LIST OF CONTENTS

LIST OF FIGURES

LIST OF TABLES

LIST OF ABBREVIATIONS

%	percentage
°C	degrees Celsius
•OH	hydroxyl radical
2-NI	2-nitroimidazole
αMEM	α-modified minimal essential medium
λ_{em}	emission wavelength
λ_{ex}	excitation wavelength
ACSRC	Auckland Cancer Society Research Centre
ACTB	β-actin
ADM	adrenomedullin
AKR1C3	aldo-keto reductase 1C3
ALDOA	aldolase A
ANKRD37	ankyrin repeat domain 37
ANOVA	analysis of variance
ATCC	American Type Culture Collection
AU	arbitrary units
B2M	beta-2 microglobulin
BCA	bicinchoninic acid
BNIP3	BCL2/adenovirus E1B 19kDa interacting protein 3
BNIP3L	BCL2/adenovirus E1B 19kDa interacting protein 3-like
BODIPY-FL-azide	boron-dipyrromethene fluorescein-like azide
BODIPY-TR-azide	boron-dipyrromethene Texas Red-like azide
bp	base pairs
BPDS	bathophenanthroline disulfonate disodium salt
BrdU	5-bromo-2'-deoxyurdine
BSA	bovine serum albumin
BTTAA	bis[(tert-butyltriazoyl)methyl]-[(2-carboxymethyltriazoyl)methyl]-amine
CA9	carbonic anhydrase IX
CBP	CREB-binding protein
cDNA	complementary deoxyribonucleic acid
CHIP	Hsc70-interacting protein
Cmpd	compound
CO_2	carbon dioxide

C_t	threshold cycle
CuAAC	Copper(I)-catalysed azide-alkyne cycloaddition
Cu(II)-ATSM	Cu-diacetyl-bis(N4-methylthiosemicarbazone)
CYB5R3	NADH:cytochrome b_5 reductase 3
dAMP	2'-deoxyadenosine 5'-monophosphate
dCMP	2'-deoxycytidine 5'-monophosphate
DDR	DNA damage response
DEAC-azide	diethylaminocoumarin azide
dGMP	2'-deoxyguanosine 5'-monophosphate
DMACA-azide	dimethylaminocoumarin acetic acid azide
DMEM	Dulbecco's Modified Eagle Medium
DMSO	dimethyl sulfoxide
DNA	deoxyribonucleic acid
DNase	deoxyribonuclease
DSB	double strand break
EC	Enzyme Commission
ECM	extracellular matrix
EDTA	ethylenediaminetetraacetic acid
EdU	5-ethynyl-2'-deoxyuridine
EF5	2-(2-Nitro-1H-imidazol-1-yl)-N-(2,2,3,3,3-pentafluoropropyl)acetamide
EGLN3	egl-9 family hypoxia-inducible factor 3
ELISA	enzyme-linked immunosorbent assay
ER	endoplasmic reticulum
ERK/MAPK	extracellular signal-regulated kinase/mitogen-activated protein kinase
EtOH	ethanol
FACS	fluorescence-activated cell sorting
FAM162A	family with sequence similarity 162, member A
FAZA	flouroazomycin arabinoside
FBS	fetal bovine serum
FCS	foetal calf serum
FDXR	adrenodoxin reductase
FIH-1	factor inhibiting HIF-1
FMISO	fluoromisonidazole
FOXRED2	FAD-dependent oxidoreductase domain containing 2
g	grams
× *g*	times gravity
gDNA	genomic deoxyribonucleic acid
GFP	green fluorescent protein

GLUT1	glucose transporter 1
GSH	glutathione
h	hours
HAF	hypoxia-associated factor
HAP	hypoxia-activated prodrug
HER	HIF-responsive element
HGP	human genome project
HHR	homologous recombination repair
HIF	hypoxia inducible factor
HIV/AIDS	human immunodeficiency virus infection/acquired immunodeficiency syndrome
HNSCC	head and neck squamous cell carcinoma
HPLC	high performance liquid chromatography
HPV	human papilloma virus
HRP	horseradish peroxidase
Hsp	heat shock protein
i.p.	intraperitoneal
KCTD11	potassium channel tetramerization domain containing 11
kDa	kilodalton
L	litres
LC/MS	liquid chromatography/mass spectrometry
LC-MS/MS	liquid chromatography triple quadrupole tandem mass spectrometry
LCM	laser capture microdissection
LOX	lysyl oxidase
m	milli
M	moles per litre
MCL	multicellular layer
Mdm2	murine double minute 2
MeOH	methanol
MFI	median fluorescence intensity
mg	milligrams
MGB	minor groove binder
min	minutes
mL	millilitres
mm Hg	millimetres of Mercury
mM	millimoles per litre
MMC	mitomycin
MRI	magnetic resonance imaging
mRNA	messenger ribonucleic acid

mTOR	mammalian target of rapamycin
MTRR	methionine synthase reductase
MWC	Maurice Wilkins Centre
n	nano
NADPH	nicotinamide adenine dinucleotide phosphate
NDRG1	N-myc downstream regulated 1
NDOR1	NADPH-dependent diflavin oxidoreductase 1
NFQ	nonfluorescent quencher
NLCQ-1	4-[3-(2-nitro-1-imidazolyl)-propylamino]-7-chloroquinoline hydrochloride
nM	nanomoles per litre
NOS	nitric oxide synthase
NOS1	neuronal nitric oxide synthase
NOS2A	inducible nitric oxide synthase
NOS3	endothelial nitric oxide synthase
NQO1 (2)	NAD(P)H:Quinone oxidoreductase 1 (2)
NRH	dihydronicotinamide riboside
NSCLC	non-small cell lung cancer
O_2	molecular oxygen
ODD	oxygen-dependent degradation
ODN	oligodeoxyribonucleotides
OPN	osteopontin
p	pico
P4HA1	prolyl 4-hydroxylase, alpha polypeptide I
P4HA2	prolyl 4-hydroxylase, alpha polypeptide II
PBS	phosphate buffered saline
PCR	polymerase chain reaction
PDK1	pyruvate dehydrogenase kinase, isozyme 1
Pfa	paraformaldehyde
PET	positron emission tomography
PFKFB3	6-phosphofructo-2-kinase/fructose-2,6-biphosphatase 3
pH	measure of acidity or basicity of a solution
PHD	prolyl hydroxylase domain
pH_e	extracellular pH
PI	propidium iodide
pO_2	partial pressure of oxygen
POR	NADPH:cytochrome P450 oxidoreductase
PS	penicillin/streptomycin
psi	pound per square inch
p-value	probability

rcf	relative centrifugal force
RFU	relative fluorescence units
RH1	2,5-di(aziridin-1-yl)-3-(hydroxymethyl)-6-methylcyclohexa-2,5-diene-1,4-dione
RIN	RNA integrity number
RIPA buffer	radioimmunoprecipitation buffer
RNA	ribonucleic acid
RNase	ribonuclease
ROS	reactive oxygen species
rpm	revolutions per minute
rRNA	ribosomal ribonucleic acid
RT	room temperature
RT-qPCR	quantitative reverse transcription real-time polymerase chain reaction
s	seconds
s.c.	subcutaneous
SD	standard deviation
SDS	sodium dodecyl sulfate
SEM	standard error of the mean
siRNA	small interfering RNA
SLC2A1	solute carrier family 2, facilitated glucose transporter member 1
SPAAC	strain-promoted azide-alkyne cycloaddition
SPECT	single photon emission computed tomography
STR	short tandem repeat
SUMO	small ubiquitin-like modifier
TAD	transactivation domain
TAMRA-azide	tetramethylrhodamine azide
TBS	tris-buffered saline
TBTA	tris(benzyltriazolylmethyl)amine
TCEP	tris(2-carboxyethyl)phosphine
TLDA	TaqMan® Low-Density Array
THPTA	tris(hydroxypropyltriazolylmethyl)amine
TPZ	tirapazamine
TXNRD1	thioredoxin reductase
UPR	unfolded protein response
UV	ultraviolet
v	version
v/v	volume/volume
VEGF	vascular endothelial growth factor

VHL	von Hippel-Lindau protein
WHO	World Health Organization
WT	wild-type
µg	micrograms
µL	microlitres
µM	micromoles per litre

Chapter 1. Literature review

Cancer is an enormous global health burden and accounts for one in every four deaths in the United States (Siegel, Naishadham, & Jemal, 2012) and one in every eight deaths worldwide today, which is more than human immunodeficiency virus infection/acquired immunodeficiency syndrome (HIV/AIDS), tuberculosis, and malaria combined (Palazon, Aragones, Morales-Kastresana, de Landazuri, & Melero, 2012). As the leading cause of death in economically developed countries and the second leading cause of death in developing countries (WHO, 2008), cancer has become one of the most feared health issues of humankind, touching every region and socioeconomic level (Jemal et al., 2011).

International cancer surveillance has been carried out principally by the World Health Organization (WHO) (WHO, 2010). According to the official report released by GLOBOCAN 2008, 12.7 million cancer cases and 7.6 million cancer deaths are estimated to have occurred in 2008 worldwide (Ferlay et al., 2010b). Of these, 56% of cases and 64% of deaths occurred in the economically developed world (Ferlay et al., 2010a, 2010b; Jemal et al., 2011). The global burden of cancer continues to grow at an alarming pace, especially in economically developed countries, as a result of population aging and growth, as well as an increasing adoption of lifestyles associated with economic development and urbanization (Ferlay et al., 2010b).

1.1 Tumour Vasculature and Blood Flow

Solid tumours are heterogeneous three-dimensional structures (Joyce, 2005; Tredan, Galmarini, Patel, & Tannock, 2007). There are multiple cell types and many different extracellular elements involved in this complex system (Hanna, Quick, & Libutti, 2009; Joyce, 2005). These components are collectively termed the tumour microenvironment, or stroma consisting, beside tumour cells, of endothelial cells, pericytes, fibroblasts, inflammatory cells, leucocytes, and elements of the extracellular matrix (ECM) (Hanna et al., 2009; Ronnov-Jessen, Petersen, & Bissell, 1996). Tumour epithelial cells are part of this microenvironment in which the tumour grows (Hu & Polyak, 2008).

With the accumulation of knowledge in cancer biology, there is a tendency to treat tumours as a functional organ-like structure (Tredan et al., 2007). Generally, solid tumours comprise various types of cells, embedded in an extracellular matrix and nourished by a vascular network (Hanna et al., 2009; Tredan et al., 2007). These components affect tumour growth, invasion, and metastasis by interacting with each other in a dynamic and independent manner (Blavier, Lazaryev, Dorey, Shackleford, & DeClerck, 2006; Shekhar, Werdell, Santner, Pauley, & Tait, 2001; Tredan et al., 2007).

Cells require oxygen and other nutrients for their survival, growth, and normal physiological functions. These requirements are satisfied by exchange of gas, nutrients, and metabolites across the capillary wall (Fens, Storm, & Schiffelers, 2010; Hanahan & Weinberg, 2011; Stewart et al., 2010). The vascular system not only plays essential roles in embryogenesis and development but also contributes to the achievement and maintenance of normal homeostasis in adult tissues (Furuya, Yonemitsu, & Aoki, 2009; Stewart et al., 2010).

1.1.1 Tumour vasculature

The vascular system is also actively involved in a wide range of pathological events, including wound repair, metabolic diseases, and tumour progression (Furuya et al., 2009). A functioning vasculature is necessary for solid tumours to efficiently deliver nutrients and remove toxic waste products associated with cellular metabolism (Siemann, 2006). The uncontrolled proliferation of neoplastic cells forces the cell population away from the existing vasculature, consequently leading to impaired oxygen and nutrient delivery (Folkman, 2003; Gatenby & Gillies, 2004). This critically limits the growth of avascular tumours to a certain size, typically about 1–2 mm in diameter (Folkman, 1971). In order to compensate for this, tumours induce an independent blood supply by establishing vasculature for themselves. Such vascular network requirement by tumours can be, at least, partially achieved by the incorporation of existing host blood vessels (Fens et al., 2010; Li et al., 2000). Simultaneously, the altered tumour microenvironment is also able to recruit heterogeneous precursors of main constituent cells for constructing blood vessels and localise them in close proximity of tumour vasculature (Furuya & Yonemitsu, 2008; Lyden et al., 2001; Yang et al., 2004). With the development of cancer, tumour expansion eventually necessitates the

formation of novel blood vessels (Fens et al., 2010). As a consequence, tumour growth, development, and survival are generally associated with the parallel proliferation of microvascular endothelial cells comprising the tumour blood vessel network (Huang & Chen, 2008). Unlike tumour cells themselves, these microvascular endothelial cells recruited by tumours are genetically stable (Folkman, 2001). This angiogenic vasculature is aberrant from normal host vasculature and has become a crucial second target in cancer therapy (Fens et al., 2010; Satchi-Fainaro, 2002).

In general, tumour blood vessels possess a highly irregular morphology. They are often dilated and tortuous/convoluted (Tredan et al., 2007). Different to the vasculature in normal tissues, blood vessels have branching patterns featuring excessive loops and arteriolar-venous shunts, which are associated with specific structures, such as blind ends, in tumours (Jain, 1988). Instead of being organised in arterioles-capillaries-venules, individual tumour blood vessels share features from more than one or all of these structures (Brown & Wilson, 2004; Tredan et al., 2007). The walls of tumour vessels, including both blood and lymphatic vessels, may have fenestrations, incomplete or even absent endothelial linings and basement membrane (Brown & Giaccia, 1998; Tredan et al., 2007). In addition, fewer pericytes than associated with normal vessels and lack of perivascular smooth muscle may directly lead to compromised physiological function (Benjamin, Golijanin, Itin, Pode, & Keshet, 1999; Carmeliet & Jain, 2000). Consequently, vessels are much “leakier” than those in normal tissues, which offers cancer cells more possibilities to intravasate into vessels and facilitates metastatic spread (Brown & Giaccia, 1998; Hashizume et al., 2000).

1.1.2 Tumour blood flow

Blood flow in many tumours is both disorganised and variable (Carmeliet & Jain, 2000). In a vascular network, the pressure difference between the arteries and the veins is directly proportional to the flow rate that is inversely proportional to the viscous and geometric resistance (Tredan et al., 2007). In tumour tissues, the difference in pressure between arterioles and venules is diminished (Brown & Giaccia, 1998; Tredan et al., 2007), while the viscous and geometric resistance is augmented (Sevick & Jain, 1989, 1991). All of these changes induced by tumour genesis/development increases resistance to blood flow (Padera et al., 2004). Moreover, similar

to vascular morphology, these alternations in blood flow may also vary with location and/or time even in the same tumour (Gillies, Schornack, Secomb, & Raghunand, 1999; Vaupel, 2004).

This sluggish blood flow consequently causes the reduction in both supply of nutrients and clearance of unwanted metabolic products, which ultimately contributes to the formation of hypoxia (Tatum et al., 2006; Vaupel, 2004), decrease in proliferation rates (Hirst & Denekamp, 1979; Tannock, 1968), and acidic regions in tumours (Helmlinger, Yuan, Dellian, & Jain, 1997; Tannock & Rotin, 1989).

1.2 Tumour Hypoxia

Hypoxia is a low oxygen condition often found in tumours. Over time, we have gained a better understanding of the correlations between cancer and hypoxia. The accumulated evidence from a large body of literature clearly demonstrates that hypoxia is not only playing an essential role in resistance to cancer therapy but also is a potent inducer of numerous critical tumour phenotypes with the rationale of inducing tumourigenesis (Moeller, Richardson, & Dewhirst, 2007).

1.2.1 Discovery of hypoxia

From a long-term study of the anatomy of the capillary bed as well as a mathematical model of oxygen diffusion and consumption, the Nobel Laureate, August Krogh, first introduced the concept that oxygen diffusion was limited to 100-200 μM from capillary vessels (Krogh, 1922). This theory was confirmed about 30 years later. In 1955, similar “cord”-like structures were identified in human lung cancer (Thomlinson & Gray, 1955). Meanwhile, necrotic cells were detected in tumour tissue located beyond 180 μM from blood vessels, presumably as a consequence of oxygen deprivation (Stewart et al., 2010).

Regions of hypoxia and necrosis commonly develop at sites generally over 100 μM from blood vessels in solid tumours due to their structurally abnormal vasculature, through which oxygen and other essential nutrients cannot be efficiently supplied to all cells (Brown & Wilson, 2004; Helmlinger et al., 1997). For example, instead of ~65 mmHg in surrounding normal tissue, the

oxygen tension was shown to be ~10 mmHg in hypoxic breast tumours (Vaupel, Mayer, & Höckel, 2004).

Due to rapid proliferation and insufficient blood supply, progressive tumours easily become hypoxic and necrotic (Figure 1.1) (Pugh & Ratcliffe, 2003). Some aggressive tumour cells located far from blood vessels can still survive at low levels of oxygen. Hypoxia can function as a selection pressure and has a great impact on tumour progression through induced vascularization and resistance to therapy. This autocrine-like hypoxia-mediated tumour progression subsequently decreases overall patient survival, increases tumour mutation rate, and contributes to enhanced metastatic phenotypes (Bacon & Harris, 2004; Holmquist, Lofstedt, & Pahlman, 2006). Because of this, hypoxic tumour cells are usually associated with poor prognosis and increased rates of recurrence, which was demonstrated as a 3-fold increase in resistance to radiotherapy compared to well-oxygenated control tumour cells both *in vitro* and in a clinical study of 30 consecutive patients with cervical cancer (Harrison, Chadha, Hill, Hu, & Shasha, 2002; Suzuki et al., 2006).

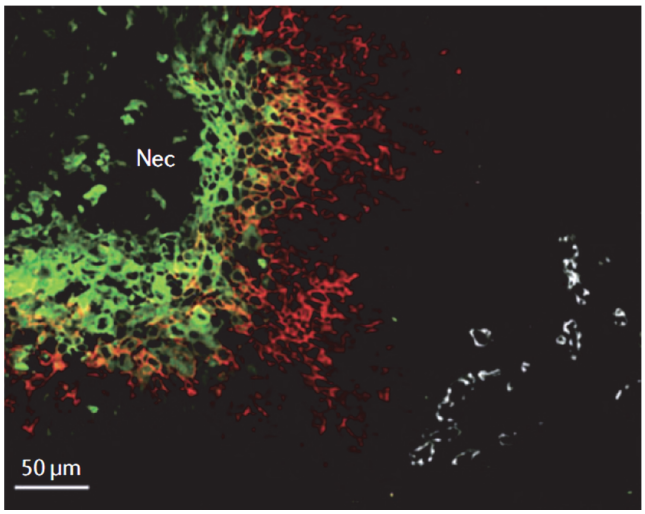

Figure 1.1: Detection of hypoxia in human squamous cell carcinoma by using exogenous and endogenous markers.

Photomicrograph of a biopsy of a human squamous cell carcinoma of the larynx showing hypoxia (green, by use of exogenous hypoxia marker; red, by use of endogenous hypoxia marker) in relation to vasculature (white) and necrosis (Nec). Modified from: Wilson and Hay (2011).

1.2.2 Classification of hypoxia

Depending on the duration of low oxygen tension in tumour cells, tumour hypoxia is generally classified into two types, chronic and acute hypoxia (Brown & Wilson, 2004). This is a somewhat artificial separation as there is no precise temporal boundary to distinguish and define these two states (Chaudary & Hill, 2007).

Tumour cells may experience chronic or “diffusion-limited” hypoxia when located at the outer limits of oxygen diffusion from properly functioning blood vessels. The reason to term it “chronic” is from the fact that such hypoxic conditions typically last for relatively long periods from hours to days (Martin Brown, 2007). On the other hand, tumour vasculature abnormalities can also lead to short-term or transient changes in oxygen tension in some regions of the tumour due to the intermittent blood supply (Fukumura, Duda, Munn, & Jain, 2010; Fukumura & Jain, 2007). These pathological alternations may make cells suffer acute or “perfusion-limited” hypoxia characterized by rapid reoxygenation or hypoxic-oxic cycles with periodicities of minutes to hours (Kimura et al., 1996). More recently, a new form of hypoxia, macro-regional hypoxia, was also identified as a consequence of both diffusion-limited and perfusion-modulated hypoxia in a relatively large tumour region (Koch et al., 2013). All three types of hypoxia develop when oxygen supplies cannot satisfy tissue oxygen demands due to aberrant blood vessel formation, fluctuation in blood flow, and elevated oxygen consumption from rapid tumour expansion (Meng, Kong, & Yu, 2012).

1.2.3 Reoxygenation and intratumoural hypoxia

Through the elimination of tumour cells that cannot adapt by apoptosis and other means of cell death, hypoxic stress is able to provide a selection pressure on the mutation rate by inducing changes in the proteome and genome of neoplastic cells. It has been demonstrated that tumour hypoxia may impact on the development of metastases in different ways (Rofstad, Galappathi, Mathiesen, & Ruud, 2007). The reoxygenation process following hypoxia or even repeated hypoxia-reoxygenation alternations is capable of promoting the generation of superoxide and other oxygen-derived radicals that likely contribute to the accumulation of mutations. During gene amplification or DNA replication under hypoxic conditions, the locally enriched oxygen free radicals may lead to chromosomal breaks or chromosomal rearrangements (Al-Waili et al., 2005), which

was supported by the 3.4-fold increase in point-mutation frequency of tumorigenic cells cultured under severe oxygen tension instead of normal gassing conditions (Höckel & Vaupel, 2001).

The existence of intratumoral hypoxia does not only depend on the size but also on the growing stage of tumour (Casazza et al., 2014). Sustained hypoxia in a growing tumour has been implicated in the elevation of clinically more aggressive phenotypes by inducing cell morphology changes and causing mutations selectively in crucial oncogenes (Vaapil et al., 2012). As a consequence, the promotion of regional and distant tumour cell metastases contributes to the aggressive phenotype of tumours (Zhang, Li, Yao, & Chen, 2007).

1.2.4 Significance of tumour hypoxia in clinical therapies

Tumour hypoxia is associated with aggressive disease and poor treatment outcomes for radiotherapy and chemotherapy (Graves, Maity, & Le, 2010; Mees, Dierckx, Vangestel, & Van De Wiele, 2009; Vikram, Zweier, & Kuppusamy, 2007).

It has been known for a long time that hypoxic cells are resistant to ionising radiation (Figure 1.2) (Gray, Conger, Ebert, Hornsey, & Scott, 1953). Induction of cell death is the most straight-forward strategy of cancer treatment. Under normal conditions, the cell killing function requires oxygen to rapidly react with free-radical damage produced by ionising radiation in DNA for ‘fixing’ and causing permanent DNA damage (Martin Brown, 2007; Roots & Smith, 1974). Under low oxygen tension, the majority of initial radical damage can be restored to the corresponding non-damaged form by reacting with hydrogen donated from non-protein sulfhydryls, particularly glutathione (GSH), and cysteine (Biaglow, Varnes, Clark, & Epp, 1983; Bump, Cerce, al-Sarraf, Pierce, & Koch, 1992; Horan & Koch, 2001; Little & Williams, 2010; Mitchell, Biaglow, & Russo, 1988; Revesz, 1985).

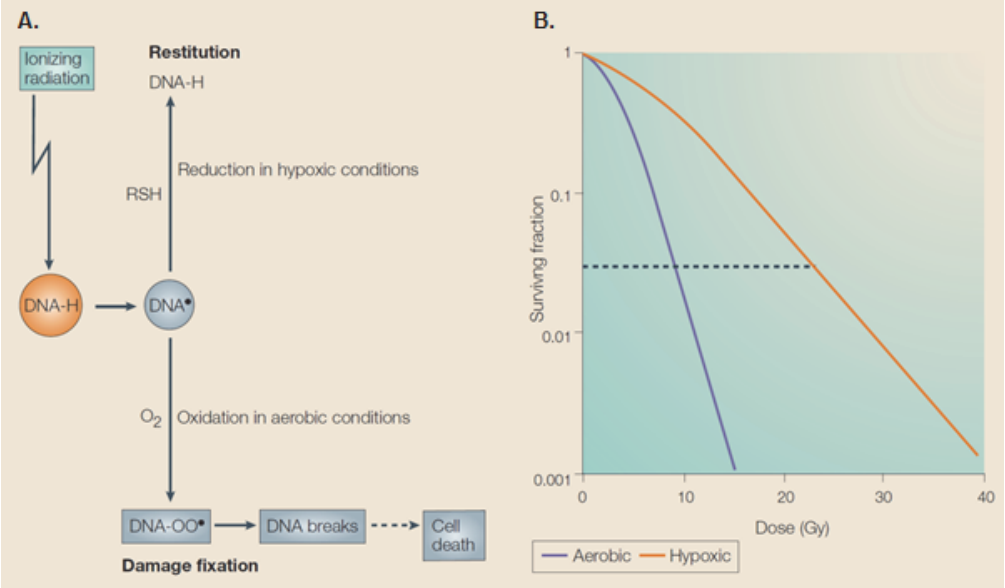

Figure 1.2: Radiation resistance of hypoxic cells.

Ionizing radiation conducts the cell killing function by inducing DNA damage. (A) A radical on the DNA (DNA·) produced by ionizations enters into a competition for oxidation or reduction. (B) DNA damage is oxygen-dependent. This effect of oxygen in sensitizing cells to radiation is illustrated in the cell-survival curve and is quantified as the ratio of dose in the absence of oxygen to dose in the presence of oxygen needed to obtain the same surviving fraction of cells. Studies in head and neck cancers (HNSCCs) have indicated that more hypoxic tumours (typically those with a median *p*O2 less than 10 mmHg) are associated with a higher level of radio-resistance. Modified from: Brown and Wilson (2004).

In order to improve the therapeutic efficacy of radiation in hypoxic tumours, a group of molecules coined as hypoxic radiosensitizers have been developed, initially in the 1960's (Adams & Cooke, 1969). Their potent electron-affinic nature allows them to mimic O_2 to react with the short-lived DNA free radicals generated by ionizing radiation, consequently sensitizing radiation-induced cytotoxic responses in hypoxic tumour cells (Ahn & Brown, 2007). Unfortunately, all hypoxic radiosensitizers so far have limited clinical application, because the radiation doses used in clinically relevant fractionated irradiation schedules lead to a reduction of the radiosensitization efficacy in tumours (Denekamp & Stewart, 1978; Hill & Bush, 1978; Sheldon & Fowler, 1978).

Under oxygen deprivation, cells are considered to carry chemotherapeutic resistance predominantly due to their physiological and genetic changes in response to hypoxia. The primary events contribute to this kind of treatment resistance include the slow proliferation or even non-

cycling state of hypoxic cells (Green & Giaccia, 1998; Kennedy et al., 1997; Tannock, 1968); the limited accessibility of hypoxic cells to drugs delivered by blood flow (Hicks et al., 2006; Kyle, Huxham, Yeoman, & Minchinton, 2007; Minchinton & Tannock, 2006; Tannock, Lee, Tunggal, Cowan, & Egorin, 2002); selective stress against p53 followed by loss of sensitivity to hypoxia-induced apoptosis (Graeber et al., 1996); the lack of molecular oxygen similar to the reason of resistance in radiotherapy (Batchelder, Wilson, Hay, & Denny, 1996; Teicher, Lazo, & Sartorelli, 1981); as well as induction of proteins whose expressions mediate resistance of some tumours to some chemotherapeutics, such as p-glycoprotein (Comerford et al., 2002).

1.3 Hypoxia-inducible factors

The hypoxia-inducible factors (HIFs) are transcriptional factors that function as pivotal master regulators of oxygen homeostasis and are expressed in all existing metazoan species investigated to date (Loenarz et al., 2011). They are critical in the adaptation of cells to hypoxic stress in order to survive.

1.3.1 Regulation of HIFs

Both HIF-1α and HIF-1β are constitutively transcribed and translated in cells. HIF-1α, however, demonstrates an extremely short half-life of less than 5 min in well-oxygenated cells (Huang, Arany, Livingston, & Franklin Bunn, 1996). The rigid regulation of HIF protein activity is mediated primarily through the instability of the α subunit by several mechanisms, dominantly through the degradation pathways (Figure 1.3).

1.3.1.1 Oxygen/PHDs/VHL-dependent HIF-α regulation

Under normoxic conditions, prolyl hydroxylase domain protein 2 (PHD2), cooperating with non-heme, oxygen-, Fe(II)-, and 2-oxoglutarate-dependent dioxygenases, hydroxylates HIF-1α on its specific proline residues (Pro402 and/or Pro564) within the oxygen-dependent degradation (ODD) domain by utilising O_2 and α-ketoglutarate as substrates (Kaelin Jr & Ratcliffe, 2008; Loboda, Jozkowicz, & Dulak, 2010). This reaction converts HIF-1α into the prolyl-hydroxylated form, by which it is possible to establish the association between HIF-1α and von Hippel-Lindau tumour

suppressor protein (VHL). Subsequently, VHL recruits the elongin-C/elongin_B/cullin-2 E3-ubiquitin-ligase complex and thus targets HIF-1α for degradation by the 26S proteasome (Cockman et al., 2000; Maxwell et al., 1999). Additionally, asparagine 803 (N803) in the transactivation domain (TAD) of HIF-1α can be hydroxylated by factor inhibiting HIF-1 (FIH-1) in well-oxygenated cells. This process functionally regulates HIF-1α in a negative manner by blocking the access of coactivators p300 and CREB-binding protein (CBP) to their binding sites (Kaelin Jr & Ratcliffe, 2008; Lando, Peet, Gorman, et al., 2002; Lando, Peet, Whelan, Gorman, & Whitelaw, 2002).

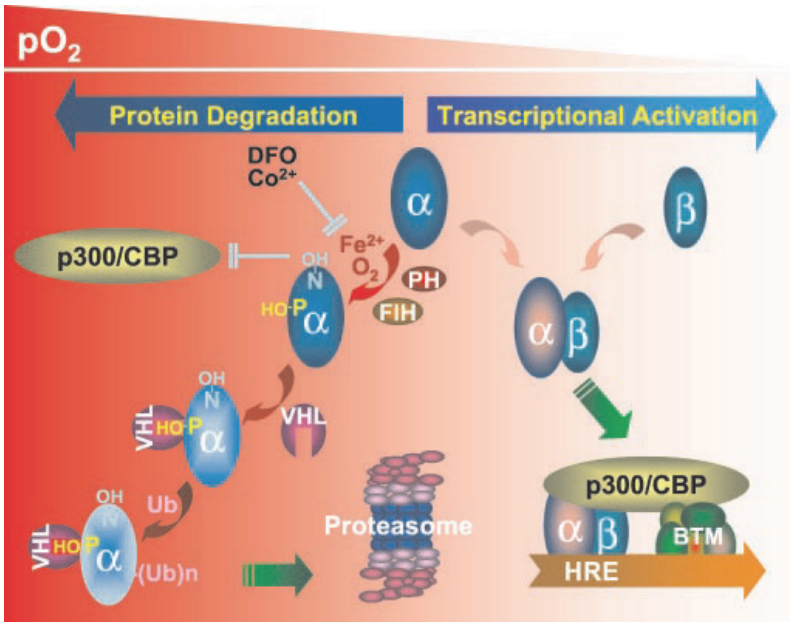

Figure 1.3: Oxygen-dependent regulation of HIF depends on site-specific hydroxylation of the HIF-α subunit.

When the levels of O_2 and Fe(II) are above a threshold, some specific proline and asparagine residues in HIF-1 are hydroxylated under the catalysation of prolyl 4-hydroxylase (PH) and asparaginyl hydroxylase (FIH), respectively. The hydroxylated prolines (P-OH) provide docking sites for VHL interaction, accordingly triggering ubiquitin conjugation and proteasomal degradation of HIF-1. The hydroxylated asparagine (N-OH) blocks p300/CBP binding site in HIF-1, thereby hindering subsequent transcriptional activation. The prolyl hydroxylase activity is repressed by low oxygen tension, desferrioxamine (DFO), or cobalt ion (Co^{2+}). Such inhibitions stabilise HIF α-subunit. The HIF heterodimer recruits p300/CBP and binds to the HRE in the promoter or enhancer region of target genes, activating the basal transcription machinery (BTM). The intensity of red background decreasing from left to right indicates the level of oxygen tension. From: Huang and Bunn (2003).

During hypoxia, both prolyl and asparaginyl hydroxylation reactions are repressed by substrate deprivation, the limited O_2 accessibility. In addition, the mitochondrially generated reactive oxygen

species (ROS) may oxidize Fe(II), the major cofactor of PHD2, into inactivated Fe(III), thereby diminishing the overall activities of the hydroxylases (Guzy et al., 2005; Guzy & Schumacker, 2006). Since the inactivated PHDs prevent the VHL-initiated ubiquitination and proteasomal degradation, HIF-1α/2α can be transported into the nucleus and undergo dimerisation with HIF-1β (Chilov et al., 1999). Subsequently, various coactivators are recruited to form a functional complex by coupling with dimerised HIF (Semenza et al., 1996). Due to the histone acetyltransferase activities provided by coactivators, the activated HIF complex eventually binds to the highly conserved HIF-responsive element (HER) sequence at the target gene loci and initiates downstream expression events (Loboda et al., 2010).

1.3.1.2 Oxygen/PHDs/VHL -independent HIF-α regulation

The presence of VHL-independent regulation of HIF-1α is supported by accumulated evidence generated from a range of studies. To date, several oxygen/PHDs/VHL–independent mechanisms have been identified.

Hypoxia-associated factor (HAF) is a novel HIF-1α isoform specific E3 ligase with a unique expression pattern. HAF has been detected in both normal and tumour-derived cell lines, but only in proliferating, not all, tissues. This molecule has been proven to induce oxygen-independent HIF-1α degradation even in hypoxic cells (Koh, Darnay, & Powis, 2008).

Tumour suppressor p53 has been reported to mediate the recruitment of the murine double minute 2 (Mdm2) ubiquitin-protein ligase, which promotes the ubiquitination and proteasomal degradation of HIF-1α (Ravi et al., 2000). This regulating mechanism explains why the loss of p53 is usually associated with increased HIF-1α levels in tumour cells.

HIF-1α is also functional as the client protein of some molecular chaperones, such as extracellular heat shock proteins (Hsp). Hsp family protein Hsp90, Hsp70, and a carboxyl terminus of Hsc70-interacting protein (CHIP) were demonstrated to selectively protect only HIF-1α, not HIF-2α, from ubiquitination and degradation (Liu, Baek, et al., 2007; Liu, Hubbi, et al., 2007; Luo et al., 2010).

The hypoxia induced HIF-1α small ubiquitin-like modifier (SUMO)ylation has been reported to regulate VHL-mediated oxygen-dependent HIF-1α degradation. Different to mechanisms discussed above, SUMOylation has specially Janus-style bifacial features. Such posttranslational modifications can regulate the stability of HIF-1α in either a positive (Bae et al., 2004; Carbia-Nagashima et al., 2007) or a negative direction (Berta, Mazure, Hattab, Pouysségur, & Brahimi-Horn, 2007; Cheng, Kang, Zhang, & Yeh, 2007). Besides, the process of HIF-2α degradation can also be regulated by SUMO modifier-mediated mechanisms (van Hagen, Overmeer, Abolvardi, & Vertegaal, 2010).

In addition, phosphorylation through the classic extracellular signal-regulated kinase/mitogen-activated protein kinase (ERK/MAPK) signalling pathway has been indicated to stabilize HIF-1α and in turn elicit enhanced transcriptional activities by several research groups (Richard, Berra, Gothié, Roux, & Pouysségur, 1999). Both HIF-1α and HIF-2α have been shown to act as the phosphorylation substrates of p42/44 kinase and p38 kinase by *in vitro* studies (Richard et al., 1999; Sodhi et al., 2000). Interestingly, phosphorylation of p300 by the MAPKs pathway facilitates the recruitment of p300-CBP coactivator family proteins (p300/CBP) to the C-TAD of HIF-1α, which contributes to the enhanced transcription activities of downstream target genes (Sang et al., 2003).

Another key signalling pathway, PI-3K/Akt/mTOR, is also implicated in the regulation of both HIF-1 expression and activity in an oxygen-independent manner in various cancer cell lines (Alvarez-Tejado et al., 2001; Howes et al., 2003). Applications of inhibitors specific to these signalling pathways were able to significantly interfere with the expression patterns of HIF-1α mediated reporter genes (Hur, Chang, Lee, Lee, & Park, 2001).

1.3.2 Significance of HIF in cancer

The adaptation of tumour cells to hypoxic scenarios makes HIFs either directly or indirectly key players in cancer biology (Figure 1.4). HIFs are functional regulators of gene expression at transcription level and play pivotal roles in a number of subdivisions of cancer research that include cell immortalization and stem cell maintenance; genetic instability; glucose and energy metabolism; pH regulation; vascularization; autocrine growth factor signalling; migration, invasion, and

metastasis; immune evasion; and resistance to chemotherapy and radiation therapy (reviewed in: Semenza, 2010).

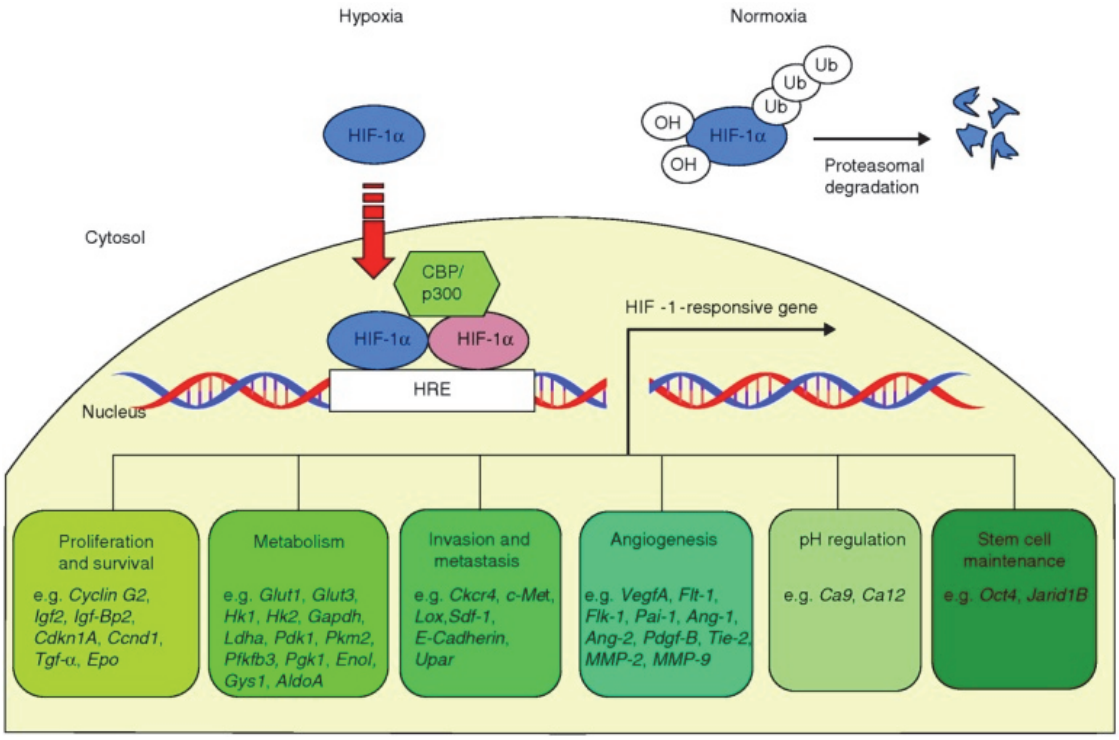

Figure 1.4: Target genes transcriptionally activated by HIF-1α.

Genes are grouped by biological function. Redrawn and modified from: GenomeMedicine (2012).

1.4 Hypoxia gene signatures in tumours

Hypoxia mediates a wide spectrum of biological pathways, which makes it a key factor promoting solid tumour progression and resistance to therapy. Understanding hypoxia is important for the development of novel therapies and thus to improve prognosis.

Up to 1.5% of the human genome is estimated to be transcriptionally responsive to hypoxia (Denko et al., 2003). Any single factor, such as the expression profile of an individual gene, does not possess sufficient capability in adequately describing this complicated response (Winter et al.,

2007). Gene expression signatures are clusters of genes discriminating different statuses of the cells, which is critical for understanding the complicated molecular mechanisms behind diseases (Fardin et al., 2009). Since the prognostic potential to predict benefit from particular interventions, a robust and clinically applicable hypoxia gene expression signature (or metagene) is required (Buffa, Harris, West, & Miller, 2010).

Denko *et al.* identified 110 hypoxia-responsive genes from large-scale cDNA array analysis in 6 different cell lines including 3 carcinoma cell lines (FaDu, SiHa, and C33a) under a not clearly ooof defined “long term hypoxia” (Denko et al., 2003).

A microarray based study of the expression of genes induced *in vitro* by hypoxia in a panel of normal cell lines was first accomplished by Chi *et al.*, who published a gene expression signature of cellular response to hypoxia in epithelial cells. This metagene was dependent not only on cell type but also the intensity/duration of hypoxia. Even though derived from normal cell types, it has been successfully applied in predicting relapse rates in ovarian and breast cancers (Chi et al., 2006).

Lambin and colleagues used the same published data from the microarray work of Chi *et al.* to establish gene signatures of specific time points during the process of hypoxic induction to obtain the time-dependent patterns of gene expression during hypoxia. They emphasized the significant value of early hypoxia signatures in prognosis and indicated that *in vitro* gene signatures could contribute to clinical cases via providing a means to select patients for individualized therapy (Seigneuric et al., 2007).

Through microarray results generated from an mRNA study in 59 head and neck cancer tissues, Harris and co-workers defined an *in vivo* hypoxia metagene containing 99 genes in head and neck squamous cell carcinomas (HNSCCs) by clustering around the RNA expression of a group of known hypoxia-regulated genes (Winter et al., 2007). This gene expression signature of cellular response to hypoxia slightly overlapped the *in vitro* one defined by Chi *et al*.. In both univariate and multivariate analyses, Harris’ signature demonstrated the advantage in retaining prognostic significance over Chi’s. The 99-gene hypoxic expression profile was prognostic for relapse-free survival in HNSCC and breast cancer validation cohorts (Winter et al., 2007).

The ability to promote new blood and lymphatic vessel formation is the major part of the response to hypoxia. The expression profile of a gene set, involving vascular endothelial growth factor (VEGF) *per se* and 12 other VEGF-related genes, was identified as a compact *in vivo* hypoxia signature and indicated prognostic significance on tests of patients with breast and lung cancer and glioblastoma. The upregulated expression of this gene set was correlated to poor patient prognosis by causing *de novo* vessel formation and providing a dual conduit for metastatic spread (Hu et al., 2009).

The response to hypoxia is highly heterogeneous in different cell lines (Chi et al., 2006). Unlike Chi *et al.*, Varesio's group worked on the gene expression profile of 11 hypoxia responsive neuroblastoma cell lines with the analysis of differential gene expression to eventually derive 62 probesets (NB-hypo), a robust *in vitro* hypoxia signature. Gene expression of the tumours of 88 neuroblastoma patients was profiled, by which the neuroblastoma patients were divided into good and poor prognosis groups. In the overall survival studies, the patients with good prognosis demonstrated a survival rate of 73.2% compared with a survival rate of 25.5% for the patients with poor prognosis. A survival rate of 67.7% for the patients with good prognosis was shown in the event-free survival curves, compared with a survival rate of 27.7% for the patients with poor prognosis. As a significant independent predictor, NB-hypo successfully illustrated its ability to stratify the neuroblastoma patients according to their prognostic outcome, which consequently improved the effectiveness of risk related therapy (Fardin et al., 2010).

More recently, Buffa *et al.* selected genes that consistently co-expressed with the previously validated hypoxia-regulated genes (seeds) in multiple cancers. By combining knowledge of multiple genes' function together with analysis of *in vivo* co-expression patterns/networks, they defined a more general and compact hypoxia signature (including 51 genes) with clinical application value from three head and neck and five breast cancer studies in a meta-analysis context for clinical use. This signature constructed by the hypoxia co-expression cancer networks is important for improved prognosis or development of novel therapies (Buffa et al., 2010).

Tumour pH is generally in the range of 6.15-7.4 (Helmlinger et al., 1997; Vaupel, Kallinowski, & Okunieff, 1989). It has been demonstrated that hypoxia related gene expression is to a large

degree influenced by extracellular pH (pH_e) (Sørensen, Alsner, Overgaard, & Horsman, 2007; Sørensen et al., 2005). Suppression in hypoxia-induced upregulation of expression has been identified in a number of genes in tumour microenvironments with low pH_e. In order to establish expression profile of genes that are regulated by hypoxia but independent of other factors, Alsener and co-workers derived a robust hypoxia signature of 27 genes unaffected by pH_e across 4 human squamous carcinoma cell lines (Sørensen, Toustrup, Horsman, Overgaard, & Alsner, 2010). Those 27 genes composing the profile therefore could be candidates for endogenous markers of tumour hypoxia with increased confidence.

The microarray study of hypoxic gene expression profiling done by Marotta *et al* directly compared *in vivo* hypoxia gene signatures, derived by total RNA samples from normoxic and hypoxic regions in the rat 9L glioma tumour model grown in its isogenic host, with two *in vitro* counterparts which were generated from rat 9L gliomas cells in culture exposed to hypoxia or normoxia for either 6 or 16 hours (Marotta et al., 2011). Two *in vitro* samples showed very similar clustering of these specific mRNAs. However, there was a more pronounced increase in number of mRNAs responsible to hypoxia *in vivo* versus *in vitro*, which was in agreement with other studies indicating a more robust gene signature with clinical significance in response to hypoxic stresses *in vivo*.

Patients with hypoxic tumours will most likely benefit from hypoxic modification. To characterise the hypoxic status of a tumour and identify patients who would potentially benefit from hypoxic modification of radiotherapy (hypoxia-modifying therapy), a hypoxia responsive gene expression classifier containing 15 genes was developed in Overgaard's research group and validated clinically for hypoxic modification or placebo in combination with radiotherapy (Toustrup, Sørensen, Alsner, & Overgaard, 2012; Toustrup et al., 2011).

Tumours display heterogeneity in degrees of hypoxia (Mortensen et al., 2010). Apart from the limited applications in human papilloma virus (HPV)-negative tumours (Toustrup, Sørensen, Lassen, et al., 2012), this hypoxia gene expression classifier can classify patients with HNSCC as having either ''more'' or ''less'' hypoxic tumours correlating with poor and good prognosis, respectively (Toustrup et al., 2011). In a retrospective study of 320 patients, the 2-nitroimdazole radiosensitiser nimorazole improved radiotherapy outcomes in hypoxic, but not normoxic HNSCC.

Hypoxia was identified according to the 15-gene signature by scoring formalin-fixed paraffin-embedded tissue samples. Tumours above the median hypoxic value were associated with poor radiotherapy outcomes and significant benefit from nimorazole. The patients classified as ‘‘more’’ hypoxic had a significant benefit regarding locoregional tumour control and disease-specific survival from hypoxic modification with nimorazole compared with patients with ‘‘less’’ hypoxic tumours (Toustrup, Sørensen, Lassen, et al., 2012).

1.5 Detection of tumour hypoxia

Gatenby and co-workers indicated that the degree and extent of tumour hypoxia at the time of diagnosis strongly correlated with tumours' radio-therapeutic responses (Gatenby et al., 1988). Overwhelming experimental and clinical data from studies in the correlations between hypoxia status and therapeutic resistance indicated that determinations of tumour oxygenation status are necessary for all patients where tumour hypoxia may be of concern (Chapman, 1991).

The existence of hypoxic cells in human solid tumours was determined by using traditional histology-based techniques at first (Thomlinson & Gray, 1955). Unfortunately, the oxygenation status of individual human tumours cannot be predicted from tumour histology, tumour volume, and tumour growth rate (Chapman, 1991). To address this problem, a group of metabolic sensitizer-adducts, hypoxic radiosensitizers, were proposed as markers of tissue oxygenation status in the 1970s (Chapman, 1979). However, most methods were based on measuring concentrations of tumour metabolites associated with cellular respiration during that time were not practical as rapid approaches for tumour oxygenation status. A range of techniques were created to achieve the requirements of tumour internal oxygenation quantification in either an invasive or non-invasive manner.

1.5.1 Invasive measurement of tumour hypoxia

Through physically inserting an oxygen-sensitive electrode into the tumour, the level of oxygen tension can be determined rapidly in a real-time manner. In this technique, a microelectrode needle is inserted into the tumour and sequential pO_2 measurements are recorded as the needle advances in a stepwise fashion through the tissue (Mortensen et al., 2010). It is one of a handful

of methods which have shown prognostic significance in pilot clinical studies to date (Brizel, Dodge, Clough, & Dewhirst, 1999; Nordsmark et al., 2005). A collection of rapid and reliable pO_2 values in the form of a histograph can be provided by this electrode-based approach, which is extremely valuable in the identification and characterization of hypoxic stress in different tumour types (Vaupel & Harrison, 2004). Hence, it has been considered as the "gold standard" for measuring tissue oxygen tension (Höckel & Vaupel, 2001; Menon & Fraker, 2005; Milosevic, Fyles, Hedley, & Hill, 2004; Olive, Banath, & Aquino-Parsons, 2001). With the application of polarographic microelectrodes, patients with non-small cell lung cancer (NSCLC) demonstrated lower *in vivo* tumour pO_2 (Le et al., 2006). Experimental and clinical data have proven a clear inverse correlation (P = 0.018) between tumour hypoxia and patient prognosis (Meng et al., 2012).

Hypoxia is often associated with necrotic regions. All methods based on the application of oxygen-sensitive electrodes are unable to distinguish viability of target cells in tumours. Due to the invasive nature, each measurement performed by pO_2 electrode only provides the hypoxic stress data in a limited region, which is thus subject to sampling error. Furthermore, the application is restricted to superficially accessible lesions (Evans et al., 2004; Milosevic et al., 2004). The number of independent measurements depends on what is intended to be achieved, which makes such methodology limited in screening overall hypoxia status across a tumour (the limited spatial resolution).

1.5.2 Non-invasive measurement of tumour hypoxia

Alternatively, direct measures of absolute pO_2 have been achieved by utilizing magnetic resonance imaging (MRI) assays based on paramagnetic agents (Padhani, Krohn, Lewis, & Alber, 2007; Vikram et al., 2007). A validation study has shown the correlations of tumour oxygenation data provided by Eppendorf pO_2 electrode and dynamic contrast-enhanced MRI (Cooper et al., 2000). MRI-based blood oxygenation level dependent assays have demonstrated reliable performance in several experimental tumour-based *in vivo* studies, suggesting its future clinical potential in identifying patients for selected oxygen-modifying treatment according to pre-treatment pO_2 levels as well as evaluating early treatment responses (Dunn et al., 2002; Foo, Abbott, Lawrentschuk, & Scott, 2004; Landuyt et al., 2001; Rodrigues, Howe, Griffiths, & Robinson, 2004).

1.5.2.1 Endogenous hypoxia-specific markers

The expression patterns of certain hypoxia-regulated proteins represent the alternations of oxygen tension in tumour cells. This characteristic allows them to be employed as indicators. Detection of hypoxic status can be accomplished through surveillance of their expression profiles. For instance, HIF-1α was reported to be employed for this purpose and analysed by immunohistochemistry (Hung et al., 2009).

Overexpression of HIF-1α was found in around one third of primary tumour clinical samples (Zhong et al., 1999). This aberrant expression pattern was related to both shorter overall survival and recurrence-free survival (Sun et al., 2012; Zheng, Ni, Huang, Wang, & Han, 2013). Some proteins encoded by HIF-mediated target genes, for example glucose transporter 1 (*GLUT1*) and carbonic anhydrase IX (*CA9*), have also been selected as indicators of hypoxic stress by their expression levels (Ilie et al., 2010). Osteopontin (OPN) belongs to a group of circulating proteins secreted by tumour and surrounding stromal cells in response to hypoxic stress. As a circulating hypoxia marker, enhanced OPN expression and elevated protein concentration in blood were normally correlated with poorer prognosis in NSCLC patients (Mack et al., 2008).

In contrast to the inaccessibility of microelectrodes, the development and application of hypoxia-specific markers provided a novel way of monitoring oxygen tension (Meng et al., 2012). The understanding of endogenous hypoxia-related cell marker expression in response to the tumour microenvironment is necessary for their applications in clinical practice (Ljungkvist, Bussink, Kaanders, & van der Kogel, 2007).

1.5.2.2 Exogenous hypoxia-specific markers

Positron emission tomography (PET), single photon emission computed tomography (SPECT), and magnetic resonance spectroscopy are often used for molecular imaging purposes (Dolbier, Li, Koch, Shiue, & Kachur, 2001). Characteristics of PET, including quick response, simultaneously monitoring of multiple targets, relatively good spatial and temporal resolution, make it a popular candidate for characterizing oxygen tension in hypoxia-specific marker labelled tumour cells. Clinical applications of PET have been reported in optimizing and individualizing

selected therapy for cancer patients based on hypoxia (Krause, Beck, Souvatzoglou, & Piert, 2006; Sloka, Hollett, & Mathews, 2007).

Several types of molecules including the 2-nitroimidazoles (2-NIs) accumulate inside hypoxic cells, where they are reduced into reactive intermediary metabolites by intracellular reductases. These metabolites covalently link to thiol groups of intracellular proteins and are enriched within viable hypoxic cells with the amount directly proportional to the level of hypoxia *in situ.*

Simply labelling 2-nitroimidazole molecules with a PET tracer to generate hypoxia-specific PET tracer successfully introduced the PET imaging method as the detection procedure of hypoxia measurement and combined advantages from both methods. Cellular uptake of this hypoxia-specific PET tracer should also correlate with the oxygenation profile in the tumours(Koh et al., 1992).

In this category, the most widely applied and intensively investigated molecule is ^{18}F-fluoromisonidazole (^{18}F-FMISO) (Cherk et al., 2006; Rasey et al., 1996). Unfortunately, ^{18}F-FMISO was associated with low tumour to background contrast ratios in applications. Additionally, the slow clearance of ^{18}F-FMISO from background tissue causes long delay period (about 2 hours) to acquire image with optimal contrast. The short half-life of ^{18}F leads to further decrease in signal to noise ratio (Meng et al., 2012).

2-(2-Nitro-1H-imidazol-1-yl)-N-(2,2,3,3,3-pentafluoropropyl)acetamide (EF5) is another popular nitromidazole hypoxia marker with a uniform biodistribution and stable structure *in vivo* (Evans et al., 2006). The long half-life (about 12 hours) of EF5 tends to increase the association with aerobic cells and reduce the excretion speed of the unmetabolised marker from normal tissues. Such drawbacks brought by the nature of EF5 interfere with its performance in hypoxia-specific imaging process (Meng et al., 2012). In order to overcome disadvantages of EF5 mentioned above, another notable hypoxia-specific radiotracer, ^{18}F-FAZA, was developed (Kumar et al., 1999). Comparison studies of ^{18}F-FAZA to ^{18}F-FMISO illustrated that both compounds shared similar cellular uptake levels in sites of oxygen tension on early PET imaging. However, ^{18}F-FAZA was associated with relatively diminished background signals, because it was rapidly eliminated from

the circulation system and non-target normal tissues (Souvatzoglou et al., 2007; Trinkaus et al., 2013).

Different to the exogenous hypoxia-specific markers discussed above, Cu-diacetyl-bis(N4-methylthiosemicarbazone) (Cu(II)-ATSM) exploits different mechanism to selectively target cells under hypoxic stress (Fujibayashi et al., 1997). The neutral lipophilic molecule Cu(II)-ATSM displays a high level of membrane permeability. Following application, random diffusion creates a uniform distribution of Cu(II)-ATSM because of its highly permeable nature. Under low oxygen tension, such as inside hypoxic cells, the copper atom of Cu(II)-ATSM is reduced because of cellular reducing equivalents, generating Cu(I)-ATSM^{-}. The negative charge carried by the reduced form of the molecule makes it membrane impermeable, and the molecule is selectively trapped inside hypoxic cells (Chao et al., 2001; Dehdashti, Grigsby, et al., 2003; Lewis, McCarthy, McCarthy, Fujibayashi, & Welch, 1999). Although animal studies indicated that ^{18}F-FMISO tumour uptake was more responsive than ^{64}Cu(II)-ATSM in imaging hypoxic tumours (Matsumoto et al., 2007), Cu(II)-ATSM has demonstrated both decreased target to background contrast ratio and elevated speed in clearance from background tissue in comparison to ^{18}F-FMISO (Takahashi et al., 2000; Zhang et al., 2007). The metal ion carried by this molecule, copper, provides a convenient option for further radiolabelling purposes. The molecule labelled by either ^{60}Cu or ^{64}Cu has been used in rapidly delineating tumour hypoxia with low background noise, which has been reported in several cancer clinical studies to predict patient response to therapy (Dehdashti, Grigsby, et al., 2003; Dehdashti, Mintun, et al., 2003; Padhani, 2005).

1.6 Current approaches to isolate hypoxic cell populations from tumour tissues

Profiling gene signature responses to hypoxia in cancer are started by separating cells suffering hypoxic stress from non-hypoxic tumour tissues. *In vitro*, cell lines can be stably transfected with hypoxia-inducible reporter expression vectors that are constructed with reporter gene(s), coding fluorescent proteins, under the regulation of a hypoxia-inducible promoter (He et al., 2008). According to oxygen stress in the microenvironment, those stably transfected cells express

reporter proteins at different levels. Fluorescence-activated cell sorting approaches can be used to isolate fractions based on hypoxia status.

In vivo hypoxia mediated cellular responses in tumours were initially investigated by using fluorescence-activated cell sorting techniques (Chaplin, Olive, & Durand, 1987; Olive, Luo, & Banáth, 2002; Young & Hill, 1990). Employment of DNA binding/diffusion properties of bisbenzamide fluorochrome Hoechst dye (H33342) via intravenous injection allowed tumour cells to be sorted on the basis of their Hoechst staining intensity/concentration gradient after tumour excision and preparation of tumour cell suspension using enzymatic disaggregation. Since the staining intensity of each cell represented its individual blood supply status inside the tumour, cell sorting according to the hypoxic stress could be achieved to a certain extent. The application of this technique is limited by the very short distribution half-life and highly variable cellular tolerance of Hoechst dyes. Meanwhile, Hoechst dyes also demonstrated both potent radioprotective properties and inhibiting activities in cell cycle progression (Young & Hill, 1989). These features further restricted its application value.

Since the development of EF5 and antibodies specific to its cellular adducts (Lord, Harwell, & Koch, 1993), cells in hypoxic regions can be labelled by EF5 and then analysed using fluorescence immunohistochemistry, which is followed by fluorescent activated cell sorting to separate enzymatically disaggregated cells into fractions corresponding to status of hypoxia (Lin & Hahn, 2012). Another nitroimidazole compound, ^{18}F-labeled fluoroazomycin arabinoside (^{18}F-FAZA) was used by Busk and co-workers as an indicator to evaluate the hypoxia status of tissue samples. This study demonstrated a strong correlation between *CA9*, *GLUT1* and lysyl oxidase (*LOX*) transcript abundance and hypoxia in human head and neck cancer xenograft model (FaDu; hypopharyngeal carcinoma). However, hypoxia-associated increased gene expression was only observed for *CA9* and *GLUT1* in murine squamous cell carcinoma (Busk et al., 2011).

Immunohistochemistry-guided laser capture microdissection (LCM) has been utilised to isolate pure populations of cells from solid tumours on the basis of distinct immunophenotypical criteria (Buckanovich et al., 2006). Prototypical hypoxia markers, such as EF5, combined with

corresponding fluorophore-labelled antibodies have been successfully employed to isolate total RNA from normoxic and hypoxic regions in the same rat 9L glioma tumour (Marotta et al., 2011).

Compared to tissue dissociation and cell immunopurification approaches, this technique is straightforward, less time-consuming, and less tissue is required. The sample fixation procedure involved in the immunohistochemistry part of this technique maintains the physical/structural features of cells extremely close to their physiologic settings in the native microenvironment. But the tumour has to be of sufficient size to allow large tissue areas to be collected by LCM.

By using different fluorophores, measurement of hypoxia markers can be combined with other predictive or prognostic factors. PET hypoxia imaging is usually limited by long diffusion distances, lack of an active uptake mechanism, and slow clearance of tracer without specific binding. Current preclinical development work in improving these aspects may help to circumvent these problems. But more efforts are still required to increase its resolution (Busk et al., 2008; Souvatzoglou et al., 2007; Yapp et al., 2007). Single-cell analysis is limited in detecting the therapeutically relevant hypoxic cells. Unlike the invasive methods that mix up intact and necrotic cells, single-cell analysis, however, is not able to identify the repopulation potential remaining in target cells (Olive & Aquino-Parsons, 2004). It furthermore requires either a large-scale biopsy or multiple examinations on a smaller scale to guarantee the representativeness of the sample to be investigated. In this case, calibration procedures are necessary to ensure the accurate measurement of oxygen level (Koch, 2002). The ideal method would be a non-invasive method. And it will be very useful if the method can be applied both before treatment to determine the presence of hypoxia and during therapy to assess tumour reoxygenation (Olive & Aquino-Parsons, 2004).

1.7 Click Chemistry

The modern biological sciences have made extraordinary progress in mechanistic understanding of living systems. The improvements in genetics, biochemistry, molecular/cellular biology and other related fields have accomplished impressive achievements in the structural and functional knowledge of biological molecules including DNA, RNA, and proteins. In the last decade, the human genome project (HGP) has provided entire genome sequencing information, which offered

especially remarkable insight into a myriad of biological processes and mechanisms in humans (Boyce & Bertozzi, 2011; International Human Genome Sequencing, 2004).

Whatever the object of biological study in such complicated living system is, scientists consistently attempt to deal with the same challenge, in this case, finding a way to single out a target biomolecule among all of the molecular diversity inherent to cells or organisms for analysis (Boyce & Bertozzi, 2011). The application of monoclonal antibodies opened a new era in biological research in the 20th century (Winter & Milstein, 1991). The unique nature of antibodies allows to selectively target a single type of molecule among multitudinous distractions and bind with high affinity.

As everything has its pros and cons in the world, antibodies have also demonstrated some inherent limitations when employed as tools to specifically target molecules inside cells. Antibodies do not pass through the membrane of living cells due to their large size. This limits their applications to the extracellular environment and also leads to poor tissue penetration in animals. Besides, antibodies have to be generated *de novo* for each individual new antigen, which makes the preparation work very labour intensive and expensive.

1.7.1 Bioorthogonal chemistry in biomedical sciences

In 1998, Tsien and co-workers reported that single target selectivity could be achieved via covalent reactions in live cells (Adams et al., 2002; Griffin, Adams, & Tsien, 1998). This ground-breaking research opened a new door to solve the scientific equivalent of finding a needle in a haystack. Instead of utilising the exquisite selectivity of antibody-antigen binding, a range of chemical reactions exploit the establishment of covalent association between reactants bearing complementary functional groups to achieve the aim of targeting selected biomolecules (Sletten & Bertozzi, 2011).

The term of bioorthogonal chemistry was first coined by Carolyn R. Bertozzi in 2003 (Hang, Yu, Kato, & Bertozzi, 2003). It refers to chemical reactions among abiotic reactants that are able to proceed inside of living systems without interfering with the native biological milieu (Prescher & Bertozzi, 2005; Prescher, Dube, & Bertozzi, 2004; Sletten & Bertozzi, 2009). According to the

concept of bioorthogonal chemistry, methods exploiting the mechanism of bioorthogonal reaction allow the real time study of biomolecules, such as proteins, glycans (Plass, Milles, Koehler, Schultz, & Lemke, 2011), and lipids (Neef & Schultz, 2009), in living systems without cellular toxicity (Boyce & Bertozzi, 2011).

To optimise performance, the bioorthogonal reactions designed for the purpose of biological research must have the following characteristics (Boyce & Bertozzi, 2011):

- The reactions have to proceed smoothly in water at physiological temperature, pH, and pressure;
- The reactions must give good yield and reasonable kinetics at low reagent concentrations;
- The reactions should be maximally inert to plentiful biological nucleophiles, electrophiles, as well as redox-active metabolites;
- The reactions must merely generate nontoxic or leave no side products.

A wide array of chemical ligation strategies have been developed so far in accordance with the requirements of bioorthogonality. The common strategy incorporates one reaction partner into the target biomolecules as the label, and then covalently binds that label to an exogenously applied probe. According to the experimental system and goals, the reaction is able to attach an affinity tag, imaging marker or other functional moiety with the target biomolecules (Boyce & Bertozzi, 2011).

1.7.2 Click chemistry

The concept of click chemistry was first introduced to public by Dr Karl Barry Sharpless at the 217th American Chemical Society annual meeting in 1999 (Hein, Liu, & Wang, 2008; Kolb, Finn, & Sharpless, 2001). It almost revolutionised molecular synthesis to be as simple as either building a LEGO® toy or assembling IKEA® furniture.

The definition of click chemistry was originally from a landmark review in 2001 (Kolb et al., 2001). The Nobel Prize laureate Dr Sharpless first fully described the reaction as “modular, wide in scope, giving very high yields, generating only inoffensive byproducts that can be removed by nonchromatographic methods, and be stereospecific (but not necessarily enantioselective). The

required process characteristics include simple reaction conditions, readily available starting materials and reagents, the use of no solvent or a solvent that is benign (such as water) or easily removed, and simple product isolation. Purification (if required) must be by nonchromatographic methods, such as crystallization or distillation, and the product must be stable under physiological conditions" (Evans, 2007; Kolb et al., 2001).

Numerous types of potent linking reactions meet the requirements of click chemistry. All of these reactions generally share some common properties to ensure maximum efficiency. Those features include rapid kinetics, high yield but deficiency of unwanted by-products, wide solvent compatibility, and readily accessible starting materials as implicated previously.

To date, click reactions have been divided into four major classifications based on the mechanism (Hein et al., 2008). Among these four major classifications, cycloadditions, especially the copper(I)-catalysed azide-alkyne Huisgen 1,3-dipolar cycloaddition, are most widely employed across a wide range of diverse research areas, such as biomedical science and material science (Hein et al., 2008). According to a multi-database search via SciFinder®, the number of click chemistry-related publications, which indicates the popularity of click chemistry applied in various fields of scientific research, increased exponentially (Figure 1.5).

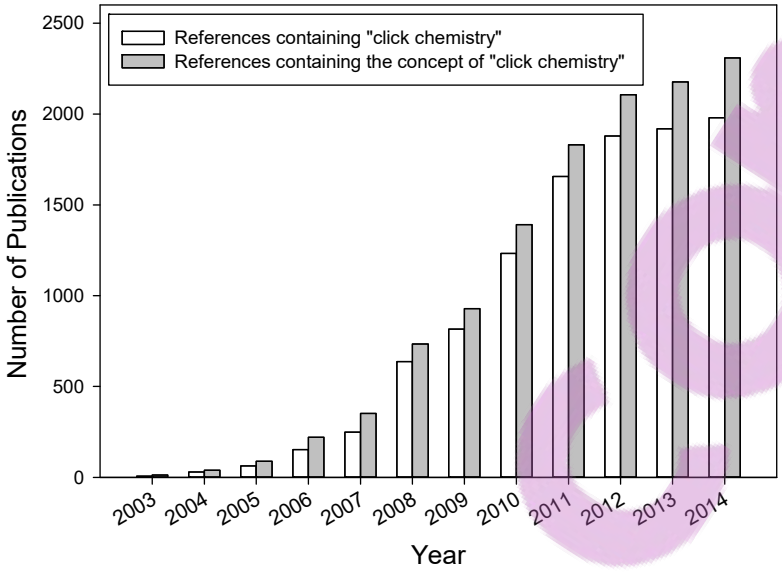

Figure 1.5: Number of publications in SciFinder® database.

A database search was performed by using the keywords “click chemistry” on August 20th, 2015. The search results covered articles published between 2003 and 2014. Types of publications included dissertations, journal articles, letters, patents, preprints, reports, as well as reviews. "References containing the concept" include all references when the entered term(s), synonymous term(s), or similar term(s) are found within the record.

1.7.3 Azide–alkyne Huisgen cycloaddition

The Huisgen 1,3-dipolar cycloaddition of alkynes to azides fulfils many of the prerequisites of click chemistry. The concept of azide-alkyne Huisgen cycloaddition was first introduced by Rolf Huisgen in the early 1960’s based on a type of reaction that generates a mixture of 1,4- and 1,5-disubstituted triazoles via cycloaddition between azide and acetylene, discovered by Dimroth at the beginning of the 20th century (Huisgen, 1961). Briefly, this type of reaction is a 1,3-dipolar cycloaddition between a terminal or internal alkyne (**1**) and an azide (**2**) to give a 1,2,3-triazole (**3**) as a mixture of 1,4-adduct and 1,5-adduct (Figure 1.6).

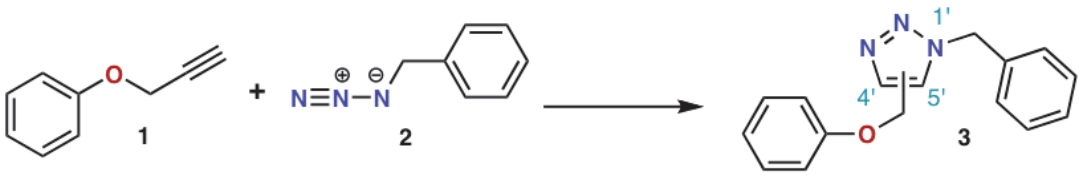

Figure 1.6: Azide-alkyne Huisgen cycloaddition.

Re-drawn and modified from: Wikipedia (2015).

The Huisgen 1,3-dipolar cycloaddition illustrates the characteristic of reliably covalently linking readily accessible building blocks in the presence of other functional groups across a wide spectrum of conditions. Due to this unparalleled feature, the azide-alkyne Huisgen cycloaddition is one of the most useful tools for assembling novel molecular architectures with specific functional properties (Hein & Fokin, 2010) and possesses massive potential of applications in diverse areas ranging from functional materials (Casas-Solvas et al., 2009; Juricek, Kouwer, & Rowan, 2011; Lutz, 2007) to biological chemistry (Ackermann & Potukuchi, 2010; Amblard, Cho, & Schinazi, 2009; Best, Rowland, & Bostic, 2011; Bock, Hiemstra, & van Maarseveen, 2006; Diez-Gonzalez, 2011; Fekner, Li, Lee, & Chan, 2009; Hein & Fokin, 2010; McNulty, Keskar, & Vemula, 2011; Meldal & Tornoe, 2008; Sletten & Bertozzi, 2011; Wang, Winblade Nairn, Johnson, Tirrell, & Grabstein, 2008). These wide ranging applications have let cycloaddition be referred as "the cream of the crop" of click chemistry (Kolb et al., 2001).

1,3-dipolar cycloaddition between azide and alkyne also possesses an inherent defect, namely the low reaction rate (Evans, 2007; Lwowski, 1984). As a result, this type of reaction generally requires certain thermal conditions to overcome the activation threshold of deforming the alkyne's bond angle to form the triazole (Jewett & Bertozzi, 2010). Although both the azides and alkynes are kinetically stable, this weakness will still limit its application potential especially in the click context until the discovery of reliable and efficient specific metal ions.

1.7.4 Copper(I)-catalysed azide–alkyne cycloaddition

The copper(I)-catalysed variant of the Huisgen 1,3-dipolar cycloaddition was first reported in independent publications by Morten Meldal at the Carlsberg Laboratory in Denmark (Tornøe, Christensen, & Meldal, 2002) as well as American chemists, Valery Fokin and Karl Barry Sharpless, at the Scripps Research Institute (Rostovtsev, Green, Fokin, & Sharpless, 2002) in 2002.

Copper(I) catalysis significantly decreases the activation barrier of the cycloaddition with terminal alkynes, which allows the reaction to proceed with high rate at room temperature (RT). The recruitment of this catalytic system also simplifies the reaction product as 1,4-disubstituted 1,2,3-triazoles exclusively (Rodionov, Fokin, & Finn, 2005).

1.7.4.1 Copper(I) species

Copper(I) species undergo metal insertion to react and associate with terminal alkynes. With the assistance from copper(I), the pKa of the alkyne C-H can be reduced by up to 9.8 units during the step to generate acetylide (Evans, 2007).

The copper(I) species may be directly introduced into the reaction system as preformed commercial cuprous complexes, such as cuprous bromide or iodide. In this case, reactions have to be performed in a deoxygenated environment. Either organic or mixed solvent is also required to maintain the oxidative state of copper, which probably necessitates some protection groups along with a base (Orgueira, Fokas, Isome, Chan, & Baldino, 2005).

Another way to create the copper(I) catalyst is to oxidise copper metal *in situ* with an amine salt (Himo et al., 2004; Orgueira et al., 2005). Unfortunately, this approach usually requests longer reaction times, larger amounts of copper, and a relatively acidic environment to dissolve the metal. These particular requirements consequently limit any applications of the reactants with acid-sensitive functional groups (Bock et al., 2006).

In general, the reaction performs much better and reliably by utilising copper(I) species (Hein & Fokin, 2010; Rostovtsev et al., 2002). There are several improved ways to achieve such a goal by

linking a copper(I) generating reaction to the cycloaddition reaction and guaranteeing they work simultaneously in the same system.

The most popular way is to bring a mixture of copper(II) salt and reducing agent into the cycloaddition reaction system. Sodium ascorbate is the most widely used candidate to convert copper(II) into copper(I) by a reduction in a 3- to 10-fold concentration excess (Bock et al., 2006). Other reducing agents, such as hydrazine (Golas, Tsarevsky, Sumerlin, & Matyjaszewski, 2006) and tris(2-carboxyethyl)phosphine (TCEP) (Zhan, Barnhill, Sivakumar, Tian, & Wang, 2005), have demonstrated promising performances as well. Due to the presence of reducing agent, copper(II) ions are reduced to the +1 oxidation state *in situ*. Copper(II) sulphate ($CuSO_4$) is the common copper source to provide catalyst by reacting with the reducing agent.

By generating copper(I) species *in situ*, an amine base is no longer essential in the reaction system. In addition, the existence of reducing agent may consume any oxygen present in the system to maximally maintain copper in the desired +1 oxidation state (Meldal & Tornoe, 2008). As a backup plan, halides of copper are applied as the source of copper(II) to replace $CuSO_4$ when solubility becomes a concern. Certain harsh conditions, including the presence of amines or higher temperatures, are specifically required in cycloadditions with copper(II) iodide salt or copper(II) bromide salt involved (Meldal & Tornoe, 2008).

Controlling the oxidation state of copper is the key to achieve the best cycloaddition by maintaining the availability of copper(I) catalyst. The chief drawback is that copper(I) might be further reduced down to copper(0) (Hein et al., 2008). A proper ratio of reducing agent to catalyst and/or employment of a copper-stabilising agent therefore is critical to the reaction (Bock et al., 2006).

1.7.4.2 The limitations of CuAAC for the functionalization of biomacromolecules

The copper(I)-catalysed azide–alkyne cycloaddition (CuAAC) has been recognized as the greatest exponent among the entire collection of click reactions currently available (Kolb et al., 2001; Rostovtsev et al., 2002). CuAAC is a powerful coupling technology for conjugation of proteins, nucleic acids, and polysaccharides (Lallana, Riguera, & Fernandez-Megia, 2011).

However, the copper(I) catalyst induces severe structural damage to biomolecules, while the rate of CuAAC reaction is often the concern at low micromolar concentrations typically required for bioconjugation purposes (Lallana et al., 2011). The cytotoxicity of metals including copper by inducing oxidative stress has been well recognised (Brewer, 2010). Copper ions are directly involved in the generation of reactive oxygen species (ROS). ROS has been demonstrated to induce degradation of amino acids and cleavage of the polypeptide chain (Stadtman, 2006; Stadtman & Berlett, 1998). Both damaging processes in proteins have been identified under CuAAC conditions (Kumar, Li, & Cai, 2011). Copper(I) from CuAAC is also involved in the production of the hydroxyl radical (•OH) and ultimately contributes to biological damage, including RNA degradation and DNA damage (Biaglow, Manevich, Uckun, & Held, 1997; Tabbi, Fry, & Bonomo, 2001; Temple, Perrone, & Dawes, 2005).

Only a very few cases of applications in living cells or organisms have been reported (McKay & Finn, 2014). In an attempt to extend the application of bioorthogonal click chemistry to living organisms, researchers have been focusing on developing rapid reactions proceeding with extremely fast kinetics and without compromising the function and metabolic processing of biomolecules (Kennedy et al., 2011). The application of CuAAC reactions in complex living systems requires copper catalysts effective for *in vivo* labelling strategies, otherwise prolonged catalyst exposures and noninterfering with the surrounding cellular milieu cannot be avoided (Kennedy et al., 2011). Meanwhile, the membrane permeability and the sequestration of copper(I) ions by the thiol-containing compound glutathione in the cytosol are also crucial in performing CuAAC reactions inside living cells (Uttamapinant, Sanchez, Liu, Yao, & Ting, 2013).

1.7.4.3 Copper(I)-chelating ligands

Oxidative degradation by reactive oxygen species and sample contamination by copper are major limitations of CuAAC. The presence of copper ions is responsible for both of them. One strict requirement of this catalytic system is the presence of copper(I)-chelating ligands in the reaction on account of the catalyst's unstable oxidation state in aqueous solutions (Lallana et al., 2011). Apart from the stabilization effect, utilisation of ligands significantly improves the reaction outcome by accelerating the cycloaddition reaction, preventing the formation of unwanted by-products, as well as sequestering copper ions to avoid biomolecule damage and simplify removal (Besanceney-

Webler et al., 2011; Timothy R Chan & Fokin, 2007; Hein, Krasnova, Iwasaki, & Fokin, 2011; Rodionov, Presolski, Diaz, Fokin, & Finn, 2007; del Amo et al., 2010).

Different types of ligands have been used, including tris(benzyltriazolylmethyl)amine (TBTA), tris(hydroxypropyltriazolylmethyl)amine (THPTA), and bathophenanthroline disulfonate disodium salt (BPDS) (Chan, Hilgraf, Sharpless, & Fokin, 2004; Hein et al., 2011; Lewis, Magallon, Fokin, & Finn, 2004).

The tetradentate binding ability of the tris(triazolylmethyl)amine ligand family, including TBTA and THPTA, leads to the formation of stable copper(I) chelates. A 5-fold molar excess of tris(triazolylmethyl)amine ligand relative to copper(I) has been recommended in order to minimise oxidative degradation (Hong, Presolski, Ma, & Finn, 2009; Lallana et al., 2011; Wang et al., 2003).

As the first member of this ligand family to be identified (Hein et al., 2011), TBTA is the most commonly used for bioorthogonal conjugation (Chan et al., 2004). The presence of TBTA in the reaction system efficiently overcomes limitations and allows the reaction to take place in a variety of solvents, even mixtures of water and a number of miscible organic solvents, including alcohols, dimethyl sulfoxide (DMSO), and acetone (Chassaing, Kumarraja, Sani Souna Sido, Pale, & Sommer, 2007; Meldal & Tornoe, 2008; del Amo et al., 2010). Fortunately, the starting reagents need not be completely soluble for the reaction to be successful. In many cases, the product can simply be filtered from the solution as the only purification step required.

The application of this technique was initially hampered by the deleterious effects associated with copper ions. Copper-mediated *in situ* generation of ROS induced strand breakage of nucleic acids by both metal-assisted and free radical mechanisms (Burrows & Muller, 1998). Nucleic acids represent a highly demanding platform for bioconjugation by means of CuAAC (El-Sagheer & Brown, 2010b; Gramlich, Wirges, Manetto, & Carell, 2008). Without ligand, roughly 50% CuAAC induced degradation in nucleic acids was observed by Liu and co-workers after only 10 min at room temperature (Kanan, Rozenman, Sakurai, Snyder, & Liu, 2004). Introducing TBTA into the reaction system paved the way for CuAAC as a reliable tool for nucleic acid modification. TBTA was reported to significantly accelerate the CuAAC process and potently stabilise the copper(I) oxidation state to enhance the catalytic activity in aqueous solutions (Chan et al., 2004; Hein &

Fokin, 2010). In the presence of TBTA, the successful modification of oligodeoxyribonucleotides (ODN) and long DNA chains by means of CuAAC has been reported by the groups of Rajski (Weller & Rajski, 2005) and Carell (Gierlich, Burley, Gramlich, Hammond, & Carell, 2006). Based on this pioneering work, the further success in CuAAC coupling of ODN to self-assembled monolayers was accomplished (Devaraj et al., 2005). CuAAC functionalization of the resulting alkyne-modified DNA with saccharides proceeded in excellent yields in the presence of TBTA, with no sign of DNA degradation (Gierlich et al., 2007; Wirges et al., 2007).

The lack of solubility in water is a great limitation of TBTA. A small volume (ca. 10%) of organic solvent is always required to solubilise TBTA. To overcome this, water-soluble tris(triazolylmethyl)amine ligands, such as THPTA, were developed (Wang et al., 2003). In addition to the improvement in solubility, THPTA was also found to prevent ROS-mediated protein degradation by acting as a radical scavenger and strongly accelerating the decomposition of H_2O_2 formed in the course of the reaction (Hong et al., 2009). The group led by Brown has proposed the use of THPTA as an alternative to TBTA for the functionalization of nucleic acids (El-Sagheer & Brown, 2008; El-Sagheer & Brown, 2010b; El-Sagheer et al., 2008; Kocalka, El-Sagheer, & Brown, 2008; Kumar et al., 2007).

1.7.4.4 Mechanism of copper(I)-catalysed azide-alkyne cycloaddition

As the premier example of click chemistry, CuAAC is the most well-studied and a wildly utilised straight-forward click chemistry approach (Hein & Fokin, 2010). Based on the mechanism of CuAAC described in Figure 1.7, it is obvious that the efficacious candidates of ligand should be able to maintain the balance between sturdy association with copper(I) to preclude the formation of unreactive polymeric complexes and sufficient approach to allow azide to access to the coordination sphere of acetylide copper(I) centre (Hein et al., 2008; Hein & Fokin, 2010).

With the correct selection of the catalytic system, CuAAC is a safe and efficient tool for the bioconjugation of proteins and bionanoparticles (Lallana et al., 2011). By copper(I) catalysis, applications of azide-alkyne cycloaddition has extended far beyond organic synthesis to further challenging goals in chemistry, polymer science, and biology (Bock et al., 2006; Iha et al., 2009;

Lutz, 2007; Meldal, 2008; Meldal & Tornoe, 2008; van Dijk, Rijkers, Liskamp, van Nostrum, & Hennink, 2009).

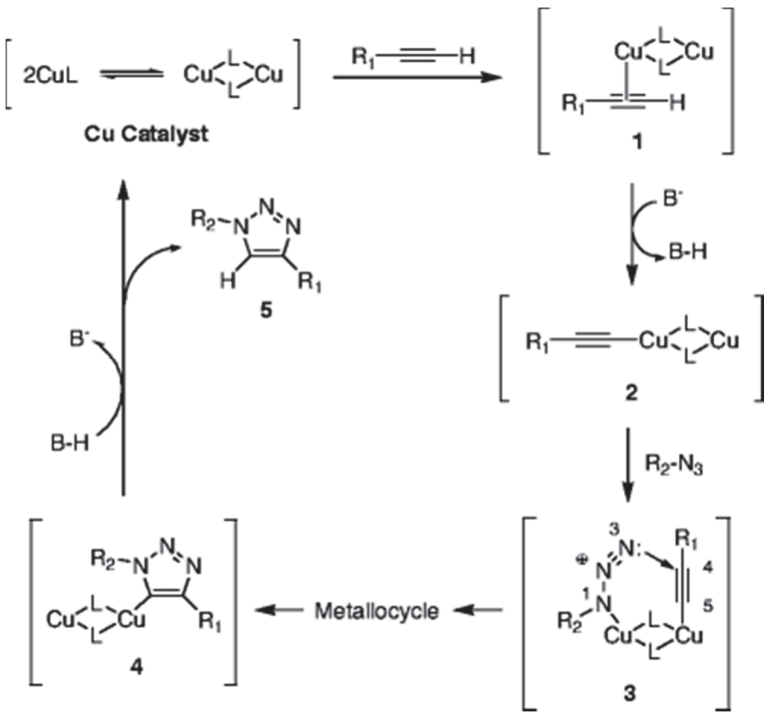

Figure 1.7: Generally accepted mechanism of CuAAC.

The CuAAC initiates with the formation of the structure (**1**) by linking the copper(I) dimer-ligand complex (functional as a catalyst) with terminal alkyne via π complexation. This step is followed by deprotonation of the terminal hydrogen of alkyne to generate an intermediate structure, copper(I)-acetylide (**2**). Both structure (**2**) and organic azide are essential to the fundamental reactivity of CuAAC. Addition to the thermal and photochemical decomposition, the reactivity of organic azide generally depends on the reactions with nucleophiles at its terminal N3 atom. The N(1) of azide, thereafter, displaces one of the ligands from the second copper in the copper(I)-acetylide (**2**). Owing to proximity and electronic factors, N(3) of azide, in turn, associates with C(4) of the copper(I)-acetylide (**2**) via the stage of intriguing six-membered metallocycle (**3**). The formation of this structure (**3**) from the copper(I)-acetylide (**2**) and the azide has been postulated to serve as the rate-determining step during the whole CuAAC procedure. Within structure (**3**), the lone pair of electrons from N(1) then attack C(5) to induce contraction of the metallocycle and form a metalated triazole (**4**) in a preference for the stepwise addition, respected the calculations based on density functional theory. In the last step, the metalated triazole is protonated to yield only the 1,4-isomer of 1,2,3-triazole as the final product (**5**), meanwhile regenerating the catalyst. Redrawn and modified from: Hein *et al.* (2008)**.**

1.7.4.5 Applications of copper-catalysed click chemistry in biological sciences

In the context of tumour hypoxia, the green fluorescent protein (GFP) and tetra-cysteine motifs have been utilised as genetically encoded reporters or to tag selected proteins (Le et al., 2014; Martin, Giepmans, Adams, & Tsien, 2005; Melillo, 2013; Mihich & Kaelin, 2004; Vordermark, Shibata, & Brown, 2001). Unfortunately, such genetic incorporation-mediated techniques are not amenable to label molecules if they are not encoded directly in the genome, such as glycans, lipids, metabolites, and myriad posttranslational modifications (Coralli, Cemazar, Kanthou, Tozer, & Dachs, 2001).

By taking advantage of the major progress made in immunology, antibodies generally demonstrate high specificity to selected targets with a relatively broad range of applications that are not limited to protein molecules (Arlen et al., 2014; Pandey & Mahadevan, 2014). However, the labour-intensive preparation and purification of antibodies and their restricted permeability and transport in intact cells have somewhat limited their application in effective targeting molecules especially those that are located intracellularly (Barbet et al., 2012; Goebl, Berridge, Wroblewski, & Brown-Augsburger, 2007; Tabrizi, Bornstein, & Suria, 2010).

In general, labelling specific biomolecules by the utilisation of click reactions is achieved by a two-step protocol. It firstly requires that one reactant is stable enough to be somehow incorporated into the target biomolecule, which is followed by exposure to another reactant modified to carry a specific probe, such as functional motif or reporter molecule. The subsequent reaction links the two bioorthogonal partners together, tagging the target biomolecule with the probe (Jewett & Bertozzi, 2010). However, the dipolar cycloaddition of organic azides with alkynes fulfils the click criteria but with an inherently low reaction rate.

The application of this latter reaction did not show much potential until the discovery of the catalysis by copper(I) (Rostovtsev et al., 2002; Tornøe et al., 2002). Copper catalysis severely alters both the mechanism and the outcome of the reaction. In contrast to the uncatalysed reaction, which demands much higher temperatures and produces mixtures of triazole regioisomers, the copper-catalysed version transforms organic azides and terminal alkynes exclusively into the corresponding 1,4-disubstituted 1,2,3-trizoles (Rostovtsev et al., 2002; Tornøe et al., 2002). Being

the most prominent member of click chemistry with a stable triazole product, the significantly increased number of applications of copper(I)-catalysed azide-alkyne cycloaddition (CuAAC) has been well-documented and this is continually enriched by scholars in numerous fields (Berg & Straub, 2013; Besanceney-Webler et al., 2011; Bevilacqua et al., 2014; Boyce & Bertozzi, 2011; Kennedy et al., 2011; Presolski et al., 2011; Schilling, Jung, & Bräse, 2010).

Employment of the simple copper(I) catalytic system has brought remarkable improvements in the Huisgen 1,3-dipolar azide-alkyne cycloaddition. The rapid reaction kinetics, high degree of reliability, and bioorthogonality offer CuAAC great advantages which have been applied extensively in both the selective labelling of biological molecules (Wu & Fokin, 2007) and the establishment of small molecule libraries for drug discovery purposes (Kolb & Sharpless, 2003; Moses & Moorhouse, 2007).

Techniques for the purpose of bioconjugation are usually built up on the covalent association between synthetic probes and biomolecular frameworks. The latter includes the modification of proteins and nucleic acids by attaching labels for specific detecting methods; or synthesis of simple peptides or carbohydrate-modified peptide complexes by using simple proteins and carbohydrates as building “bricks” (Moses & Moorhouse, 2007).

Molecules carrying bioorthogonal functional groups with the abilities to metabolically associate with nucleic acids have been synthesized for imaging cells undergoing replication or other cellular processes related to the alternations of genetic materials (Gramlich et al., 2008; Salic & Mitchison, 2008). 5-ethynyl-2’-deoxyuridine (EdU) was used to metabolically incorporate into DNA during the genome replication stage, which could be subsequently detected by an azido fluorophore through CuAAC. Compared to the traditional immunology based 5-bromo-2’-deoxyurdine (BrdU) labelling (Gratzner, 1982), EdU and its CuAAC counterpart, the fluorophore conjugated azide, provided the reaction with fast rate and good sensitivity.

The targeting techniques based on click chemistry enable visualisation and tracking of complex biopolymers (Speers, Adam, & Cravatt, 2003; Speers & Cravatt, 2004). To date, such applications have been mostly limited to *in vitro* studies or *in vivo* after sacrifice and lysation of the animal. The

biological toxicity induced by metal ions from catalytic system became the biggest concern in the application of this technique.

To ameliorate this drawback of CuAAC, two different approaches were developed. One is to eliminate the requirement of copper(I)-catalyst, for example, utilization of ring stain catalysis (Jewett & Bertozzi, 2010; Kuzmin, Poloukhtine, Wolfert, & Popik, 2010; Mbua, Guo, Wolfert, Steet, & Boons, 2011). Another is to enhance cell compatibility by using ligands with higher water solubility, such as THPTA (Hong et al., 2009), bis[(*tert*-butyltriazoyl)methyl]-[(2-carboxymethyltriazoyl)methyl]-amine (BTTAA) (Besanceney-Webler et al., 2011), or bis(L-histidine) (Kennedy et al., 2011).

Recently, Ting and co-workers reported the third tactic to achieve the same goal (Uttamapinant et al., 2012), in which an azide reaction partner carrying an internal copper-chelating moiety was introduced into CuAAC. Due to the existence of this functional structure, the effective copper concentration was able to be elevated particularly around the reaction site but with a reduced overall concentration which, in turn, diminished toxicity and increased biocompatibility.

In the field of drug discovery, CuAAC has provided a novel approach to the development of high throughput methodology for screening compound libraries to discover and select molecules with pharmaceutical values (Lee et al., 2003). Meanwhile, it has also enabled the rapid and efficient synthesis of molecules for pharmaceutical purposes (Sharpless & Manetsch, 2006). Because CuAAC dynamically prefers thermal scenarios; does not involve any side reactions or third party participants; and is inert in the presence of biomolecules or physiological conditions. Beside functioning as a linkage, the 1,4-triazole products generated from CuAAC have also been reported as a crucial section of candidate pharmacophores, indicating further possible applications of the triazole functionality (Moorhouse et al., 2006).

1.7.5 Strain-promoted azide–alkyne cycloaddition

The most effective way to improve the biocompatibility of azide-alkyne cycloaddition is to eliminate the requirement for copper(I)-catalysis. Considerable effort has been devoted by scholars towards the development of copper-free variants of CuAAC as biocompatible alternatives.

Instead of copper ion, the cycloaddition is accelerated with a cyclooctyne that is activated by ring strain (Agard, Baskin, Prescher, Lo, & Bertozzi, 2006; Agard, Prescher, & Bertozzi, 2004). This strain-promoted azide-alkyne cycloaddition (SPAAC) was first coined by Bertozzi *et al*. (Agard et al., 2004). Considering the possible reaction between the strained alkyne and thiols, this copper-free version of the click reaction is not truly bioorthogonal (van Geel, Pruijn, van Delft, & Boelens, 2012). But the exclusion of the cytotoxic copper catalyst allows a copper-free click reaction to be performed in living cells without noticeable toxicity. Although the kinetics of SPAAC are sluggish (usually 10 to 100 times slower than CuAAC) (Jewett & Bertozzi, 2010; Jewett, Sletten, & Bertozzi, 2010), it has been applied effectively in a broad range of *in vivo* contexts including cultured cells, live zebrafish, and mice (Agard et al., 2004; Baskin et al., 2007; Laughlin, Baskin, Amacher, & Bertozzi, 2008).

1.7.6 Prospects of applied click chemistry

The applications of conventional tagging technologies are limited in glycans, lipids, and some metabolites (Agard et al., 2006). The bioorthogonal chemistry based probing strategy, in a complementary manner, provides powerful methods for those molecules without the requirement of direct genetic encoding (Prescher & Bertozzi, 2005).

Small in size and stable in physiological sittings make azide the most capable candidate for a bioorthogonal chemical reporter (Agard et al., 2006). To tag azide-labelled biomolecules, three types of reactions have been used so far by the bioorthogonal chemistry based methodology (Figure 1.8).

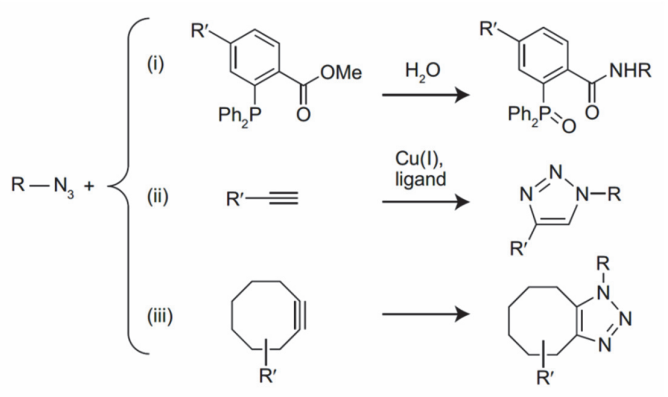

Figure 1.8: Bioorthogonal reactions with azide.

Biomolecules containing azide react via Staudinger ligation (i), click chemistry (ii), or a strain-promoted cycloaddition (iii) to give ligated products. Redrawn and modified from: Agard *et al.* (2006).

Among these reaction types, the balance point between sensitivity and biocompatibility needs to be considered according to the particular requirements during the experimental designing stage. Generally, click chemistry has been demonstrated to be ideal for high sensitivity protein labelling due to superior kinetics. When viability is the concern, only the Staudinger ligation or stain-promoted cycloaddition can be employed because of their superior biocompatibility. In the latter situation, the final decision will be dictated by the nature of the azide employed (Agard et al., 2006).

High sensitivity and biocompatibility are two top priorities essential in the development of bioorthogonal chemistry based target tagging technology. At the current stage, these two essential attributes are still in conflict with each other in the repertoire of candidate reactions. Development of tight binding copper ligands to mitigate copper(I)-induced cytotoxicity and further substitutions on the cyclooctyne scaffold to enhance reacting rate are possibly reasonable options to further optimise cycloaddition reagents (Agard et al., 2006; Baskin et al., 2007; Boyce & Bertozzi, 2011; DeForest, Polizzotti, & Anseth, 2009).

1.8 Aims and objectives

Hypoxia is a pathological condition in which the body or a region of the body is deprived of adequate oxygen supply (Prabhakar, 2013). In the context of cancer, hypoxic conditions are in part responsible for resistance of tumour cells to ionising radiation and many forms of chemotherapy. These cells usually lead to more aggressive tumours with increased metastatic potential (Dhani, Fyles, Hedley, & Milosevic, 2015; Wilson, Hicks, Wang, & Pruijn, 2014). Cellular responses to hypoxic stress have been successfully investigated in low cell density cultures. However, information is still limited both on responses to hypoxia in the tumour microenvironment and on molecular targets in these cells primarily due to lack of suitable research tools.

Drs Pruijn and Tercel have recently developed a new click chemistry-based strategy for detecting, imaging, and isolating hypoxic cells from tumours by use of a 'clickable' 2-nitromidazole (2-NI) hypoxia markers (SN33267) bearing a side chain containing a terminal alkyne group which can be derivatised via CuAAC with azides.

This thesis mainly focused on establishing and optimising a novel methodology on the basis of an approach with preincubation/preinjection and detection of a metabolically-bound exogenous clickable hypoxia tracer, SN33267. The ultimate goal was the application of the optimised methodology to specifically label tumour cells in a hypoxia-dependent manner *in vivo* and sort these cells according to their cellular hypoxia status *in situ* to investigate genes that are differentially regulated between the oxic and hypoxic compartments of the tumour microenvironment.

On the basis of their previous work, the first part of this thesis aims to continue establishing and optimising a fast and sensitive method for fluorescence-based detection and flow cytometric sorting of hypoxic cells from tumours for subsequent study of gene and protein expression in the sorted fractions. The second part of this thesis aims to evaluate the hypoxia-mediated expression of 10 oxidoreductases involved in the activation of hypoxia-activated anticancer prodrugs (HAPs) in the tumour microenvironment by use of this CuAAC-based approach after it has been optimised and validated by correlating with transcript abundance of 15 clinically-validated hypoxia marker genes (Toustrup et al., 2011).

Once fully established, optimised, as well as validated independently using a hypoxia gene signature, this novel CuAAC-based method will be much faster and more versatile than the established antibody-based hypoxic cell detection techniques and provides at least the same sensitivity. It will provide a powerful and user-friendly tool for pre-clinical study of the hypoxia-mediated effects in the tumour microenvironment by gene and/or corresponding protein expression in tumours *in situ*.

The specific objectives of the thesis are as follows:

- To characterise candidate fluorophores and select the best fluorophore(s) in conjunction with SN33267 for hypoxia-specific cell labelling by testing the performance of each candidate fluorophore in labelling SiHa cells via CuAAC using an initial non-optimised protocol;
- To identify the optimal conditions and/or settings of each component involved in the CuAAC reaction in attempts to improve hypoxia-selectivity of cell labelling;
- To maximise the compatibility of the click chemistry-based method with high-quality RNA and validate the optimised methodology in human cancer cell lines under different hypoxic stress;
- To validate the optimised click chemistry-based methodology *in vitro* and *ex vivo* by assessment of the expression of 15 clinically validated hypoxia marker genes (Toustrup et al., 2011);
- To evaluate the *in vitro* and *ex vivo* expression of prodrug-activating reductase genes in response to hypoxic stress by applying the optimised methodology for fluorescence-based detection and flow cytometric sorting of cells in a hypoxia-selective manner.

Chapter 2. Materials and methods

2.1 General materials and compounds

Milli-Q water (18.2 MΩ·cm), used to prepare solutions, was purified by filtering through ion exchange columns and a 0.22 µm filter (Milli-Q® purification system, Millipore Corporation, MA, USA) unless stated otherwise.

To achieve a high degree of accuracy, chemical compounds were weighed using a Sartorius Type 1712 analytical balance (Sartorius GmbH, Göttingen, Germany).

Reagents, chemicals, materials, and consumables were purchased as listed in Table 2.1, Table 2.2, as well as Table 2.3 unless stated otherwise.

Table 2.1: Laboratory consumables.

Laboratory Consumable	Manufacturer or Supplier
1 mL Luer Slip Tuberculin Syringe	BD Biosciences, Singapore
96-Well Plates	Greiner Bio-One Ltd, Frickenhausen, Germany
ABI Prism™ 384-Well Clear Optical Reaction Plate, with Barcode	Applied Biosystems, CA, USA
Axygen® 0.2 mL Polypropylene Thin Wall PCR Tubes, with Flat Cap	Corning Life Sciences, MA, USA
Axygen® 1.7 mL MaxyClear Snaplock Microcentrifuge Tube	Corning Life Sciences, MA, USA
BD Falcon® Tissue Culture Flask, with Vented Cap	BD Biosciences, MA, USA
BD Falcon® 5 mL Polystyrene Round-Bottom Tube	BD Biosciences, MA, USA
BD Falcon® 5 mL Polystyrene Round-Bottom Tube, with Cell-Strainer Cap	BD Biosciences, MA, USA
BD Falcon® 14 mL Polystyrene Round-Bottom Tube	BD Biosciences, MA, USA
BD Falcon® 15 mL High-Clarity Polypropylene Conical Tube	BD Biosciences, MA, USA
BD Falcon® 50 mL Polypropylene Conical Tube	BD Biosciences, MA, USA
BD Integra™ Blunt Filter Needle	BD Biosciences, Singapore
Cryovials	Nunc, Roskilde, Denmark
LCMS Vials	Agilent Technologies, CA, USA
MAXYMUM RECOVERY™ Pre-Sterilized Filter Tips	Corning Life Sciences, MA, USA
MicroAmp™ Optical Adhesive Film	Applied Biosystems, CA, USA
Micro-Cuvettes (Absorbance)	Bio-Rad Laboratories, CA, USA
Micro-Cuvettes (Fluorescence)	Hewlett-Packard, CA, USA
Micro-Touch® DermaClean® Powder-Free Latex Examination Gloves	Ansell Limited, VIC, Australia
Micro-Touch® NitraFree™ Pink Nitrile Examination Gloves	Ansell Limited, VIC, Australia
Nitrocellulose Membrane	Bio-Rad Laboratories, CA, USA
Supreno® Powder-Free Nitrile Exam Gloves	Microflex Corporation, NV, USA

Table 2.2: Materials, reagents, and chemical compounds.

Materials, Reagent, and Chemical Compound	Manufacturer or Supplier
1 kb Plus DNA Ladder	Invitrogen, Life Technologies, CA, USA
Agilent RNA 6000 Nano Kit	Agilent Technologies, CA, USA
Alpha Minimal Essential Media	Gibco, Life Technologies, CA, USA
Bicinchoninic Acid	Sigma-Aldrich, MO, USA
Bovine Serum Albumin	Thermo Fisher Scientific, MA, USA
Chloroform	Merck KGaA, Darmstadt, Germany
Collagenase	Sigma-Aldrich, MO, USA
Copper(I) Acetate, 97% (CuOAc)	Sigma-Aldrich, MO, USA
Copper(II) Sulphate ($CuSO_4$)	Sigma-Aldrich, MO, USA
DNase I	Sigma-Aldrich, MO, USA
Dimethyl Sulphoxide (DMSO)	Merck KGaA, Darmstadt, Germany
Disodium Hydrogen Phosphate (Na_2HPO_4)	Sigma-Aldrich, MO, USA
Ethylenediaminetetraacetic Acid (EDTA)	AppliChem GmbH, Darmstadt, Germany
Foetal Calf Serum	Moregate Biotech, New Zealand
High Capacity RNA-to-cDNA Kit	Applied Biosystems, CA, USA
Hydrogen Chloride (HCl)	Reidel-de Haën, Seelze, Germany
4-(2-hydroxyethyl)-1-piperazineethanesulfonic acid (HEPES)	Sigma-Aldrich, MO, US
Kaleidoscope™ Precision Plus Protein™ Standard	Bio-Rad Laboratories, CA, USA
2-Mercaptoethanol	Gibco, Life Technologies, CA, USA
Methanol	Merck KGaA, Darmstadt, Germany
Molecular Probes™ Tetramethylrhodamine (TAMRA) Azide (Tetramethylrhodamine 5-Carboxamido-(6-Azidohexanyl)), 5-isomer	Molecular Probes Inc., OR, USA
Non-Fat Milk Powder	Pams Products Ltd, New Zealand
NuPAGE® LDS Sample Buffer (4X)	Invitrogen, Life Technologies, CA, USA
NuPAGE® MES SDS Running Buffer	Invitrogen, Life Technologies, CA, USA
NuPAGE® Novex® 4-12% Bis-Tris Pre-Cast Polyacrylamide Gel	Invitrogen, Life Technologies, CA, USA
Penicillin	Sigma-Aldrich, MO, USA
Pronase	Sigma-Aldrich, MO, USA
2-Propanol	BDH Laboratory Supplies, England, UK
Protease Inhibitor Cocktail	Sigma-Aldrich, MO, USA
PureLink® DNase Set	Ambion™, Life Technologies, CA, USA
PureLink® RNA Mini Kit	Ambion, Life Technologies, CA, USA
Qiaquick® PCR purification kit	Qiagen GmbH, Hilden, Germany

RNase AWAY® Decontamination Reagent	Ambion™, Life Technologies, CA, USA
RNaseZap® RNase Decontamination Solution	Life Technologies, CA, USA
Sodium Bicarbonate ($NaHCO_3$)	Merck KGaA, Darmstadt, Germany
Sodium Chloride (NaCl)	Merck Millipore, MA, USA
Sodium Hydroxide (NaOH)	Ajax Chemicals, NSW, Australia
(+)-Sodium L-ascorbate	Sigma-Aldrich, MO, USA
Streptomycin	Sigma-Aldrich, MO, USA
SuperSignal® West Pico Chemiluminescent Substrate	Pierce Rockford, Thermo Fisher Scientific, IL, USA
TaqMan® Custom Array	Applied Biosystems, CA, USA
TaqMan® Gene Expression Master Mix	Applied Biosystems, CA, USA
Tetramethylrhodamine (TAMRA) Azide (Tetramethylrhodamine 5-Carboxamido-(6-Azidohexanyl)), 5-isomer	Molecular Probes, Life Technologies, OR, USA
TRIzol® LS Reagent	Ambion, Life Technologies, CA, USA
Trypsin EDTA (0.5%)	Gibco, Life Technologies, CA, USA
Tween 20	Sigma-Aldrich, MO, USA
UltraPure™ DEPC-Treated Water	Invitrogen, Life Technologies, CA, USA

Table 2.3: Equipment and software.

Equipment and Software	Manufacturer or Supplier
ABI 7900HT Sequence Detection Systems (SDS; Version 2.4.1)	Applied Biosystems, CA, USA
ABI Prism® 7900HT Fast Real-Time PCR System	Applied Biosystems, CA, USA
AccuBlock™ Digital Dry Bath	Labnet International, NJ, USA
Agilent 2100 Bioanalyzer	Agilent Technologies, CA, USA
Agilent 2100 Expert Software (Version B.02.08)	Agilent Technologies, CA, USA
Agilent 8453 UV-Vis Spectrophotometer	Agilent Technologies, CA, USA
Agilent UV-Visible ChemStation (Version A.10.01 [81])	Agilent Technologies, CA, USA
Barnstead Lab-Line SHKA2000-1CE Open Air Shaker	Thermo Fisher Scientific, OH, USA
BD FACSAria™ II Cell Sorter	BD Biosciences, MA, USA
BD FACSDiva™ Software (Version 6.1.3)	BD Biosciences, MA, USA
BD LSR II Flow Cytometer	BD Biosciences, MA, USA
BioTek® EL808 Microplate Absorbance Reader	BioTek Instruments, VT, USA
BioTek® Gen5 (Version 1.11.5)	BioTek Instruments, VT, USA
Chip Priming Station	Agilent Technologies, CA, USA
Class II Biological Safety Cabinet	Contamination Control Laboratories Pty Ltd, Sydney, Australia
EndNote for Windows (Version X7.3.1)	Thomson Reuters, NY, USA
Eppendorf Research® Adjustable-Volume Pipettes	Eppendorf AG, Hamburg, Germany
Fisher & Paykel E388 Freezer	Fisher & Paykel Appliances Limited, Auckland, New Zealand
Fisher & Paykel E450 Refrigerator	Fisher & Paykel Appliances Limited, Auckland, New Zealand
FlowJo software (Version 7.6.4, or 10.0.7)	Tree Star Inc,, OR, USA
Forma™ -86 °C Upright Ultra-Low Temperature Freezer (Model 705)	Thermo Scientific, Thermo Electron Corporation, MA, USA
Forma™ 8600 Series -86 °C Ultra-Low Temperature Chest Freezer (Model 8606)	Thermo Fisher Scientific, OH, USA
Forma™ Series II 3110 Water-Jacketed CO_2 Incubator	Thermo Fisher Scientific, OH, USA
Fume Cupboard	Thermoplastic Engineering Limited, Wellington, NZ
GraphPad Prism for Windows (Version 5.01)	GraphPad Software, CA, USA
Heating Circulator	Grant Instruments Ltd, Cambridgeshire, UK
Heraeus® Multifuge® 1S Centrifuge	Thermo Fisher Scientific, OH, USA
Heraeus® Multifuge® 3S+ Centrifuge	Kendro Laboratory Products GmbH, Hanau, Germany
Heraeus® Multifuge® 3S-R Centrifuge	Kendro Laboratory Products GmbH, Hanau, Germany

IKAMAG EOA 9 Multipoint Stirrer	IKA® Werke GmbH & Co. KG, Staufen, Germany
IKA MS 3 Vortex Mixer	IKA® Werke GmbH & Co. KG, Staufen, Germany
Janke & Kunkel IKA-WERK ES5 Controller	IKA® Werke GmbH & Co. KG, Staufen, Germany
LabMini™ 6 Six-Place Mini-Centrifuge	Southwest Science, NJ, USA
LABOPORT® Vacuum Pump	KNF Neuberger GmbH, NJ, USA
Mastercycler® Gradient Thermal Cycler	Eppendorf AG, Hamburg, Germany
MicroAmp™ Adhesive Film Applicator	Applied Biosystems, CA, USA
Microfuge® 22R Centrifuge	Beckman Coulter, CA, USA
Mini LabRoller™ Dual Format Rotator	Labnet International, NJ, USA
MiniSpin® Plus Microcentrifuge	Eppendorf AG, Hamburg, Germany
NanoDrop 1000 Measurement Software (Version 3.8.1)	Thermo Fisher Scientific, DE, USA
NanoDrop® ND-1000 Spectrophotometer	Thermo Fisher Scientific, DE, USA
Olympus CKX41 Inverted Microscope	Olympus Corporation, Tokyo, Japan
RQ Manger (Version 1.2.2)	Applied Biosystems, CA, USA
Sartorius Type 1712 Analytical Balance	Sartorius GmbH, Göttingen, Germany
SigmaPlot for Windows (Version 11, 12, or 12.5)	Systat Software Inc., CA, USA
SoftMax® Pro Software (Version 5.0.1)	Molecular Devices Co., CA, USA
SpectraMax® M2 Multi-Mode Microplate Reader	Molecular Devices Co., CA, USA
TaqMan® Custom Array	Applied Biosystems, CA, USA
Techne® TE-10A Tempette Clip-on Thermoregulator	Bibby Scientific Limited, UK
VSR-50 Laboratory Platform Rocker	PRO Scientific Inc., CT, USA
VX100 Vortex	Labnet International, NJ, USA
Z2 Coulter® Particle Count and Size Analyser	Beckman Coulter, CA, USA

2.2 Cell lines and culture

2.2.1 Culture medium

Alpha minimal essential medium (αMEM) was prepared by dissolving αMEM powdered medium (Gibco®, Life Technologies Inc., CA, USA) in Milli-Q water (18.2 MΩ·cm), purified by a Milli-Q® water purification system (Millipore Corporation, MA, USA), with 2.2 g/L $NaHCO_3$. The pH of the medium was adjusted to 7.2 with 12 M HCl or 5 M NaOH. The medium was sterilised through 0.22 µm filters under positive pressure, after which 400 mL or 900 mL volumes were aliquoted into sterile 500 mL or 1000 mL DURAN® laboratory bottles (DURAN Group GmbH, Wertheim, Germany), respectively. Medium was stored at 4 °C (Fisher & Paykel E450 Refrigerator, Fisher & Paykel Appliances Limited, Auckland, New Zealand) and used within two months from the time of preparation.

Culture medium was supplemented with 5% foetal calf serum (FCS; Moregate Biotech, New Zealand), which was heat-inactivated at 56 °C for 40 minutes, stored at -20 °C (Fisher & Paykel E388 Freezer, Fisher & Paykel Appliances Limited, Auckland, New Zealand) and thawed prior to use. Antibiotics, 100 units/mL penicillin and 100 µg/mL streptomycin (Sigma-Aldrich, MO, USA), were added to culture medium during certain experiments but not during passage of cell cultures.

2.2.2 Cell culture conditions

All the cell lines were propagated as monolayers in tissue culture flasks with vented cap (BD Falcon™, BD Biosciences, MA, USA) housed in humidified Forma™ Series II 3110 Water-Jacketed CO_2 Incubator (Thermo Fisher Scientific, OH, USA) at 37 °C in 5.0% CO_2. Cells were passaged every 6-7 days or when the cells were 70-80% confluent. All of cell lines were cultured for short periods, typically less than 2 months cumulative passage, from frozen stocks confirmed to be free of Mycoplasma by PCR-ELISA (Roche Diagnostics, Mannheim, Germany). Cell counts were obtained using a Z2 Coulter® Particle Count and Size Analyzer (Beckman Coulter, CA, USA).

2.2.3 Authentication of cell lines

Cell line misidentification is an endemic problem in cancer research. A recent study pointed out that between 18% and 36% of sampled cell lines were incorrectly designated (Lacroix, 2008). Carcinoma cell lines described in this thesis (Table 2.4) were either authenticated by CellBank Australia (HT-29) or DNA Diagnostics (FaDu) using short tandem repeat (STR) profiling (Masters et al., 2001) or in our laboratory using a GeneScan™ kit (SiHa and HCT116; Applied Biosystems, CA USA).

Table 2.4: Panel of carcinoma cell lines used in this thesis and tumour types from which they were derived.

Cell line	Tissue of origin	Organism	Source
FaDu	Pharyngeal squamous cell carcinoma	Homo sapiens	ATCC
HCT116	Colorectal carcinoma	Homo sapiens	ATCC
HT-29	Colorectal adenocarcinoma	Homo sapiens	Dr David Ross, University of Colorado, USA
SiHa	Cervical squamous cell carcinoma	Homo sapiens	Dr David Cowan, Ontario Cancer Institute, Canada

2.3 Xenograft models

2.3.1 Animals

Animal studies were performed in accordance with the *New Zealand Animal Welfare Act 1999* and Research Approvals CR830 and CR001190 from the Animal Ethics Committee of the University of Auckland. All experiments utilised specific pathogen-free, female, 18-21 g CD1-nude mice bred at the University of Auckland from founders purchased from Charles River Laboratories (Wilmington, MA). Mice were housed in Tecniplast microisolator cages (≤ 6 per cage) with free access to water and standard certified commercial rodent diet (2018 Teklad Global 18% Protein Rodent Diet; Harlan Laboratories, IN, USA) in a temperature-controlled room (20 ± 2 °C) with a 12 h light/dark cycle.

2.3.2 Cell line-derived xenografts

In the late 1950's, the introduction of the experimental armamentarium began an era of using human cancer material heterotransplanted into murine immune-deficient mice as xenograft models in cancer drug development (Chesterman, 1959).

Cell line-derived, subcutaneous xenografts were cultivated on the flank or back of mice. A total of 10×10^6 SiHa or FaDu cells in 0.1 mL of serum-free αMEM were inoculated into non-anaesthetised mice on the left flank using 21-gauge needles. Tumour growth was monitored by electronic calliper measurement of two orthogonal dimensions (length and width, where length ≥ width) using the formula volume = 0.5 × length × width^2. Tumours were grown to treatment size of 500-900 mm^3 for click chemistry-based hypoxic cell labelling assays.

2.4 Hypoxic cell labelling using click chemistry

2.4.1 Labelling of cultured human cancer cells with clickable 2-nitroimidazole

Cancer cells, grown as a subconfluent monolayer culture, were harvested in trypsin/EDTA. After a wash with PBS to remove residual trypsin by centrifugation (1000 rpm, 5 min, RT), cell density was determined using Z2 Coulter® Particle Count and Size Analyser (Beckman Coulter, CA, USA). Cells were resuspended in fresh culture medium (αMEM, 5% FCS) at a density of 1×10^6 cells/mL and divided into aliquots of 10 mL. Each aliquot of the cell suspension was incubated at 37 °C with low-speed stirring and exposed to selected atmospheric conditions (Table 2.5) for 90 min (the pre-gassing incubation). Then, clickable 2-NI at the selected concentration (by diluting from 20 mM stock solution in DMSO) was added to the cell suspension, which was followed by 2-hour incubation in the original gas phase at 37 °C with low-speed stirring. Instead of clickable 2-NI, an equal volume of DMSO was added to another aliquot of cells and incubated under the conditions identical to the experimental sample for purposes of control.

Table 2.5: The compositions of the gassing mixtures used in *in vitro* studies.

	N_2	CO_2	O_2
Hypoxic conditions [a, b]	95%	5%	
Oxic conditions [b]		5%	95%

Note:
a. When experimental manipulation of cells under anoxic conditions (95% N2, 5% CO2) was performed, 'anoxic' and 'hypoxic' are used interchangeably to describe such conditions in this thesis. Both refer to strict anoxia;
b. Gassing at 50 psi and ambient temperature.

When cell fixation and permeabilisation was not required, cells were washed once with ice-cold PBS and pelleted down by centrifugation at 1000 rpm for 5 min at RT after the 2-hour incubation. Following careful removal of the supernatant and gentle dislodgement of the pellet, cells were then washed with ice-cold 1% (w/v) bovine serum albumin (BSA; Thermo Fisher Scientific, MA, USA) in PBS and pelleted down by centrifugation at 1000 rpm for 5 min at RT and the supernatant was removed. The light inside the tissue culture hood was switched off and the sample tube was wrapped in aluminium foil to prevent or minimise exposure to light from this step onwards.

For experiments requiring cell fixation and permeabilisation, cells were washed once with ice-cold PBS and pelleted down by centrifugation at 1000 rpm for 5 min at RT after the 2-hour incubation. Cells were then resuspended in ice-cold PBS containing 1% (w/v) BSA (a volume of 100 µL was required for every $1x10^7$ cells). The sample tube was wrapped with aluminium foil to prevent or minimise exposure to light from this step onwards. An equal volume of 4% (w/v) paraformaldehyde (Pfa) in PBS used as fixative was added in and mixed well to dislodge and resuspend any remaining pellet and to ensure a homogenous sample. The cells were incubated for 15 min at RT. After washing once with 3 mL 1% (w/v) BSA in PBS, cells were pelleted down by centrifugation at 1000 rpm for 5 min at RT. The supernatant was removed and the cell pellet was completely dislodged. A volume of 1 mL of PBS with 0.3% (v/v) Tween 20 (Sigma-Aldrich, MO, USA; PBStt) was added (Koch, 2008). The cells were mixed well to ensure a homogenous sample and incubated for 30 min at 4 °C in the dark. At the end of incubation, cells were washed one more time with 3 mL ice-cold PBStt and pelleted down by centrifugation at 1000 rpm for 5 min at RT.

2.4.2 Labelling of cells in human tumour xenografts with clickable 2-NI

CD1-nude mice were inoculated with 10×10^6 human tumour cells in 100 µL of serum-free culture medium subcutaneously on the left flank as described in section 2.3.2.

About 3–4 weeks later, the dosing solution was prepared by diluting clickable 2-NI SN 33267 stock solution dissolved in DMSO with saline to achieve a final concentration of 3 mg/mL. Mice were dosed by intraperitoneal (i.p.) injection with SN 33267 at 60 mg/kg, using an injection volume of 0.02 mL/g.

After 2 hours, the mice were euthanized and the tumours excised. The tumour tissue was minced using scissors or scalpels until a fine minceate was obtained. Up to 500 mg of minceate was transferred into a pre-tared 14 mL polystyrene round-bottom tube (BD Falcon®, BD Biosciences, MA, USA) containing a magnetic spin bar and weighed on a Sartorius Type 1712 analytical balance (Sartorius GmbH, Göttingen, Germany).

Chilled, filter-sterilised enzyme cocktail was prepared freshly (Table 2.6). After the weighing of the tumour, a volume of 1 mL of enzyme cocktail was immediately added for every 50 mg of tumour minceate as soon as a fine minceate was obtained by mincing tumour with scissors or scalpels. The tumour minceate was incubated with enzyme cocktail in a 37 °C water bath (Techne® TE-10A Tempette Clip-on Thermoregulator, Bibby Scientific Limited, UK) for 30 min. The mixture solution was stirred with a magnetic stir bar throughout the whole incubation period to achieve a maximum level of enzymatic digestion (IKAMAG EOA 9 multipoint stirrer with Janke & Kunkel IKA-WERK ES5 Controller, IKA® Werke GmbH & Co. KG, Staufen, Germany).

Table 2.6: Enzyme cocktail for dissociation of tumours.

Component	Final Concentration
Pronase	2.5 mg/mL
Collagenase	1 mg/mL
DNase I	0.2 mg/mL
FCS	10% (v/v)
PS	1% (v/v)

Dissociated cells were transferred into a fresh 50 mL polypropylene conical tube (BD Falcon®, BD Biosciences, MA, USA) and pelleted by centrifugation at 1000 rpm for 5 min at RT (Heraeus® Multifuge® 3S-R Centrifuge, Kendro Laboratory Products GmbH, Hanau, Germany). Cells were washed once with culture medium, followed by centrifugation at 1000 rpm for 5 min at RT. After removing the supernatant, cells were resuspended in a small volume (5-10 mL) of fresh culture medium and cell counting was performed using a Z2 Coulter® Particle Count and Size Analyser (Beckman Coulter, CA, USA).

Based on the counting result, the suspension of dissociated tumour cells was further diluted with fresh culture medium to achieve at the cell density of 1×10^6 cells/mL, which was followed by 2 washing steps. First, cells were washed with ice-cold PBS and pelleted down by centrifugation at 1000 rpm for 5 min at RT. After carefully removing the supernatant and gently dislodging the pellet, cells were then washed with ice-cold 1% (w/v) bovine serum albumin (BSA; Thermo Fisher Scientific, MA, USA) in PBS and pelleted down by centrifugation at 1000 rpm for 5 min at RT. The supernatant was removed. The light inside the tissue culture hood was switched off and sample tube was wrapped in aluminium foil to prevent or minimise exposure to light from this step onwards.

2.4.3 Staining of clickable 2-NI labelled cells using copper(I)-catalysed alkyne-azide click chemistry

Similar to most applications of bioorthogonal reactions, the click chemistry-based methodology discussed in this thesis is based on a two-step bioorthogonal labelling strategy that requires introduction of chemical exogenous functionality (see 2.4.1 and 2.4.2) followed by modification of the biomolecule with the tailor-designed highly specific bioorthogonal probe (Hanson et al., 2007; Laughlin & Bertozzi, 2009; Yang, Ascano, & Hang, 2010).

The optimisation of this methodology will be outlined in Chapters 4 and 5. The complete optimisation process of the methodology is illustrated in Figure 2.1. The final version of the optimised protocol is as follows.

After gently dislodging the pellet, 100 µL of freshly prepared[1] reaction cocktail #7 (Table 2.7) was added in for every 1 × 10^6 cells. Cells and click reaction cocktail were mixed well and incubated for 20 min at RT with gentle agitation (120 rpm; Barnstead Lab-Line SHKA2000-1CE Open Air Shaker, Thermo Fisher Scientific, OH, USA), protected from light.

An equal volume of the second dose of freshly prepared reaction cocktail #7 was directly added into cell sample following the first 20-minute incubation. Cells were incubated with click reaction cocktail for a further 20 min at RT with gentle agitation (120 rpm), protected from light. At the end of the incubation, 4mL PBS was added, cells were pelleted by centrifugation at 1000 rpm for 5 min at RT, and pelleted cells were gently dislodged after the supernatant was carefully removed.

The cells were resuspended in 50% (v/v) ethanol (EtOH) in PBS and incubated for 1 min. The volume of 50% (v/v) EtOH-PBS solution required in this step depended on the sample size. When the sample size was less than 3 × 10^6 cells, 3.5 mL was used; for sample containing 3 × 10^6 to 8 × 10^6 cells, 8 mL was used. Cells were pelleted down by centrifugation at 1000 rpm for 5 min at RT, followed by removal of the supernatant and dislodging the pellet.

Next, cells were resuspended in and incubated with PBS for 1 min. The volume of PBS used in this step was same as the volume of 50% (v/v) EtOH-PBS in previous step. Again, cells were centrifuged at 1000 rpm for 5 min at RT and the supernatant was carefully removed. Cells were finally resuspended in a small volume of PBS and subsequently transferred into a fresh 5 mL polystyrene round-bottom tube with cell-strainer cap (BD Falcon®, BD Biosciences, MA, USA) by passing through the 35 µm cell-strainer to remove cell clumps. Samples were kept on ice and protected from light. Flow cytometry or fluorescence-activated cell sorting (FACS) was performed immediately.

[1] Based on suggestions from published studies of CuAAC, during the preparation of reaction cocktail in this thesis, as a matter of routine, the copper source was first mixed with the ligand, which was followed by adding a solution of an azide-modified fluorophore into this mixture. The whole preparation procedure was completed by the addition of the freshly prepared reducing agent to the desired concentration (Hong et al., 2009).

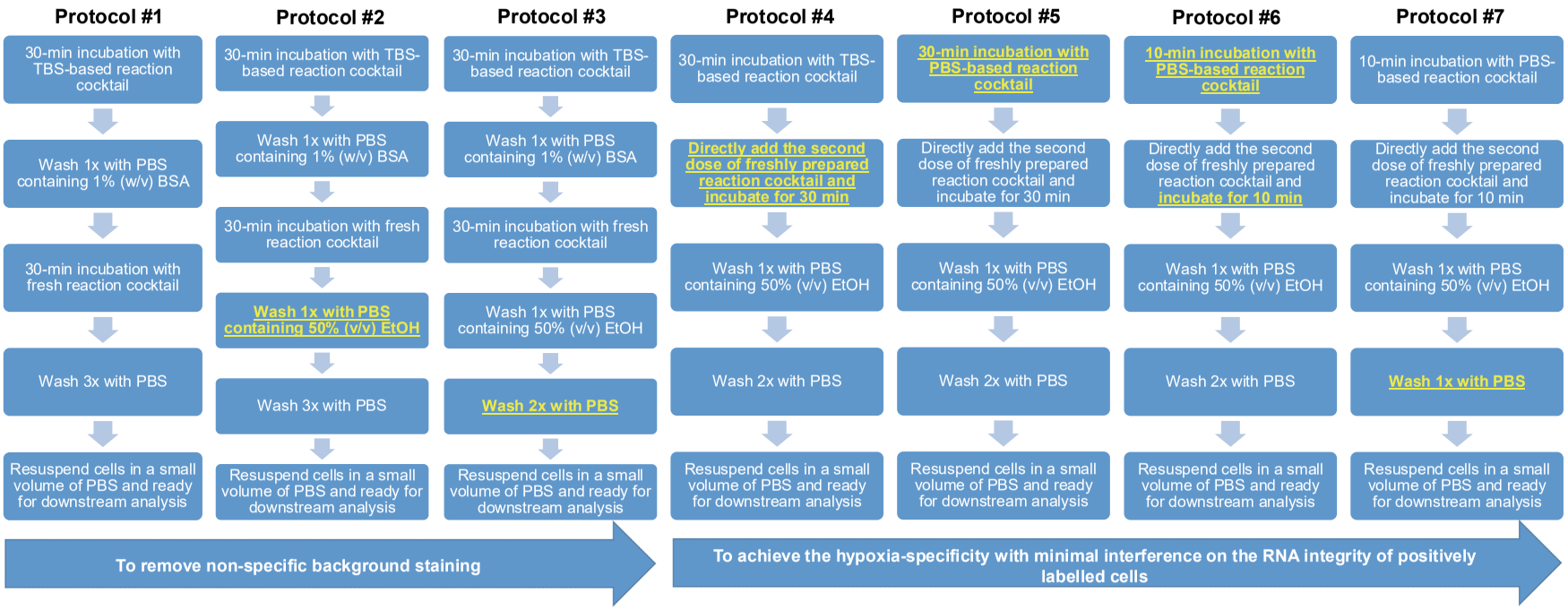

Figure 2.1: Schematic view of the modifications made in experimental protocols to optimise the click chemistry-based methodology.

The modifications made in each version of the experimental protocol are underlined and highlighted in yellow. The two horizontal at the bottom indicate the order of modifications have been made and the major intention(s) of modifying experimental protocol at each stage.

Table 2.7: The composition of click reaction cocktails[a] used in this thesis.

Component	Cocktail #1	Cocktail #2	Cocktail #3	Cocktail #4	Cocktail #5	Cocktail #6	Cocktail #7 (Optimised)
Copper salt	1 mM $CuSO_4$	1 mM $CuSO_4$	1 mM CuOAc	1 mM CuOAc	1 mM CuOAc	1 mM CuOAc	1 mM CuOAc
Ligand	1 mM TBTA	100 µM TBTA	1 mM TBTA	1 mM THPTA	100 µM TBTA	100 µM THPTA	100 µM TBTA
Reducing agent	100 mM Sodium ascorbate	500 µM TCEP	100 mM Sodium ascorbate	100 mM Sodium ascorbate	500 µM TCEP	500 µM TCEP	500 µM TCEP
Buffer	TBS [b]	TBS [b]	TBS [b]	TBS [b]	TBS [b]	TBS [b]	PBS [c]
Fluorophore azide				10 µM			

Notes:

a. The majority of click reactions involved in this PhD project used reaction cocktails listed in this table unless stated otherwise;

b. Tris-buffered saline (TBS; 150 mM NaCl, 10 mM Tris, pH 7.4) to a final volume of 100 µL for every 10^6 cells;

c. Phosphate-buffered saline (PBS; 137 mM NaCl, 2.68 mM KCl, 1.47 mM KH_2PO_4, 8.16 mM Na_2HPO_4, pH 7.4) to a final volume of 100 µL for every 10^6 cells.

2.4.4 Nomenclature of clicked samples

One major objective of this PhD project was to continue work on establishing and subsequently optimising a hypoxia-specific cell labelling methodology on the basis of click chemistry. To achieve this goal, a considerable number of *in vitro* experiments were conducted. All cell samples were named following the same rules in those experiments unless stated otherwise.

Each sample name consists of 3 parts linked by 2 underscores. The first part of the sample name is either the word “Oxic” or the word “Hypoxic” to indicate the atmospheric conditions in which cells were incubated both during the pre-gassing stage and with clickable 2-NI. The middle part is the name of 2-NI used in the experiment followed by either “+” (cells incubated with 2-NI) or “-” (cells incubated with the equal volume of DMSO). The third part is the word “Azide” followed by either “+” (cells incubated with selected reaction cocktail) or “-” (cells incubated with selected reaction cocktail including all components but the azide-modified fluorophore). For example, cells in the sample named “Oxic_SN33267+_Azide-” were prepared by 1.5-h pre-gassing incubation following 2-h incubation with SN33267 under the same oxic conditions and subsequently incubating with a reaction cocktail without containing azide-modified fluorophore.

In some experiments, an additional sample with the name of “Hypoxic_SN33267-_Blank” was employed to account for the background signals. The sample with such name is the cells incubated

with the solvent of 2-NI in hypoxic conditions for 2 h following the 1.5 h pre-gassing incubation in hypoxic conditions and incubated with the buffer on which the selected reaction cocktail was based.

2.5 Flow cytometric analysis

Cellular fluorescence was measured using either a Becton Dickinson FACSAria™ II Cell Sorter (for TAMRA dyes) or a Becton Dickinson LSR II Flow Cytometer (for other dyes) with BD FACSDiva™ software (version 6.1.3; BD Biosciences, MA, USA). Single cells were gated using a selected laser for the forward-scatter and side-scatter signals. Integrated fluorescence measurements were recorded for 30,000 single cells. Laser excitation wavelength, optical configuration, and filter specifications for instruments of flow cytometric analysis in this study are given in Table 2.8. Data were analysed and plotted using FlowJo (version 7.6.4, or 10.0.7; Tree Star, OR, USA).

Table 2.8: The settings for instruments employed in flow cytometric analysis in this study.

Azide-modified Fluorophore	Laser	Bandpass Filter	Longpass Dichroic Mirror
Alexa Fluor 488-azide	488 nm	530/30	505LP
BODIPY-650/665-azide	640 nm	670/30	blank
BODIPY-FL-azide	488 nm	530/30	505LP
DMACA-azide	355 nm	530/30	505LP
TAMRA-azide	552 nm	585/15	blank

2.6 Fluorescence-activated cell sorting

Cells labelled with azide-modified fluorophores were resuspended in 3 mL of PBS. Cells were gated into quartiles and sorted into 4 fractions defined by approximately equivalent cell number with a sorting rate giving ≥ 90% efficiency using a Becton Dickinson FACSAria™ II Cell Sorter (BD Biosciences, MA, USA) operated by Mr Stephen Edgar (University of Auckland). The sorted cells were collected using Falcon® 5 mL polystyrene round-bottom tubes (BD Biosciences, MA, USA) with 1.5 mL TRIzol® LS Reagent (Ambion™, Life Technologies, CA, USA) or with 1 mL culture media (αMEM with 5% FBS) for the purpose of RNA extraction or protein extraction, respectively.

2.7 RNA extraction and quality control

In order to ensure an RNase-free environment required when working with RNA, either RNase AWAY® Decontamination Reagent (Ambion™, Life Technologies, CA, USA) or RNaseZap® RNase Decontamination Solution (Life Technologies, CA, USA) was employed to perform surface decontamination and effectively eliminate RNase as well as DNA contamination without inhibiting subsequent enzymatic reactions.

2.7.1 Cell lysis

2.7.1.1 Homogenization in TRIzol

Total RNA was isolated from FACS-sorted cells using a combination of homogenization in TRIzol® LS Reagent and RNA extraction by silica gel-based membrane filtration using PureLink® RNA Mini Kit (both from Ambion™, Life Technologies, CA, USA). Both sample homogenisation and phase separation with TRIzol® were performed in a fume cupboard (Thermoplastic Engineering Limited, Wellington, New Zealand)

To achieve a sufficient yield of total RNA for each sample, approximately 500,000 cells collected from FACS in a Falcon® 5 mL polystyrene round-bottom tube (BD Biosciences, MA, USA) with 1.5 mL of TRIzol® LS Reagent were processed. After incubating the cells with TRIzol® LS Reagent at RT for 5 min to achieve complete dissociation of the nucleoprotein complex, 400 µL of chloroform (LiChrosolv®, Merck KGaA, Darmstadt, Germany) was added to samples, which were mixed by vigorously shaking for 15 s and incubated for 3 min at RT.

All samples were centrifuged at 12,000 × *g* for 15 min at 4 °C (Microfuge® 22R Centrifuge, Beckman Coulter, CA, USA). After centrifugation, the upper aqueous phase was transferred to a fresh RNase-free 1.7 mL microcentrifuge tube (Axygen®, Corning Life Sciences, MA, USA). For each sample, a volume of ethanol (EMSURE®, Merck KGaA, Darmstadt, Germany) was then added to obtain a final ethanol concentration of 35%. Samples were mixed immediately by vortexing (Labnet VX100 Vortex, Labnet International, NJ, USA) and kept on ice before proceeding to silica-cartridge purification.

2.7.1.2 Homogenization in lysis buffer

For un-sorted cells used to determine the effect of the CuAAC-mediated cell labelling procedure on hypoxia-regulated expression of hypoxia marker gene set in Chapter 6, PureLink® RNA Mini Kit was used to perform both homogenization and total RNA extraction according to the manufacturer's instructions. Briefly, a fresh amount of Lysis Buffer containing 1% 2-mercaptoethanol (Gibco™, Life Technologies, CA, USA) was prepared for each extraction procedure. Cells were centrifuged at 2,000 × *g* for 5 min at 4 °C to pellet (Heraeus® Multifuge® 3S-R Centrifuge, Kendro Laboratory Products GmbH, Hanau, Germany).

For samples containing less than 1×10^6 cells, 300 µL of freshly prepared Lysis Buffer was added; for samples containing a total number of cells between 1 and 5×10^6, 600 µL of freshly prepared Lysis Buffer was used. Each sample was lysed firstly by vortexing at high speed until the cell pellet was completely dispersed and then homogenised by passing through an 18 gauge BD Integra™ blunt filter needle (BD Biosciences, Singapore) 20 times using a 1 mL Luer Slip Tuberculin Syringe (BD Biosciences, Singapore). The homogenate was centrifuged at 2,600 × *g* for 5 min at RT. The supernatant was then transferred to a fresh RNase-free microcentrifuge tube.

Based on the volume of Lysis Buffer applied in each sample, an equal volume of 70% ethanol, prepared using RNase-free water, was added. Samples were vortexed to mix thoroughly and kept on ice before proceeding to RNA extraction.

2.7.2 RNA extraction by silica gel-based membrane filtration

Up to 700 µL of sample was loaded onto a Spin Cartridge with Collection Tube from PureLink® RNA Mini Kit (Ambion™, Life Technologies, CA, USA), which was then centrifuged at 12,000 × *g* for 15 s at RT (MiniSpin® plus microcentrifuge, Eppendorf AG, Hamburg, Germany). If the sample volume exceeded 700 µL successive aliquots were applied to the same Spin Cartridge as above. Flow-through was discarded after each centrifugation. A volume of 350 µL of Wash Buffer I was added to each Spin Cartridge and centrifuged at 12,000 × *g* for 15 s at RT.

On-column DNase treatment was performed using a PureLink® DNase Set (Ambion™, Life Technologies, CA, USA). A volume of 80 µL PureLink® DNase mixture, containing 8 µL of 10× DNase I Reaction Buffer, 10 µL of Resuspended DNase (~3 U/µL), and 62 µL RNase Free Water, was added directly on to the surface of the Spin Cartridge membrane. After 15-minute incubation at RT, the Spin Cartridge was washed by adding 350 µL of Wash Buffer and centrifuging at 12,000 × *g* for 15 s at RT.

The Spin Cartridges were then transferred to fresh Collection Tubes. A volume of 500 µL of Wash Buffer II was added and the Spin Cartridges were centrifuged again at 12,000 × *g* for 15 s at RT. Flow-through was discarded and this wash step was repeated with a 15-s centrifugation time followed by a final 1-min centrifugation to dry the membrane with bound RNA. Each Collection Tube was replaced with a fresh Recovery Tube. RNA was eluted with 30 µL of RNase-Free Water by incubating Spin Cartridge with eluant for 1 min at RT then centrifuging at 12,000 × *g* for 1.5 min at RT.

To obtain a higher total RNA concentration, the first elution was reapplied to the Spin Cartridge which was spun again at 12,000 × *g* for 1 min at RT. After the second elution, two 1 µL aliquots were removed from each RNA sample for quantitation and determination of RNA integrity/quality detailed below in section 2.7.3. Total RNA samples were subsequently stored at -80 °C (Forma™ 8600 Series -86 °C Ultra-Low Temperature Chest Freezer (Model 8606), Thermo Fisher Scientific, OH, USA) until further analysis.

2.7.3 Quantification of RNA

Purity and integrity were determined for all RNA samples prior to use in real-time qPCR experiments. The concentration and purity of all RNA samples was initially quantified by measuring sample absorbance at 260 nm and 280 nm using a NanoDrop® ND-1000 Spectrophotometer with NanoDrop 1000 Measurement Software v3.8.1 (Thermo Fisher Scientific, DE, USA).

RNA sample integrity and purity were further tested using an Agilent 2100 Bioanalyzer with 2100 Expert Software (Agilent Technologies) as follows. Briefly, a 1 µL aliquot of each RNA sample was denatured at 70 °C for 2 min. Up to 12 heat-denatured samples and Agilent RNA 6000 nano ladder

were loaded onto a gel-filled RNA nano chip (RNA 6000 Nano LabChip® Kit, Agilent Technologies, CA, USA). The RNA nano chip was vortexed for 1 min at 2400 rpm (IKA MS 3 vortex mixer, IKA® Werke GmbH & Co. KG, Staufen, Germany), then loaded into the Agilent 2100 Bioanalyzer, and analysed using the option of Eukaryote Total RNA Nano Series II Assay v2.6.

For each sample, an electropherogram trace and an RNA integrity number (RIN) were generated. The RIN number provides an unambiguous assessment of RNA integrity that allows RNA quality to be standardised cross multiple samples (Schroeder et al., 2006). RIN values ranged from 1 to 10 with 10 indicating completely intact RNA and 1 indicating complete degradation (Schroeder et al., 2006). All RNA samples used in this thesis were with RIN greater than 5.2 and demonstrated no signs of genomic DNA contamination on either the electropherogram trace or gel-like image.

2.8 Reverse transcription of RNA to cDNA

cDNA was synthesised from 200 ng of total RNA using the High Capacity RNA-to-cDNA Kit (Applied Biosystems, CA, USA) according to the manufacturer's instructions. Briefly, 200 ng of total RNA, in a volume up to 9 µL, was combined with 10 µL of 2× RT Buffer and 1 µL of 20× RT Enzyme Mix in a 0.2-mL polypropylene thin wall PCR tube (Axygen®, Corning Life Sciences, MA, USA). Sample volumes were made up to 20 µL with UltraPure™ DEPC-Treated Water (Invitrogen™, Life Technologies, CA, USA). This reaction mixture was gently mixed, spun down by brief centrifugation (LabMini™ 6 six-place mini-centrifuge, Southwest Science, NJ, USA), and incubated at 37 °C for 60 min using a Mastercycler® gradient thermal cycler (Eppendorf AG, Hamburg, Germany). The reaction was terminated by incubating at 95 °C for 5 min and then placing samples on ice for at least 1 min. After a brief centrifugation, cDNA products were purified using a Qiaquick® PCR purification kit (Qiagen GmbH, Hilden, Germany) according to the manufacturer's protocol. cDNA samples were transferred into fresh RNase-free 1.7 mL microcentrifuge tubes and stored at -20 °C (Fisher & Paykel E388 Freezer, Fisher & Paykel Appliances Limited, Auckland, New Zealand) until further use.

Since it is almost impossible to completely eliminate genomic DNA (gDNA) from RNA, it is essential to involve a minus-reverse transcriptase control in real-time PCR experiments for each cDNA sample, especially when the assay is not cDNA-specific. The presence of an amplification

product in minus-reverse transcriptase control indicates the contamination of gDNA in the corresponding sample.

The minus-reverse transcriptase control is a mock reverse transcription containing all the RT-PCR reagents, except the reverse transcriptase. For each RNA sample, 200 ng of total RNA, in a volume up to 10 µL, was mixed with 10 µL of 2× RT Buffer and incubated at same thermal cycler conditions. -RT controls were also transferred into fresh RNase-free 1.7 mL microcentrifuge tubes and stored at -20 °C (Fisher & Paykel Appliances Limited, Auckland, New Zealand) until further use.

2.9 Real-time quantitative PCR using TaqMan® gene expression assays

TaqMan® Gene Expression Assays (Applied Biosystems, CA, USA) were used to perform gene expression analysis by real-time quantitative PCR. Pre-formulated expression assays consisted of a single 20× mix containing 1 pair of unlabelled gene specific PCR primers (each primer at a final concentration of 900 nM) and 1 FAM™ dye-labelled TaqMan® minor groove-binder probe (250 nM final concentration). The following human-specific assays were used in the qPCR experiments detailed in this thesis (Table 2.9).

Assays with the suffix "_m1" are designed over exon-exon boundaries. Assays with the suffix "_g1" are also designed over exon-exon boundaries but have the potential to detect both the functional transcript and non-transcribed pseudogenes, in the presence of high levels of contaminating genomic DNA. Similarly, "_s1" indicates an assay whose probes and primers are designed within a single exon also with the possibility of genomic DNA detection.

Table 2.9: TaqMan® Gene Expression Assays.

Gene Symbol	Assay ID
18S	Hs99999901_s1
ADM	Hs00969450_g1
AKR1C3	Hs00366267_m1
ALDOA	Hs00605108_g1
ANKRD37	Hs00699180_m1
B2M	Hs99999907_m1
BNIP3	Hs00969291_m1
BNIP3L	Hs01087963_m1
CYB5R3	Hs01060717_m1
EGLN3	Hs00222966_m1
FAM162A (C3orf28)	Hs01055825_m1
FDXR	Hs01031617_m1
FOXRED2	Hs00227920_m1
HPRT1	Hs99999909_m1
KCTD11	Hs00922550_s1
LOX	Hs00942480_m1
NDRG1	Hs00608387_m1
NDOR1	Hs00180881_g1
NQO1	Hs02512143_s1
NQO2	Hs01056948_m1
P4HA1	Hs00914594_m1
P4HA2	Hs00990001_m1
PDK1	Hs01561850_m1
PFKFB3	Hs00998700_m1
POR	Hs01016332_m1
PPIA	Hs99999904_m1
RPL13A	Hs04194366_g1
RPLP0	Hs99999902_m1
SLC2A1 (GLUT1)	Hs00892681_m1
TXNRD1	Hs00917067_m1
UBC	Hs00824723_m1
YWHA	**Hs00237047_m1**

Notes: TaqMan® probe with a FAM™ dye label on the 5' end, and minor groove binder (MGB) nonfluorescent quencher (NFQ) on the 3' end. Candidate reference genes are indicated in **bold**.

2.9.1 Selection of reference genes

To identify stable reference (endogenous control) genes from a set of tested candidate reference genes in a given experimental condition, an implementation of the popular algorithm qBase+ (version 1.3.5; Biogazelle NV, Zwijnaarde, Belgium), geNorm™ (version 3.5), was employed according to according to the manufacturer's protocol.

2.9.2 Assay protocol and real-time qPCR cycling conditions

2.9.2.1 Using 384-well plate

All qPCR reactions were singleplex reactions with a total volume of 20 µL. All reactions were set up in ABI Prism™ 384-well clear optical reaction plates (Applied Biosystems, CA, USA). Within each plate well 9 µL of cDNA template, amounting to an input amount of 300 ng cDNA (equivalent to approximately 2 ng of total RNA), was combined with 11 µL of real-time PCR reaction mix (Table 2.10).

Table 2.10: Components and volumes of master mix per well in qPCR reaction.

Component	Volume
TaqMan® Gene Expression Assay (20×)	1 µL
TaqMan® Universal Master Mix (2×)	10 µL
cDNA sample (~2 ng of total RNA) made up with UltraPure™ DEPC-Treated Water	9 µL

All samples were assayed in triplicate. Also in triplicate were no-template control reactions, loaded with RNase free H_2O. After loading the wells, 384-well plates were sealed with an ABI MicroAmp™ Optical Adhesive Film (Applied Biosystems, CA, USA). Experimental plates were run under standard universal thermal cycling conditions (Table 2.11) in an ABI 7900HT Fast Real-Time PCR System (Applied Biosystems, CA, USA).

Each 384-well plate had a unique barcode, and Sequence Detection System (SDS) plate documents stored information on the plate type, detector, sample/target gene configurations, thermal cycling conditions, data collection, and raw fluorescence data at each cycle.

Data were analysed with RQ documents and the RQ Manager Software (version 1.2.2; Applied Biosystems, CA, USA) for automated data analysis.

The relative level of expression for the target gene was normalized to the averaged expression of 18S and B2M genes and calculated using the $2^{-\Delta\Delta C_t}$ relative quantification method as described in section 2.9.3.

Table 2.11: qPCR thermal-cycling conditions (using 384-well plate).

	Step	Time	Temperature	Number of cycles
Holding/Activation	AmpErase® UNG activation	2 min	50 °C	N/A
	AmpliTaq Gold® DNA polymerase activation	10 min	95 °C	N/A
Cycling	Denaturation	15 sec	95 °C	45
	Annealing/Extension	1 min	60 °C	

2.9.2.2 Using TaqMan® Array Card (384-well microfluidic card)

TaqMan® Low-Density Arrays (TLDA, Array Microfluidic Cards; Applied Biosystems, CA, USA) were also used in a 2-step real-time PCR process.

Apart from 18S rRNA and B2M as endogenous controls, the TaqMan® probe and primer sets for 10 human flavin reductase genes were carefully selected from predesigned TaqMan® Gene Expression Assays (see Table 2.12; Applied Biosystems, CA, USA). The sets were factory-loaded into the 384-well plate to create TLDA cards.

Table 2.12: Pre-selected TaqMan® Gene Expression Assays in TLDA cards.

Gene Symbol	Assay ID
18S	Hs99999901_s1
AKR1C3	Hs00366267_m1
B2M	Hs99999907_m1
CYB5R3	Hs01060717_m1
FDXR	Hs01031617_m1
FOXRED2	Hs00227920_m1
MTRR	Hs00985015_m1
NDOR1	Hs00180881_g1
NQO1	Hs02512143_s1
NQO2	Hs01056948_m1
POR	Hs01016332_m1
TXNRD1	Hs00917067_m1

Notes: TaqMan® probe with a FAM™ dye label on the 5' end, and minor groove binder (MGB) nonfluorescent quencher (NFQ) on the 3' end.

PCRs were then carried out in Micro Fluidic Cards using the QuantStudio™ 12K Flex Real Time PCR System (Applied Biosystems, CA, USA). The probes were labelled with the fluorescent reporter dye 6-carboxyfluorescein (FAM®; Applera corp.) on the 5′-end and with a nonfluorescent quencher (NFQ) on the 3′-end. The exact locations and the sequences of the oligonucleotides used in all assays can be downloaded from the Life Technologies website by selecting the Assays IDs. About 800 ng of cDNA (equivalent to approximately 5.3 ng of total RNA) combined with 2× TaqMan® Universal Master Mix (Applied Biosystems, CA, USA) was loaded into each fill reservoir according to the manufacturer's protocol (Table 2.13).

Table 2.13: Components and volumes of master mix per reservoir in qPCR reaction.

Component	Volume
TaqMan® Universal Master Mix (2×)	50 µL
cDNA sample (~5.3 ng of total RNA) made up with UltraPure™ DEPC-Treated Water	50 µL

TaqMan® Array Microfluidic Cards were thermal-cycled at 50 °C for 2 min and 94.5 °C for 10 min followed by 45 cycles at 97 °C for 30 s and 59.7 °C for 1 min (Table 2.14). Data were collected with instrument spectral compensations by QuantStudio™ 12K Flex Real Time PCR System Software (version 1.2.2; Applied Biosystems, CA, USA) and analysed using the $2^{-\Delta\Delta C_t}$ relative quantification method as described in section 2.9.3.

Table 2.14: qPCR thermal-cycling conditions (using TLDA card).

	Step	Time	Temperature	Number of cycles
Holding/Activation	AmpErase® UNG activation	2 min	50 °C	N/A
	AmpliTaq Gold® DNA polymerase activation	10 min	94.5 °C	N/A
Cycling	Denaturation	30 sec	97 °C	45
	Annealing/Extension	1 min	59.7 °C	

2.9.3 Real-time quantitative PCR data analysis

The abundance of transcripts in a test sample relative to calibrator sample was computed using the comparative threshold cycle (C_t) method with *18S* and *B2M* as an internal reference (Lo, Chiu, & Chan, 2006; Schmittgen & Livak, 2008). This multi-step data analysis was conducted with the concern of propagation of uncertainty in this thesis.

First, expression of the target gene was normalized relative to expression of the endogenous reference gene for each sample to produce ΔC_t ($\Delta C_t = C_{t\ target} - C_{t\ reference}$). Then, a calibrator sample was selected and used to set an arbitrary baseline. In this thesis, sample with the lowest hypoxic stress in the group was chosen as the calibrator. $\Delta\Delta C_t$ was the difference between ΔC_t of the test sample and the ΔC_t of the calibrator sample ($\Delta\Delta C_t = \Delta C_t$ test sample $- \Delta C_t$ calibrator sample). The fold change of the differential gene expression, normalised to an endogenous reference and relative to the selected baseline, is calculated using the relative quantification with the equation: $2^{-\Delta\Delta C_t}$ (Livak & Schmittgen, 2001).

2.10 Western blotting

Western blotting was utilised to detect and semi-quantitate BCL2/adenovirus E1B 19kDa interacting protein 3 (BNIP3) and NADPH:cytochrome P450 oxidoreductase (POR) expression at the level of translation in SiHa xenografts.

2.10.1 Protein extraction from cells collected by FACS

Cells labelled with azide-modified fluorophores were divided into quartiles of roughly equal cell numbers by gating their fluorescent intensity and sorted into 4 fractions by FACS (BD FACSAria™ II Cell Sorter with BD FACSDiva™ Software (version 6.1.3; BD Biosciences, MA, USA). For each sample, 250,000 events were collected in Falcon® 5 mL polystyrene round-bottom tube (BD Biosciences, MA, USA) with 1 mL of αMEM media. Cells were washed once with ice-cold PBS and re-pelleted by centrifugation at 6000 × *g* for 5 min at 4 °C.

Working solution of cell lysis buffer was prepared by diluting 1 volume of NuPAGE® LDS sample buffer (4×; Invitrogen™, Life Technologies, CA, USA) with 3 volumes of ice-cold radioimmunoprecipitation (RIPA) buffer containing 50 mM Tris-HCl pH 7.4, 1% (v/v) NP-40, 0.25% (v/v) sodium-deoxycholate, 150 mM NaCl (Merck Millipore, MA, USA), and 1 mM EDTA (AppliChem GmbH, Darmstadt, Germany) with an added 1% (v/v) protease inhibitor cocktail (Sigma-Aldrich, MO, USA). Whole cell lysate was prepared from each sample by resuspending cell pellet with 15 µL of 1× cell lysis working solution. Lysis was allowed to proceed for 30 min at 4 °C with regular agitation. Each sample was then centrifuged at 1000× relative centrifugal force (rcf) for 5 min at 4 °C to remove cell debris and the supernatant was stored at -80 °C.

2.10.2 Gel electrophoresis

The bicinchoninic acid (BCA; Sigma–Aldrich®) assay using standard protocols was not suitable to assess total protein concentration in each lysate prepared from FACS-sorted cells due to insufficient sample (Smith et al., 1985). Instead of measuring total protein concentration, the entire volume of cell lysate prepared from each cell sample containing equal number of sorted cells was mixed with 5% (v/v) 2-mercaptoethanol (Gibco, Life Technologies, CA, USA) and heated to 95 °C

for 5 min (AccuBlock™ digital dry bath, Labnet International, NJ, USA). A volume of 5 µL of molecular weight marker (Kaleidoscope™ Precision Plus Protein™ Standard; Bio-Rad Laboratories, CA, USA) and the lysates were loaded onto NuPAGE® Novex® 4-12% Bis-Tris pre-cast polyacrylamide gel (Invitrogen™, Life Technologies, CA, USA). Proteins were separated by electrophoresis at 150 V in 1× NuPAGE® MES SDS running buffer (Invitrogen™, Life Technologies, CA, USA) for 1 h. The gel was blotted onto a nitrocellulose membrane (Bio-Rad Laboratories, CA, USA) using Mini Trans-Blot Electrophoretic Transfer Cell (Bio-Rad Laboratories, CA, USA) at 100 V for 1 h in transfer buffer containing 25 mM Tris-HCl (pH 8.5), 200 mM glycine, and 20% (v/v) methanol. The membrane was then blocked with 5% (w/v) non-fat milk powder in Tris-buffered saline (TBS) containing 0.1% (v/v) Tween 20 (Sigma-Aldrich®) for 1 h at RT with gentle agitation (VSR-50 Laboratory Platform Rocker, PRO Scientific Inc., CT, USA).

2.10.3 Band detection

Blocked nitrocellulose membranes were probed with primary antibodies (Table 2.15) diluted in 0.5% milk/TBS-0.1% Tween 20 overnight at 4 °C with gentle agitation. After washing 3 times with TBS-0.1% Tween 20 for 10 min each, the membranes were probed with secondary antibodies (Table 2.15) diluted in 0.5% (w/v) milk/TBS-0.1% (v/v) Tween 20 for 1 h at room temperature with gentle agitation. Then, secondary antibodies were decanted and membranes were washed with TBS-0.1% Tween 20 (3 times for 10 min each). Chemiluminescent images were acquired using an ImageQuant™ LAS-4000 (GE Healthcare, Buckinghamshire, UK) with SuperSignal® West Pico Chemiluminescent Substrate (Thermo Fisher Scientific, IL, USA).

For BNIP3, these conditions detected a band at approximately 30 kDa, corresponding to the expected molecular weight of this protein, with weaker non-specific bands at two sizes (approximately 20 and 60 kDa). The antibodies against POR and ACTB were highly specific and targeted protein bands of approximately 76 and 42 kDa, respectively. The applications of these antibodies in immunoblotting have been validated previously (Guise et al., 2010; Guise et al., 2012).

Table 2.15: Primary and secondary antibodies used for Western blotting.

Antigen	Antibody	Supplier	Dilution
BNIP3 (human)	Goat polyclonal AF4147	R&D Systems, Inc., MN, USA	1:1000
POR (human)	Mouse monoclonal sc-25263	Santa Cruz Biotechnology Inc., CA, USA	1:2000
ACTB (all vertebrates)	Mouse monoclonal MAB1501R	Chemicon®, Merck Millipore, MA, USA	1:10,000
IgG (mouse)	Goat anti-mouse IgG-HRP sc-2055	Santa Cruz Biotechnology Inc., CA, USA	1:1000 (ACTB) 1:5000 (POR)
IgG (goat)	Rabbit anti-goat IgG-HRP sc-2768	Santa Cruz Biotechnology Inc., CA, USA	1:1000 (BNIP3)

2.10.4 Densitometry of Western blots

Expression of BNIP3 and POR in SiHa xenografts was quantified by comparing band density normalised against ACTB (i.e. beta actin) as a loading control in ImageJ (v1.48v of the public domain software) using unprocessed images. To clarify band densitometry analysis, blots in the main text have been cropped to retain about 3 bandwidths both above and below bands.

2.11 Statistical Analysis

The statistical significance of difference between the means and trends were assessed using linear regression analysis, two-tailed Student's *t*-test, 2-way analysis of variance (ANOVA) with Bonferroni *post-hoc* pairwise analysis for multiple comparisons were performed when appropriate. Statistical tests were performed using GraphPad Prism (version 5.01 for Windows; GraphPad Software, CA, USA) or SigmaPlot (version 11, 12, or 12.5 for Windows; Systat Software Inc., CA, USA).

Means and standard error of the mean (SEM) derived from either technical replicates or multiple independent experiments were typically used. A *P*-value less than 0.05 was regarded as indicating statistically significant differences.

Chapter 3. Selection of fluorophores for click chemistry-based detection of hypoxic cells

3.1 Introduction

Fluorescence is a widely used key technique in life science applications (Drummen, 2012; Fili & Toseland, 2014; Lakowicz, 2007). Each fluorescent compound is characterised by an excitation spectrum (the wavelength and amount of light absorbed) and an emission spectrum (the wavelength and amount of light emitted), usually referred to as compound's fluorescence signature or fingerprint (Valeur & Berberan-Santos, 2012). The principle that all fluorophores have relatively distinct fluorescence signatures makes fluorometry a highly specific analytical technique (Drummen, 2012; Taraska & Zagotta, 2010).

By selectively generating the wavelength of light required to excite the analyte of interest, selectively transmitting the wavelength of light emitted, and measuring the intensity of the emitted light, fluorescence can be measured based on the principle that the emitted light is proportional to the concentration of the analyte being measured within a certain range of concentration (Fili & Toseland, 2014; Neef & Schultz, 2009; Valeur & Berberan-Santos, 2012).

Due to the ability of labelling biomolecules and staining cells, the use of exogenous synthetic organic fluorophores is still the most-adopted approach to visualise or analyse biological molecules in cells and organisms. Fluorophore-based technologies have made significant contributions to the understanding of dynamic and complicated processes in biological systems since the first attempt to achieve fluorescence staining of cells by von Prowazek exactly a century ago (Lam, Law, Lee, & Wong, 2014; von Prowazek, 1914). Fluorescent probes are versatile research tools, and offer exquisite sensitivity and outstanding selectivity, by which the limits of detecting particular components of complex biomolecular assemblies can be accomplished at the level of single molecules (Valeur & Berberan-Santos, 2012).

Click chemistry is an exciting development in biological chemistry in recent years. As the most widely utilised type of click chemistry, the copper(I)-catalysed reaction between an azide and a

terminal alkyne is one of the most successful and versatile bioorthogonal reactions providing novel platforms for development of cell labelling methodologies (Amblard et al., 2009; Best, 2009; Kolb et al., 2001; Meldal & Tornoe, 2008).

Both reaction partners of the copper(I)-catalysed azide-alkyne cycloaddition (CuAAC) are small in size without cross-reactivity with molecules found in living cells (Lim & Lin, 2010; Sletten & Bertozzi, 2009). Before the reaction takes place, both reactants are non-toxic and stable kinetically, thermodynamically, and metabolically. The click chemistry reaction takes place under physiological conditions, i.e. ambient temperature and pressure, neutral pH, and aqueous conditions (Lang & Chin, 2014). During the reaction, the two reactants react selectively with each other and form extremely stable 1,4-disubtituted-1,2,3-triazole covalent linkages between the azide and alkyne in a regiospecific manner without any innocuous byproducts (Agard et al., 2006; Hong et al., 2009; Sletten & Bertozzi, 2009). In the presence of a copper(I) catalyst and a stabilising ligand, the reaction rate of this process is boosted approximately one million times faster than the very sluggish uncatalysed [3+2] cycloaddition (Becer, Hoogenboom, & Schubert, 2009; Lewis et al., 2002; Rodionov et al., 2007).

To establish a methodology capable of selectively labelling target cells using copper(I)-catalysed azide-alkyne cycloaddition, one of the reaction partners has to be modified to carry a specifically designed motif that functions as a biomarker to the feature of interest (Nadler & Schultz, 2013; Uttamapinant et al., 2012).

2-Nitroimidazoles (2-NI) have been demonstrated to undergo hypoxia-selective metabolism. By forming covalent associations (adducts) with cellular macromolecules, their reduction products are able to selectively accumulate in hypoxic cells (Arteel, Thurman, & Raleigh, 1998; Franko & Chapman, 1982). This inherent feature has led to derivatives of nitroimidazole being widely used as hypoxia markers (Arteel et al., 1998; Evans et al., 2006).

A 2-NI compound named SN33267 was synthesised by Dr Moana Tercel for this thesis. Due to the presence of a terminal alkyne moiety, SN33267 is capable of incorporating into cellular macromolecules via covalent associations under a reducing environment. To transfer the information of these covalent adducts into an analytically useful signal, indicators are designed by

combining an analyte recognition site with a fluorescent reporter moiety (Boens, Leen, & Dehaen, 2012; Finn & Fokin, 2010; Presolski, Hong, & Finn, 2011; Spiteri & Moses, 2010). In the particular case of this thesis, azide-modified fluorophores were utilised to translate the binding between the analyte (alkyne SN33267) and the recognition site (azide moiety) into a fluorescence output signal by CuAAC.

3.2 Aims

A group of seven complementary candidate azide-modified fluorophores belonging to three chemical families were synthesised by Dr Moana Tercel. This Chapter evaluated the spectral properties of each fluorophore, in relation to the instrument used. On the basis of their fluorescence properties and capability of labelling hypoxic cells via CuAAC, the selected candidate(s) combined with the clickable 2-NI, SN33267, would be employed to optimise the click chemistry-based hypoxia-dependent cell labelling methodology in the following chapters. The specific objectives of this Chapter were:

- To characterise candidate fluorophores by determining absorption- and emission spectra, and ranking the candidates by fluorescence intensity;
- To test the performance of each candidate fluorophore in labelling SiHa cells via CuAAC in a hypoxia-dependent manner;
- To compare microplate reader with flow cytometer in the assessment of fluorescence in cell suspensions labelled with fluorophores via CuAAC;
- To select the best fluorophore(s) in conjunction with SN33267 for hypoxia-selective cell labelling using an initial non-optimised protocol.

3.3 Compounds

One clickable 2-nitroimidazole (SN33267) and 7 azide-modified fluorophores were tested in this chapter (Figure 3.1) (Tercel & Pruijn, 2011). Alexa Fluor 488-azide is commercially available and purchased from Invitrogen New Zealand Limited. The other six azide-modified fluorophores, boron-dipyrromethene 650/665 azide (BODIPY-650/665-azide), boron-dipyrromethene fluorescein-like azide (BODIPY-FL-azide), boron-dipyrromethene Texas Red-like azide (BODIPY-

TR-azide), dimethylaminocoumarin acetic acid azide (DMACA-azide), diethylaminocoumarin azide (DEAC-azide), and a mixture of 5- and 6-isomers of tetramethylrhodamine azide (TAMRA-azide), were made in a single step from the corresponding commercially available fluorophore-succinimide esters.

Apart from the commercially available one, all compounds were synthesised by Dr Moana Tercel at the Auckland Cancer Society Research Centre. Each compound was confirmed for >95% purity by HPLC and stored as concentrated stock solution (20 mM for SN33267, 2 mM for all other fluorophores) in DMSO (Merck KGaA, Darmstadt, Germany) at -80 °C.

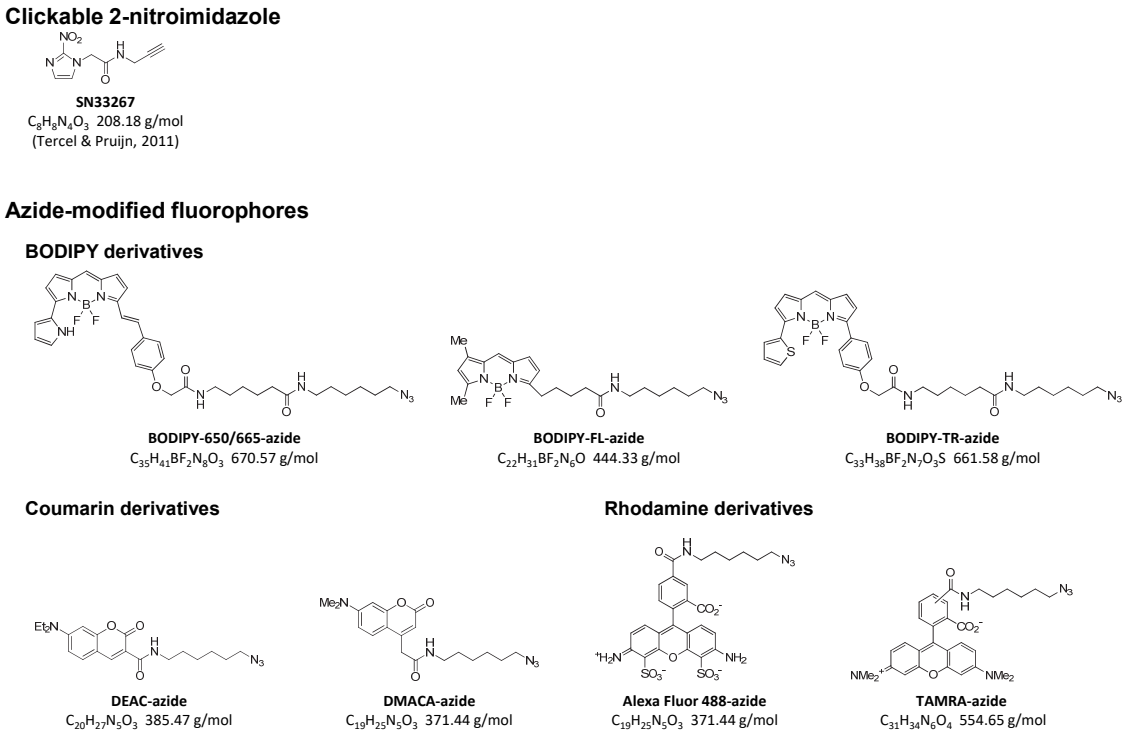

Figure 3.1: Chemical structures of clickable 2-nitroimidazole and candidate azide-modified fluorophores used in this study.

3.4 Results

3.4.1 Characterising fluorescence properties of candidate azide-modified fluorophores

All fluorescence molecules have two characteristic spectra, an excitation spectrum and an emission spectrum. The excitation or emission spectrum depicts the dependence on wavelength of the exciting or emitting light of the fluorescence intensity at a fixed emission or excitation wavelength, respectively.

For each fluorophore an excitation and an emission spectrum were acquired using 200 µL of 100 nM fluorophore PBS solution containing 5% (v/v) DMSO. Both excitation and emission scan were performed using a SpectraMax® M2 multi-mode microplate reader with SoftMax® Pro software (Version 5.0.1; Molecular Devices Co., CA, USA) according to the manufacturer's instructions.

The cutoff filter was able to improve the fluorescence signal to background ratio by allowing the longer wavelength fluorescence to be transmitted but blocking the scattered excitation light. As soon as the optimal excitation (λ_{ex}) and emission wavelengths (λ_{em}) were determined for each fluorophore, a suitable cutoff filter was selected on the basis of its capability to improve the detection of fluorescence signal at the selected optimal emission wavelength (Table 3.1). Those optimal settings of microplate reader were further confirmed by at least 2 independent experiments.

Table 3.1: The optimal settings of microplate reader for quantifying fluorescence signal of candidate fluorophores.

Fluorophore-azide[a]	Parent fluorophore absorption (max.) / emission (max.) [b]	Optimal λ_{ex}	Optimal λ_{em}	Cutoff filter	Signal / Background ratio (max.) [c]	Maximum fluorescence (AU)
Alexa Fluor 488-azide	491/519 nm	488 nm	526 nm	515 nm	314	343
BODIPY-650/665-azide	650/665 nm	610 nm	672 nm	665 nm	61	25
BODIPY-FL-azide	504/513 nm	488 nm	528 nm	515 nm	254	119
BODIPY-TR-azide	588/617 nm	560 nm	624 nm	610 nm	142	32
DEAC-azide	432/472 nm [d]	430 nm	476 nm	455 nm	68	84
DMACA-azide	376/468 nm [e]	380 nm	494 nm	475 nm	148	224
TAMRA-azide	547/574 nm	540 nm	580 nm	570 nm	152	127

Notes:
a. Fluorescence properties of azide-modified fluorophores were determined in 100 nM solutions prepared with PBS (pH 7.4) containing 5% (v/v) DMSO at room temperature using microplate reader;
b. Data courtesy of Molecular Probes (Thermofisher, 2013), unless otherwise noted.
c. Signal / Background ratio was calculated by dividing the microplate reader reading of 100 nM fluorophore solution by the reading of PBS (pH 7.4) containing 5% (v/v) DMSO under the optimal settings;
d. Data courtesy of the product webpage of AnaSpec, Inc. (AnaSpec, 2013a);
e. Data courtesy of the product webpage of AnaSpec, Inc. (AnaSpec, 2013b).

3.4.2 Linear dynamic range

For each azide-modified fluorophore, 100 μM working solution in PBS (pH 7.4) containing 5% (v/v) DMSO was prepared by diluting corresponding 2 mM DMSO stock solution 20 times with PBS (pH 7.4). A series of solutions with different concentrations of the fluorophore were prepared by diluting this 100 μM working solution with PBS (pH 7.4) containing 5% (v/v) DMSO. The intensity of fluorescence emitted from an identical volume (200 μL) of each solution containing a specific concentration of the candidate fluorophore was measured using the optimised settings summarised in Table 3.1 by a microplate reader.

All candidate fluorophores demonstrated that the intensity of the emitted fluorescence was directly proportional to the concentration of the fluorescent substance within a certain range (Figure 3.2). In comparison to other fluorophores that exhibited linearity of fluorescence as a function of concentration over the entire concentration range tested in this experiment, BODIPY-650/665-azide (Figure 3.2A) and BODIPY-TR-azide (Figure 3.2C) showed a relatively narrow linear dynamic range. These two BODIPY-based fluorophores reached a fluorescence intensity plateau

at a relatively low concentration of 100 nM; above 100 nM the fluorescence response was no longer linearly proportional to concentration. Subsequent studies with BODIPY-650/665-azide and BODIPY-TR-azide demonstrated that linear dependency of fluorescence intensity on fluorophore concentration was restricted to the same concentration range of 1-100 nM with both BODIPY-based fluorophores (Figure 3.3 and Table 3.2).

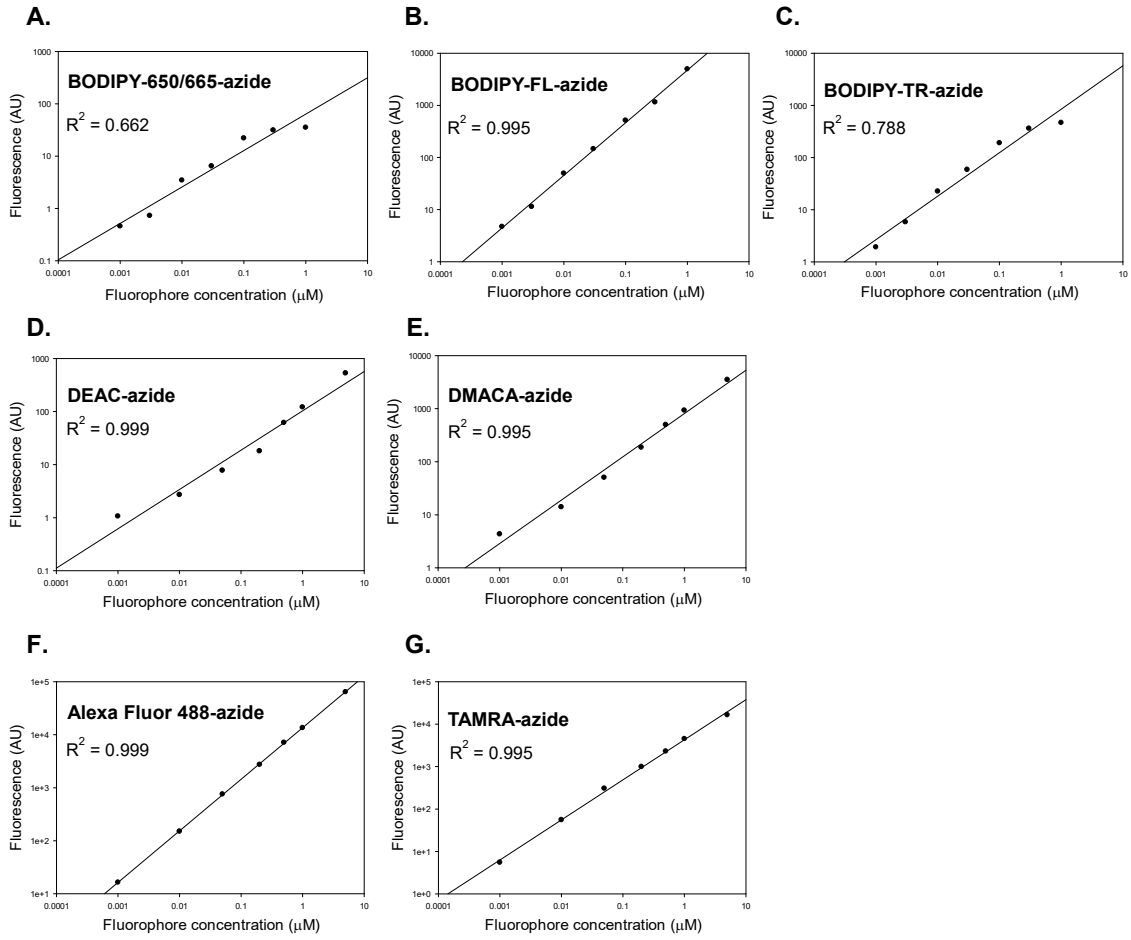

Figure 3.2: Linear dependency of fluorescence intensity on concentration of candidate fluorophores.

(A) BODIPY-650/665-azide; (B) BODIPY-FL-azide; (C) BODIPY-TR-azide; (D) DEAC-azide; (E) DMACA-azide; (F) Alexa Fluor 488-azide; (G) TAMRA-azide. Intensity of fluorescence was measured in a series of solutions with different concentrations of the fluorophore dissolved in PBS (pH 7.4) containing 5% (v/v) DMSO using microplate reader with the settings summarised in Table 3.1. Data points show the intensity of fluorescence emitted from solutions at different concentrations of fluorophore in one representative example of 3 independent experiments. Black lines represent linear regression lines with coefficients of determination (R^2) indicated.

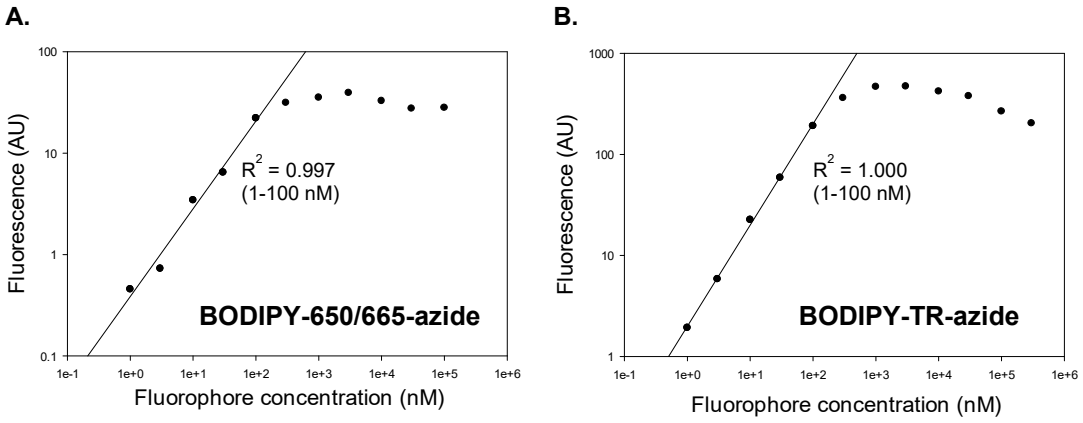

Figure 3.3: Restricted linear dependency of fluorescence intensity and fluorophore concentration.

(A) BODIPY-650/665-azide; (B) BODIPY-TR-azide. Intensity of fluorescence was measured in a series of solutions with different concentrations of the fluorophore dissolved in PBS (pH 7.4) containing 5% (v/v) DMSO using microplate reader with the settings summarised in Table 3.1. Data points show intensity of fluorescence emitted from solutions with different concentrations of fluorophore in one representative example of 3 independent experiments. Black lines represent linear regression lines with coefficients of determination (R^2) indicated. The linear dynamic ranges are indicated in brackets.

Table 3.2: The linear dynamic range of candidate fluorophores in PBS (pH 7.4) containing 5% (v/v) DMSO.

Compound	Linear dynamic range
Alexa Fluor 488-azide	1 nM – 5 µM
BODIPY-650/665-azide	1 nM – 100 nM
BODIPY-FL-azide	1 nM – 1 µM
BODIPY-TR-azide	1 nM – 100 nM
DEAC-azide	30 nM – 5 µM
DMACA-azide	30 nM – 5 µM
TAMRA-azide	1 nM – 5 µM

3.4.3 Correlation of fluorescence with cell number by microplate reader

Characterising the relationship between fluorescence response and particles positively labelled with fluorophores is a fundamental basis for comparison of experimental results in all quantitative fluorescent staining and labelling techniques. To expedite the selection process we tested the possibility that a microplate reader could replace flow cytometry for comparing fluorescence intensity of cells labelled with candidate fluorophores in a hypoxia-dependent manner by click chemistry. We used a non-optimised click chemistry-based hypoxia-dependent cell labelling methodology[2] and investigated the correlation between intensity of fluorescence and density of cell suspension in both cell suspensions containing various densities of fluorophore-labelled cells and cell suspensions consisting of fluorophore-labelled cells mixed with unlabelled cells using a microplate reader.

3.4.3.1 Cell suspensions consisting of a single homogeneous population of cells

To study the correlation between intensity of fluorescence emitted from cells positively labelled with azide-modified fluorophores via click chemistry-based methodology and cell density, we deployed hypoxic SiHa cells incubated with SN33267. Following fixation and permeabilisation, cells were covalently labelled with selected azide-modified fluorophore via the click chemistry-based methodology (see section 2.4) by following the protocol #1 (Figure 2.1) and using the reaction cocktail #1 (Table 2.7).

In both Alexa Fluor 488-azide and BODIPY-FL-azide labelled hypoxic SiHa cells, the emitted fluorescence was proportional to the total number of cells suspended in PBS throughout the entire range of cell densities tested (Figure 3.4). In single cell suspensions consisting of hypoxic SiHa cells labelled with Alexa Fluor 488-azide, a linear regression was calculated to predict fluorescence emitted based on cell density in suspension. A significant regression equation was found ($P < 0.001$), with an R^2 of 0.981. The regression equation was fluorescence intensity (AU) = 7.460 + 0.00159 * cell density (cells/mL). In the case of SiHa cells labelled with BODIPY-FL-

[2] All click chemistry-based hypoxia-specific cell labelling experiments in Chapter 3 were performed by following the unoptimised protocol (protocol #1 in Figure 2.1) and using the reaction cocktail #1(Table 2.7). All other technical details are outlined in section 2.4.

azide, a linear regression was calculated to predict fluorescence emitted based on cell density in suspension. A significant regression equation was found ($P < 0.001$), with an R^2 of 0.995.

The fluorescent signal emitted from fixed and permeabilised SiHa cells labelled with BODIPY-FL-azide suspended in PBS solution was relatively stable for at least 35 min at RT and ambient light conditions (Figure 3.5).

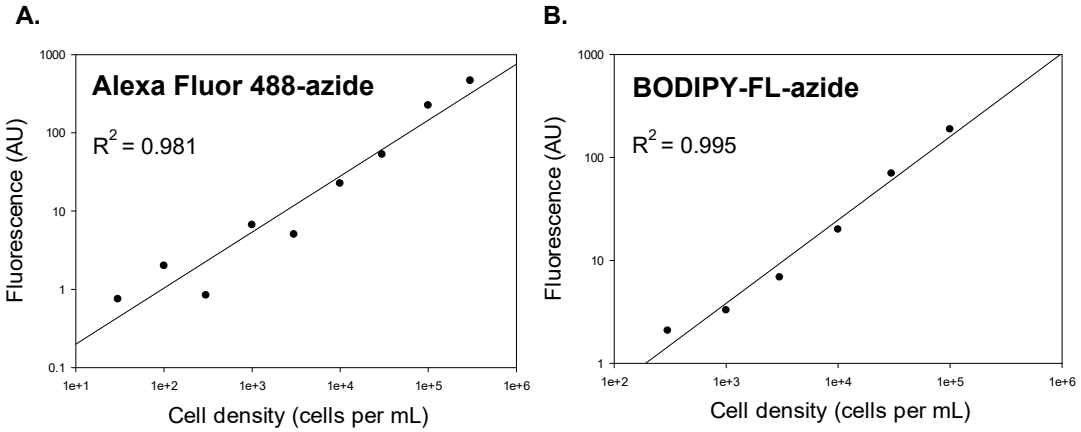

Figure 3.4: Linear dependency of fluorescence intensity and density of fluorophore-labelled cells in suspensions consisting of a single homogeneous population.

After a 2-h incubation with 100 µM SN33267 under hypoxic conditions, SiHa cells were fixed and permeabilised, which was followed by labelling with azide-modified fluorophore, Alexa Fluor 488-azide (A) or BODIPY-FL-azide (B), using click chemistry-based methodology. A series of suspensions of positively labelled SiHa cells were made using PBS (pH 7.4) as the diluent. Aliquots of each suspension (200 µL) were pipetted into microplates. An equal volume of PBS was used for background. The fluorescence was determined using the settings listed in Table 3.1 by microplate reader. Background reading was subtracted. Representative data from 3 independent experiments are shown. Data points show intensity of fluorescence emitted from cell suspension samples with different density of fluorophore-labelled cells. Black lines represent linear regression lines with coefficients of determination (R^2) indicated.

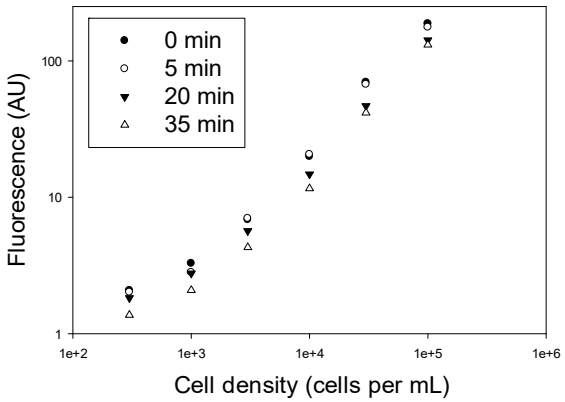

Figure 3.5: Stability of fluorescent signals of hypoxic SiHa cells labelled with BODIPY-FL-azide.

The same series of suspensions of hypoxic SiHa cells labelled with BODIPY-FL-azide from Figure 3.4B were used to test the stability of fluorescent signals. The fluorescence was determined immediately after loading the microplate (the t = 0 min time point) and at each indicated time point (see the legend) using the settings listed in Table 3.1 by microplate reader. Aliquots loaded into the microplate were kept at RT and exposed to ambient light between measurements. Data points show intensity of fluorescence emitted from cell suspension samples with different density of fluorophore-labelled cells. Plot is representative of at least 2 independent experiments.

3.4.3.2 Cell suspensions consisting of two heterogeneous populations of cells

The correlation between intensity of emitted fluorescence and density of cells labelled with fluorophore was further investigated. Instead of cell suspensions consisting of a single homogeneous population of positively labelled hypoxic cells with different cell densities, a series of cell suspensions consisting of two types of cells were used. By mixing fluorophore-labelled cells (Hypoxic_SN33267+_Azide+) with unlabelled cells (Hypoxic_SN33267+_Azide-), single cell suspensions at identical cell density were prepared with different fractions of fluorophore-labelled cells.

All three azide-modified fluorophores (Alexa Fluor 488-azide, BODIPY-FL-azide, and TAMRA-azide) showed similar trends of augmented intensity of fluorescence in relation to increased percentage of fluorophore-labelled cells in the cell suspension (Figure 3.6 and Figure 3.7). Unlike the results generated by cell suspensions consisting of a single homogeneous population of cells

(section 3.4.3.1), the linearity of data of all three fluorophores shown in both Figure 3.6 and Figure 3.7 was restricted to the range of 0.3–100% positively labelled cells.

In single cell suspension made by mixing hypoxic SiHa cells labelled with Alexa Fluor 488-azide and unlabelled cells, a relationship was calculated to predict fluorescence emitted based on the percentage of fluorophore positively labelled cells in suspension within the range of 0.3–100% positively labelled cells (Figure 3.6A). An equation was found ($F(1, 5) = 4545.081$, $P < 0.001$), with an R^2 of 0.999. The equation was fluorescence intensity (AU) = 2.325 + 3.203 * percentage of fluorophore positively labelled cells.

In single cell suspension made by mixing hypoxic SiHa cells labelled with BODIPY-FL-azide and unlabelled cells, the relationship was calculated to predict fluorescence emitted based on the percentage of fluorophore positively labelled cells in suspension within the range of 0.3–100% positively labelled cells (Figure 3.6B). An equation was found ($F(1, 5) = 3857.256$, $P < 0.001$), with an R^2 of 0.999. The equation was fluorescence intensity (AU) = 6.952 + 5.337 * percentage of fluorophore positively labelled cells.

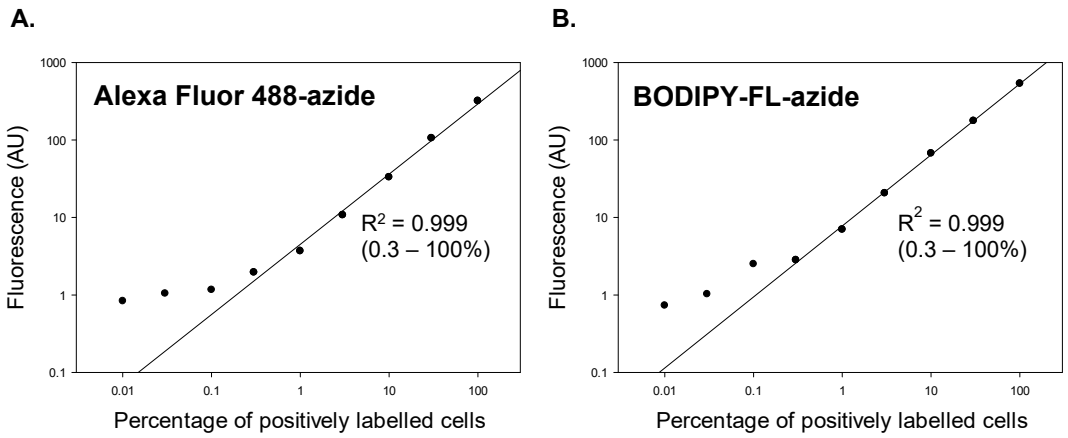

Figure 3.6: Relationship between fluorescence intensity and percentage of fluorophore-labelled cells in suspension consisting of two heterogeneous populations.

(A) Alexa Fluor 488-azide; (B) BODIPY-FL-azide. SiHa cells were incubated with 100 μM SN33267 for 2 h under hypoxic conditions. Following fixation and permeabilisation, cells were split into two samples. One sample was labelled with azide-modified fluorophore using the click chemistry-based methodology (positively labelled cells). Another sample was served as negative control by incubating with fluorophore-free reaction cocktail following the same protocol. A series of suspensions with equal density (3×10^5 cells/mL) were carefully prepared by mixing the two types of cells in PBS (pH 7.4). Each suspension contained a different percentage of cells positively labelled with fluorophore. Aliquots of each suspension (200 μL) were pipetted into microplates. The fluorescence was determined using the settings listed in Table 3.1 by microplate reader. Representative data from 3 independent experiments are shown. Data points indicate intensity of fluorescence emitted from cell suspension samples with different percentage of fluorophore-labelled cells. Black lines represent linear regression lines with coefficients of determination (R^2) indicated. The linear dynamic ranges are indicated in brackets.

Both assays using TAMRA-azide demonstrated linearity within the same percentage range of positively labelled cells as indicated by coefficients of determination. In cell suspension obtained by mixing fixed and permeabilised hypoxic SiHa cells labelled with TAMRA-azide and unlabelled cells (Figure 3.7A), a significant association ($F(1, 5) = 790.418$, $P < 0.001$, $R^2 = 0.995$) was calculated to predict fluorescence emitted based on the percentage of fluorophore positively labelled cells in suspension within the range of 0.3–100% positively labelled cells by use of the equation fluorescence intensity (AU) = 0.713 + 0.423 * percentage of fluorophore positively labelled cells. In the assay of cell suspensions containing two types of non-fixed hypoxic SiHa cells (Figure 3.7B), a significant association was also found between fluorescence intensity and percentage of fluorophore-labelled cells ($F(1, 5) = 2816.886$, $P < 0.001$, $R^2 = 0.999$). An equation, fluorescence intensity (AU) = 0.651 + 0.760 * percentage of fluorophore positively labelled cells, was valid within the range of 0.3–100% positively labelled cells.

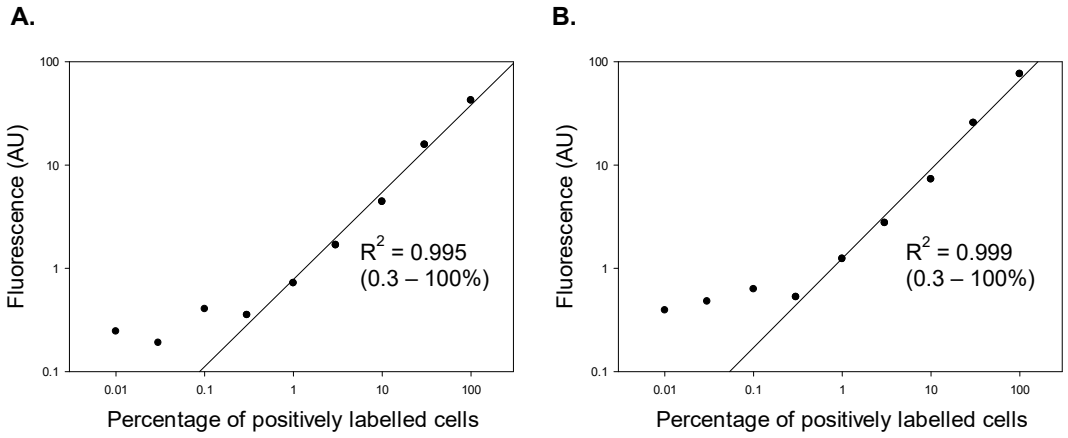

Figure 3.7: Relationship between fluorescence intensity and percentage of TAMRA-labelled cells in suspension consisting of two heterogeneous populations.

(A) Fixed and permeabilised cells; (B) Unfixed cells. SiHa cells were incubated with 100 µM SN33267 for 2 h under hypoxic conditions. Cells, with or without fixation and permeabilisation, were split into two samples. One sample was labelled with TAMRA-azide using the click chemistry-based methodology (positively labelled cells). Another sample was served as negative control by incubating with fluorophore-free reaction cocktail following the same protocol. A series of suspensions with equal density (3×10^5 cells/mL) were carefully prepared by mixing the two types of cells in PBS (pH 7.4). Each suspension contained different percentage of cells positively labelled with fluorophore. Aliquots of each suspension (200 µL) were pipetted into microplates. The fluorescence was determined using the settings listed in Table 3.1 by microplate reader. Representative data from 3 independent experiments are shown. Data points show intensity of fluorescence emitted from cell suspension samples with different percentage of fluorophore-labelled cells. Black lines represent linear regression lines with coefficients of determination (R^2) indicated. The linear dynamic ranges are indicated in brackets.

3.4.4 Selection of candidate azide-modified fluorophores by flow cytometer based hypoxia-selective cell labelling

Fluorescence intensity was evaluated by use of a microplate reader in section 3.4.3. Experimental data generated by two fluorophore-modified azides indicated that the CuAAC-mediated cell labelling was in a hypoxia-dependent manner and the microplate reader was capable of assessing fluorescence intensity in cell suspensions as an alternative solution to replace flow cytometry.

3.4.4.1 Experimental design

Fluorescence detection sensitivity is severely influenced by background signals. The major sources of background signals include the signal originated from endogenous sample constituents (autofluorescence) and the signals from unbound or non-specifically bound probes (reagent background) (Drummen, 2012; Fritzsche & Mandenius, 2010; Monici, 2005). In order to isolate the contribution of background signals in CuAAC-mediated cell labelling with fluorophores, five different sample-treatments were used to investigate the labelling selectivity for hypoxic cells with each candidate fluorophore (Table 3.3). Click chemistry-based cell labelling experiments using SiHa cells incubated for 3.5 hr under oxic or hypoxic conditions were performed following a non-optimised protocol (protocol #1; Figure 2.1) using reaction cocktail #1 (Table 2.7). The labelling selectivity for hypoxic cells was used as the most important criterion for the selection of candidate azide-modified fluorophores. Fluorescence intensity was determined using both microplate reader and flow cytometry (BD FACSAria™ II Cell Sorter for TAMRA dye and BD LSR II Flow Cytometer for others with BD FACSDiva™ Software; version 6.1.3; BD Biosciences, MA, USA).

In each experiment, a ratio was calculated using the fluorescence intensity reading of the Hypoxic_SN33267+_Azide+ sample divided by the reading of the Oxic_SN33267+_Azide+ sample was termed “hypoxic/oxic ratio”. This ratio indicated the labelling selectivity of hypoxic cells and was a measure of the performance of the click chemistry-based cell labelling approach. Alternatively, this ratio can also be calculated by readings of these two samples after background subtraction. Since the background signal (the fluorescence reading of Hypoxic_SN33267+_Azide-) was low compard with fluorescence intensities of these two samples labelled with azide, the influence of background signals was ignored here.

Table 3.3: Experimental samples used in the selection of candidate fluorophores.

Sample Name	Incubation with 2-NI		Click reaction with azide-modified fluorophore	Research Purpose
Hypoxic_SN33267-_Blank	anoxic	DMSO	TBS buffer	Measure of autofluorescence
Hypoxic_SN33267+_Azide-	anoxic	SN33267	Reaction cocktail without fluorophore	Measure of background signal induced by 2-NI
Hypoxic_SN33267-_Azide+	anoxic	DMSO	Reaction cocktail including 10 μM fluorophore	Measure of background signal induced by fluorophore via non-covalent interactions
Oxic_SN33267+_Azide+	oxic	SN33267	Reaction cocktail including 10 μM fluorophore	Measure of designed labelling selectivity
Hypoxic_SN33267+_Azide+	anoxic	SN33267	Reaction cocktail including 10 μM fluorophore	To detect hypoxic-selective labelling via click reaction

Notes: Concentration of SN33267 was 100 μM.

The assessment of relationship between two groups of data was performed using Pearson correlation. These statistical procedures were undertaken using SigmaPlot for Windows (version 11, 12, or 12.5; Systat Software Inc., CA, USA). For each statistical test, a *P*-value less than 0.05 was regarded as a statistically significant difference.

3.4.4.2 Alexa Fluor 488-azide

Alexa Fluor 488-azide demonstrated very good labelling results in SiHa cells with fixation and permeabilisation (Figure 3.8). Hypoxic/oxic ratio of 13.1 and 55.1 were calculated using fluorescence intensity determined by a microplate reader (Fluorescence AU) and flow cytometry (median fluorescence intensity; MFI), respectively. In the flow cytometric histogram, the peak (blue) representing the SiHa cells labelled with Alexa Fluor 488-azide was completely separated from the peak (dark green) representing the oxic SiHa cells (Figure 3.8B).

To determine if the fluorescence intensity data measured using microplate reader were correlated to the data determined by flow cytometry, linear regression was used to analyse the relationship between these values. The linear regression was highly significant ($P < 0.001$) with the R^2 value of 0.996 (Figure 3.8C), indicating there was a strong correlation between microplate reader data and flow cytometry data.

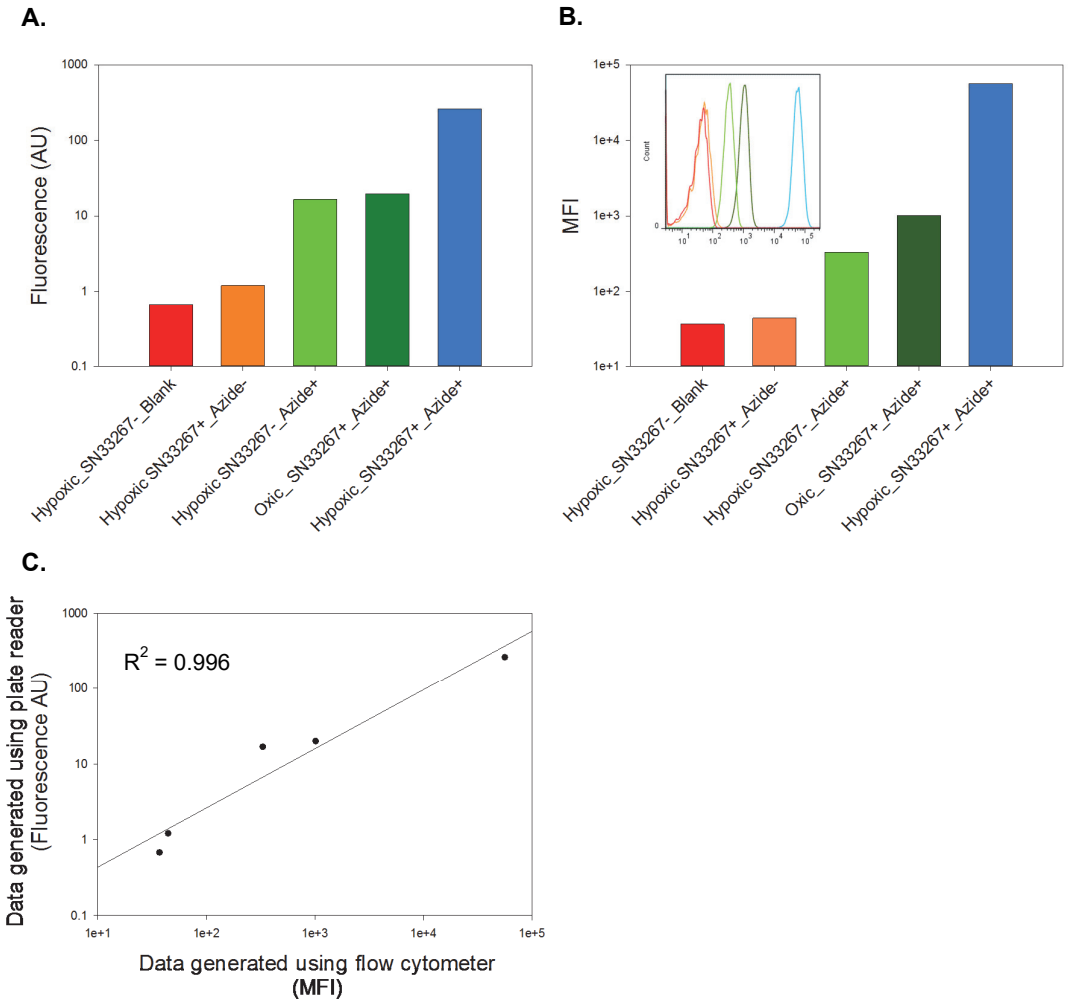

Figure 3.8: Test of hypoxia-specific cell labelling by Alexa Fluor 488-azide.

Measurement of fluorescence intensity in fixed and permeabilised SiHa cells labelled with Alexa Fluor 488-azide in a hypoxia-selective manner. (A) Fluorescence intensity determined by microplate reader. Each cell sample was diluted with PBS (pH 7.4) to reach an equal final density of 50,000 cells/mL. Fluorescence was measured using a volume of 200 µL. (B) Fluorescence intensity determined by flow cytometry. Each bar represents the median fluorescence intensity (MFI) of sample read from the flow cytometry histogram. (C) Data of fluorescence intensity generated using two different instruments were analysed by linear regression to predict relationship. Representative data from 3 independent experiments are shown.

3.4.4.3 BODIPY-FL-azide

Similar trends of fluorescence intensity among the samples were observed in SiHa cells with or without fixation and permeabilisation and labelled with BODIPY-FL-azide (Figure 3.9A and B). Unlike the promising hypoxic/oxic ratios calculated from the Alexa Fluor 488-azide data, the difference in fluorescence intensity between oxic cells and hypoxic cells generated by labelling with BODIPY-FL-azide, however, was not as marked as Alexa Fluor 488-azide. Hypoxic/oxic ratios of 1.8 and 2.8 were produced using fluorescence intensity determined by microplate reader (Fluorescence AU) and flow cytometry (MFI), respectively.

The peak (blue) representing the fluorescence signals of the hypoxic SiHa cells labelled with BODIPY-FL-azide was only partially separated from the peak (dark green) representing the signals of the oxic SiHa cells in the flow cytometric histogram (Figure 3.9B).

In the case of BODIPY-FL-azide, the click chemistry-based labelling was also tested in non-fixed SiHa cells. The trend of fluorescence intensity among samples shared the same pattern as seen with fixed and permeabilised SiHa cells (Figure 3.9D and E). Hypoxic/oxic ratios of 1.9 and 4.9 were calculated using fluorescence intensity determined by microplate reader (Fluorescence AU) and flow cytometry (MFI), respectively.

In the flow cytometric histogram, the peak (blue) representing the fluorescence signals of the hypoxic SiHa cells labelled with BODIPY-FL-azide still partially overlapped with the peak (dark green) representing the signals of the oxic SiHa cells (Figure 3.9E).

To determine if the fluorescence intensity data measured using microplate reader were related to the data determined by flow cytometry, the analysis was performed to analyse the relationship between these two groups of data. In both cases, the data generated by microplate reader were strongly correlated with the data generated by flow cytometry ($R^2 = 0.996$, $P < 0.001$ in fixed and permeabilised SiHa cells, Figure 3.9C; $R^2 = 0.913$, $P = 0.0011$ in non-fixed SiHa cells, Figure 3.9F).

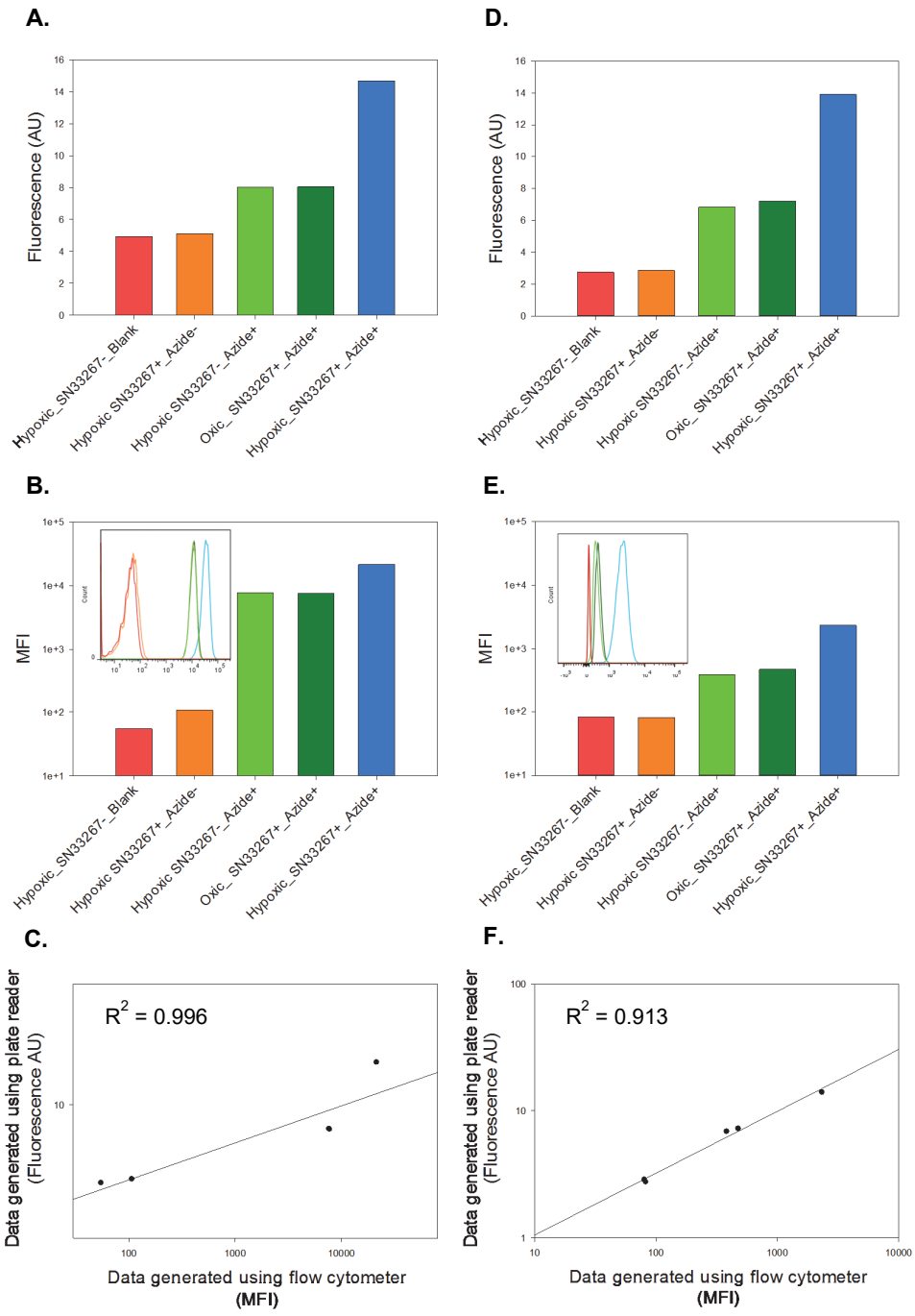

Figure 3.9: Test of hypoxia-selective cell labelling by BODIPY-FL-azide.

SiHa cells were incubated under oxic or hypoxic conditions and labelled with BODIPY-FL-azide in a hypoxia-specific manner. Graph A to C are data generated by SiHa cells with fixation and permeabilisation. Graph D to F are data generated by non-fixed SiHa cells. A and D show the fluorescence intensity of cell samples quantified by using microplate reader. Each cell sample was diluted with PBS (pH 7.4) to reach the equal final density of 25,000 cells/mL. Fluorescence was measured using 200 µL of aliquot. B and E show the histogram and the median fluorescence intensity (MFI) of the same group of cell samples determined using flow cytometry. In graph C and F, data of fluorescence in cell samples generated using two different instruments were analysed by Pearson correlation to predict relationship. Representative data from 3 independent experiments are shown.

3.4.4.4 TAMRA-azide

In fixed and permeabilised SiHa cells, TAMRA-azide did not show obvious selectivity in labelling hypoxic cells based on the fluorescence data determined by microplate reader (Figure 3.10A). The same group of samples provided better results in hypoxic-selective labelling when the measurement of fluorescence was accomplished by using flow cytometry (Figure 3.10B). Such differences in experimental data produced by using different approaches in fluorescence signal quantitation can also be indicated by hypoxic/oxic ratios. The hypoxic/oxic ratio calculated using flow cytometry data is 11.6 that is considerably greater than the ratio generated from the microplate reader data, 1.3.

The flow cytometric histogram in Figure 3.10B shows that the spike (dark green) representing the fluorescence signals carried by hypoxic SiHa cells labelled with TAMRA-azide is nearly completely separated from the spike (light green) representing the signals carried by oxic SiHa cells.

Similar to BODIPY-FL-azide, the hypoxia-mediated selectivity of TAMRA-azide in click chemistry-based labelling was also tested in non-fixed SiHa cells. The trend of fluorescence intensity among samples shared the same pattern from fixed and permeabilised SiHa cells. But the labelling-selectivity to non-fixed hypoxic cells is not as good as in SiHa cells with fixation and permeabilisation. The hypoxic/oxic ratio of 1.8 and 3.4 were calculated using fluorescence intensity measured by microplate reader (Fluorescence AU) and flow cytometry (MFI), respectively.

In the flow cytometric histogram, the spike (dark green) representing the fluorescence signals carried by hypoxic SiHa cells labelled with TAMRA-azide still partially overlapped with the spike (light green) representing the signals carried by oxic SiHa cells (Figure 3.10E).

To determine if the fluorescence intensity data measured using microplate reader were related to the data determined by flow cytometry, Pearson correlation was performed to analyse the relationship between these two groups of data. In fixed and permeabilised SiHa cells, the result is $R^2 = 0.632$, $P = 0.108$. The trend is in the expected direction, but it is not quite significant (Figure 3.10C). In non-fixed SiHa cells, there is a strong association between the data generated by

microplate reader and the data generated by flow cytometry with R^2 value of 0.919 (P = 0.010; Figure 3.10F).

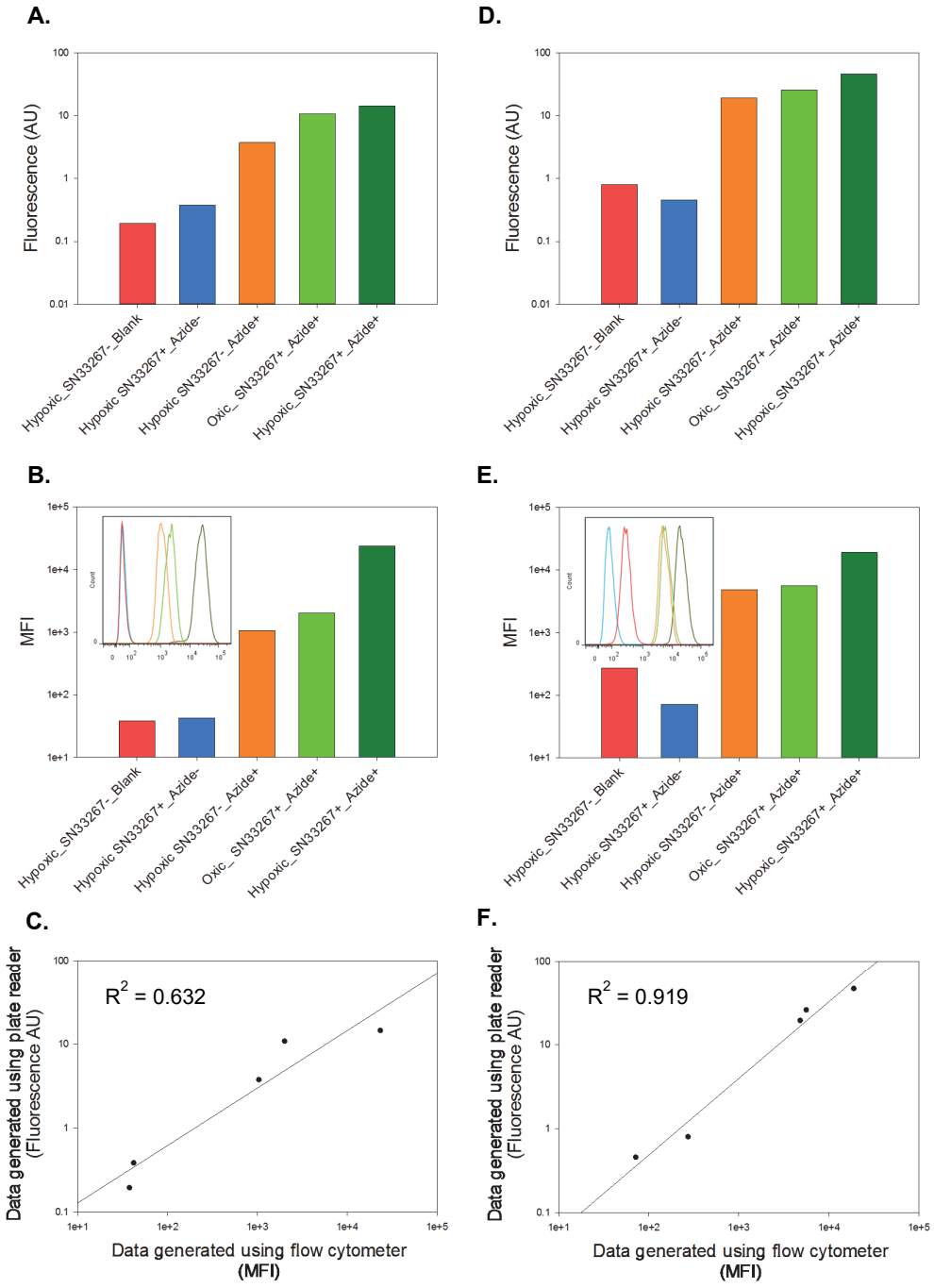

Figure 3.10: Test of hypoxia-selective cell labelling by TAMRA-azide.

SiHa cells were incubated under oxic or hypoxic conditions and labelled with TAMRA-azide in a hypoxia-selective manner. Graph A to C are data generated by SiHa cells with fixation and permeabilisation. Graph D to F are data generated by non-fixed SiHa cells. A and D show the fluorescence intensity of cell samples quantified by using microplate reader. Each cell sample was diluted with PBS (pH 7.4) to reach the equal final density of 40,000 cells/mL. Fluorescence was measured using 200 µL of aliquot. B and E show the histogram and the median fluorescence intensity (MFI) of the same group of cell samples determined using flow cytometry. In graph C and F, data of fluorescence in cell samples generated using two different instruments were analysed by Pearson correlation to predict relationship. Representative data from 3 independent experiments are shown.

3.4.4.5 BODIPY-650/665-azide

BODIPY-650/665-azide demonstrated highly limited selectivity in labelling hypoxic SiHa cells with fixation and permeabilisation. Based on the data generated by microplate reader, the sample of hypoxic cells with access to both SN33267 (clickable 2-NI) and BODIPY-650/665-azide (fluorophore), technically supposed to be labelled with high selectivity, even demonstrated lower level of fluorescence in comparison with oxic cells (hypoxic/oxic ratio of 0.7). All 3 samples labelled with the BODIPY-650/665-azide during the experiment showed very similar intensity of fluorescence independent to individual hypoxic status (Figure 3.11A). Such observations were further confirmed by flow cytometry data (Figure 3.11B). In the flow cytometric histogram, the spikes in light green, dark green, and blue represent the fluorescence signals carried by 3 samples that had access to BODIPY-650/665-azide during the incubation with reaction cocktail. All 3 spikes almost overlap to each other (hypoxic/oxic ratio of 1.7), which indicate that BODIPY-650/665-azide may label fixed and permeabilised SiHa cells in a manner independent to cell hypoxia status and clickable 2-NI.

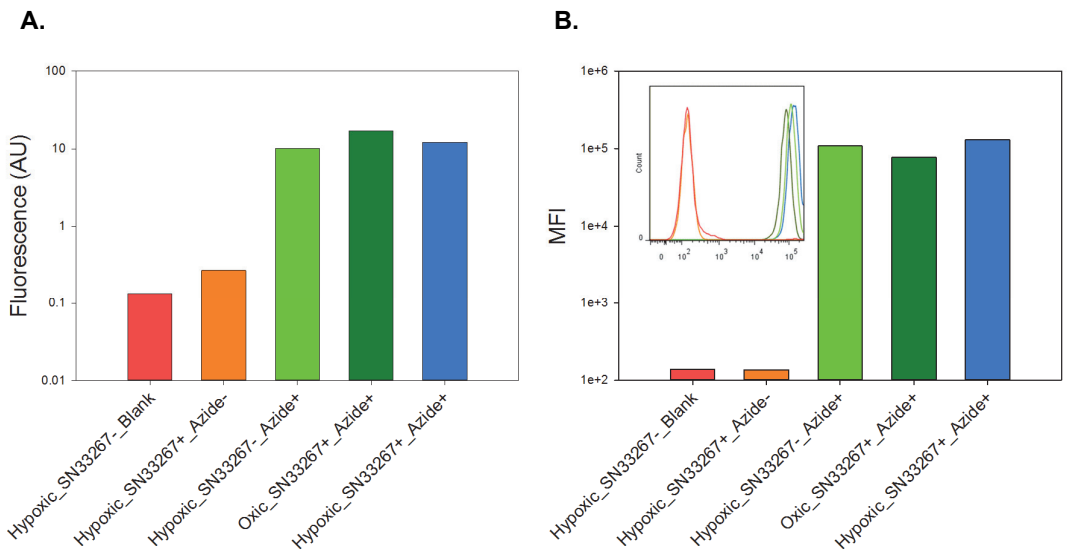

Figure 3.11: Test of hypoxia-selective cell labelling by BODIPY-650/665-azide.

SiHa cells were incubated under oxic or hypoxic conditions. After fixation and permeabilisation, cells were labelled with BODIPY-650/665-azide, which supposed to be in a hypoxia-selective manner. (A) Fluorescence intensity determined by microplate reader. Each cell sample was diluted with PBS (pH 7.4) to reach the equal final density of 40,000 cells/mL. Fluorescence was measured using 200 µL of aliquot. (B) Fluorescence intensity determined by flow cytometry. Each bar represents the median fluorescence intensity (MFI) of sample read from the flow cytometry histogram. Data are representative of 3 independent experiments.

3.4.4.6 BODIPY-TR-azide

Since the strong correlations between fluorescence data generated by different technical approaches (microplate reader and flow cytometry) have been demonstrated in cells labelled with different types of fluorophore, microplate reader was used alone to investigate the features of BODIPY-TR-azide in hypoxia-selective cell labelling.

Two azide-modified BODIPY fluorophores shared very similar characters in labelling fixed SiHa cells. Two independent experiments profiled very similar features of BODIPY-TR-azide in cell labelling. The hypoxic sample with access to both SN33267 (clickable 2-NI) and BODIPY-TR-azide (fluorophore) showed lower level of fluorescence in comparison with the oxic counterpart (hypoxic/oxic ratio of 0.7). All samples with access to BODIPY-TR-azide during the experiment showed very similar intensity of fluorescence independent to individual hypoxic status or even clickable 2-NI (Figure 3.12).

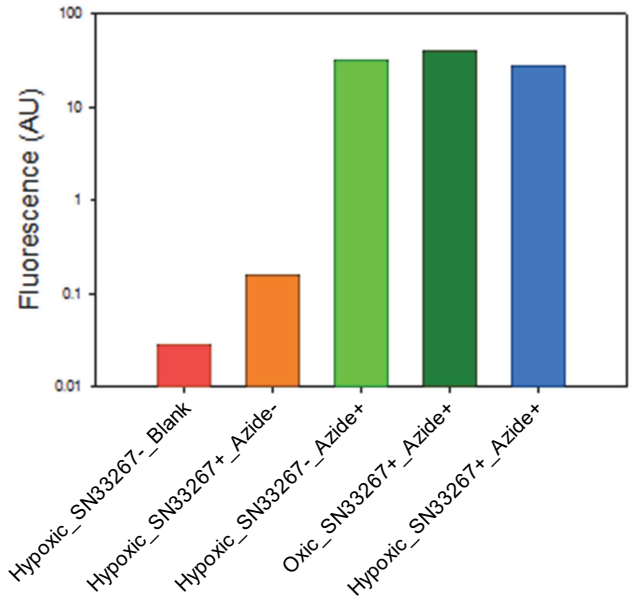

Figure 3.12: Test of hypoxia-selective cell labelling by BODIPY-TR-azide.

Fluorometry analysis of BODIPY-TR-azide in fixed and permeabilised SiHa cells using microplate reader. Each cell sample was diluted with PBS (pH 7.4) to reach the equal final density of 40,000 cells/mL. Fluorescence was measured using 200 µL of aliquot. Data are representative of 2 independent experiments.

3.4.4.7 DEAC-azide

Similar to both BODIPY-650/665-azide and BODIPY-TR-azide, another azide-modified fluorophore, structurally belonging to coumarin family, also shows very similar characters in labelling fixed SiHa cells. The hypoxic sample with access to both SN33267 (clickable 2-NI) and DEAC-azide (fluorophore) showed nearly equal level of fluorescence in comparison with the oxic counterpart (hypoxic/oxic ratio of 0.5). All samples with access to DEAC-azide during the experiment showed very similar intensity of fluorescence independent to either individual hypoxic status or even clickable 2-NI (Figure 3.13).

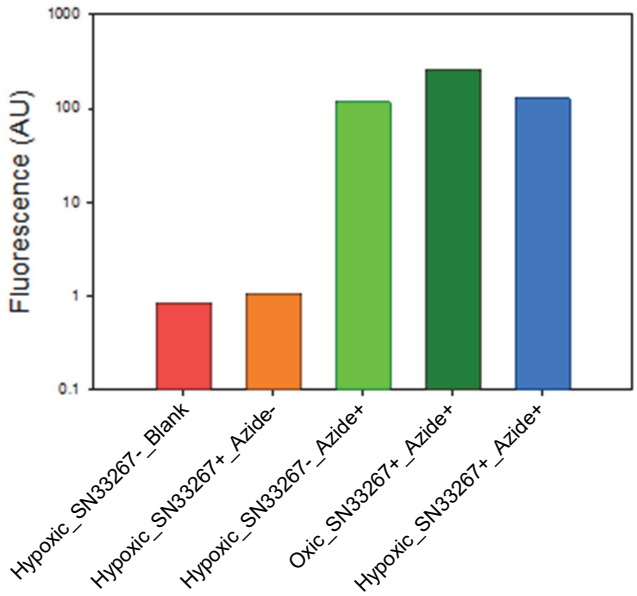

Figure 3.13: Test of hypoxia-selective cell labelling by DEAC-azide.

Fluorometry analysis of DEAC-azide in fixed and permeabilised SiHa cells using microplate reader. Each cell sample was diluted with PBS (pH 7.4) to reach the equal final density of 40,000 cells/mL. Fluorescence was measured using 200 µL of aliquot. Data are representative of 2 independent experiments.

3.4.4.8 DMACA-azide

Another member of coumarin family, DMACA-azide, also did not demonstrate hypoxia-selectivity in labelling fixed and permeabilised SiHa cells based on the data generated by using microplate reader as an approach to quantify fluorescence intensity (hypoxic/oxic ratio of 1.0; Figure 3.14A).

Since we planned that one from each chemical family on the candidate list could be selected and used in optimising click chemistry based hypoxia-selective labelling methodology, flow cytometry was also deployed in the study of DMACA-azide.

According to the data generated by using flow cytometry as an approach to quantify fluorescence intensity, the overall fluorescence intensity of cells labelled with DMACA-azide was about one order of magnitude lower than labelling with other fluorophores mentioned previously in this Chapter under the same experimental conditions. The difference in fluorescence intensity determined from hypoxic sample (blue bar) and the oxic counterpart (dark green bar) indicated a certain level of hypoxia selectivity (hypoxic/oxic ratio of 4.9) in click chemistry-based cell labelling mediated by DMACA-azide (Figure 3.14B). In the flow cytometric histogram, the spike (blue) representing the fluorescence signals carried by hypoxic SiHa cells labelled with TAMRA-azide nearly completely separated from the spike (dark green) representing the signals carried by oxic SiHa cells (Figure 3.14B).

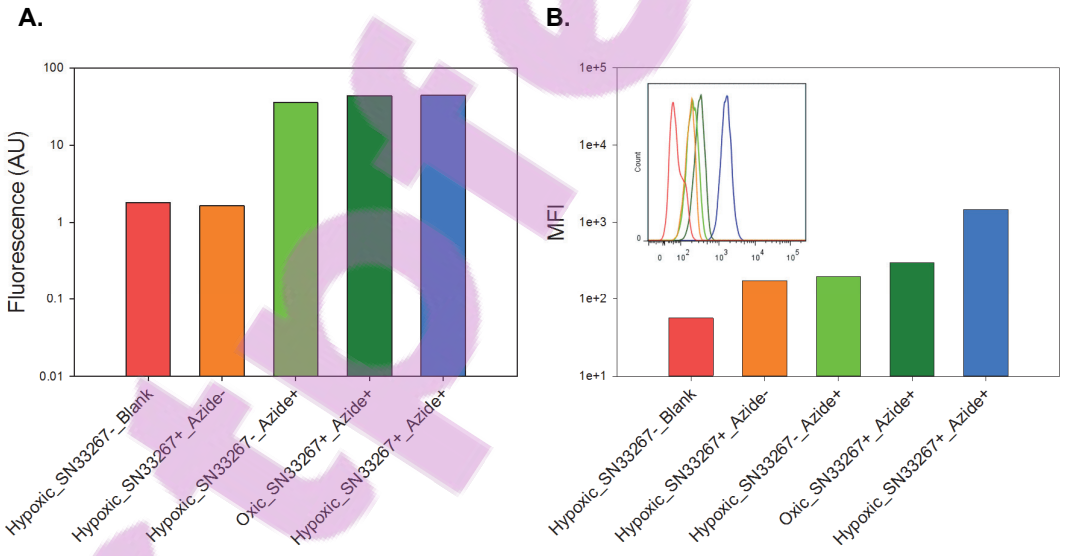

Figure 3.14: Test of hypoxia-selective labelling by DMACA-azide in fixed cells.

SiHa cells were incubated under oxic or hypoxic conditions. After fixation and permeabilisation, cells were labelled with DMACA-azide in a hypoxia-selective manner. (A) Fluorescence intensity determined by microplate reader. Each cell sample was diluted with PBS (pH 7.4) to reach the equal final density of 40,000 cells/mL. Fluorescence was measured using 200 µL of aliquot. (B) Fluorescence intensity determined by flow cytometry. Each bar represents the median fluorescence intensity (MFI) of sample read from the flow cytometry histogram. Representative data from 3 independent experiments are shown.

In non-fixed SiHa cells, DMACA-azide also demonstrated a certain level of hypoxia-selectivity (hypoxic/oxic ratio of 5.3) in click chemistry-based cell labelling according to flow cytometry data (Figure 3.15A). Under the same experimental conditions, there was generally about one order of magnitude reduction in fluorescence intensity in non-fixed SiHa cells in comparison with fixed and permeabilised cells.

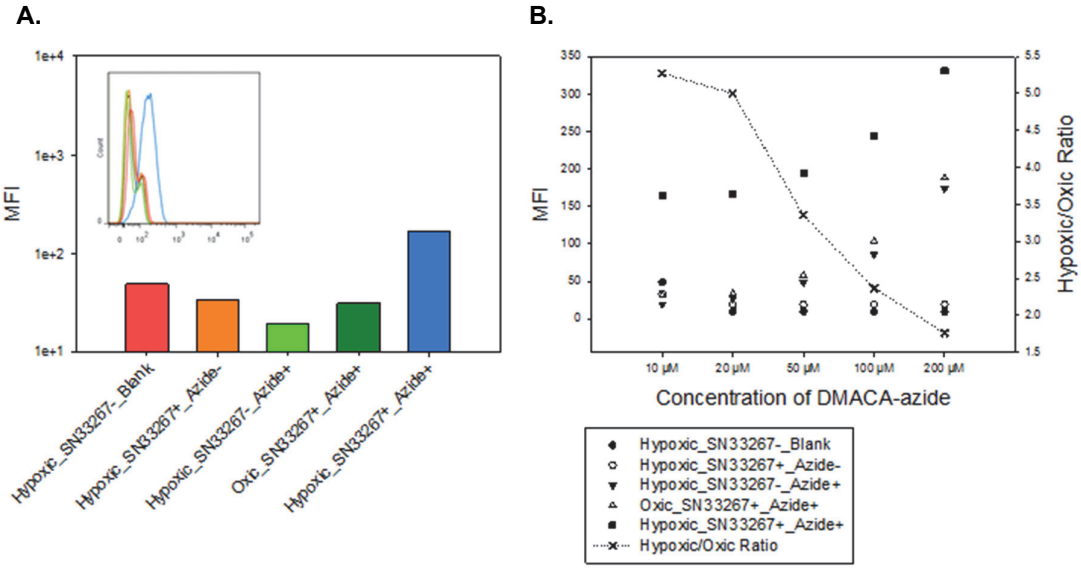

Figure 3.15: Flow cytometry analysis of non-fixed cells labelled with DMACA-azide in a hypoxia-selective manner.

SiHa cells were incubated under oxic or hypoxic conditions. Cells were labelled with DMACA-azide in a hypoxia-selective manner. (A) Fluorescence intensity determined by flow cytometry. 10 µM DMACA-azide was used in reaction cocktail. Each bar represents the median fluorescence intensity (MFI) of sample read from the flow cytometry histogram. (B) SiHa cells labelled with DMACA-azide in a concentration-dependent manner. Representative data from at least 2 independent experiments are shown.

To test if elevated concentrations of DMACA-azide in the reaction cocktail could improve the hypoxic/oxic ratio by selectively enhancing the fluorescence labelling in hypoxic cells, a range of concentrations (10-200 µM) of DMACA-azide were tested in non-fixed SiHa cells (Figure 3.15B). With increasing concentration of DMACA-azide, the intensity of fluorescence was increased in the hypoxic sample. However, enhanced fluorescence intensity was also observed in both the oxic sample and in the hypoxic sample incubated without SN33267. As a consequence, the hypoxic/oxic ratio, indicating the overall performance of hypoxia-selective labelling, dropped down with increasing concentration of DMACA-azide.

3.4.5 Correlation between fluorescence data determined by microplate reader and flow cytometry

As shown above a strong correlation existed between microplate reader data and flow cytometry data in quantifying fluorescence intensity in SiHa cells labelled with 10 μM of Alexa Fluor 488-azide (in cells with fixation and permeabilisation; section 3.4.4.2), BODIPY-FL-azide (in both cells with fixation and permeabilisation and non-fixed cells; section 3.4.4.3), as well as TAMRA-azide (in non-fixed cells; section 3.4.4.4).

Experimental data determined by both approaches demonstrated the dose-dependent increase in fluorescence intensity of hypoxic cell samples. However, very similar dose-dependent effects were also observed in both oxic and hypoxic cell samples without incubating with clickable 2-NI across the gradient of applied TAMRA-azide concentrations, which severely compromised the hypoxic/oxic ratio (Figure 3.16A and B). Above a certain concentration of TAMRA-azide, when the increase of fluorescence intensity in hypoxic samples was not able to respond as fast as oxic samples to the increase in applied concentration of TAMRA-azide, the labelling selectivity for hypoxic cells started to decrease. As the indicator of the overall performance of hypoxia-selective cell labelling, the hypoxic/oxic ratio responded to the increase in the applied concentration of TAMRA-azide in the exactly same manner. The hypoxic/oxic ratio was elevated with the increase in applied concentration of TAMRA-azide in the range of 0.05-5 μM. With a further rise in TAMRA-azide concentration (5-100 μM), the ratio decreased. Both measurement methods for fluorescence intensity showed that a concentration of 5 μM achieved optimal hypoxia-selectivity in labelling non-fixed SiHa cells (Figure 3.16A and B).

To determine if the fluorescence intensity data measured using microplate reader were related to the data determined by flow cytometry, data generated by each approach in different concentration of TAMRA-azide were pooled together and correlation analysis was used to analyse the relationship between 2 groups of data. The association was highly significant ($P < 0.001$) with the R^2 value of 0.750 (Figure 3.16C), indicating there was a strong correlation between microplate reader data and flow cytometry data.

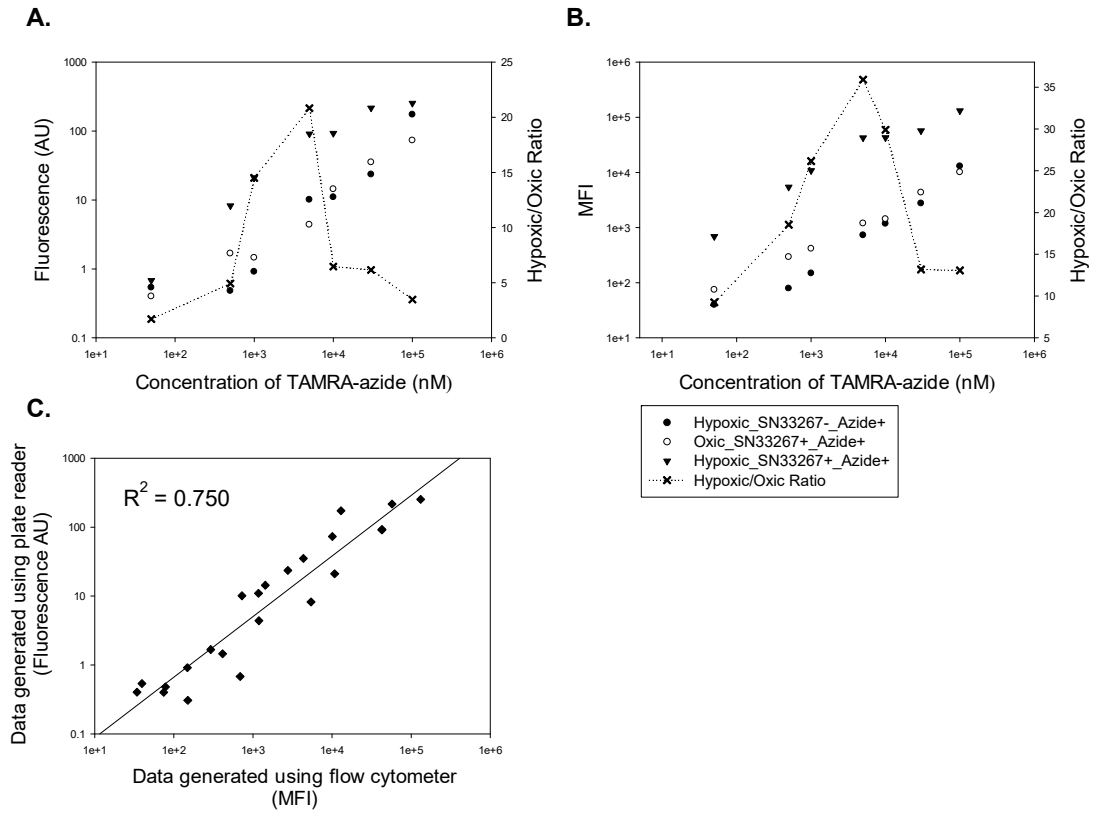

Figure 3.16: Measurement of fluorescence intensity in non-fixed SiHa cells labelled with different concentrations of TAMRA-azide.

(A) Fluorescence intensity determined by microplate reader. (B) Fluorescence intensity determined by flow cytometry. (C) Relationship of data of fluorescence in cell samples generated using two different instruments was analysed. Data are representative of 6 independent experiments.

3.5 Discussion

This Chapter describes the characterisation and the selection of candidate azide-modified fluorophores using microplate reader and flow cytometry. Experimental data acquired using the two different types of instruments were compared. The possibility of using microplate reader as a substitute of flow cytometry in determining fluorescence intensity in cells will be discussed.

The fluorescence signatures of all candidate azide-modified fluorophores were determined and the optimal instrument settings were selected for each (Table 3.1). Generally, the fluorescence intensity increases in direct proportion to the concentration of the fluorophore in a reasonable concentration range (Fili & Toseland, 2014). The majority of candidate azide-modified fluorophores demonstrated a linear relationship between fluorescence intensity and concentration in PBS solution containing 5% DMSO (Figure 3.2). However, this relationship was restricted to a range of 1-100 nM of fluorophore in PBS solution containing 5% DMSO for BODIPY-650/665-azide and BODIPY-TR-azide (Figure 3.3). The proportionality was no longer satisfied when concentration above 100 nM with these two BODIPY fluorophores.

As the concentration increases, one of at least three things can happen. First, the fluorophore solubility is exceeded. The insoluble fluorophore molecules undergo precipitation, which prevents the fluorescence intensity from increasing further (Zhang, Gao, Liu, Yang, & Fang, 2012). Second, short-range interactions between the molecules of the fluorophore themselves occur, which lead to loss of fluorescence signal by aggregation forming stable non-fluorescent complexes. As a special case of fluorescence quenching in concentrated solutions of fluorophores, the fluorescence of the sample is decreased since the quencher is essentially reducing the number of fluorophores which can emit (Zhuang et al., 2000). The last one is the inner filter effect. The fluorophore absorbs all the incident exciting and possibly emitted light in samples with very high absorbance. In addition, the excitation light cannot penetrate deeply enough to the point at which the detection optics are focused. So, the detected fluorescence reduces with the increase of the sample absorbance (Larsson, Wedborg, & Turner, 2007). Apart from those three major reasons mentioned above, saturation of the detector by too much light can also appear to cause a plateau in fluorescence intensity as the sample concentration increases, which is directly related to

extremely strong fluorescence signals and definitely not applicable to these cases. In my case, the second reason was probably the main cause resulting in the plateau phase of fluorescence intensity following the linear phase in which fluorescence was directly proportional to fluorophore concentration.

The selection of candidate fluorophores to design azide-modified fluorescent probes is done on the basis of fluorescence efficiency, photostability, the spectral range used for excitation and detection, the convenience of applying the new created fluorescent probe into the biological system of interest, and in this case the hypoxic to oxic ratio (Eisold et al., 2015).

For each candidate azide-modified fluorophore, a pilot experiment was run to test the hypoxia-mediated cell labelling specificity *in vitro* by using an initial click chemistry-based protocol (protocol #1 in Figure 2.1) and SiHa cells (results are summarised in Table 3.4). BODIPY-FL-azide and TAMRA-azide demonstrated promising hypoxia-selective labelling in both fixed and permeabilised and non-fixed SiHa cells (Figure 3.9 and Figure 3.10), which was further validated by the strong associations between fluorescence intensity and density of fluorophore-labelled cells in suspension with both azide-modified fluorophores (Figure 3.6 and Figure 3.7).

Table 3.4: Summary of hypoxia-selective labelling by candidate fluorophores in SiHa cells.

Candidate fluorophore	Cell type	Hypoxic/Oxic ratio (by microplate reader)	Hypoxic/Oxic ratio (by flow cytometer)	Flow cytometry histogram separation
Alexa Fluor 488-azide	Fixed	13.1	55.1	Complete
BODIPY-FL-azide	Fixed	1.8	2.8	Partial
	Non-fixed	1.9	4.9	Almost
TAMRA-azide	Fixed	1.3	11.6	Almost
	Non-fixed	1.8	3.4	Partial
BODIPY-650/665-azide	Fixed	0.7	1.7	None
BODIPY-TR-azide	Fixed	0.7	-	-
DEAC-azide	Fixed	0.5	-	-
DMACA-azide	Fixed	1.0	4.9	Almost
	Non-fixed	-	5.3	Partial

BODIPY and rhodamine derivatives are widely used among the fluorescence probes by satisfying all these criteria, which makes technical equipment for fluorescence detection and quantitation compatible for both families of fluorescence probes. In addition, they are commercially available in different chemical forms offering extra flexibilities in structural modification to fulfil specific design purposes (Lakowicz, 2007).

Two fluorophores on the candidate list from the coumarin family, DEAC-azide and DMACA-azide, exhibited limited utility in hypoxia-selective labelling of SiHa cells (Figure 3.13 and Figure 3.14). Efforts were made to improve the interactions between DMACA-azide and cell-incorporated SN33267 adducts by increasing concentration of DMACA-azide in reaction medium (Figure 3.15). However, the non-specific staining in oxic cells became an issue when the concentration of DMACA-azide was increased in reaction medium. It might be possible to develop a protocol for hypoxia-selective cell labelling mediated by DMACA-azide by including additional steps aimed to reduce background staining, e.g. extra wash steps.

Microplate reader and flow cytometry were used to quantitate fluorescence intensity emitted from the same cell samples after click chemistry-based hypoxia-selective labelling. In five out of six experiments, association analyses in experimental data generated from the same group of samples by two measurement approaches illustrated strong correlations with P values less than 0.05 (Figure 3.8C, Figure 3.9C and F, Figure 3.10F, as well as Figure 3.16C). Such consistent associations between data generated by 2 instruments from multiple independent experiments and three different types of fluorophores strongly suggest that it is possible to use microplate reader as a substitute of flow cytometer.

Basically, microplate reader and flow cytometry are both designed to determine the intensity of fluorescence but in different ways. The advantages of plate reader include cheaper cost, easier operation, and higher throughput. Microplate readers measure the average properties, the fluorescence intensity of entire cell suspensions on a microlitre to millilitre scale, and are designed to read whole-sample fluorescence (Jahan-Tigh, Ryan, Obermoser, & Schwarzenberger, 2012; MolecularDevices, 2006). However, microplate readers only provide moderate sensitivity and specificity in comparison to flow cytometry. Based on the data described in this Chapter, the

difference between data generated from same cell sample by the two types of instruments is usually more obvious in samples emitting high levels of fluorescence intensity. Thus, there are certain research goals that can only be achieved by use of flow cytometry since it is capable of generating correlative information about single cells within heterogeneous sample preparations via simultaneous multiparametric analysis in a high-throughput fashion (Jahan-Tigh et al., 2012; Pitsillides et al., 2011).

Considering the technical features of each fluorescence measuring approach, in the following chapters, flow cytometry will be predominantly utilised to quantitate fluorescence in fluorophore-labelled cells due to its sensitivity, accuracy, and the capabilities of selecting uniform population of cells as well as excluding any debris. In addition, microplate reader will be mostly used in pilot experiments for a quick check on hypoxia-mediated cell labelling selectivity.

Alexa Fluor 488-azide showed linear dependency on cell numbers (Figure 3.4A and Figure 3.6A) and good hypoxic to oxic ratio (Figure 3.8) when it was used in CuAAC-based hypoxia-selective cell labelling. However, such favourable features were only limited in fixed and permeabilised cells since Alexa Fluor-488 dyes exhibited no cell permeability (van de Linde et al., 2013). BODIPY-FL-azide and TAMRA-azide illustrated proportional associations between fluorescence intensity and fluorophore concentration in PBS. Studies of the association between density of hypoxic cells and intensity of fluorescence in cell suspension indicated a highly significant linear relationship when BODIPY-FL-azide and TAMRA-azide were used to label hypoxic SiHa cells via CuAAC reactions. These two fluorophore-modified azides also demonstrated promising interactivities with cell-incorporated SN33267 adducts with relatively low levels of non-specific staining. Thus, they were selected to optimise the click chemistry-based methodology.

Chapter 4. Optimisation of click chemistry-based hypoxia-selective cell labelling method

4.1 Introduction

To understand the role of hypoxia in a broad variety of cellular processes associated with metastasis and tumour progression, labelling tumour cells in their native environment in a manner that is selective for hypoxia and separating/isolating cells on the basis of their hypoxic stress *in situ* have become increasingly popular (Jones et al., 2012; Marotta et al., 2011; Stany et al., 2011; Zhu, Ning, Yao, Chen, & Xu, 2010).

Click reactions are characterised by extraordinary features including simplicity, versatility, high efficiency, as well as bioorthogonality (Breinbauer & Köhn, 2003; Kolb et al., 2001). CuAAC with its inherited bioorthogonality operates efficiently in aqueous medium and demonstrates a large tolerance for a number of functional groups, which makes it a powerful tool and thus highly favoured for biological applications such as measuring hypoxia (Accurso et al., 2014; Boyce & Bertozzi, 2011; Diaz, Rajagopal, Strable, Schneider, & Finn, 2006; El-Sagheer & Brown, 2010a; Finn & Fokin, 2010; Hein & Fokin, 2010; Hong, Steinmetz, Manchester, & Finn, 2010). One key advantage of the cell labelling approach based on CuAAC over immunohistochemical methods is the cell permeability due to the small particle size in reactants of CuAAC. At the same time, the distinctively narrow reactivity profiles of the reactants in CuAAC make these two reaction partners unparalleled candidates for deployment of novel CuAAC-based approaches for probing selected target molecules to aid investigations of complex biological systems (Berg & Straub, 2013; Chan et al., 2004). Thus, bioorthogonal chemistry has become a solution in targeting new classes of biomolecules relying on a single covalent reaction between complementary functional groups with exquisite selectivity comparable with antibody-antigen interactions (Boyce & Bertozzi, 2011).

4.2 Aims

Apart from an azide and terminal alkyne, the CuAAC reaction also requires a coordinating ligand, a copper source, and a reducing agent to participate for the purpose of catalysis. The *in situ*

generated copper(I) ions result in cytotoxicity due to the formation of reactive oxygen species (ROS) (Besanceney-Webler et al., 2011). The presence of ROS is capable of inducing RNA degradation in cells (Temple et al., 2005).

This Chapter aims to optimise the protocol of tagging cells with the 2-NI hypoxia marker SN33267 in a hypoxia-dependent manner and labelling with the fluorophores identified in Chapter 3. The optimisation procedure of click chemistry methodology was achieved through the introduction of defined reaction conditions for CuAAC along with CuAAC-accelerating ligands to overcome limitations during the conjugation of terminal alkynes with azides in a biological setting. The specific objectives are:

- To determine the optimal reaction temperature;
- To determine the optimal concentration of each participant;
- To improve hypoxia-selectivity of cell labelling.

4.3 Results

4.3.1 Reaction temperature

The rate of a chemical reaction can be changed by altering the temperature. Generally, an increase in temperature causes the reacting particles to move faster and more vigorously by elevating their kinetic energy, which thus increases the chances for particle collisions in order to initiate a reaction (Levine, 2005).

As mentioned in the previous chapter, the SiHa cell line was predominately used as the model system throughout this thesis to explore the features and optimise the protocol of this novel click chemistry-based hypoxia-selective cell labelling methodology. To investigate if the click chemistry-based hypoxic cell labelling could be influenced by a change in reaction temperature, SiHa cells were labelled with SN33267 and then clicked with BODIPY-FL-azide in a hypoxia-selective manner at both ambient temperature and 37 °C.

There was no obvious difference in clicking rates at these two temperatures. Also, no change in background fluorescence was detected (Figure 4.1). The increase in reaction temperature from

RT to 37 °C did not improve the hypoxia-selective labelling efficiency through enhanced reaction kinetics of CuAAC.

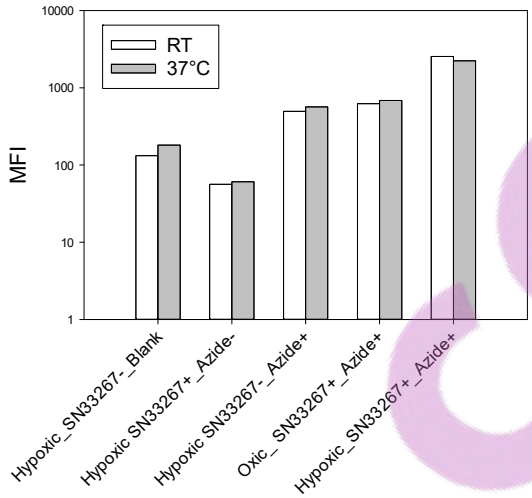

Figure 4.1: Hypoxia-selective clicking of SiHa cells under different temperatures.

SiHa cells were incubated under oxic or hypoxic conditions and clicked with BODIPY-FL-azide by following protocol #1 (see Figure 2.1) and using reaction cocktail #1 (see Table 2.7). Fluorescence intensity was determined by flow cytometry. Each bar represents the median fluorescence intensity (MFI) of a sample derived from the corresponding flow cytometry histogram. Data are representative of 2 independent experiments.

4.3.2 Trypsinisation

Subculturing is an essential task in the routine maintenance of cell cultures. During the passage of adherent cell lines, the trypsin-EDTA solution is frequently applied to detach adhesive cells from the substratum. It has been well-documented that the proteolytic activity of trypsin is able to cleave cell surface proteins, which can induce dysregulation of cellular functions and functional changes in the cell membrane (Huang et al., 2010; Mayrhofer, Krieger, Allmaier, & Kerjaschki, 2006).

To investigate if the time interval between the last subculturing and the experiment could affect the entire two-step process of CuAAC-based hypoxia-selective cell labelling, two SiHa cell samples with different time intervals (24 and 48 h) were prepared. For each sample, the experiment was performed following the procedures described in section 2.4.1. The fluorescence

intensities of cells labelled with a cell-permeable fluorophore, TAMRA-azide, in two groups of samples with different time intervals (24 and 48 h) were compared. There were no obvious changes in the hypoxic/oxic ratio caused by the 24 h difference in the interval between the last subculturing and the experiment in all five cell samples in terms of fluorescence intensity (Figure 4.2).

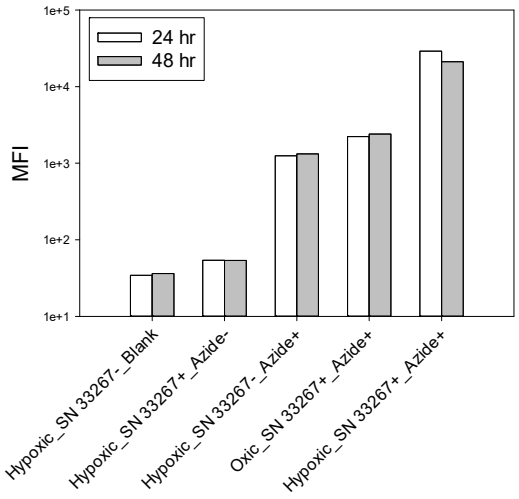

Figure 4.2: Comparison of the hypoxia-selectivity of click chemistry-based approach in SiHa cells with different recovery period from trypsinisation.

SiHa cells, grown as a subconfluent monolayer culture, were harvested in trypsin-EDTA solution, transferred into new tissue culture flasks, and housed in an incubator under standard cell culture conditions for 24 or 48 h. On the day of experiments, SiHa cells were incubated under oxic or hypoxic conditions and labelled with TAMRA-azide in a hypoxia-selective manner by following protocol #1 (see Figure 2.1) and using reaction cocktail #1 (see Table 2.7). Fluorescence intensity determined by flow cytometry. Each bar represents the median fluorescence intensity (MFI) derived from the corresponding flow cytometry histogram. Data are representative of 2 independent experiments.

4.3.3 Ligand and copper source

A series of reaction cocktails containing identical components except for the concentration of ligand were prepared. The CuAAC-mediated hypoxia-selective labelling was performed in the same group of cell samples using these reaction cocktails. Cells labelled with SN33267 were clicked with TAMRA-azide. The fluorescence intensity of each sample was determined and quantitated by flow cytometry. The data generated by the same group of samples with reaction

cocktails with various concentrations of ligand were compared to determine the hypoxia-selectivity of CuAAC-mediated cell labelling in response to the ligand to copper ratio in the reaction cocktail.

4.3.3.1 TBTA and $CuSO_4$

$CuSO_4$ was selected as the copper source. Under the catalysis provided by 1 mM $CuSO_4$ and 500 µM sodium ascorbate, hypoxic SiHa cells showed a slight increase in fluorescence intensity when the concentration of Tris(benzyltriazolylmethyl)amine (TBTA) was increased from 0.1 to 0.5 mM in the reaction cocktail. The further increase in ligand concentration (1 mM), however, led to a reduction in of the fluorescence signal. A different pattern was observed with oxic cells. They consistently demonstrated a slight increase in fluorescence intensity across the tested range of TBTA concentrations (0.1 – 1 mM). Consequently, the hypoxic to oxic ratio initially increased with increasing concentration of TBTA in the reaction cocktail. The maximum ratio, indicating the optimal hypoxia-selectivity, was achieved when the CuAAC-mediated cell labelling was facilitated by 0.5 mM TBTA (Figure 4.3A).

Controls were included to account for the contribution of auto-fluorescence and non-selective binding of TAMRA-azide. The hypoxic cell sample without exposure to clickable 2-NI (SN33267) but incubated with TAMRA-azide showed much higher fluorescence than cells that were not incubated with TAMRA-azide. This suggested non-selective binding of TAMRA-azide to macromolecules independent of CuAAC with covalent adducts of SN33267 (Figure 4.3A).

The fluorescence intensity of the oxic cells exposed to SN33267 clicked with TAMRA-azide was similar to that seen in cells without prior exposure to SN33267 (i.e. non-specific binding of TAMRA-azide). This suggested that very little, if any, covalent adducts were formed from SN33267 under oxic conditions, which is consistent with the very low K-value of a close analogue of SN33267, the 2-nitroimidazole EF5 under oxic conditions (Wang et al., 2012).

When sodium ascorbate was replaced by TCEP as the reducing agent at the same concentration in the reaction cocktail, the CuAAC-based cell labelling with TAMRA-azide showed a different pattern as a function of TBTA concentration in the reaction cocktail.

As can be seen from Figure 4.3B, data generated by three concentrations of TBTA (0.1, 0.2, and 0.5 mM) were used; 1 mM of TBTA caused severe precipitation during the preparation of the reaction cocktail. Under the catalysis provided by 1 mM $CuSO_4$ and 500 μM TCEP, the fluorescence signals of hypoxic SiHa cells) decreased with increasing TBTA concentration in the reaction cocktail. There was no obvious change in fluorescence intensity of oxic cells with the use of reaction cocktails containing 0.1 or 0.2 mM of TBTA. However, the fluorescence intensity was markedly increased in oxic cells when the concentration of TBTA was further increased from 0.2 to 0.5 mM. The hypoxic to oxic ratio dropped about 60% predominantly due to the decrease in fluorescence signals of hypoxic cells when increasing the concentration of TBTA from 0.1 to 0.2 mM. The increased fluorescence intensity in oxic cells when the concentration of TBTA was further increased to 0.5 mM in the reaction cocktail also contributed to the further decrease in the hypoxic to oxic ratio (Figure 4.3B).

In addition to showing very similar levels of fluorescence intensity, the hypoxic cell sample without exposure to clickable 2-NI (SN33267) but incubated with TAMRA-azide and the oxic cells demonstrated almost identical changes in fluorescence across the concentration gradient of TBTA. This might again indicate non-selective binding between TAMRA-azide and macromolecules independent of CuAAC. Again, the cell samples that were not incubated with TAMRA-azide showed very low levels of fluorescence intensity, presumably auto-fluorescence (Figure 4.3B).

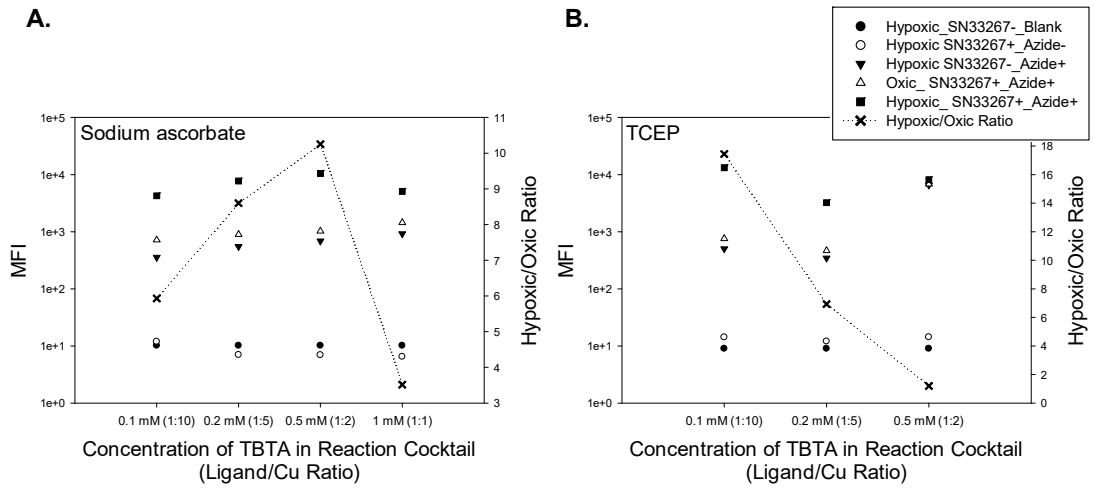

Figure 4.3: The effect of TBTA concentration on hypoxia-selective cell labelling with TAMRA-azide.

SiHa cells were incubated under oxic or hypoxic conditions and labelled with TAMRA-azide in a hypoxia-selective manner by following protocol #1 (see Figure 2.1). Apart from different concentrations of TBTA, the reaction cocktails also contained 10 μM TAMRA-azide, 1 mM $CuSO_4$, and 500 μM reducing agent. (A) Fluorescence intensity of each sample when using sodium ascorbate as reducing agent. (B) Fluorescence intensity of each sample when using TCEP as reducing agent. The MFI of sample is read from the corresponding flow cytometry histogram. The data are represented with different types of plot symbols according to the figure legend. Each plot is representative of at least 3 independent experiments.

As mentioned above severe precipitation was induced by 1 mM TBTA in the presence of 10 μM TAMRA-azide, 1 mM $CuSO_4$, and 500 μM TCEP in the reaction cocktail. When the concentration of $CuSO_4$ was fixed at 1 mM, only a very narrow range of TBTA concentrations could be investigated. This limited the *in vitro* study of hypoxia-selective cell labelling as a function of a change in the ligand to copper ratio. To overcome this limitation, a series of reaction cocktails with different concentrations of $CuSO_4$ (10 μM – 2 mM) with a fixed concentration of TBTA (100 μM) were used to study the role played by ligand to copper ratio in the selectivity of CuAAC-mediated hypoxic cell labelling with 10 μM TAMRA-azide under the reduction of 500 μM TCEP.

The fluorescence intensity of hypoxic samples initially increased as a function of increasing concentration of $CuSO_4$ in the reaction cocktail, which was followed by reaching a maximum when 1 mM $CuSO_4$ was applied in the reaction cocktail to give a ligand to copper ratio of 1:10. There was no obvious change in fluorescence signals in oxic samples in a concentration-dependent

manner, which made the trend of hypoxic to oxic ratio as a function of the concentration of $CuSO_4$ in the reaction cocktail very similar to the trend of fluorescence of the hypoxic samples across the gradient of ligand to copper ratio (Figure 4.4). Thus the highest labelling selectivity to hypoxic cells was observed with 1 mM $CuSO_4$ (the ligand to copper ratio of 1:10) in the reaction cocktail. The optimal ligand to copper ratio determined by this experiment was consistent with the finding from the previous experiment (Figure 4.3B).

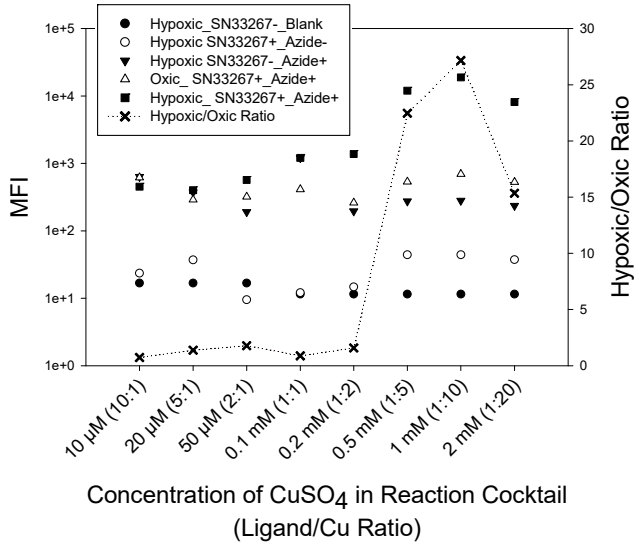

Figure 4.4: The effect of $CuSO_4$ concentration on hypoxia-selective cell labelling with TAMRA-azide.

SiHa cells were incubated under oxic or hypoxic conditions and clicked with TAMRA-azide in a hypoxia-selective manner by following rotocol #1 (see Figure 2.1) and using a series of reaction cocktails containing various concentrations of $CuSO_4$ (10 µM – 2 mM) based on reaction cocktail #2 (see Table 2.7). Fluorescence intensity of each sample is graphed using the MFI read from the corresponding flow cytometry histogram. The data are represented with different types of plot symbols according to the figure legends. Plot is representative of at least 3 independent experiments.

4.3.3.2 THPTA and $CuSO_4$

The same experimental design was also used to evaluate the performance of CuAAC-mediated hypoxia-selective cell labelling as a function of the concentration of Tris(3-hydroxypropyltriazolylmethyl)amine (THPTA) ligand in the reaction cocktail.

When 500 μM sodium ascorbate was used as reductant, the hypoxic samples labelled with TAMRA-azide demonstrated a reduction in fluorescence intensity when the concentration of THPTA was increased from 0.1 to 1 mM in the reaction cocktail. Similar to the results with TBTA, the fluorescence signals of the oxic samples did not change with THPTA concentration. The reaction cocktail containing 0.2 mM THPTA (ligand to copper ratio of 1:5) provided the best hypoxia-selectivity (Figure 4.5A).

Unlike TBTA, no precipitation occurred during the preparation of the reaction cocktail containing 1 mM THPTA and 500 μM of TCEP as the reducing agent. With increasing concentration of THPTA in the reaction cocktail, the fluorescence intensity went down in the hypoxic samples. However, no concentration-dependent response in fluorescence intensity was observed across the gradient of THPTA concentrations in the oxic samples. Among the tested THPTA concentrations, the reaction cocktail containing 0.1 mM THPTA (ligand to copper ratio of 1:10) provided the best hypoxia-selectivity in CuAAC-mediated cell labelling (Figure 4.5B).

Similar to what had been observed when TBTA was used as ligand (Figure 4.4), the fluorescence intensity of the oxic cells exposed to SN33267 and clicked with TAMRA-azide was similar to that seen in cells without prior exposure to SN33267 (i.e. non-specific binding of TAMRA-azide) independent of the selection of reducing agent when THPTA was used as ligand (Figure 4.5).

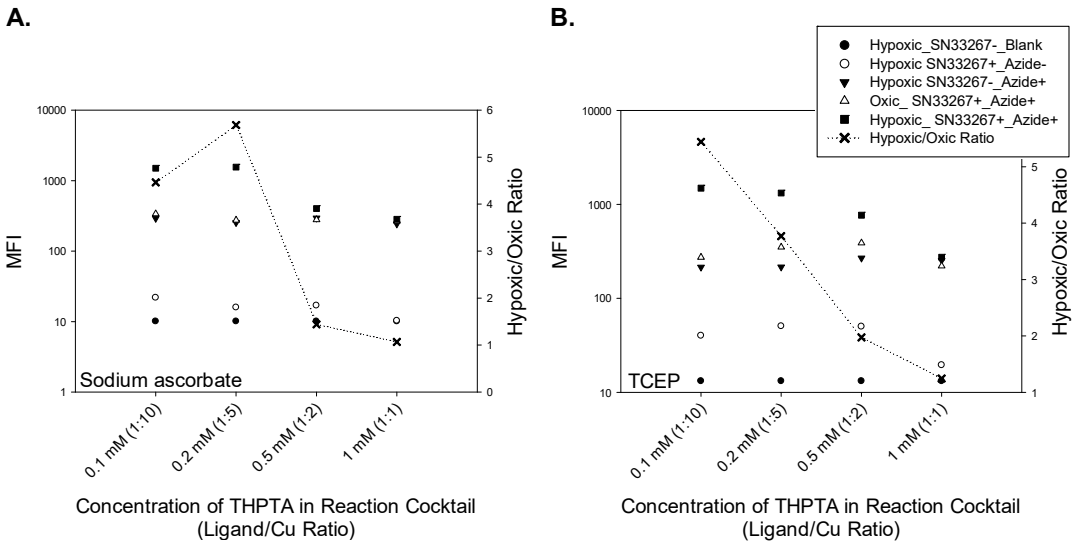

Figure 4.5: The effect of THPTA concentration on hypoxia-selective cell labelling.

SiHa cells were incubated under oxic or hypoxic conditions and clicked with TAMRA-azide in a hypoxia-selective manner by following protocol #1 (see Figure 2.1). Apart from different concentrations of THPTA, the reaction cocktails also contained 10 μM TAMRA-azide, 1 mM $CuSO_4$, and 500 μM reducing agent. (A) Fluorescence intensity of each sample when using sodium ascorbate as reducing agent. (B) Fluorescence intensity of each sample when using TCEP as reducing agent. The MFI of sample is read from the corresponding flow cytometry histogram. The data are represented with different types of plot symbols according to the figure legends. Each plot is representative of at least 3 independent experiments.

4.3.4 Reducing agent

Two reducing agents were tested in CuAAC-mediated hypoxia-selective cell labelling at different concentrations.

Based on the recipe of reaction cocktail #1 (Table 2.7), five reaction cocktails containing a series of sodium ascorbate concentrations ranging from 1 to 100 mM were used to determine the role of reductant concentration in clicking SiHa cells with TAMRA-azide in a hypoxia-selective manner (Figure 4.6A). Across the tested range of sodium ascorbate concentrations, fluorescence intensity did not show an obvious concentration-dependency. SiHa cells clicked with TAMRA-azide using the reaction cocktail containing 2 mM sodium ascorbate gave the best hypoxic selectivity on the basis of the calculated hypoxic to oxic ratio. The hypoxic to oxic ratio, however, varied slightly between 6.5 and 9.0 in the tested range of sodium ascorbate concentrations.

Similar to sodium ascorbate, five reaction cocktails, based on the recipe of reaction cocktail #2 (Table 2.7) and containing a series of TCEP concentrations ranging from 0.1 to 10 mM, were tested in the same way.

Across the tested range of TCEP concentrations, fluorescence intensity of the hypoxic samples increased with increasing concentration of TCEP in the reaction cocktail and reached a maximum value when 1 mM TCEP was used. At a TCEP concentration of 10 mM, a dramatic decrease in fluorescence signal was seen in labelled hypoxic sample. In the other tested cell samples in this experiment, fluorescence intensity did not show any obvious concentration-dependency. Both fluorescence intensity in the hypoxic samples and the hypoxic to oxic ratio thus responded to the concentration of TCEP in the reaction cocktail in a similar manner. SiHa cells labelled with TAMRA-azide using the reaction cocktail containing 1 mM of TCEP provided the best hypoxic cell labelling selectivity based on the calculated hypoxic to oxic ratio (Figure 4.6B).

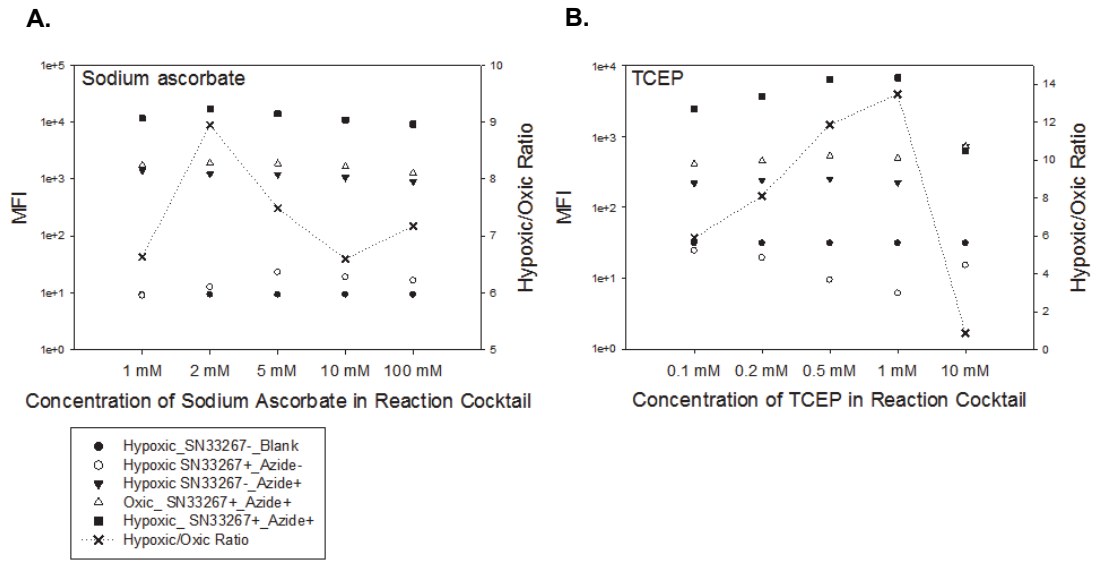

Figure 4.6: The effect of reducing agent concentration on clicking TAMRA-azide with cells in a hypoxia-selective manner.

SiHa cells were incubated under oxic or hypoxic conditions and clicked with TAMRA-azide in a hypoxia-selective manner by following protocol #1 (see Figure 2.1) and using a series of reaction cocktails containing various concentrations of reducing agent (1 – 100 mM sodium ascorbate or 0.1 – 10 mM TCEP) based on reaction cocktail #1 or #2 (see Table 2.7), respectively. (A) Fluorescence intensity of each sample when using sodium ascorbate as reducing agent. (B) Fluorescence intensity of each sample when using TCEP as reducing agent. The MFI of sample is read from the corresponding flow cytometry histogram. The data are represented with different types of plot symbols according to the figure legends. Each plot is representative of at least 3 independent experiments.

4.3.5 Modification of methodology to minimise non-specific binding

4.3.5.1 Non-specific binding

To determine the optimal concentration of TAMRA-azide in reaction medium, SiHa cells were incubated with SN33267 under oxic or hypoxic conditions and clicked with TAMRA-azide in a hypoxia-selective manner following protocol #1 (Figure 2.1) and using a series of reaction cocktails containing various concentrations of TAMRA-azide (50 nM – 100 µM) based on reaction cocktail #1 (Table 2.7).

This experiment was independently repeated three times within a 5-month time window. The fluorescence intensity of each simple increased with increasing in concentration of TAMRA-azide in the range from 50 nM to 100 µM and followed the same pattern in all three experiments (Figure 4.7A).

With increasing concentration of TAMRA-azide in the reaction cocktail, the hypoxic to oxic ratio increased and reached a maximal maximum value at 5 µM TAMRA-azide, which was followed by a drastic reduction of the ratio when further increasing the concentration of TAMRA-azide to 100 µM due to the large increase in fluorescence of the oxic samples. This pattern was observed in three independent experiments performed over a 5-month period (Figure 4.7B). The increases in fluorescence intensity of the oxic samples were due to non-specific binding of TAMRA-azide independent of CuAAC.

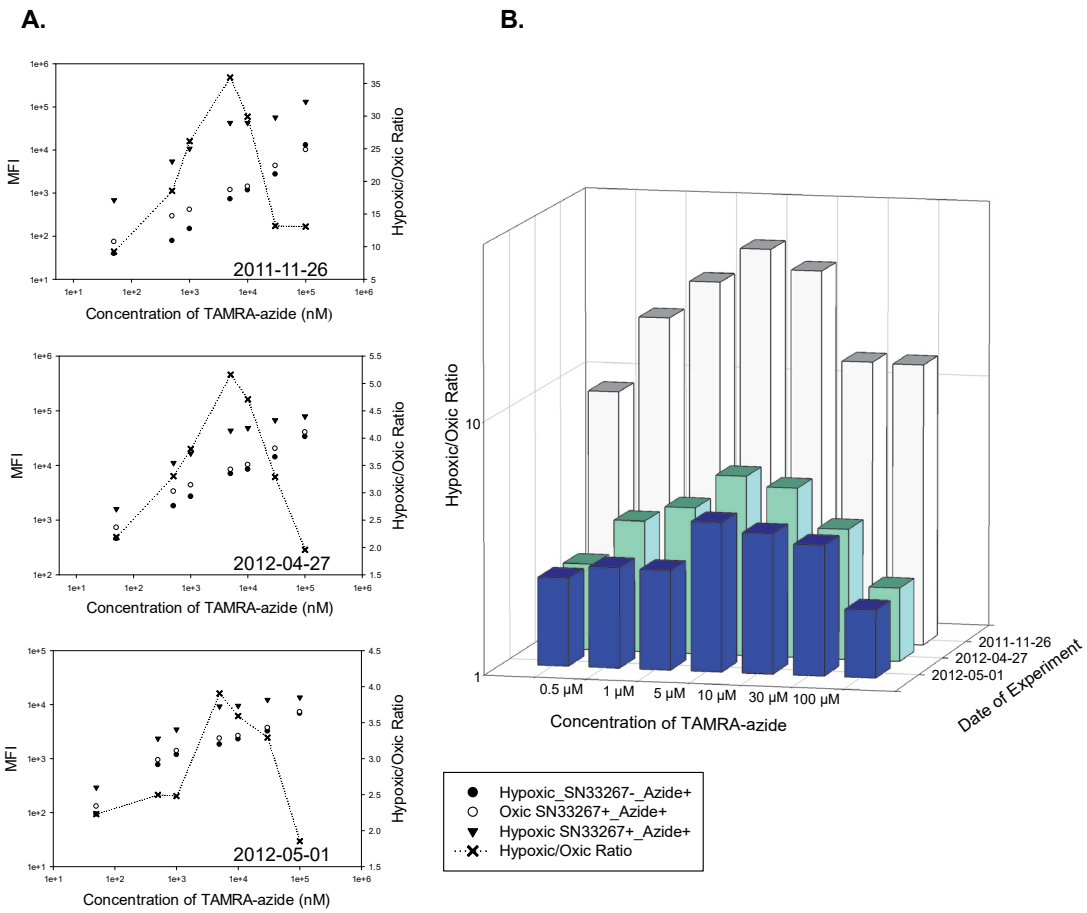

Figure 4.7: The effect of TAMRA-azide concentrations on hypoxia-selective cell labelling.

SiHa cells were incubated under oxic or hypoxic conditions and clicked with TAMRA-azide in a hypoxia-selective manner by following the protocol #1 (see Figure 2.1) and using a series of reaction cocktails containing various concentrations of TAMRA-azide (50 nM – 100 µM) based on reaction cocktail #1 (see Table 2.7). (A) Fluorescence intensity of each sample against TAMRA-azide concentration. The plots are from three independent experiments. The date of experiment is indicated on the corresponding graph. The MFI of sample is read from the corresponding flow cytometry histogram. The data are represented with different types of plot symbols according to the figure legend. Each plot is representative of 27 independent experiments over a 5-month period. (B) Hypoxia-mediated selectivity in clicking TAMRA-azide with SiHa cells from the three independent experiments shown in (A). Each bar represents the hypoxic/oxic ratio as the indicator of hypoxia selectivity. The same data are indicated by black crosses in (A).

4.3.5.2 Concentration of ethanol applied in the additional wash step

In order to minimise the fluorescence caused by non-specific staining by TAMRA-azide, an additional wash step was added in the original protocol (protocol #1, see Figure 2.1) following the second 30-min incubation with the reaction cocktail and before the three PBS wash steps. Ethanol-PBS solution was used in this additional wash step. It is known that high concentrations of ethanol are able to affect the structure of some proteins, produce dehydratation of the cell membrane, and remove significant quantities of membrane lipids, which can induce changes in cell mophology as well as cause significant damage to cells (Schnell, Dijk, Sjollema, & Giepmans, 2012). The optimal concentration of ethanol used in the washing solution was carefully determined by examining the capability of a series of ethanol-PBS solutions covering a range of ethanol concentrations (v/v) from 0% to 50% in improving the hypoxia-selectivity in CuACC-mediated cell labelling. Two fluorophore azides were selected in Chapter 3 since their promising interactivities with cell-incorporated SN33267 adducts with relatively low levels of non-specific staining. Owing to the choice of two reductants, in total four experiments covering all possible combinations of reductant and azide-modified fluorophore were performed in parallel to determine the optimal concentration of ethanol in the washing solution.

In all four experiments, the fluorescence of the oxic samples was notably reduced as a consequence of the elevated concentration of ethanol in the washing solutions used during the additional wash step. In contrast to the responses of fluorescence in oxic samples, changes in ethanol concentration did not show any obvious effects on the fluorescence intensity of the hypoxic samples (Figure 4.8). Thus, the additional washing step using ethanol-PBS solution selectively reduced the fluorescence intensity in oxic samples in an ethanol concentration-dependent manner within the range of concentrations examined. The application of 50% (v/v) ethanol-PBS solution in the additional wash step demonstrated the best efficiency in selectivly removing non-specifically bound fluorophores in the oxic samples. Based on this modified protocol, the hypoxia-selectivity of this CuAAC-based methodology, indicated by the hypoxic to oxic ratio, was significantly and consistently improved.

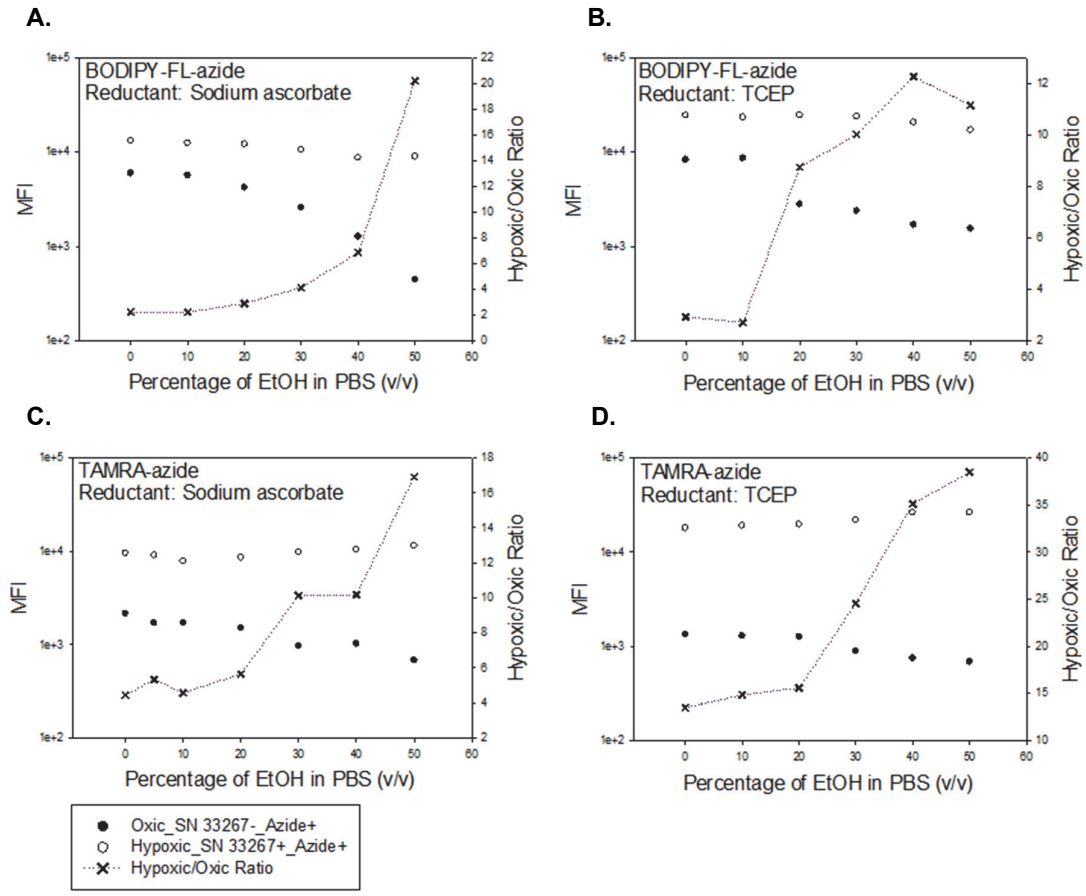

Figure 4.8: The effect of washing with ethanol-PBS solution on removal of non-specific binding of fluorophore azide.

SiHa cells were incubated under oxic or hypoxic conditions and clicked with azide-modified fluorophores in a hypoxia-selective manner by following the modified version of protocol #1 (see Figure 2.1) and using reaction cocktail #1 or #2 (see Table 2.7) when sodium ascorbate or TCEP was selected as reductant during the click reaction, respectively. In comparison with protocol #1, an ethanol wash step was added in experimental procedure between the second 30-min incubation with reaction cocktail and three PBS wash steps in the modified protocol. (A) Fluorescence intensity of each sample clicking with BODIPY-FL-azide against the ethanol concentration used in additional wash step when sodium ascorbate was used as reducing agent. (B) Fluorescence intensity of each sample clicking with BODIPY-FL-azide against the ethanol concentration used in additional wash step when TCEP was used as reducing agent. (C) Fluorescence intensity of each sample clicking with TAMRA-azide against the ethanol concentration used in additional wash step when sodium ascorbate was used as reducing agent. (D) Fluorescence intensity of each sample clicking with TAMRA-azide against the ethanol concentration used in additional wash step when TCEP was used as reducing agent. The MFI of sample is read from the corresponding flow cytometry histogram. The data are represented with different types of plot symbols according to the figure legend. Each plot is representative of at least 4 independent experiments.

4.3.5.3 The new protocol with modified wash steps

After 50% (v/v) ethanol-PBS solution was selected for use in the additional wash step, hypoxic SiHa cells without prior exposure to SN33267 and clicked with BODIPY-FL-azide were used to determine the performance of each single wash step in removing background fluorescence signals following the modified protocol (protocol #2 in Figure 2.1) by flow cytometry (Figure 4.9A).

Any detected fluorescence from the BODIPY dye was assumed to be caused by non-specific binding independent of cellular hypoxic stress or CuAAC. In comparison to the level of fluorescence intensity in cells at the end of the second 30-min incubation with reaction cocktail containing 3 μM BODIPY-FL-azide, 94% of fluorescence signals was removed by the wash step containing 50% ethanol, which was followed by three wash steps with PBS-alone to further decrease the fluorescence intensity by 4%, 0.7%, and 0.04%, respectively (Figure 4.9B). The first two wash steps removed the majority of non-specific fluorescence (98%). The third PBS wash step was removed since its limited function in eliminating background staining.

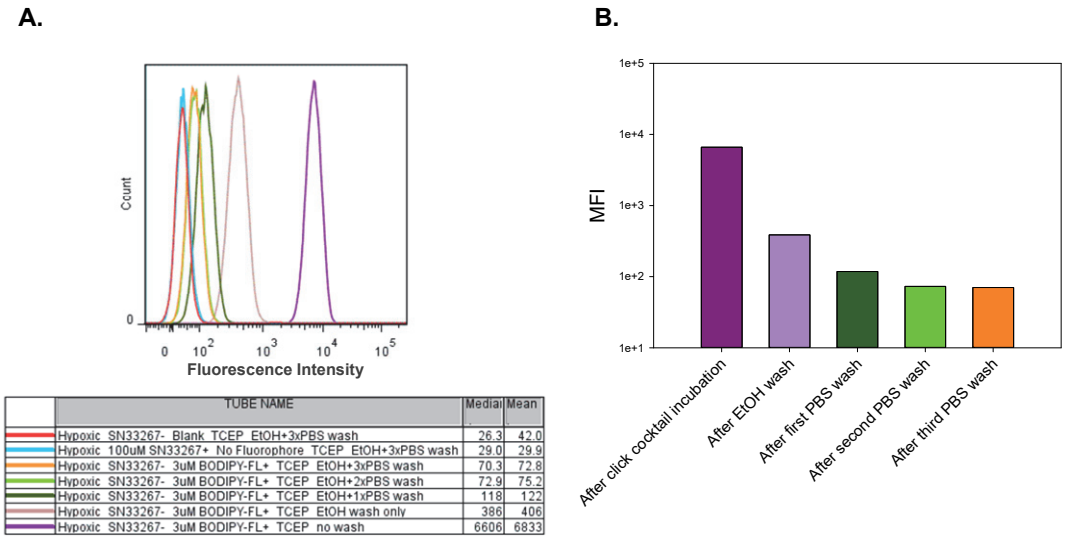

TUBE NAME	Median	Mean
Hypoxic_SN33267-_Blank_TCEP_EtOH+3xPBS wash	26.3	42.0
Hypoxic_100uM SN33267+_No Fluorophore_TCEP_EtOH+3xPBS wash	29.0	29.9
Hypoxic_SN33267-_3uM BODIPY-FL+_TCEP_EtOH+3xPBS wash	70.3	72.8
Hypoxic_SN33267-_3uM BODIPY-FL+_TCEP_EtOH+2xPBS wash	72.9	75.2
Hypoxic_SN33267-_3uM BODIPY-FL+_TCEP_EtOH+1xPBS wash	118	122
Hypoxic_SN33267-_3uM BODIPY-FL+_TCEP_EtOH wash only	386	406
Hypoxic_SN33267-_3uM BODIPY-FL+_TCEP_no wash	6606	6833

Figure 4.9: The effect of required wash steps on minimising non-specific binding of BODIPY-FL-azide.

SiHa cells were incubated under hypoxic conditions and clicked with BODIPY-FL-azide in a hypoxia-selective manner by following protocol #2 (see Figure 2.1) and using reaction cocktail #2 (Table 2.7) containing 3 μM of BODIPY-FL-azide. Hypoxic_SN33267-_Azide+ cells were sampled at the end of each individual step after the second 30-min incubation with reaction cocktail. (A) Histograms of fluorescence intensity in each sample determined by flow cytometry. (B) Residual fluorescence after each wash step to reduce non-specific background staining. Each bar represents the median fluorescence intensity (MFI) of sample read from the corresponding flow cytometry histogram in (A). Data are representative of 3 independent experiments.

4.3.5.4 Performance of the optimised protocol #3

The optimised protocol (protocol #3 in Figure 2.1) was tested by labelling SiHa cells with either BODIPY-FL-azide (Figure 4.10A) or TAMRA-azide (Figure 4.10B). By following the new protocol, the CuAAC-based method demonstrated an enhanced hypoxia-selectivity. According to the flow cytometric histograms, oxic cells were completely separated from the hypoxic cells in all tested combinations of azide-modified fluorophores and reductants. This suggested the possibility to sort cells by FACS when mixing oxic and hypoxic cells together in one sample because of the lack of overlap between the two cell populations. With both azide-modified fluorophores, the reaction cocktails using TCEP as reductant provided better hypoxic to oxic ratios than sodium ascorbate-based reaction cocktails. Compared to the flow cytometry data generated by cells labelled with BODIPY dye, TAMRA-azide offered better hypoxic to oxic ratios both when sodium ascorbate or TCEP were used as reducing agents in the reaction cocktail. Although the relatively lower hypoxic to oxic ratio with cells labelled with BODIPY-FL-azide in comparison to TAMRA-azide, the distribution of fluorescence intensities of individual cells from the same sample was generally tighter when BODIPY-FL-azide was used, as seen by the narrower peaks in the flow cytometric histograms.

A.)DIPY-FL-azide

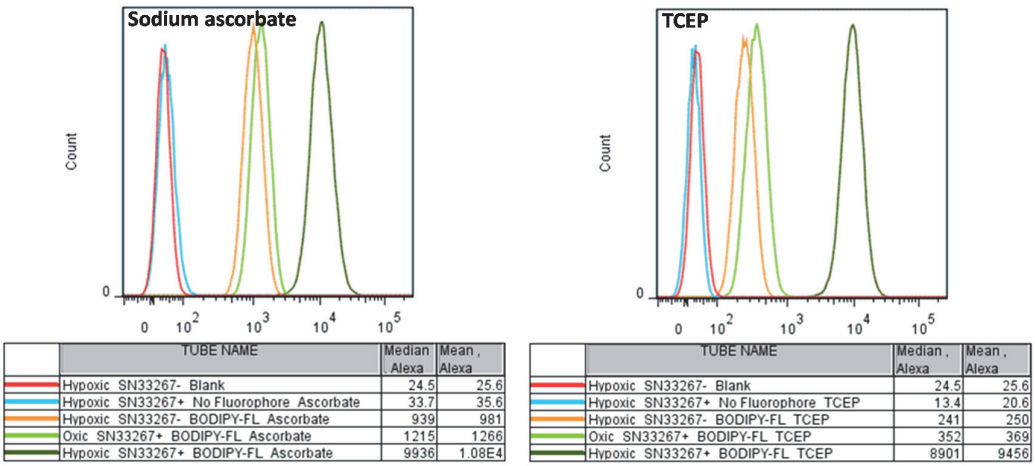

TUBE NAME	Median , Alexa	Mean , Alexa
Hypoxic SN33267- Blank	24.5	25.6
Hypoxic SN33267+ No Fluorophore Ascorbate	33.7	35.6
Hypoxic SN33267- BODIPY-FL Ascorbate	939	981
Oxic SN33267+ BODIPY-FL Ascorbate	1215	1266
Hypoxic SN33267+ BODIPY-FL Ascorbate	9936	1.08E4

Hypoxic/Oxic ratio: 8.2

TUBE NAME	Median , Alexa	Mean , Alexa
Hypoxic SN33267- Blank	24.5	25.6
Hypoxic SN33267+ No Fluorophore TCEP	13.4	20.6
Hypoxic SN33267- BODIPY-FL TCEP	241	250
Oxic SN33267+ BODIPY-FL TCEP	352	369
Hypoxic SN33267+ BODIPY-FL TCEP	8901	9456

Hypoxic/Oxic ratio: 25.3

B. \MRA-azide

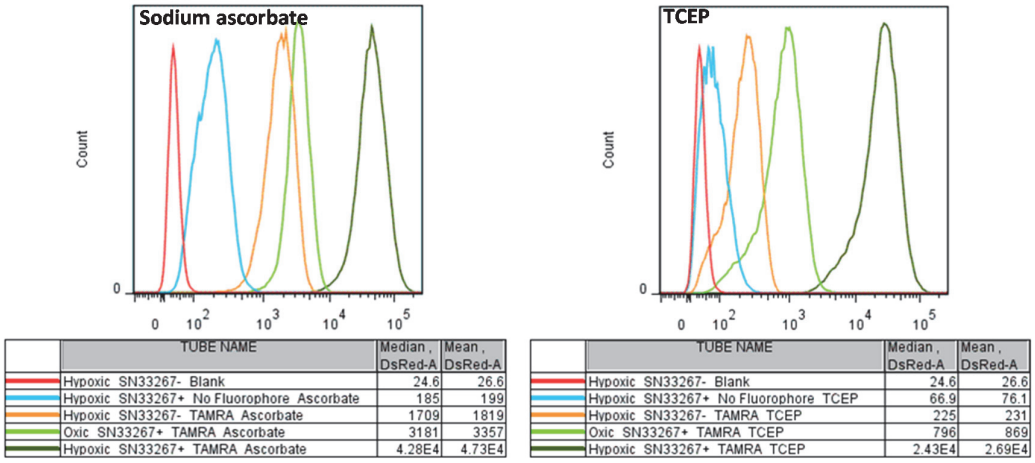

TUBE NAME	Median , DsRed-A	Mean , DsRed-A
Hypoxic SN33267- Blank	24.6	26.6
Hypoxic SN33267+ No Fluorophore Ascorbate	185	199
Hypoxic SN33267- TAMRA Ascorbate	1709	1819
Oxic SN33267+ TAMRA Ascorbate	3181	3357
Hypoxic SN33267+ TAMRA Ascorbate	4.28E4	4.73E4

Hypoxic/Oxic ratio: 13.5

TUBE NAME	Median , DsRed-A	Mean , DsRed-A
Hypoxic SN33267- Blank	24.6	26.6
Hypoxic SN33267+ No Fluorophore TCEP	66.9	76.1
Hypoxic SN33267- TAMRA TCEP	225	231
Oxic SN33267+ TAMRA TCEP	796	869
Hypoxic SN33267+ TAMRA TCEP	2.43E4	2.69E4

Hypoxic/Oxic ratio: 30.5

Figure 4.10: Hypoxia-selective labelling of SiHa cells using the optimal reaction cocktails and the optimised protocol.

SiHa cells were incubated under oxic or hypoxic conditions and clicked with azide-modified fluorophores in a hypoxia-selective manner by following protocol #3 (see Figure 2.1) and using reaction cocktails #1 or #2 (see Table 2.7) with use of sodium ascorbate or TCEP as reductant during the click reaction, respectively. Representative data from at least 3 independent experiments are shown.

4.3.6 Azide-modified fluorophore

In CuAAC-based hypoxia-selective cell labelling, the non-specific background staining was related to the concentration of azide-modified fluorophore in a concentration-dependent manner. In order to determine the hypoxia-selectivity of the method as a function of the applied concentration of fluorophore azide and the optimal concentration of azide-modified fluorophore, a series of reaction cocktails containing 30 nM – 100 μM of azide-modified fluorophore were tested utilising the modified protocol (protocol #3 in Figure 2.1) because it offered improved capability to diminishing the interference due to non-specific background staining.

4.3.6.1 BODIPY-FL-azide

With cells that were incubated with SN33267 and labelled with BODIPY-FL-azide the fluorescence intensity correlated with the concentration of fluorophore used in the reaction cocktail in a concentration-dependent manner (Figure 4.11). With increasing concentration of BODIPY-FL-azide, the fluorescence of hypoxic cells was elevated. The same trend in fluorescence intensity was also observed in both oxic and hypoxic samples without prior exposure to SN33267, which was mainly due to non-specific background staining independent of CuAAC. Apart from one outlier (3 μM BODIPY-FL-azide in panel B), SiHa cells demonstrated similar fluorescence changes to the increased BODIPY-FL-azide concentration in both types of click cocktails with different reducing agents. Based on the calculated hypoxic to oxic ratio, 3 μM of BODIPY-FL-azide in the reaction cocktail provided the highest hypoxia-selectivity when sodium ascorbate was used as a reductant. The optimal concentration of fluorophore in TCEP-reduced reaction cocktail could be either 1 or 3 μM but a firm conclusion was prevented by one measurement considered to be an outlier.

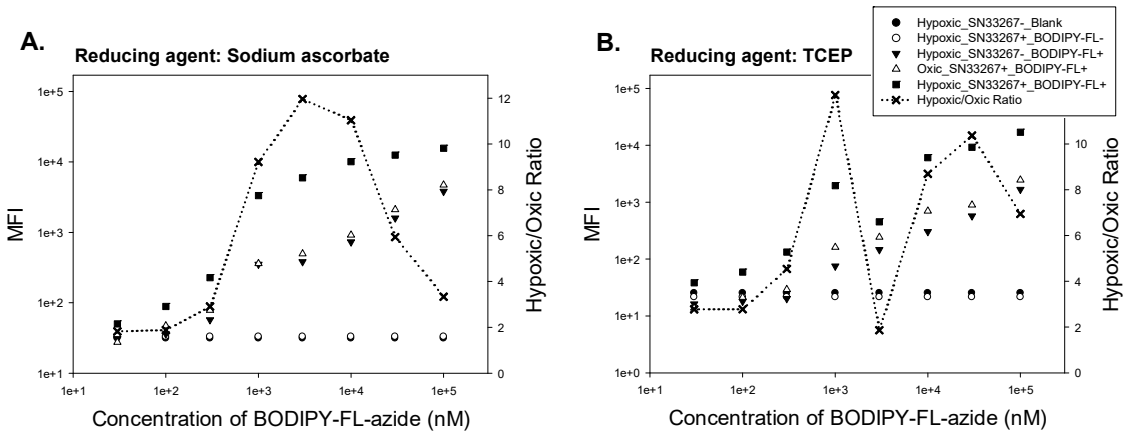

Figure 4.11: The effect of BODIPY-FL-azide concentration on clicking cells in a hypoxia-selective manner.

SiHa cells were incubated under oxic or hypoxic conditions and clicked with BODIPY-FL-azide in a hypoxia-selective manner by following protocol #3 (see Figure 2.1) and using a series of reaction cocktails containing 30 nM – 100 μM of BODIPY-FL-azide. The reaction cocktails were prepared by following the recipe of reaction cocktails #1 or #2 (see Table 2.7) when sodium ascorbate or TCEP was used as reductant during the click reaction, respectively. The MFI of sample is read from the corresponding flow cytometry histogram. The data are represented with different types of plot symbols according to the figure legend. Each plot is representative of 3 independent experiments.

4.3.6.2 TAMRA-azide

SiHa cells showed similar responses to changes in fluorophore concentration when BODIPY-FL-azide was replaced with TAMRA-azide in the reaction cocktail (Figure 4.12). Reaction cocktails with 10 and 3 μM of TAMRA-azide gave the highest hypoxic to oxic ratios when sodium ascorbate and TCEP were chosen as reducing agents, respectively. The data generated by reaction cocktails using sodium ascorbate as reductant are consistent with the data shown in Figure 4.7.

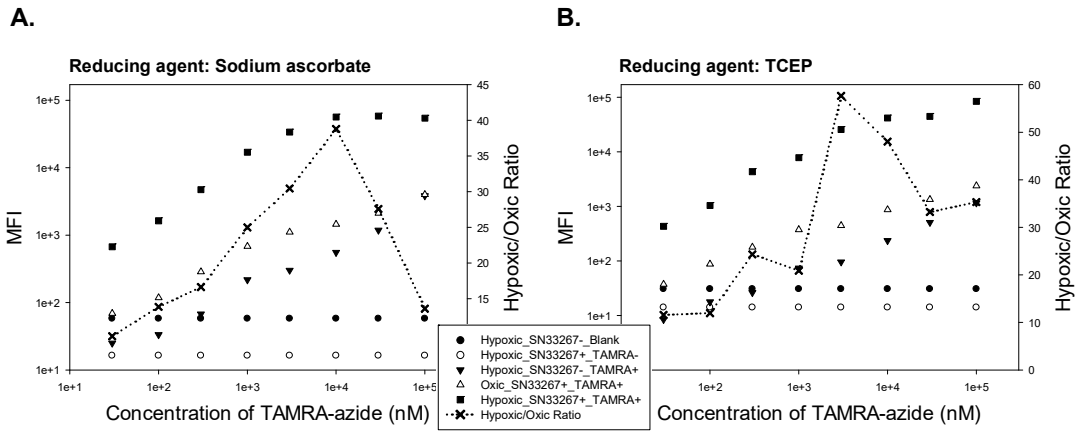

Figure 4.12: The effect of TAMRA-azide concentration on clicking with cells in a hypoxia-selective manner.

SiHa cells were incubated under oxic or hypoxic conditions and clicked with TAMRA-azide in a hypoxia-selective manner by following protocol #3 (see Figure 2.1) and using a series of reaction cocktails containing 30 nM – 100 μM of TAMRA-azide. The reaction cocktails were prepared by following the recipe of reaction cocktails #1 or #2 (see Table 2.7) when sodium ascorbate or TCEP was used as reductant during the click reaction, respectively. The MFI of sample is read from the corresponding flow cytometry histogram. The data are represented with different types of plot symbols according to the figure legend. Each plot is representative of 3 independent experiments.

4.3.7 Concentration of alkyne-modified 2-nitroimidazole SN33267

Based on the experimental results from Section 4.3.6, 3 μM of azide-modified fluorophore was used in reaction cocktail to determine the optimal concentration of SN33267 at which the cell labelling results demonstrated the best hypoxic to oxic ratio. The concentration of SN33267 within the range from 3 to 300 μM was examined in three different cell lines using the modified protocol (i.e. protocol #3 in Figure 2.1) with diminished interference caused by non-specific staining.

When sodium ascorbate was used as the reductant in the reaction cocktail containing 3 μM BODIPY-FL-azide, the fluorescence signals of the hypoxic samples increased with increasing concentration of SN33267 applied in the 2-NI-incubation step. When TCEP was employed as the reductant in the reaction cocktail containing 3 μM BODIPY-FL-azide, the fluorescence signals of the hypoxic samples increased with increasing concentration of SN33267 in a way similar to the case when sodium ascorbate was used (Figure 4.13).

In both cases, the hypoxic to oxic ratio reached a maximum at 100 μM of SN33267. The oxic samples showed a slight increase in fluorescence intensity with increasing concentration of SN33267. The other three experimental conditions did not show any notable changes in fluorescence intensities across the tested concentrations of SN33267. With both reducing agents, 100 μM of SN33267 in the 2-NI-incubation step provided the best hypoxic to oxic ratios (Figure 4.13).

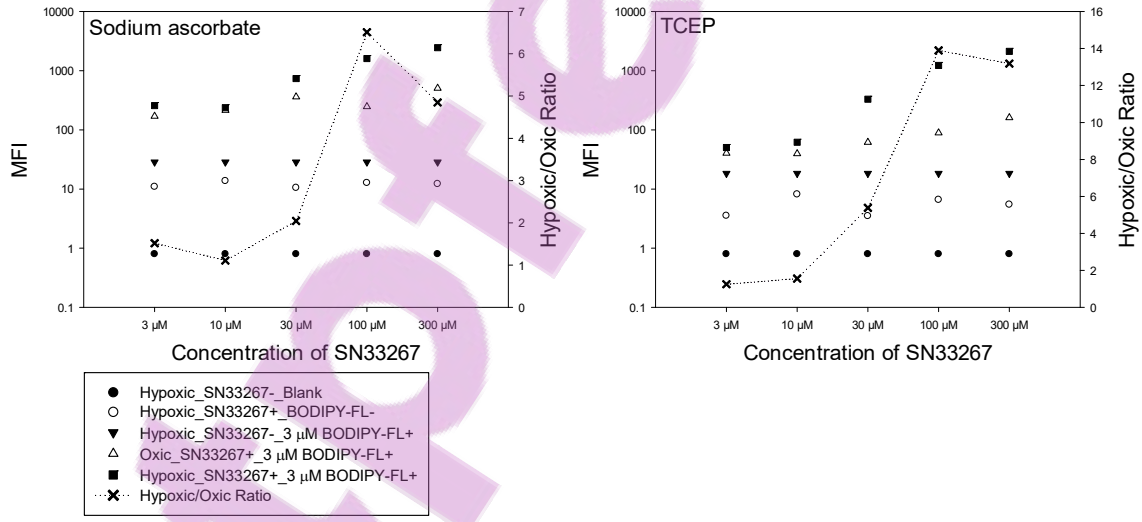

Figure 4.13: The effect of SN33267 concentration on clicking SiHa cells with BODIPY-FL-azide in a hypoxia-selective manner.

SiHa cells were incubated with 3 – 300 μM of SN33267 under oxic or hypoxic conditions and clicked with BODIPY-FL-azide in a hypoxia-selective manner by following protocol #3 (see Figure 2.1). Reaction cocktails contained 3 μM of BODIPY-FL-azide and prepared by following the recipe based on reaction cocktails #1 or #2 (see Table 2.7) when sodium ascorbate or TCEP was used as reductant during the click reaction, respectively. The MFI of sample is read from the corresponding flow cytometry histogram. The data are represented with different types of plot symbols according to the figure legend. Each plot is representative of at least 3 independent experiments.

In a similar experiment using sodium ascorbate and 3 µM TAMRA-azide in the reaction cocktail, the fluorescence signals of the hypoxic samples increased when the concentration of SN33267 applied in the 2-NI-incubation step was raised from 3 to 100 µM and reached a maximum at 100 µM. A further increase in the applied SN33267 concentration led to a slight reduction of fluorescence intensity in hypoxic cells. The fluorescence intensity of oxic samples slightly increased with increasing concentration of SN33267. When TCEP replaced sodium ascorbate as reductant in CuAAC, the fluorescence intensity was elevated by increasing concentration of SN33267 applied during the 2-NI-incubation step in both hypoxic samples and oxic samples. In addition, the fluorescence signals of the oxic sample markedly increased, when the applied concentration of SN33267 was raised from 100 to 300 µM. Again, 100 µM of SN33267 in the 2-NI-incubation step provided the best hypoxic to oxic ratios independent of the choice of reducing agent (Figure 4.14).

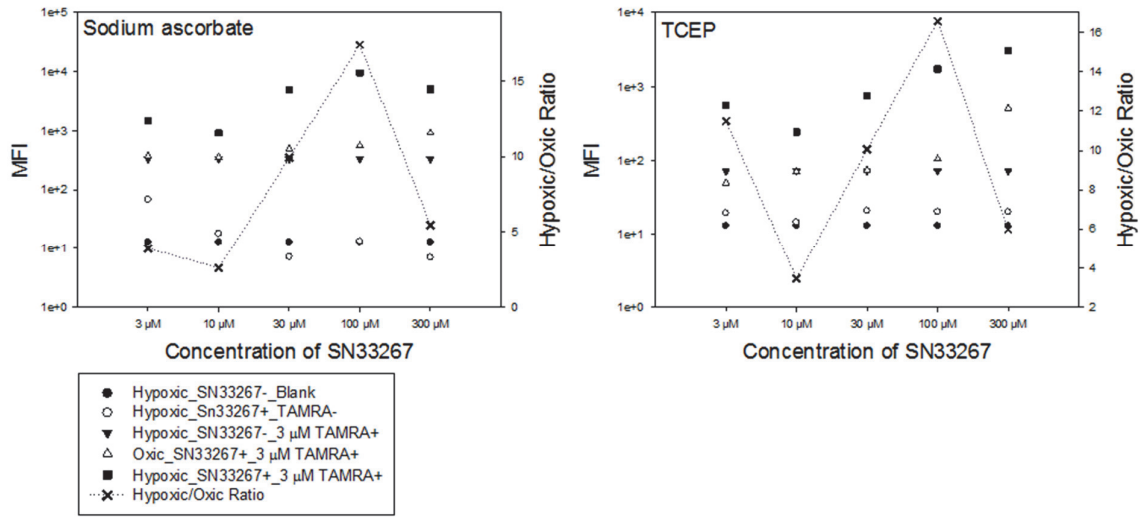

Figure 4.14: The effect of SN33267 concentration on clicking SiHa cells with TAMRA-azide in a hypoxia-selective manner.

SiHa cells were incubated with 3 – 300 µM of SN33267 under oxic or hypoxic conditions and clicked with TAMRA-azide in a hypoxia-selective manner by following protocol #3 (see Figure 2.1). Reaction cocktails contained 3 µM of TAMRA-azide and prepared by following the recipe based on reaction cocktails #1 or #2 (see Table 2.7) when sodium ascorbate or TCEP was used as reductant during the click reaction, respectively. The MFI of sample is read from the corresponding flow cytometry histogram. The data are represented with different types of plot symbols according to the figure legend. Each plot is representative of at least 3 independent experiments.

Similarly, the CuAAC-based methodology was also tested in HCT116 and HT-29 cell. In these two cell lines, a similar pattern was observed with BODIPY-FL-azide and TAMRA-azide (Figure 4.15 and Figure 4.16) as with SiHa cells (Figure 4.13 and Figure 4.14). Concentrations of 100 and 300 μM in SN33267 used during the 2-NI-incubation step provided the best hypoxic to oxic ratios irrespective of the selection of azide-modified fluorophore or reducing agent in HCT116 cells (Figure 4.15) and HT-29 cells (Figure 4.16), respectively.

In all three cell lines, the results showed high levels of similarity. For subsequent experiments, an SN33267 concentration of 100 μM was selected for the 2-NI-incubation step since it provided the best (in SiHa and HCT116 cell lines) or the second best (in HT-29 cell line) hypoxic to oxic ratios irrespective of the selection of azide-modified fluorophore or reducing agent.

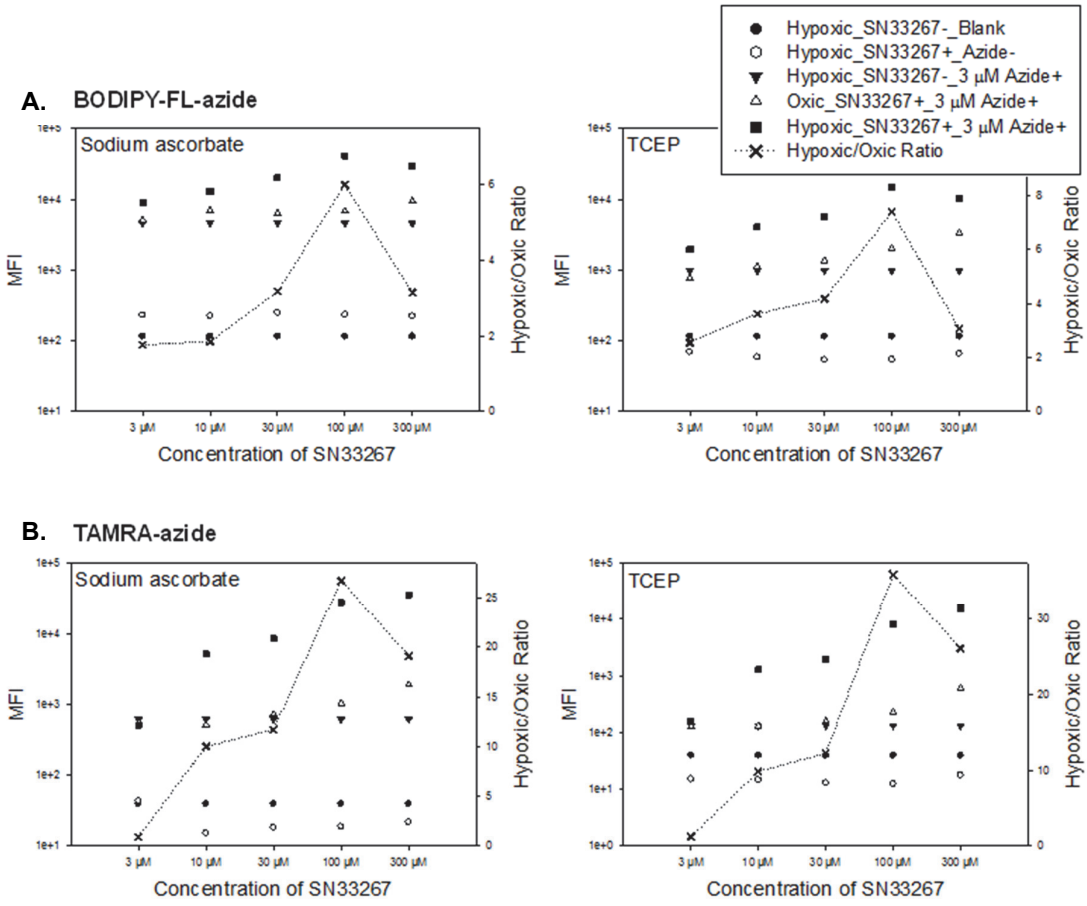

Figure 4.15: The effect of SN33267 concentration on clicking HCT116 cells with BODIPY-FL-azide or TAMRA-azide.

HCT116 cells were incubated with 3 – 300 µM of SN33267 under oxic or hypoxic conditions and clicked with azide-modified fluorophores in a hypoxia-selective manner by following protocol #3 (see Figure 2.1). Reaction cocktails contained 3 µM of the selected azide-modified fluorophore and prepared by following the recipe based on reaction cocktails #1 or #2 (see Table 2.7) when sodium ascorbate or TCEP was used as reductant during the click reaction, respectively. The MFI of sample is read from the corresponding flow cytometry histogram. The data are represented with different types of plot symbols according to the figure legends. Each plot is representative of 3 independent experiments.

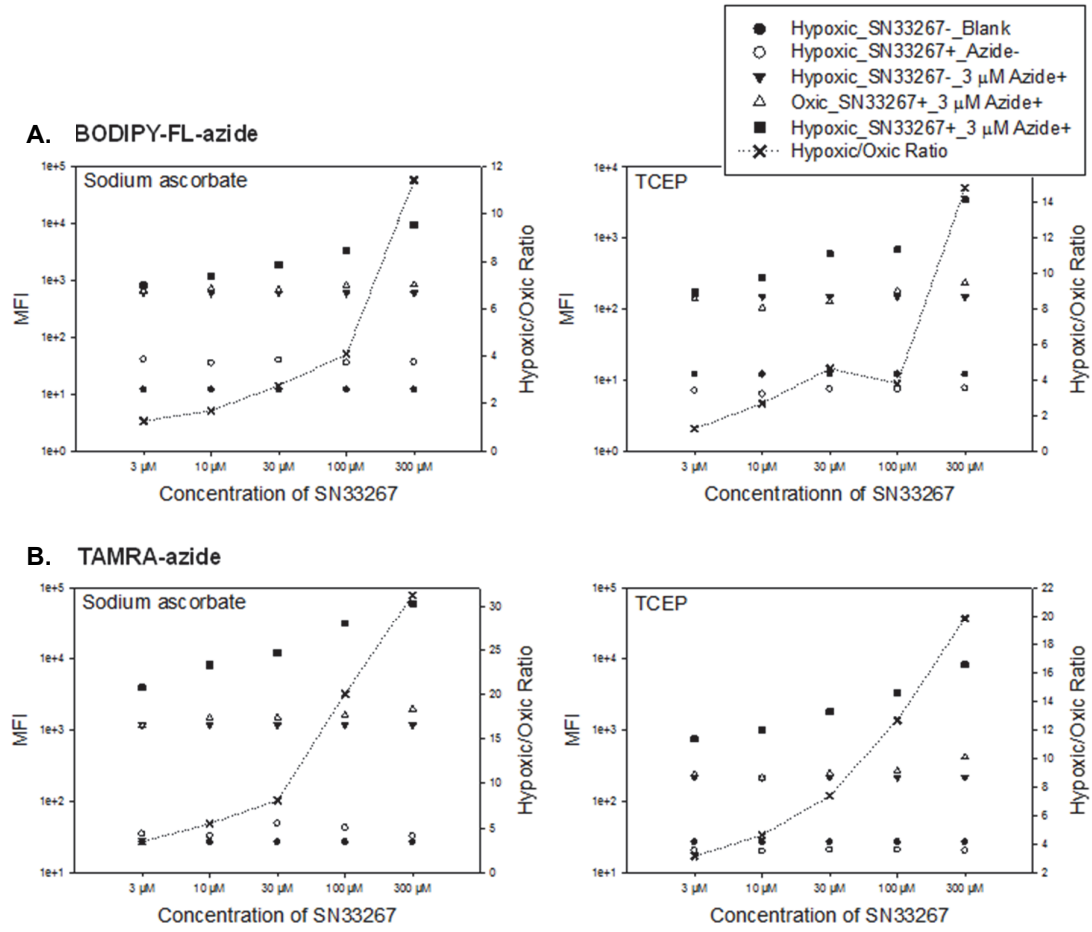

Figure 4.16: The effect of SN33267 concentration on clicking HT-29 cells with BODIPY-FL-azide or TAMRA-azide.

HT-29 cells were incubated with 3 – 300 µM of SN33267 under oxic or hypoxic conditions and clicked with azide-modified fluorophores in a hypoxia-selective manner by following protocol #3 (see Figure 2.1). Reaction cocktails contained 3 µM of the selected azide-modified fluorophore and prepared by following the recipe based on reaction cocktails #1 or #2 (see Table 2.7) when sodium ascorbate or TCEP was used as reductant during the click reaction, respectively. The MFI of sample is read from the corresponding flow cytometry histogram. The data are represented with different types of plot symbols according to the figure legends. Each plot is representative of 3 independent experiments.

4.3.8 CuAAC-mediated staining vs immunohistochemistry

Two parallel *in vitro* experiments were performed to label fixed and permeabilised SiHa cells with Alexa Fluor 488 dye either immunohistochemically (using EF5 and Alexa Fluor 488-conjugated EF5 antibody) or chemically (using SN33267 and Alexa Fluor 488-azide) in a hypoxia-selective manner.

When cells labelled chemically through the bioreductive metabolism of clickable 2-NI (SN33267) using the CuAAC-based method, the flow cytometric data demonstrated a smaller variation in fluorescence intensity of the cell sample in comparison to the immunohistochemistry-based method. Such differences in the variation of fluorescence intensity between the two methods were clearly seen in the flow cytometric histograms of three experimental samples (histograms in light green, dark green, and thistle in Figure 4.17) that were exposed to Alexa Fluor 488 fluorophores: sharp peaks with narrower base widths in the histograms of the CuAAC-based cell labelling procedure compared to the immunohistochemistry-based method.

The two histograms representing the fluorescence intensities in oxic and hypoxic samples partially overlapped when the immunohistochemistry-based method was utilised to label cells (Figure 4.17A). When cells were labelled by using CuAAC-based method, the peak representing the fluorescence intensity in the oxic sample was nearly completely separated from the one representing the hypoxic sample, which suggested the potential of this CuAAC-based method to successfully sort cells by FACS according to fluorescence intensity when the two samples were mixed together (Figure 4.17B).

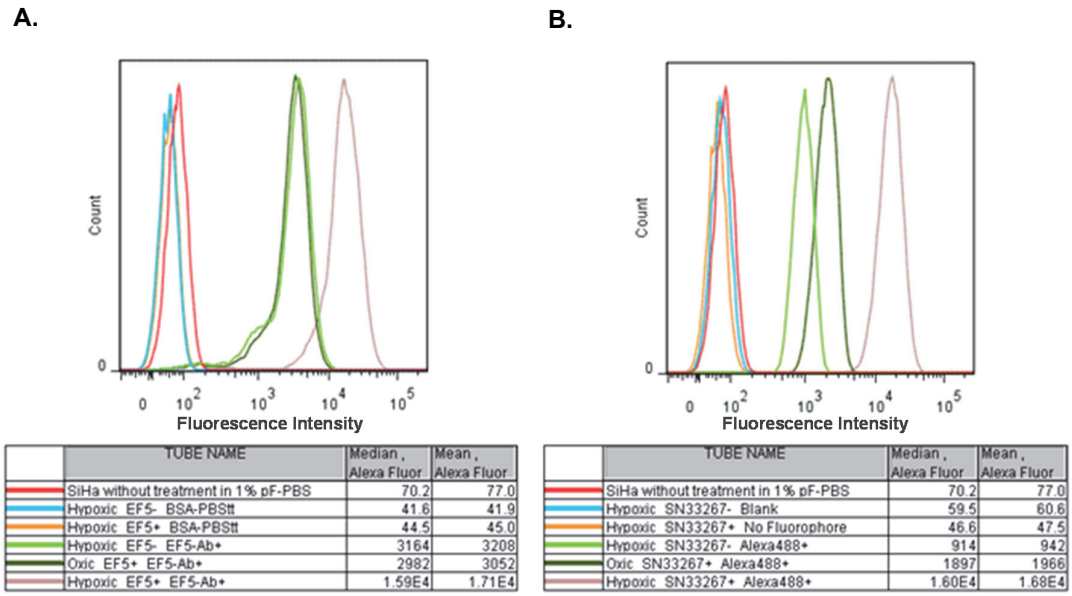

TUBE NAME	Median , Alexa Fluor	Mean , Alexa Fluor
SiHa without treatment in 1% pF-PBS	70.2	77.0
Hypoxic EF5- BSA-PBStt	41.6	41.9
Hypoxic EF5+ BSA-PBStt	44.5	45.0
Hypoxic EF5- EF5-Ab+	3164	3208
Oxic EF5+ EF5-Ab+	2982	3052
Hypoxic EF5+ EF5-Ab+	1.59E4	1.71E4

TUBE NAME	Median , Alexa Fluor	Mean , Alexa Fluor
SiHa without treatment in 1% pF-PBS	70.2	77.0
Hypoxic SN33267- Blank	59.5	60.6
Hypoxic SN33267+ No Fluorophore	46.6	47.5
Hypoxic SN33267- Alexa488+	914	942
Oxic SN33267+ Alexa488+	1897	1966
Hypoxic SN33267+ Alexa488+	1.60E4	1.68E4

Figure 4.17: Comparison of hypoxia-selective labelling of SiHa cells based on immunohistochemistry and CuAAC.

(A) Flow cytometry histograms of fluorescence signals in cell samples labelled with Alexa Fluor 488 dye via immunohistochemistry. Following a 1.5 h pre-gassing incubation, SiHa cells were incubated with 100 µM EF5 under oxic or hypoxic conditions for 2 h. After fixation and permeabilisation, cells were labelled immunochemically with Alexa Fluor 488-conjugated ELK3.1 EF5 antibody (50 µg/mL) in a hypoxia-selective manner. (B) Flow cytometry histograms of fluorescence signals in cell samples labelled with Alexa Fluor 488-azide via CuAAC-mediated conjugation with SN33267. Following a 1.5 h pre-gassing incubation, SiHa cells were incubated with 100 µM SN33267 under oxic or hypoxic conditions for 2 h. After fixation and permeabilisation, cells were labelled with Alexa Fluor 488-azide in a hypoxia-selective manner by following protocol #1 (see Figure 2.1). Reaction cocktails contained 10 µM of Alexa Fluor 488-azide and prepared by following the recipe of reaction cocktail #1 (see Table 2.7). Representative flow cytometric data from 3 independent experiments are shown.

In unpublished work done by Sarah McManaway, an NIH-III mouse bearing a subcutaneous (s.c.) A431 human tumour xenograft was co-administered the reference hypoxia marker EF5 and clickable 2-NI SN33267 (both 60 mg/kg) simultaneously by i.p. injections. The tumour was excised 2 h later. The fluorescence signals was determined by confocal microscopy on tissue sections.

Figure 4.18A shows a deparaffinised tissue sample stained immunochemically by 50 µg/mL Alexa Fluor 488-conjugated ELK3.1 EF5 antibody. The antibody-stained EF5 adducts that are formed through the covalent associations between the EF5 reductive metabolites generated in a hypoxia-dependent manner, and macromolecules. Following the immunohistochemical staining, the same section was chemically stained with 10 µM Alexa Fluor 647-azide via a CuAAC-based procedure (Figure 4.18B). The two staining patterns overlapped each other very well, which suggested that EF5 and SN33267 labelled the same (hypoxic) cells in this xenograft model and with a similar sensitivity for detection fluorescence confocal microscopy.

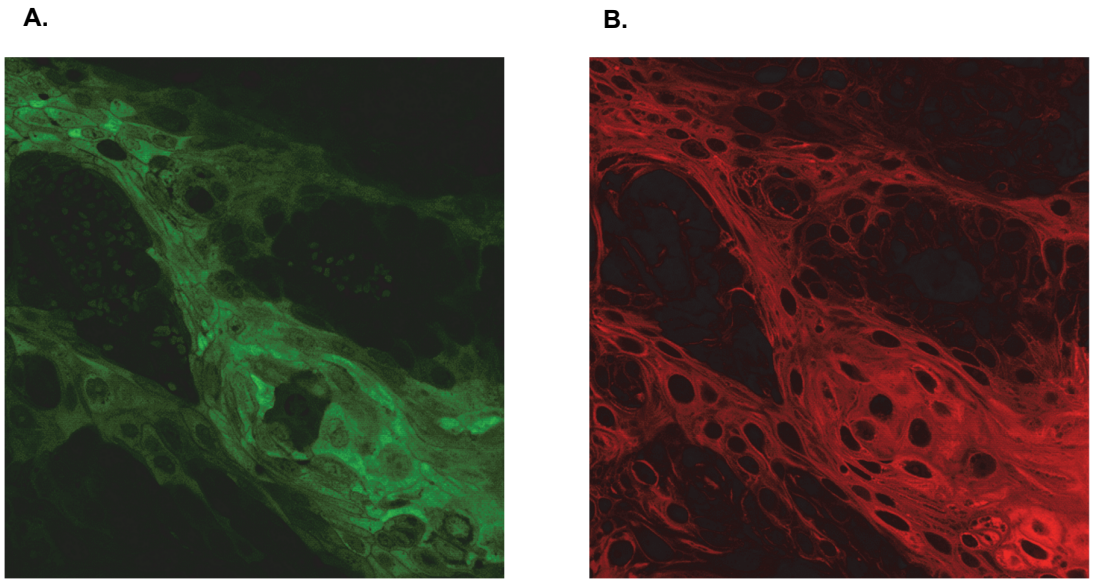

Figure 4.18: Dual staining in an A431 tumour xenograft with EF5 and SN33267 using fluorescence confocal microscopy.

(A) Alexa Fluor 488 – EF5 Antibody signal. (B) Alexa Fluor 647 – SN33267 click signal. An NIH-III mouse was inoculated with A431 tumour cells and 20 days later the mouse was dosed with both SN33267 (60 mg/kg) and EF5 (60 mg/kg) simultaneously by i.p. injection. Two hours after dosing, the mouse was euthanized and the tumour excised. Following antigen retrieval and deparaffinisation, the deparaffinised tissue sample was labelled immunochemically with Alexa Fluor 488-conjugated ELK3.1 EF5 antibody (50 µg/mL) followed by incubating with reaction cocktail #1 (see Table 2.7) containing 10 µM Alexa Fluor 647-azide. Both confocal microscopy images were taken on an Olympus FLUOVIEW FV1000 confocal laser scanning microscope with 60× oil immersion objective (Olympus Corporation, Tokyo, Japan). [Unpublished data; image courtesy of Sarah McManaway]

4.3.9 Copper-free click chemistry for labelling of hypoxic cells

The strain-promoted azide-alkyne cycloaddition (SPAAC) was first coined by Bertozzi *et al*. with improved biocompatibility due to the absence of copper(I)-catalysis (Agard et al., 2004). Two 2-NI moiety-containing compounds, a trans-cyclooctene derivative TCO (SN35189) and a cyclooctyne derivative BCN (SN34710), were also converted into reductive metabolites under hypoxic conditions and formed covalent adducts in cells by binding to macromolecules. These adducts could be tagged with a tetrazine-BODIPY conjugate, SN35580, via SPAAC reactions (Figure 4.19A). Three concentrations (10, 30, and 100 μM) of the cyclooctyne or cyclooctene derivative were tested with 2 μM of SN35580 in SiHa cells to determine the role of 2-NI concentration in the hypoxia-selectivity of SPAAC-mediated cell labelling procedure.

SiHa cells demonstrated very similar responses to the different concentrations of cyclooctyne or cyclooctene derivatives in hypoxia-selective labelling (Figure 4.19B and C). The increase in the concentration of either TCO or BCN did not cause notable changes in final fluorescence intensity of SN35580-clicked hypoxic samples. However, the fluorescence signals were elevated in oxic samples with increasing concentration of the cyclic derivatives. Among the three tested concentrations, 10 μM gave the best results in selectively labelling hypoxic SiHa cells for both TCO and BCN.

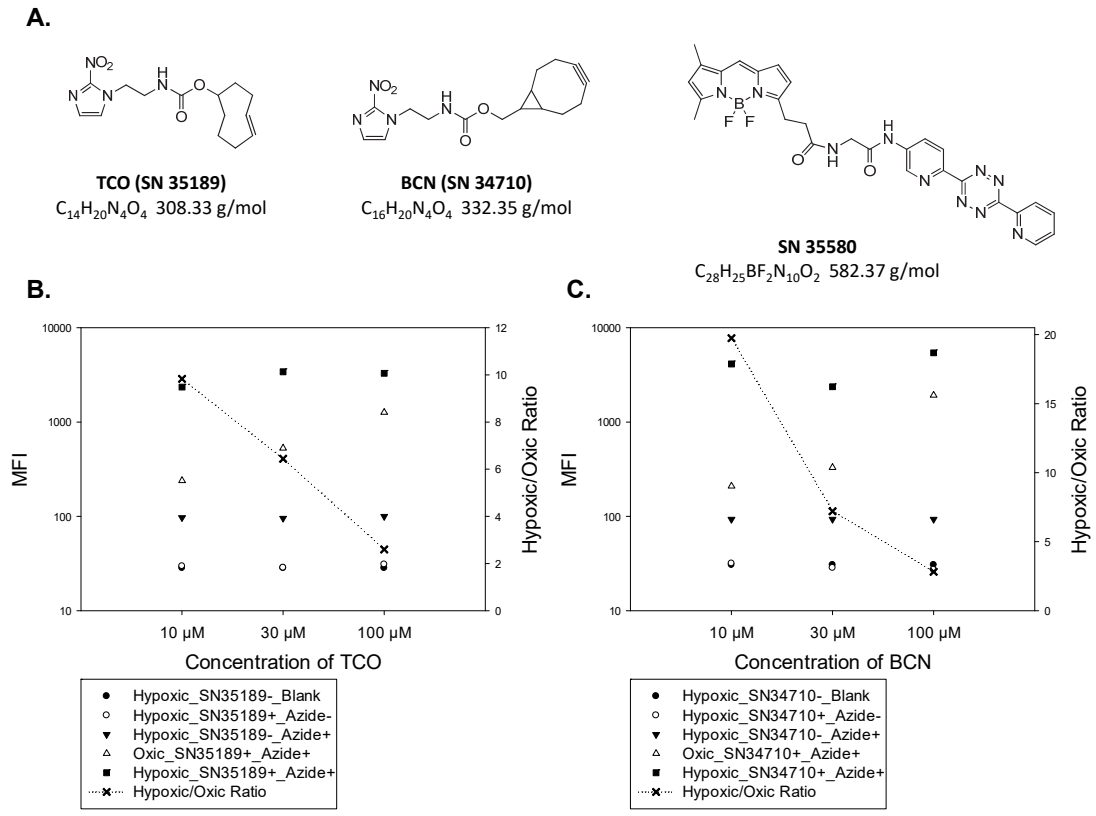

Figure 4.19: SPAAC-based hypoxia-selective labelling of SiHa cells.

SiHa cells were incubated with 10 – 100 µM of 2-NI-modified cyclooctyne under oxic and hypoxic conditions for 2 h. In SPAAC, 2 µM of BODIPY-based SN35580 in 10 mM Tris-buffered saline was used as reaction cocktail. All wash steps and reaction cocktail incubation steps were performed in the same time frame as protocol #1 (see Figure 2.1). (A) Compounds used in SPAAC-based labelling of cells. (B) Fluorescence intensity of cell sample incubated with TCO and labelled with SN35580 (C) Fluorescence intensity of cell sample incubated with BCN and labelled with SN35580. The MFI of sample is read from the corresponding flow cytometry histogram. The data are represented with different types of plot symbols according to the figure legends. Each plot is representative of 2 independent experiments.

4.4 Discussion

The presence of hypoxic regions is a common feature in most solid tumours and associated with increased metastasis, increased tissue invasion, and resistance to radio- and chemotherapy as well as surgery (Yuan et al., 2011). The distribution of hypoxic stress is spatially heterogeneous in individual tumours, characterised by gradients of oxygenation spreading from normal physiological levels close to the vasculature to near anoxia at the borders of necrotic zones (Nordsmark et al., 2005).

Fluorescent modification is by far the most popular approach in hypoxia labelling techniques by virtue of the highly sensitive detectability of the fluorescent signal with extraordinary spatial and temporal resolution with relatively reasonable cost and the potential for multichannel detection (Gonçalves, 2009; Herner, Nikic, Kallay, Lemke, & Kele, 2013; Lee et al., 2011). Chemical probes based on the 2-nitroimidazole (2-NI) functionality, such as EF5, is a widely applied probe for the immunohistochemical detection of hypoxia as well as non-invasive detection and imaging by positron emission tomography (PET) (Dolbier et al., 2001; Evans et al., 2000; Wang et al., 2012; Wilson & Hay, 2011). In the hypoxic environment, the reduction of these chemical probes mediated by one-electron reductases converts the 2-NI to a 2-(hydroxylamino)imidazole, followed by the generation of an electrophilic 2-(nitrenium)imidazole ion. The electrophilic 2-(nitrenium)imidazole ion irreversibly reacts with protein thiols and gives rise to protein-2-(amino)imidazole adducts, thereby effectively labelling the cell (Edgar et al., 2014). The success of such applications requires exquisite selectivity to maximise signal to noise ratio. During optimisation of the click chemistry-based methodology in this thesis, the hypoxic to oxic ratio was used as a major criterion to select both optimal experimental conditions and optimal concentration of each participant.

Benefitting from the small size and unobtrusive nature of the terminal alkyne and azide moieties, the majority of reported bioorthogonal reactions in the literature have been used, to date, to label proteins *in vitro* or at the cell surface with respect to selected biological functionalities (McKay & Finn, 2014). A clickable probe sensitive to cellular hypoxic stress can be created by linking an alkyne or azide moiety to a bioreductively sensitive 2-nitroimidazole scaffold. With the presence

of corresponding counterpart-modified fluorophore, the detection of hypoxia can be achieved by a chemistry-based approach.

4.4.1 Temperature

The increase of reaction temperature can benefit the reaction via boosting conformational dynamics when the azide or alkyne group on the biomolecule is sterically hindered or inaccessible to the catalyst and the coupling partner (Hong et al., 2009). Finn and co-workers reported that the CuAAC reaction benefits greatly from higher temperatures. In CuAAC bioconjugations, even modest increases of the reaction temperature within a tolerated range of some biological molecules can generally result in better kinetic behaviours (Presolski et al., 2011), especially when the metal is sequestered by competing coordinating species, including donor solvent molecules or donor groups in protein or other species present, a little heat may be what copper(I) centres need to recover from the compromised kinetics liability (Presolski, Hong, Cho, & Finn, 2010; Presolski et al., 2011). Because of concerns for RNA integrity (which will be discussed in Chapter 5), there was not much scope to increase the reaction temperature for the CuAAC reaction. A reaction temperature of 37 °C did not result in improving CuAAC-mediated cell labelling in comparison to RT. Despite the many applications of CuAAC reactions, the involvement of multiple equilibria between several reactive intermediates makes the kinetics of these processes extremely difficult to establish (Worrell, Malik, & Fokin, 2013).

4.4.2 Plasma membrane and trypsinisation

The plasma membrane plays an essential role in maintaining normal physiological activities in mammalian cells (Huang et al., 2010). For intracellular applications, the permeability of the plasma membrane is an essential physiological parameter in CuAAC-based hypoxia-specific labelling since both reactants and other components of the reaction cocktail have to cross the membrane to reach the intracellular target sites (Uttamapinant et al., 2013). Another factor to consider is the permeability of the azide-modified fluorophore. Ideally, fluorophores should extensively accumulate in cytosol with even intracellular distribution to allow them to efficiently participate in bimolecular reactions. This makes the structural and physicochemical properties essential during the design of fluorescent azide (Cunningham et al., 2010).

When cultured adherent cells reach confluence, trypsin is generally used to detach cells from the substratum via its proteolytic activity. This trypsinisation procedure may, however, physiologically affect cells by cleaving the cell surface growth factor receptors, adhesive proteins, or other types of membrane proteins (Huang et al., 2010; Soler et al., 1997). In a recent study, the proteolytic activity of trypsin provoked a leaky cell plasma membrane by trypsin-induced digestion of cell membrane proteins, leading to a change in cellular uptake within 24 h after trypsinisation (Serdiuk, Alekseev, Lysenko, Skryshevsky, & Geloen, 2014). In addition, the trypsinisation-induced dysregulation of expression of some proteins even remained after a 24-h recovery in fresh medium (Huang et al., 2010). In this thesis, a 24-h difference in recovery time after trypsinisation did not cause obvious changes in the results of click chemistry-based method (Figure 4.2). This suggested that mild trypsinisation did not cause major changes in cell integrity that could affect CuAAC-mediated labelling of SN33267-entrapped adducts.

4.4.3 Reducing agent

The catalysis of CuAAC reactions depends on the presence of copper in the oxidation state +1. For reactions performed in aqueous solvents, copper(I) ion can be introduced directly as cuprous bromide or acetate salts (Meldal & Tornoe, 2008; Rostovtsev et al., 2002; Tornøe et al., 2002). In this Chapter, the catalytically active species of copper was indirectly supplied via the *in situ* reduction of $CuSO_4$. To convert back this cupric salt to the catalytically active +1 oxidation state, two types of reducing agent, sodium ascorbate and TCEP, were tested in this study.

Since the standard protocols introduced by Sharpless and Fokin, copper(II) salts with three- to ten-fold excess of reducing agent became the most common procedure to provide catalysis for the CuAAC reaction via the *in situ* reduction (Bock et al., 2006; Rostovtsev et al., 2002). An excess of reducing agent is utilised in combination with copper(II) salts to achieve and/or preserve the stabilised copper(I) oxidation state required for the CuAAC reaction.

Previous studies suggested that TCEP could be only used at low concentrations compared with the 10- to 20-fold excess of sodium ascorbate with respect to copper (Berg & Straub, 2013; Rostovtsev et al., 2002; Rudolf & Sieber, 2013). In this Chapter, 2 mM sodium ascorbate or 1 mM TCEP in combination with 1 mM $CuSO_4$ gave the best hypoxic to oxic ratio within the concentration

ranges studied. But there was only small change in the hypoxic to oxic ratio over the increment of sodium ascorbate concentration from 1 to 100 mM. In TCEP-reduced reaction cocktail, however, concentration of TCEP had to be within a narrow range (0.5 – 1 mM) to give a good ratio.

Sieber and co-workers observed that sodium ascorbate was better than TCEP in serving as reducing agent to generate the active copper(I) species (Rudolf & Sieber, 2013). However, this difference between two reducing agents was not observed in this Chapter. One study suggested that the use of TCEP as reducing agent in CuAAC resulted in substantially lower yield and required longer incubation time for reaction completion (Lim, Mizuta, Takasu, Kim, & Kwon, 2014). Such an inhibitory impact was not identified in this thesis.

4.4.4 Copper ions

In order to both achieve a sufficient concentration to form the proper catalytic complex incorporating more than one metal centre and ensure high rates of reaction, copper concentrations have been suggested in the range from 50 to 100 μM (Hong et al., 2009). In the CuAAC reaction mediating this click chemistry-based methodology, the optimal setting of copper concentration was determined as 1 mM when $CuSO_4$ was used. To achieve a stable copper(I) ion supply, the optimal concentration of reducing agent was 100 mM for sodium ascorbate or 500 μM for TCEP combined with 1 mM $CuSO_4$ in the reaction cocktail.

The presence of copper ions can lead to degradation or aggregation of target biomolecules, which usually attributed to the production of oxygen radicals or other reactive species generated during the maintenance of copper ions in the active +1 oxidation state in the presence of atmospheric oxygen (Hong et al., 2010). Without removal of atmospheric oxygen, this ROS-induced biological damage can be either diminished by deploying copper(I)-stabilizing ligands (Chan et al., 2004) or avoided by use of SPAAC reactions (see below) (Agard et al., 2004; Marks et al., 2011).

4.4.5 Ligand

As a ligand-accelerated process, CuAAC relays on competent ligands that are capable to protect copper(I) from oxidation under aerobic aqueous conditions and facilitate copper(I)-catalysed

transformations (Chan et al., 2004; Hong et al., 2009). The functions of ligands in enhancing cell compatibility of CuAAC are predominantly accomplished by forming tight associations with the catalyst to stabilise copper ions in the +1 oxidation state and increasing its catalytic efficiency. Additionally, the function of ligand in binding copper(I) ions is to avoid damage to biomolecules (Besanceney-Webler et al., 2011; del Amo et al., 2010). The presence of ligands is particularly important in reactions involving biological molecules with relative low concentrations (Hein & Fokin, 2010). Aside from the effects on cell damage, the presence of ligand in CuAAC may also contribute to the enhanced membrane permeability (Hong et al., 2010). Proper selection of copper-binding ligand is therefore necessary (Hong et al., 2009).

A variety of ligands have been found to be functional under various conditions. The majority of the best performing ligands, so far, are oligotriazole derivatives derived from propargylamine cores. Both ligands investigated in this thesis, TBTA and THPTA, belong to this class of ligands. The shared similar structural motif allows these ligands to bind to metals by forming a five-member chelate between the N-3 of the triazole and the amine (Chan & Fokin, 2007; Chan et al., 2004; Hong, Udit, Evans, & Finn, 2008; Rodionov et al., 2007). Normally, greater amounts of copper(I) and accelerating ligand than the azide and alkyne reactants are required by the CuAAC-mediated bioconjugations (McKay & Finn, 2014).

According to the results in this Chapter, TBTA with the optimal concentration of $CuSO_4$ (1 mM) in a ratio of 1:2 or 1:10 was found to result in the best hypoxic to oxic ratio in the CuAAC-mediated cell clicking approach when 500 μM sodium ascorbate or 500 μM TCEP were used in the reaction cocktail, respectively. When THPTA was used as ligand in the reaction, 1 mM $CuSO_4$ combined with THPTA in a ligand to copper ratio of 1:5 generated the best hypoxic to oxic ratio under the reduction of 500 μM sodium ascorbate. Similar to TBTA, the ligand to copper ratio of 1:10 also gave rise to the best performance of the CuAAC-mediated approach when THPTA was used as ligand combined with 1 mM $CuSO_4$ and 500 μM TCEP in the reaction cocktail.

In aqueous buffers, TBTA shows, however, relatively low level of solubility that causes incomplete ligation especially in the case when both reactants are at micromolar concentrations (del Amo et al., 2010). The poor solubility of TBTA in water prompted the development of more polar analogues,

such as THPTA. THPTA is a member of the tris(triazolyl)methylamine family with enhanced water solubility in comparison to TBTA (Chan et al., 2004). The maximum concentration of TBTA used in this Chapter is 1 mM. This concentration of TBTA induced severe precipitation in the reaction cocktail in the presence of 1 mM $CuSO_4$ and 500 μM TCEP (Figure 4.3B). When 500 μM TCEP was replaced with the same concentration of sodium ascorbate, no precipitation was observed in reaction cocktail containing 1 mM of TBTA (Figure 4.3A).

4.4.6 Removal of background staining

High background staining was a major issue during the optimisation of the methodology to achieve better selectivity to click hypoxic cells with fluorophores. Non-specifically bound fluorescent labels can lead to very high levels of background fluorescence staining, compromising the sensitivity of detection (Herner et al., 2013).

The background fluorescence staining induced by this click chemistry-based approach can be divided into two types. Both types lead to a lower signal-to-noise ratio. Non-specific binding results from the fluorophore binding to other low-affinity binding sites and materials and thereby raising the fluorescence (Soh, 2008). In the context of CuAAC, non-specific binding is thought to be reversible. This type of background fluorescence staining could thus be washed out, in theory. Another possibility is oxic/aerobic formation of covalent SN33267 adducts and/or incomplete washout of non-covalently bound SN33267 or products thereof that could result in an elevated fluorescence signal in cell sample. However, very little, if any, covalent adducts were formed from SN33267 under oxic conditions in three experiments of detecting optimal ligand to copper ratio (Figure 4.3, Figure 4.4, and Figure 4.5). These observations are consistent with a similar very-low level of oxic formation of covalent 2-NI adducts of [^{14}C]-EF5 in SiHa cells (Wang et al., 2012).

A series of experiments were performed to determine the cause(s) of this enhanced background fluorescence induced by non-specific binding. The investigation covered SiHa cells as well as all reagents, solutions, and equipment involved in the whole SN33267-mediated cell labelling and CuAAC-based clicking processes without finding the source. Instead of tracing the source of this issue, efforts were redirected to finding a way of removing this non-specific staining. With a concern for RNA integrity (which will be discussed in Chapter 5), an RNA-friendly organic solvent

ethanol was tested, which eventually solved the problem of non-specific staining by inclusion of an additional wash step with 50% (v/v) ethanol-PBS solution. Moreover, it was identified that a single wash step with 50% (v/v) ethanol-PBS solution followed by 2× wash steps with PBS efficiently diminished background fluorescence staining in oxic samples, establishing a new protocol (protocol #3 in Figure 2.1) of the click chemistry-based technique.

Being one well-known category of the prime bioorthogonal participants, azides are absent in biological systems and practically inert in biosystems (Debets, van der Doelen, Rutjes, & van Delft, 2010; Griffin, 1994). Likewise, alkynes also possess very similar abiotic features (Grammel & Hang, 2013). In general, azides and alkynes are small in size and relatively stable to the attached structures. These features allow both reaction partners to be easily introduced to biological molecules without altering their function or metabolic processing (Grammel & Hang, 2013; McKay & Finn, 2014; Sletten & Bertozzi, 2009).

Facilitated by the additional wash step, both the optimal concentration of SN33267 used to tag cells in a hypoxia-dependent manner and the optimal concentration of azide-modified fluorophore in the reaction cocktail used to label SiHa cells were determined. The optimised protocol was confirmed with other two human cancer cell lines (HCT116 and HT-29) and showed similar capability in selectively clicking hypoxic cells with fluorophores in these cell lines.

Technically, the ethanol-PBS solution used in this wash step also to some extent fixed cells in addition to removing background fluorescence signals (Rolls, 2012). Besides morphological fidelity and protein antigenicity, fixation techniques are capable to preserve the integrity of nucleic acids when the availability of fresh sample is limited, which highly impacts on both basic and applied biomedical sciences (Antica, Paradzik, Novak, Dzebro, & Dominis, 2010). It has been well-documented that the ethanol-based fixation of tissue sample provides additional protection to both DNA and RNA, which makes such fixed-tissue specimens more useful for gene expression profiling studies (Cox et al., 2006; Gillespie et al., 2002; Milcheva, Janega, Celec, Russev, & Babal, 2013). Thus, this ethanol wash step may additionally benefit the RNA integrity in the cells, which makes the methodology more compatible with downstream analysis of gene expression (see next Chapter).

So far, considerable effort has been devoted to increasing the reaction rate, biocompatibility, and pharmacokinetic properties of the cyclooctyne components utilised in SPAAC (Marks et al., 2011; Mbua et al., 2011; McKay & Finn, 2014; Patterson et al., 2014; Sletten & Bertozzi, 2011). The relatively large size and hydrophobic nature of the cyclooctyne derivatives may influence their distribution and induce changes in biological properties of the attached functional moieties, which raises a major concern in applying SPAAC in bioconjugation (McKay & Finn, 2014). In this Chapter, a couple of *in vitro* experiments were conducted using an SPAAC-mediated protocol. SiHa cells were successfully labelled in a hypoxia-selective manner. This work with SPAAC reactions showed good prospects, demonstrating a huge potential for future exploitation in the near future.

In the dual staining study using EF5 and SN33267 in an A431 tumour xenograft, the two staining patterns were overlapped very well. It illustrated that the two approaches based on different mechanisms (click chemistry and antibody binding) labelled the same hypoxic regions, which partly validated the CuAAC methodology for labelling hypoxic cells *in situ*.

In summary, a clickable 2-nitromidazole hypoxia marker bearing a side chain with a terminal alkyne group was used to tag cancer cells in a hypoxia-selective manner. Copper(I)-catalysed click reaction with fluorophore azides was optimised to achieve maximum labelling selectivity of hypoxic cells.

4.5 Acknowledgements

We thank Dr Ralph Stevenson for the synthesis of BCN (SN34710) and Dr Andrew Marshall for syntheses of TCO (SN35189) as well as SN35580. We thank Sarah McManaway for her unpublished data of dual staining in A431 tumour xenograft with EF5 and SN33267 using fluorescence confocal microscopy (Figure 4.18).

Chapter 5. Click chemistry-based cell labelling and RNA integrity

5.1 Introduction

RNA plays an important role in transferring information encoded in genomic DNA to functional proteins. An inherent feature of RNA is that the hydroxyl group attached to the pentose ring in the 2' position of ribose renders it much less stable than DNA since it is more susceptible to hydrolysis (Shukla, 2014). The degradation of RNA is a gradual process, which can be followed by a reduction in the 18S and 28S ribosomal band ratio, i.e. less sharply defined bands, and small fragments or even a smeared appearance in slab gel electrophoresis (Fleige et al., 2006; Schroeder et al., 2006).

5.1.1 RNA integrity and RIN

In attempts to obtain meaningful gene expression data, the assessment of RNA integrity becomes a critical step for successful RT-PCR or microarray analyses (Fleige & Pfaffl, 2006; Schroeder et al., 2006). The 28S/18S ribosomal RNA (rRNA) ratio has been used to characterize the quality of RNA, which unfortunately often led to an inaccurate assessment of the RNA integrity because this method largely relied on a user-dependent interpretation of the data. A reliable, reproducible, and standardised approach to classifying the quality of RNA samples was developed to avoid user bias and variability.

To date, an automated capillary-electrophoresis system, the Agilent 2100 Bioanalyzer, and associated RNA 6000 series LabChip kits have become the most popular method to provide an industry standard for RNA quality assessment and quantitation (Mueller et al., 2000). RNA samples are separated according to molecular size by electrophoresis on microfabricated chips and subsequently detected via laser-induced fluorescence detection.

The data from each tested RNA sample are computed by the Bioanalyzer software to generate an electropherogram and gel-like image with information on sample concentration, allowing a visual

inspection of RNA integrity and the approximated ratio between the mass of ribosomal sub-units (Fleige & Pfaffl, 2006; Imbeaud et al., 2005; Schroeder et al., 2006).

In order to remove individual interpretation of RNA quality control and standardise the procedure of RNA integrity assessment, an RNA Integrity Number (RIN) software algorithm was developed by Agilent Technologies. By taking the entire electrophoretic trace into account, this RIN software algorithm allows the classification of total RNA, based on a numeric system from 1 through 10, where 1 represents the most degraded RNA and 10 is completely intact RNA (Figure 5.1). In this way, interpretation of an electropherogram is facilitated, and comparison of samples is made possible with better reproducibility due to the standardised approach (Schroeder et al., 2006). Moreover, it has been observed that the RIN scores are independent of sample concentration, instrument and analyst, which provides an unbiased comparison of samples and thereby becomes a *de facto* standard for RNA integrity (Brisco & Morley, 2012; Chen et al., 2014; Fleige et al., 2006; Kap et al., 2015; O'Brien, Costin, & Miles, 2012; Schroeder et al., 2006).

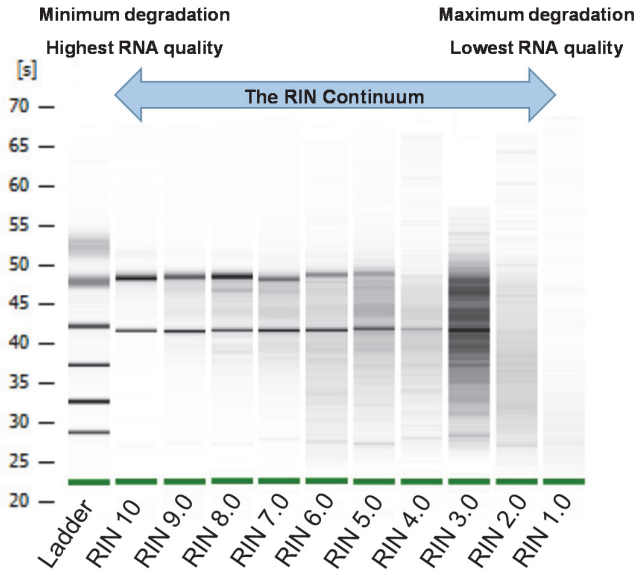

Figure 5.1: RNA integrity categories defined by RIN scores.

The Agilent 2100 Bioanalyzer software generated gel-like image of ten RNA samples generated in this thesis shows typical representatives of the ten integrity categories. RIN scores range from 10 (intact) to 1 (completely degraded).

The degradation of RNA can distort or prevent measurement of RNA transcripts (Brisco & Morley, 2012). Consequently, the ability to rapidly estimate RNA quality using minor amounts of sample, which is often precious, has become more important since subsequent measures of mRNA transcripts have become more expensive, labour-intensive, time-consuming, and comprehensive (Fleige & Pfaffl, 2006; Imbeaud et al., 2005). Before any RNA-dependent application, an iterative process of reliable and precise integrity checks is highly recommended to establish a RIN threshold value for obtaining meaningful results from downstream experiments (Brisco & Morley, 2012; Fleige et al., 2006; Schroeder et al., 2006).

5.1.2 Cytotoxic effect of Copper(I) on RNA integrity

Copper(I) plays crucial roles in biochemical processes occurring within a living cell or organism, largely because it is present in several critical metabolic enzymes that are responsible for vital electrolytic redox processes (Chan et al., 2004; Harris, 2001). Due to its general thermodynamic instability, copper(I) is easily oxidised to copper(II) and/or readily undergoes disproportionation in aqueous solutions forming copper(II) ions and copper metal [Cu(0)] (Festa & Thiele, 2011; Hein & Fokin, 2010; Kiaune & Singhasemanon, 2011; Struthers, Mindt, & Schibli, 2010). Therefore, strict experimental conditions, such as inert atmospheres and anhydrous solvents, are usually required during copper(I)-mediated processes.

Although it has excellent reaction kinetics, high specificity, and remarkable bioorthogonality, the application of CuAAC has demonstrated toxic effects in cells due to the copper(I)-mediated generation of reactive oxygen species (ROS) from O_2 (Hong et al., 2010). The potential of ROS in causing cellular damage has been intensively studied (Hensley, Robinson, Gabbita, Salsman, & Floyd, 2000). The presence of ROS is able to induce RNA degradation in cells (Temple et al., 2005).

This problem can be addressed by compromising on reaction kinetics, e.g. by replacing CuAAC with SPAAC to completely remove the requirement of copper(I)-catalysis because CuAAC is 10-100 times faster than SPAAC in aqueous solutions (Jewett & Bertozzi, 2010; Mbua et al., 2011; Presolski et al., 2010; Presolski et al., 2011; Yao et al., 2012). Alternatively, the biocompatibility of

CuAAC can be improved by deployment of ligands that help to protect cells from ROS by accelerating the reaction and acting as sacrificial reductants (Hong et al., 2009).

It has been shown that CuAAC-mediated approaches can still cause slight ROS-mediated cytotoxicity to induce protein damage even at a copper concentration of 10 – 40 μM. To ensure maximum viability in cells when CuAAC is applied with the use of the best copper(I)-stabilising ligands, the following steps have been suggested (Uttamapinant et al., 2013). Copper ions can be immediately sequestrated after labelling by the addition of bathocuproine sulfonate acting as a cell-compatible copper(I) chelator. In addition, EDTA in high molar excess has been suggested for use as additive to inactivate copper(I) catalysis by strong complexation and sequestration of the copper(II) species (Rudolf & Sieber, 2013). Moreover, the radical scavenger 4-hydroxy-2,2,6,6-tetramethylpiperidin-1-oxyl (TEMPOL) can be used to quench ROS (Uttamapinant et al., 2013).

5.1.3 Chelation-assisted CuAAC

The CuAAC-associated cytotoxicity is related to the concentration of copper in the reaction system due to the role of copper in generating ROS. Improved compatibility with cells can be simply achieved by decreasing the applied concentration of copper, which unfortunately results in a significant reduction in reaction kinetics (Besanceney-Webler et al., 2011). To satisfy the catalytic requirement of CuAAC and simultaneously minimise the copper-induced toxicity, azides containing an internal copper-chelating moiety were introduced into the field of biomolecular labelling (Uttamapinant et al., 2013; Uttamapinant et al., 2012).

Fokin *et al.* discovered that the formation of a copper(I) acetylide intermediate initiates the copper(I)-catalysed cycloaddition, which is followed by the generation of a binuclear copper intermediate through the approach of a second copper(I) (Worrell et al., 2013). According to the mechanistic rationale of CuAAC, organic azides bearing an internal copper(I)-chelating motif could further accelerate the CuAAC reaction by facilitating the coordination of the second copper(I) species (Jiang et al., 2014).

The concept of using copper-chelating azides to facilitate reaction kinetics was invented and initially explored for azide-alkyne reactions in organic solvents (Brotherton et al., 2009; Kuang,

Michaels, Simmons, Clark, & Zhu, 2010). Due to an internal copper-chelating moiety enriching the effective copper concentration at the reaction site, azides bearing strong copper-chelating moieties facilitated the formation of azide-copper complexes, which resulted in the reactions with alkynes taking place virtually instantaneously under diluted conditions (Bevilacqua et al., 2014).

Azides with proximal pyridine nitrogen atoms are able to chelate the copper(I) ions. Picolyl azides have demonstrated much faster reaction kinetics compared with standard azides due to internal chelation of the copper catalyst by increasing the electrophilicity of the azido group and facilitating the formation of the metallacycle intermediate (Brotherton et al., 2011; Brotherton et al., 2009; Kuang et al., 2010; Yuan, Kuang, Clark, & Zhu, 2012). The reaction rate of CuAAC was dramatically enhanced by application of a chelation-competent azide. A much lower concentration of copper was required for the cycloaddition involving copper-chelating azide compared to the reaction using conventional azide and to achieve the same kinetics. Additionally, reactions with copper-chelating azides were even carried out in the absence of accelerating ligand with faster reaction rates than non-chelating azides in the presence of ligand (Uttamapinant et al., 2012).

5.2 Aims

At the core of this project was the idea of taking advantage of the high efficiency and bioorthogonality of CuAAC to label hypoxic tumour cells and sort these by FACS for subsequent measurement of differential gene expression as a function of hypoxic stress *in situ*.

Following FACS of the fluorescence-labelled cells in a hypoxia-dependent manner, reverse transcriptase-quantitative PCR (RT-qPCR) was the method of choice to obtain a sensitive and reliable quantitative assessment of low-abundance mRNA as a measure of gene expression (Bar, Ståhlberg, Muszta, & Kubista, 2003; Fleige et al., 2006). The integrity of RNA during subsequent work-up is crucial for studies of transcripts as it tries to take a snapshot of gene expression at the moment of collecting the biological sample (Coulson et al., 2008; Schroeder et al., 2006). A certain RIN score has been suggested in different published studies and used as the RNA integrity cut-off for expression assessment by RT-qPCR (Fleige & Pfaffl, 2006; Fleige et al., 2006; Jahn, Charkowski, & Willis, 2008; Li et al., 2008; Marotta et al., 2011). The optimised CuAAC-mediated

method thus requires preserving maximum RNA integrity in addition to the high selectivity of cell labelling in a hypoxia-dependent manner.

The key task of this Chapter was to further optimise the methodology by which cells were successfully sorted into fractions according to their hypoxia status in such a way that the quality of RNA extracted from these sorted cells would be adequate for gene expression analysis by RT-qPCR.

In Chapter 2, BODIPY-FL-azide and TAMRA-azide were selected from the list of candidates, which was followed by determining the optimal conditions and/or settings of each component involved in the CuAAC reaction between the bioreductive metabolism of clickable 2-NI (SN33267) and fluorophore azide in attempts to improve hypoxia-selectivity of cell labelling in Chapter 3. BODIPY-FL-azide and TAMRA-azide share an identical azide moiety by carry different fluorescent moieties (Figure 3.1). In this Chapter, the majority of experiments in optimising the click chemistry based methodology were carried out by using BODIPY-FL-azide and a new copper-chelating fluorophore azide, Super-DIPY, which was also chosen to be synthesised on the basis of BODIPY fluorescent moiety. This was due to the fact of the limited accessibility for the BD FACSAria™ II Cell Sorter that was equipped with 552 nm green laser capable of generating optimal excitation wavelength for TAMRA-azide (Table 2.8).

The specific objectives are:

- To maximise the compatibility of the method optimised in Chapter 4 using BODIPY-FL-azide with extraction of high-quality RNA;
- To maximise RNA integrity of the method by introducing chelation-assisted CuAAC;
- To validate the optimised methodology in cell cultures under different hypoxic stress.

5.3 Results

In Chapter 4, the protocol was optimised and validated *in vitro* to selectively label cells with fluorophores in a hypoxia-dependent manner. The integrity of RNA was assessed using an Agilent 2100 Bioanalyzer (Agilent Technologies, CA, USA). The optimised methodology (protocol #3 with reaction cocktail #1 or #2) resulted in poor integrity RNA extracted from labelled cells (RIN < 2).

Therefore, the CuAAC-based methodology was further optimised in this Chapter to improve the quality of the extracted RNA. In order to at least maintain the same hypoxia-selectivity of labelling and in an attempt to improve RNA integrity of the labelled cells, first different reaction cocktails derived from the recipes of reaction cocktails #1 or #2 were tested using the same experimental protocol (protocol #3). Subsequently, the experimental protocol was modified in order to further improve the RNA integrity in labelled cells. In this Chapter, not only the capability of selectively clicking fluorophores with hypoxic cells but also the integrity of RNA extracted from cells labelled by the CuAAC-based approach were equally important during judgement of the performance of this click chemistry-based technique.

5.3.1 Improving compatibility of CuAAC with high-quality RNA using BODIPY-FL azide

Apart from an azide-modified fluorophore, the reaction cocktail also consists of a copper source, a reducing agent, and a stabilising ligand. Since ROS-mediated damage in cells is mainly induced by copper ions, two different ligands (TBTA vs. THPTA) and two different sources of copper ($CuSO_4$ vs. CuOAc) were compared with reduction by sodium ascorbate or TCEP based on the protocol optimised in Chapter 4 (protocol #3 in Figure 2.1). For each reducing agent, four different reaction cocktails (reaction cocktails #1, #2, #5, or #6 in Table 2.7) were examined for both hypoxia-selectivity and RNA compatibility (Table 5.1).

The reaction cocktail using TCEP as reducing agent and TBTA as stabilising ligand showed the two highest hypoxic to oxic ratios with both sources of copper. Considering the RNA integrity, the best option of reducing agent in the reaction cocktail was TCEP. The selection of CuOAc together with TCEP in the reaction cocktail gave the highest RNA integrity from labelled cells. Of all eight

tested reaction cocktails, the one (reaction cocktail #5 in Table 2.7) with copper-catalysis provided by CuOAc, TBTA and TCEP gave the second high hypoxic to oxic ratio and the highest RIN.

Table 5.1: Labelling selectivity and RNA integrity of CuAAC reaction cocktails.

Reducing Agent	Ligand	Copper Source			
		$CuSO_4$		CuOAc	
Sodium Ascorbate	TBTA	Hypoxic/Oxic ratio: 5.9	RIN: 2.3	Hypoxic/Oxic ratio: 4.6	RIN: 2.4
	THPTA	Hypoxic/Oxic ratio: 7.6	RIN: 2.2	Hypoxic/Oxic ratio: 6.5	RIN: 2.3
TCEP	TBTA	Hypoxic/Oxic ratio: 17.0	RIN: 3.2	Hypoxic/Oxic ratio: 10.6	RIN: 6.1
	THPTA	Hypoxic/Oxic ratio: 6.1	RIN: 2.4	Hypoxic/Oxic ratio: 4.4	RIN:6.6

Note: SiHa cells were incubated under oxic or hypoxic conditions with SN33267 and clicked with BODIPY-FL-azide via CuAAC in a hypoxia-selective manner by following protocol #3 (see Figure 2.1) and using reaction cocktail #1, #2, #5, or #6 (see Table 2.7). Fluorescence intensity was determined by flow cytometry. Hypoxic/Oxic ratio was calculated by use of median fluorescence intensity (MFI) derived from the corresponding flow cytometry histogram. RIN scores were generated by RNA samples extracted from the hypoxic SiHa cells labelled with BODIPY-FL-azide. Representative data from 3 independent experiments are shown.

To test the hypothesis that shorter total experiment time may improve RNA quality, SiHa cells were incubated under oxic or hypoxic conditions with SN33267 and labelled with BODIPY-FL-azide in a hypoxia-selective manner by following protocol #3 (see Figure 2.1) to test the minimal time required for the CuAAC reaction. During the incubation step with reaction cocktail, one group of cell samples was used for reference purpose (Figure 5.2C) by incubating with reaction cocktail #5 (see Table 2.7) and following protocol #3 (see Figure 2.1). The other two groups of samples were only incubated once with the same reaction cocktail for 30 (Figure 5.2A) and 60 min (Figure 5.2B), respectively.

In the standard protocol (protocol #3), the incubation with reaction cocktail is a two-stage procedure including a 30-min incubation with reaction cocktail followed by washing once with 1% (w/v) BSA-PBS and then a second 30-min incubation with a fresh second dose of reaction cocktail, termed as “30-min + 30-min incubation with two doses of reaction cocktail” or “30-min + 30-min double-clicking” in this thesis (Figure 5.2C).

The flow cytometric histograms of the hypoxic cells with both 30-min and 60-min incubation with a single dose of reaction cocktail (dark green; Figure 5.2A and B) demonstrated incomplete

labelling with BODIPY-FL-azide in comparison to the hypoxic cells in the reference group (dark green; Figure 5.2C). With an increase of reaction time from 30 to 60 min, more cell-entrapped SN33267 adducts in hypoxic cells reacted with BODIPY-FL-azide shown as a right-shift of the histogram (dark green). In contrast to the 60-min incubation with a single dose of reaction cocktail, the addition of the second dose of fresh reaction cocktail after 30 min of incubation clearly boosted the CuAAC reaction to go to completion within the same 60-min of total reaction time (Figure 5.2C). Thus, complete reaction in this CuAAC-based cell labelling procedure depends on the reaction time and/or on the addition of fresh reaction cocktail during the reaction

To identify the crucial component(s) in the second dose of reaction cocktail that was applied halfway of the click reaction, defined fresh reaction cocktails lacking certain component(s) were applied to cells to replace the standard reaction cocktail in the second 30-min incubation step. In all tested conditions, only the hypoxic cell sample incubated with 10 mM Tris-buffered saline-alone in the second 30-min incubation showed a histogram with clearly-distinguished multiple peaks in the flow cytometric analysis (Figure 5.2D). In the other four tested conditions, the flow cytometric histograms of the hypoxic samples (dark green; Figure 5.2E to H) showed a single peak but with a wider base than the one via the standard protocol (dark green; Figure 5.2C), which suggested incomplete/inefficient click reaction as well.

Selective lack of a component in the second dose of the reaction cocktail (dark green; Figure 5.2E to H) resulted in a broader diversity of fluorescence intensity in labelled hypoxic cells comparing to the control condition (Figure 5.2C). The changes were mainly observed at the front-end of the histogram while the tail-end seemed to be quite constant and similar to the reference in Figure 5.2C. All this indicated incomplete/inefficient clicking during the first 30 min and only a small boost by a second fresh cocktail regardless of its composition.

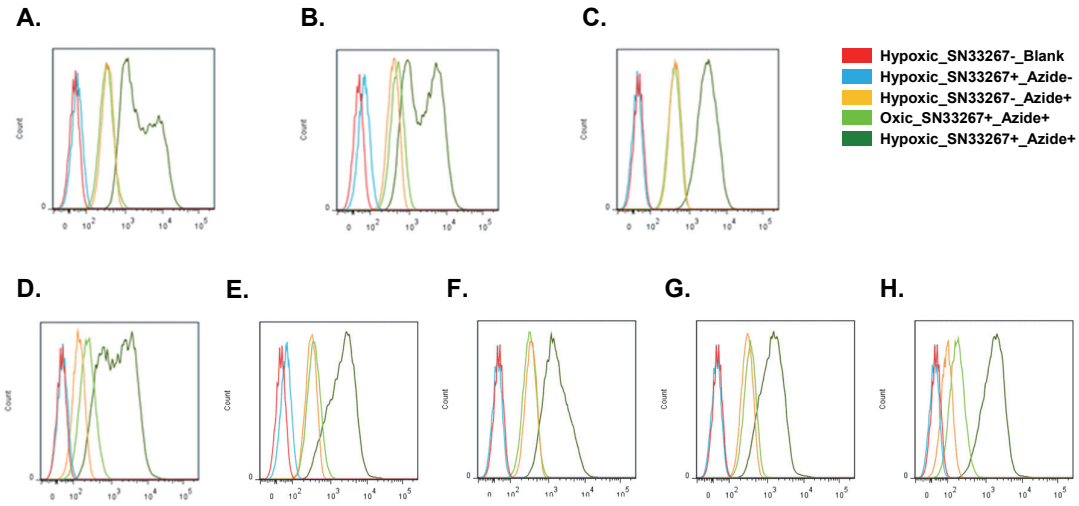

Figure 5.2: The effect of incubation time and composition of reaction cocktail on clicking cells with BODIPY-FL-azide in a hypoxia-selective manner.

Flow cytometric histograms of SiHa cells incubated under oxic or hypoxic conditions and labelled with BODIPY-FL-azide in a hypoxia-selective manner by following different protocols modified from protocol #3 (see Figure 2.1) and using reaction cocktail #5 (see Table 2.7). (A) 30-min incubation with reaction cocktail. (B) 60-min incubation with reaction cocktail. (C) Following protocol #3 and using reaction cocktail #5. In (D) to (H), cells were all incubated for 30 min with reaction cocktail followed by washing once with 1% (w/v) BSA-PBS but different modified cocktails were used in the second 30-min incubation. (D) 10 mM Tris-buffered saline. (E) Reaction cocktail #5 without CuOAc. (F) Reaction cocktail #5 without TBTA. (G) Reaction cocktail #5 without TCEP, (H) reaction cocktail #5 without BODIPY-FL-azide. Representative data from 3 independent experiments are shown.

The CuAAC reaction demonstrated reasonable RNA integrity when copper ions were supplied by CuOAc under the reduction of TCEP compared with $CuSO_4$ (Table 5.1). The ROS-mediated cellular damage is related to the concentration of copper in the reaction system due to the role of copper in generating ROS. Improved compatibility with cells can be simply achieved by decreasing the applied concentration of copper and limiting the exposure time of cells to the reaction cocktail (Besanceney-Webler et al., 2011). To determine the minimum required concentration of CuOAc and reaction time without inducing significant reduction in reaction kinetics, three different concentrations of CuOAc and two different incubation times with reaction cocktail were examined *in vitro*.

According to the flow cytometric analysis, 30-min incubation with a single dose of reaction cocktail resulted in incomplete CuAAC reaction with all three tested concentrations of CuOAc (Figure 5.3 top row). Based on the shape of the histograms generated by hypoxic cells (dark green), fewer hypoxic cells were completely labelled with BODIPY-FL-azide. The same trend of incomplete CuAAC reaction was observed in the cells labelled with BODIPY-FL-azide via the standard procedure described in protocol #3 (Figure 2.1; Figure 5.3 bottom row). Of all tested conditions, only the 30-min + 30-min incubation with two doses of reaction cocktail containing 1 mM CuOAc led to the complete CuAAC reaction between intracellular SN33267 adducts and azide-modified fluorophore (Figure 5.3 bottom-left panel). Among the three tested CuOAc concentrations in the 30-min + 30-min double clicking procedure, cells clicked by the reaction cocktail containing 1 mM CuOAc provided the RNA with the highest level of integrity. Interestingly, the RIN score slightly decreased with the reduction of CuOAc concentration in reaction cocktail (Figure 5.3 bottom row).

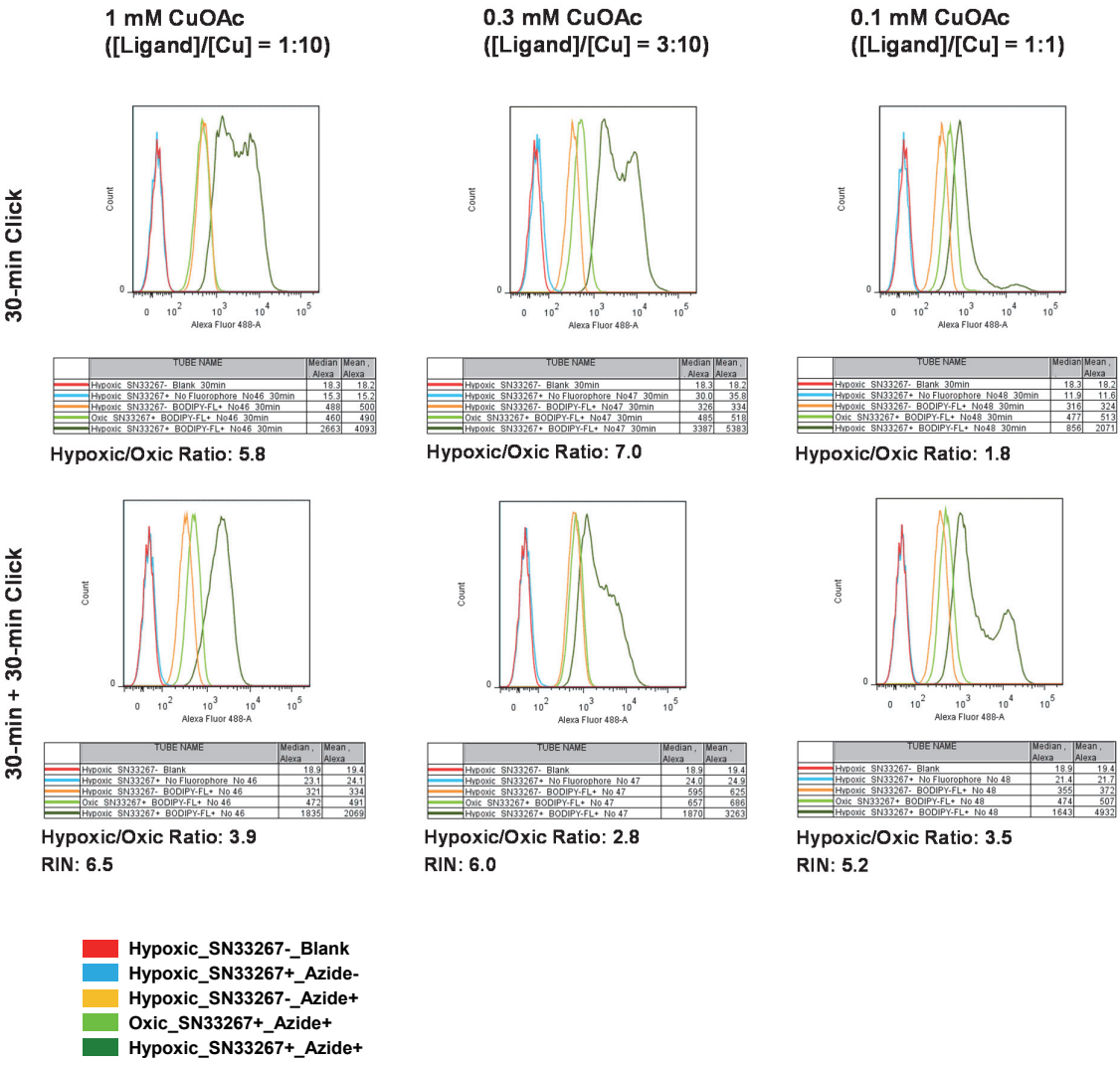

Figure 5.3: The effect of click reaction time and copper concentration on clicking cells with BODIPY-FL-azide in a hypoxia-selective manner.

Flow cytometric histograms of SiHa cells incubated under oxic or hypoxic conditions and labelled with BODIPY-FL-azide via CuAAC in a hypoxia-selective manner by following different protocols modified from protocol #3 (see Figure 2.1) and using reaction cocktails modified from reaction cocktail #5 (see Table 2.7). RIN scores were generated by RNA samples extracted from the hypoxic SiHa cells labelled with BODIPY-FL-azide. Representative data from at least 3 independent experiments are shown.

In order to achieve complete click reaction, both the total time of incubation with reaction cocktail and the application of a second dose of fresh reaction cocktail were found to be critical based on analysis by flow cytometry. Instead of the 30-min + 30-min double click procedure in the incubation step with reaction cocktail in protocol #3 (Figure 2.1), a shortened 15-min + 15-min double click procedure was utilised to check if the reduction in overall incubation time with reaction cocktail in this way was able to provide acceptable hypoxia-selective cell labelling and improved RNA integrity.

Based on the flow cytometric analysis, the fluorophore labelled hypoxic cells (dark green) were well separated from the oxic cells (light green) when either 15-min + 15-min double click procedure (Figure 5.4A) or 30-min + 30-min double click procedure (Figure 5.4B) was applied during the incubation with reaction cocktail. According to the calculated hypoxic to oxic ratio, the reduction in the total incubation time was associated with a decrease in the hypoxia-selectivity. However, the same change made in the step of incubation with reaction cocktail slightly increased the RIN value from 4.1 to 4.6 (Table 5.2).

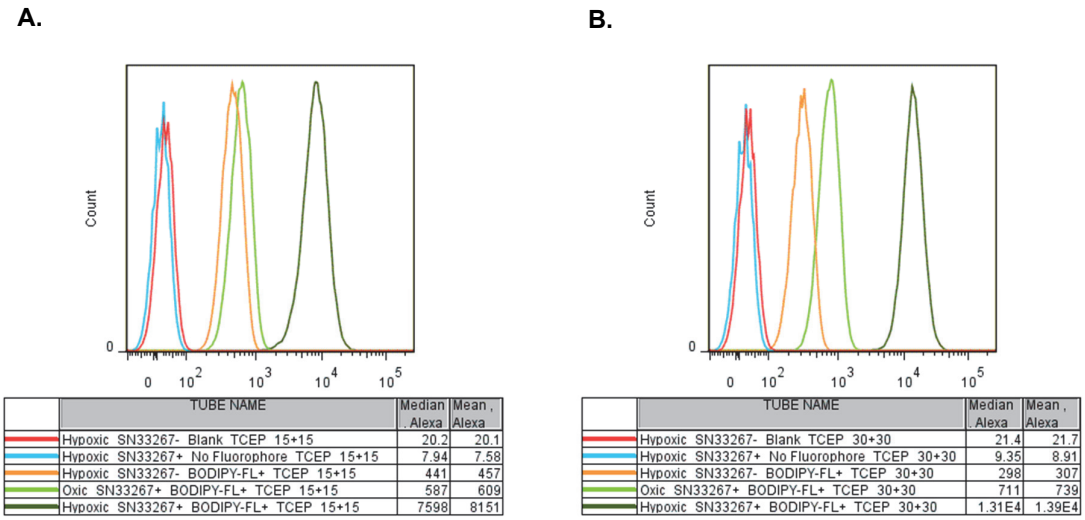

Figure 5.4: The effect of shortened click reaction time on clicking cells with BODIPY-FL-azide in a hypoxia-selective manner.

Flow cytometric histograms of SiHa cells incubated under oxic or hypoxic conditions and labelled with BODIPY-FL-azide in a hypoxia-selective manner by following protocol #3 (see Figure 2.1) and using reaction cocktail #5 (see Table 2.7). (A) 15-min + 15-min double click. (B) 30-min + 30-min double click. Representative flow cytometric data from at least 5 independent experiments are shown.

Table 5.2: RNA integrity in SiHa cells clicked with BODIPY-FL-azide in a hypoxia-selective manner after different click reaction times.

BODIPY-FL-azide	Hypoxic/Oxic Ratio	RIN
15-min + 15-min double click	12.9	4.6
30-min + 30-min double click	18.4	4.1

Note: SiHa cells were incubated under oxic or hypoxic conditions and clicked with BODIPY-FL-azide via CuAAC in a hypoxia-selective manner by following protocol #3 (see Figure 2.1) and using reaction cocktail #5 (see Table 2.7). Fluorescence intensity was determined by flow cytometry. Hypoxic/Oxic ratio was calculated by use of MFI derived from the corresponding flow cytometry histogram. RIN scores were generated by RNA samples extracted from the hypoxic SiHa cells labelled with BODIPY-FL-azide. Data are representative of at least 3 independent experiments.

5.3.2 Chelation-assisted CuAAC and Super-DIPY

The high reactivity of coordinated carbon azides in CuAAC is attributed to the fact that chelation-assisted binding between the alkylated azido nitrogen and the catalytic copper centre greatly enhances the electrophilicity of the azido group. This lowers the kinetic barrier to form the key metallacycle intermediate upon nucleophilic attack by the copper acetylide (Kuang et al., 2010). It has been well-documented that chelation-assisted azides based on this concept of chelation-assisted copper catalysis offer unprecedented reactivity in CuAAC reactions (Bevilacqua et al., 2014; Brotherton et al., 2011; Jiang et al., 2014; Jiang et al., 2011; Michaels & Zhu, 2011; Uttamapinant et al., 2013; Uttamapinant et al., 2012; Yao et al., 2012; Yuan et al., 2012).

A new BODIPY azide with an adjacent pyridine nitrogen, coined “Super-DIPY”, was synthesised by Dr Moana Tercel (Figure 5.5). In this picolyl azide, the proximal pyridine nitrogen atom is capable of coordinating with copper ions leading to improved reaction kinetics compared with standard azides due to the increased electrophilicity of the azido group, which facilitates the formation of the metallacycle intermediate (Brotherton et al., 2011; Brotherton et al., 2009; Kuang et al., 2010; Yuan et al., 2012).

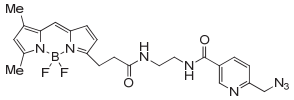

Super-DIPY (SN36482)
$C_{23}H_{25}BF_2N_8O_2$ 494.30 g/mol

Figure 5.5: Chemical structure of Super-DIPY.

To investigate the requirement for a stabilising ligand in the hypoxia-slective cell labelling, Super-DIPY was used to label cells following protocol #3 (Figure 2.1) using reaction cocktail #5 (Table 2.7) or reaction cocktail #5 without TBTA. For control purpose, a parallel group was performed using BODIPY-FL-azide.

The hypoxia-selective cell labelling using BODIPY-FL-azide demonstrated a strong ligand-dependency (Figure 5.6A). The presence of TBTA in reaction cocktail demonstrated a marked impact on the intensity of fluorescence signals of hypoxic cells. The omission of TBTA from the

reaction cocktail resulted in more than 60% decrease in the hypoxic to oxic ratio when BODIPY-FL-azide was used, which was predominantly caused by a decrease in fluorescence intensity of the hypoxic sample.

The CuAAC reaction between Super-DIPY and SN33267 adducts was independent of TBTA (Figure 5.6B). The removal of TBTA in reaction cocktail only led to 2.3% decrease in the hypoxic to oxic ratio, which was negligible. Super-DIPY demonstrated a 4.4-fold increase in the hypoxic to oxic ratio in comparison to BODIPY-FL-azide in the presence of TBTA.

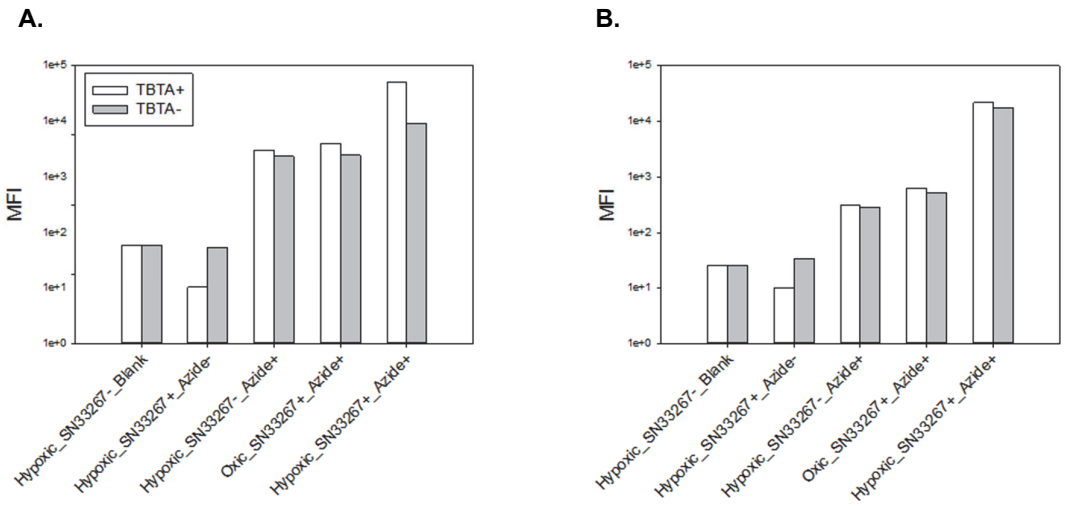

Figure 5.6: Ligand-dependency of CuAAC reaction mediated by BODIPY-FL-azide and Super-DIPY in hypoxia-selective cell labelling.

SiHa cells were incubated under oxic or hypoxic conditions and clicked with (A) BODIPY-FL-azide; (B) Super-DIPY in a hypoxia-selective manner by following protocol #3 (see Figure 2.1) and using reaction cocktail #5 (see Table 2.7). Each bar represents the median fluorescence intensity (MFI) derived from the corresponding flow cytometry histogram. Data are representative of 3 independent experiments.

The concentration of copper in the reaction system for CuAAC reaction is associated with damage of molecules in cells and effects on RNA integrity because of the damage to biomolecules induced by the copper-mediated generation of ROS from O_2 (Brewer, 2010; Hong et al., 2010; Temple et al., 2005; Wang et al., 2003). The chelation-assisted azide can enrich the concentration of copper ions *in situ* due to the presence of a proximal pyridine (Bevilacqua et al., 2014). To determine the optimal copper concentration required by Super-DIPY, $CuSO_4$ and CuOAc in a concentration

range from 0.1 to 1 mM were used to examine the hypoxia-selective labelling of SiHa cells with Super-DIPY by flow cytometry as well as the RNA integrity of the labelled cells.

Labelling hypoxic cells with higher copper concentrations resulted in higher fluorescence intensity regardless of whether the copper ions were supplied as cupric or cuprous salts. Within the tested concentration range, 1 mM copper salt reduced by 500 μM of TCEP in the presence of 100 μM TBTA gave the best hypoxic to oxic ratio (Figure 5.7A and B). The hypoxia-dependent cell labelling increased with increasing concentration of CuOAc in the same manner when the ligand was left out of reaction cocktail (Figure 5.7D). Again, Super-DIPY demonstrated the ability to react with cell-incorporated SN33267 in a ligand-independent fashion. The presence of TBTA showed a protective role with regard to RNA during the CuAAC reaction, which was more obvious when the reaction cocktail contained low concentration of CuOAc (Table 5.3). When the concentration of CuOAc was increased from 0.1 to 1 mM in ligand-free reaction cocktail, the RIN score of RNA extracted from Super-DIPY labelled cells increased from 3.7 to 6.3. In the presence of 100 μM TBTA in the reaction cocktail the RIN score increased from 5.2 to 6.5 over the same range of CuOAc concentrations.

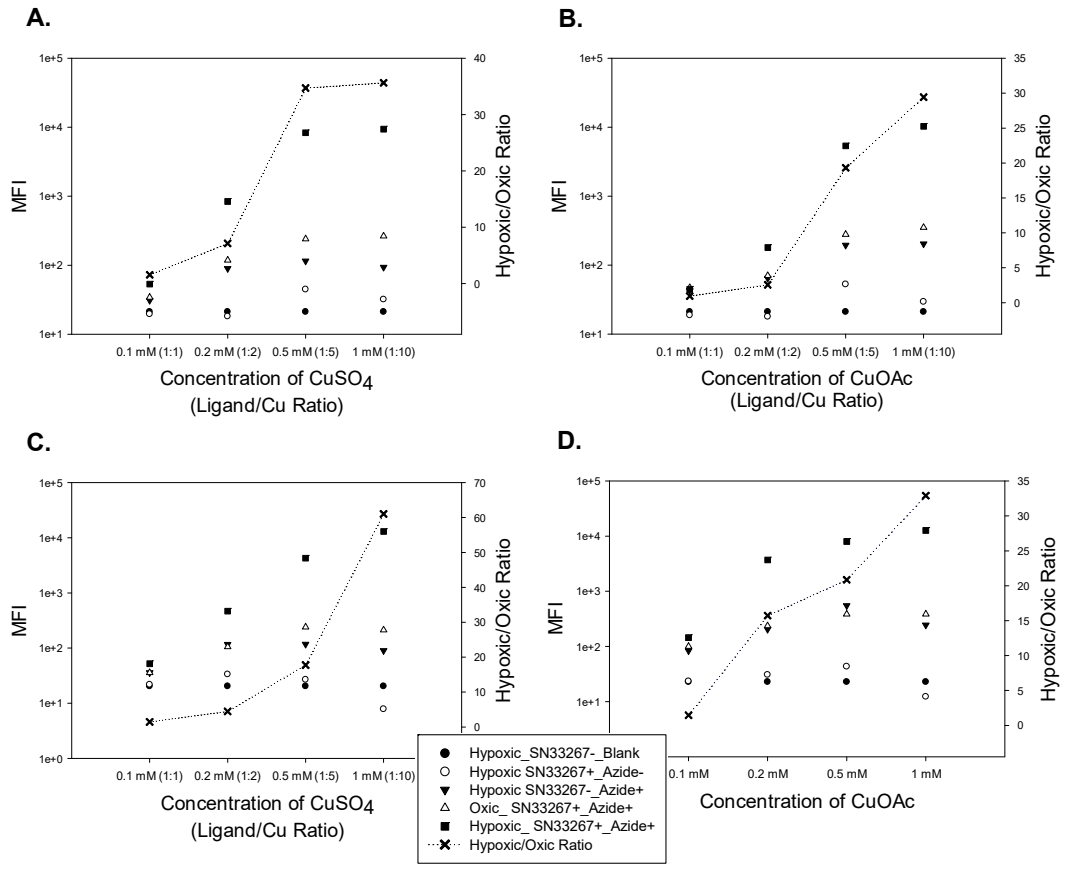

Figure 5.7: The effect of TBTA ligand and copper concentration on clicking cells with Super-DIPY in a hypoxia-selective manner.

SiHa cells incubated under oxic or hypoxic conditions and clicked with Super-DIPY in a hypoxia-selective manner by following protocol #3 (see Figure 2.1) and using following reaction media containing 500 μM TCEP. (A) Reaction medium containing 10 μM Super-DIPY, 100 μM TBTA, and 1 mM $CuSO_4$; (B) Reaction medium containing 10 μM Super-DIPY, 100 μM TBTA, and 1 mM CuOAc; (C) Reaction medium containing 3 μM Super-DIPY, 100 μM TBTA, and 1 mM $CuSO_4$; (D) Reaction medium containing 10 μM Super-DIPY, no TBTA, and 1 mM CuOAc. The MFI of sample is read from the corresponding flow cytometry histogram. The data are represented with different types of plot symbols according to the figure legend. Each plot is representative of 3 independent experiments.

Table 5.3: RNA integrity in hypoxic cells labelled with Super-DIPY in a hypoxia-selective manner as a function of copper concentration.

Concentration of CuOAc (mM)	100 μM TBTA		no TBTA
	Ligand/Cu Ratio	RIN	RIN
0.1	1:1	5.2	3.7
0.2	1:2	5.5	4.5
0.5	1:5	6.1	5.5
1	1:10	6.5	6.3

Note: SiHa cells were incubated under oxic or hypoxic conditions and clicked with Super-DIPY in a hypoxia-selective manner by following protocol #3 (see Figure 2.1) and using reaction cocktails containing 100 μM or no TBTA based on the recipe of reaction cocktail #5 (see Table 2.7). Fluorescence intensity was determined by flow cytometry. Hypoxic/Oxic ratio was calculated by use of MFI derived from the corresponding flow cytometry histogram. RIN scores were generated by RNA samples extracted from the hypoxic SiHa cells labelled with Super-DIPY. Data are representative of 3 independent experiments.

Similar to the BODIPY-FL-azide, 15-min + 15-min and 30-min + 30-min double click procedures were also investigated in the CuAAC reaction between Super-DIPY and cell-incorporated SN33267 adducts to check if the reduction in overall incubation time would simultaneously give both acceptable RNA quality and hypoxia-mediated cell labelling selectivity.

According to the results of flow cytometric analysis, the histogram representing the fluorescence of the hypoxic cells (dark green) was well separated from the one representing the oxic cells (light green) when either 15-min + 15-min (Figure 5.8A) or 30-min + 30-min double click procedure (Figure 5.8B) was applied during the step of the CuAAC reaction. A long leading front was seen in the peak of the hypoxic sample (dark green; Figure 5.8A) when 15-min + 15-min double click procedure was used, which suggested incomplete/inefficient click reaction. According to the size of this leading front, only a very small proportion of hypoxic cells was not efficiently clicked with Super-DIPY.

Based on the calculated hypoxic to oxic ratio, the reduction in the total incubation time was associated with a slight increase in the hypoxia-selectivity. The same change made in the incubation time with reaction cocktail also slightly improved the RNA integrity in Super-DIPY labelled cells from RIN value of 6.4 to 6.9 (Table 5.4).

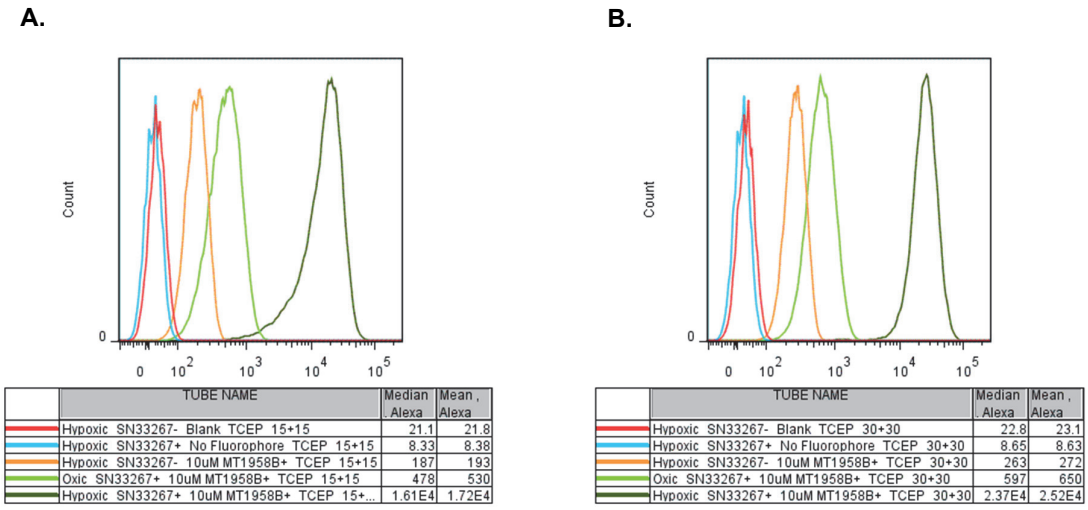

Figure 5.8: The effect of shortened click reaction time on clicking cells with Super-DIPY in a hypoxia-selective manner.

Flow cytometric histograms of SiHa cells incubated under oxic or hypoxic conditions and labelled with Super-DIPY in a hypoxia-selective manner by following protocol #3 (see Figure 2.1) and using reaction cocktail #5 (see Table 2.7). (A) 15-min + 15-min double click; (B) 30-min + 30-min double click. Representative flow cytometric data from at least 6 independent experiments are shown.

Table 5.4: RNA integrity in cells labelled with Super-DIPY in a hypoxia-selective manner as a function of different click reaction times.

Super-DIPY	Hypoxic/Oxic Ratio	RIN
15-min + 15-min double click	39.7	6.9
30-min + 30-min double click	33.7	6.4

Note: SiHa cells were incubated under oxic or hypoxic conditions and clicked with Super-DIPY in a hypoxia-selective manner by following protocol #3 (see Figure 2.1) and using reaction cocktail #5 (see Table 2.7). Fluorescence intensity was determined by flow cytometry. Hypoxic/Oxic ratio was calculated by use of MFI derived from the corresponding flow cytometry histogram. RIN scores were generated by RNA samples extracted from the hypoxic SiHa cells labelled with Super-DIPY. Data are representative of 3 independent experiments.

Two additional independent experiments of Super-DIPY following protocol #3 (Figure 2.1) with reaction cocktails based on the recipe of reaction cocktail #5 (Table 2.7) were performed to confirm the effect of shortened total click reaction time on hypoxia-selectivity as well as on RNA integrity. $CuSO_4$ was also used in both experiments to compare with the results generated with CuOAc as copper source. Consistent results were generated by thesis independent experiments. In general, application of the 15-min + 15-min double click procedure slightly increased the hypoxic to oxic ratio independent of the selection of copper source. The use of CuOAc was superior to $CuSO_4$ as copper source and resulted in improved RNA integrity in labelled cells, which was further enhanced when the 15-min + 15-min double click procedure was employed (Table 5.5).

Table 5.5: Hypoxia-selective labelling and RNA integrity in Super-DIPY labelled hypoxic cells as a function of the selected copper source and different click reaction times.

A.

Super-DIPY	$CuSO_4$		CuOAc	
15-min + 15-min double click	Hypoxic/Oxic Ratio: 56.4	RIN: 2.9	Hypoxic/Oxic Ratio: 51.1	RIN: 6.9
30-min + 30-min double click	Hypoxic/Oxic Ratio: 50.1	RIN: 2.4	Hypoxic/Oxic Ratio: 43.4	RIN: 6.2

B.

Super-DIPY	$CuSO_4$		CuOAc	
15-min + 15-min double click	Hypoxic/Oxic Ratio: 46.8	RIN: 2.8	Hypoxic/Oxic Ratio: 40.4	RIN: 6.2
30-min + 30-min double click	Hypoxic/Oxic Ratio: 45.9	RIN: 3.2	Hypoxic/Oxic Ratio: 34.7	RIN: 5.7

Note: SiHa cells were incubated under oxic or hypoxic conditions and clicked with Super-DIPY in a hypoxia-selective manner by following protocol #3 (see Figure 2.1) and using reaction cocktail #5 (see Table 2.7). Fluorescence intensity was determined by flow cytometry. Hypoxic/Oxic ratio was calculated by use of MFI derived from the corresponding flow cytometry histogram. RIN scores were generated by RNA samples extracted from the hypoxic SiHa cells labelled with Super-DIPY.

According to the experimental data shown in Figure 5.2 and Figure 5.3, use of a double clicking procedure in click step is necessary to achieve a sufficient CuAAC reaction. Exposure to RNases, ROS, or other hazardous substances results in RNA degradation (Houseley & Tollervey, 2009; Temple et al., 2005). A shortened total processing time may improve the compatibility with high-quality RNA. Thus, protocol #3 (Figure 2.1) was modified by removal of the 1% (w/v) BSA-PBS

wash step between the two 30-min incubations with reaction cocktail. In the new protocol (protocol #4 in Figure 2.1), the second dose of fresh reaction cocktail was directly applied to the cell suspension without removing the first reaction cocktail. Protocol #4 was tested in SiHa cells (Figure 5.9B) and compared with protocol #3 within the same experiment (Figure 5.9A). Removal of the wash step between the two 30-min reaction cocktail incubations did not induce any noticeable changes in the final click results as evaluated by flow cytometry.

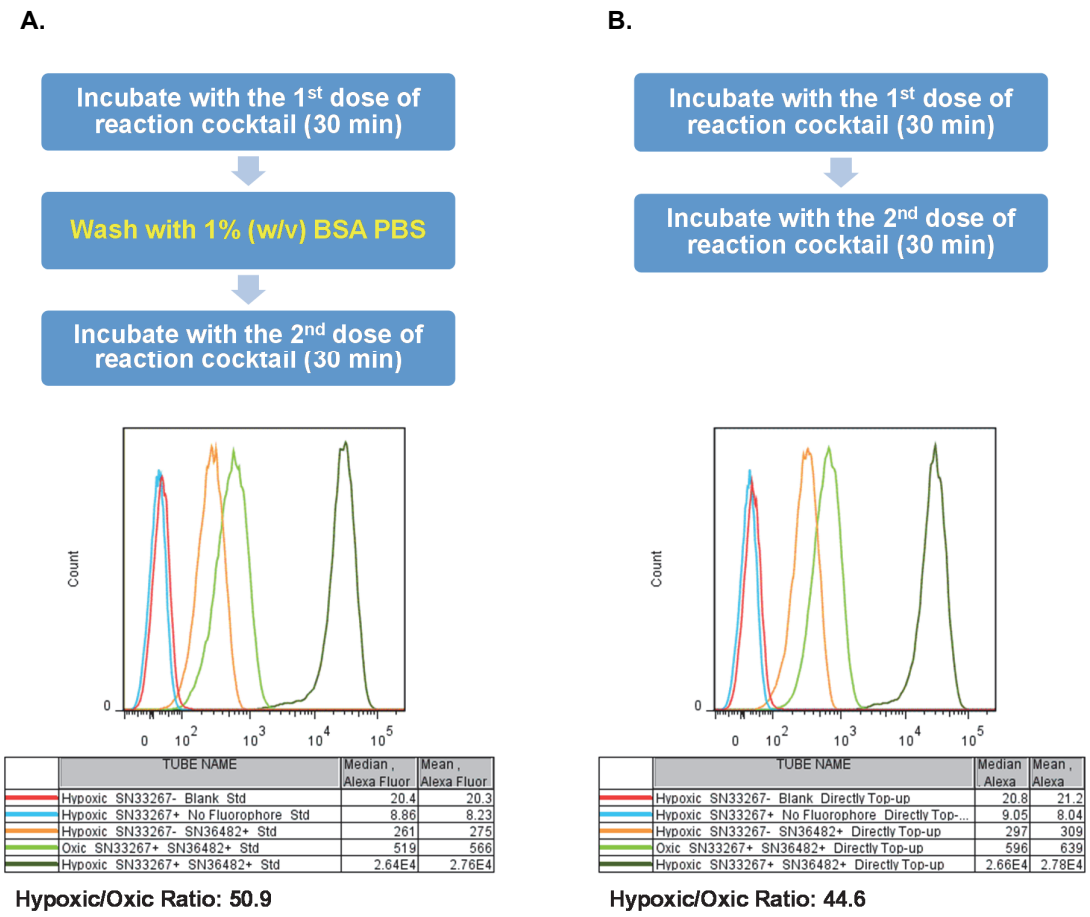

Figure 5.9: The effect of leaving out the wash step between the two 30-min click steps on clicking cells with Super-DIPY in a hypoxia-selective manner.

Flow cytometric histograms of SiHa cells incubated under oxic or hypoxic conditions and labelled with Super-DIPY using reaction cocktail #5 (see Table 2.7) in a hypoxia-selective manner. (A) Use of protocol #3 (Figure 2.1). (B) Use of the protocol #4 (Figure 2.1). Representative flow cytometric data from at least 3 independent experiments are shown.

Performing the CuAAC reaction and the following steps in an anaerobic chamber may preserve the quality of the RNA by evading the copper-mediated generation of ROS from O_2. Both 10 mM Tris-saline buffer and PBS needed to be stored in uncapped bottles and kept in the chamber for at least 72 h to equilibrate with the chamber's atmosphere.

Instead of about 0.04% CO_2 in the atmosphere (Dlugokencky & Tans, 2015), the concentration of CO_2 is 5% in an anaerobic chamber to achieve a pH of ca. 7.4 in bicarbonate-buffered media, which can cause a change in pH of solutions stored in the chamber. In comparison to storage under ambient conditions in a tissue culture hood, 72-h storage in the anaerobic chamber resulted in a decrease in pH of both 10 mM Tris-saline buffer and PBS (Table 5.6).

Table 5.6: The effect of storage conditions on buffer pH.

	PBS	10mM Tris-saline
Anaerobic chamber	6.72	6.42
Tissue culture hood	7.48	7.27

Note: Buffers were stored for 72 h and pH was measured. Temperature in the anaerobic chamber: 37 °C.

Compared to the flow cytometric histograms generated by cells labelled with Super-DIPY in a tissue culture hood (Figure 5.10B), the CuAAC-mediated cell labelling performed in the anaerobic chamber resulted in cells with relatively smaller variation in fluorescence intensity from the same sample, as seen by the histograms with narrower base widths (Figure 5.10A). There was a marginal difference in hypoxic to oxic ratio between the two experimental conditions. The integrity of RNA in labelled hypoxic cells was clearly higher when the CuAAC reaction was carried out in the absence of oxygen.

In addition to 10 mM Tris-saline, reaction cocktails based on alpha minimal essential medium (αMEM), 15 mM MOPS, and PBS were prepared following the recipe listed in Table 5.7. All three types of reaction cocktails plus the 10 mM Tris-saline based reaction cocktail as reference were examined following protocol #4 (Figure 2.1) to determine the hypoxia-selectivity and RNA integrity.

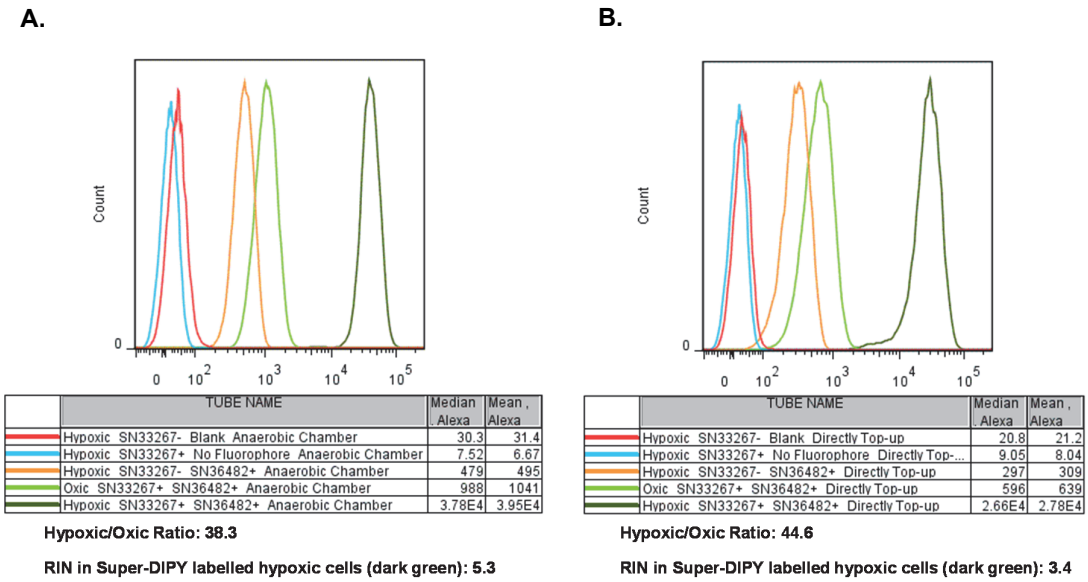

Figure 5.10: The effect of oxygen tension on clicking cells with Super-DIPY in a hypoxia-selective manner.

Flow cytometric histograms of SiHa cells incubated under oxic or hypoxic conditions and labelled with Super-DIPY by following protocol #4 (Figure 2.1) and using reaction cocktail #5 (see Table 2.7) in a hypoxia-dependent manner. (A) CuAAC-mediated cell labelling in an anaerobic chamber. (B) CuAAC-mediated cell labelling in a tissue culture hood. Data are representative of 3 independent experiments.

Table 5.7: Recipe of reaction cocktail.

Stock Solution	Final Concentration in reaction cocktail
Buffer	Top up total volume to 100 µL for every 1×10^6 cells
100 mM CuOAc	1 mM
20 mM TBTA in DMSO	100 µM
25 mM TCEP	500 µM
2 mM Super-DIPY	10 µM

This experiment was carried out in a tissue culture hood. Except for αMEM, CuAAC reactions mediated by reaction cocktails based on the other three buffers gave rise to the cell labelling highly selective for hypoxic cells, shown as the calculated hypoxic to oxic ratio above 25. The CuAAC reactions in 15 mM MOPS buffer or PBS exhibited a very good compatibility with high-quality RNA in labelled cells (Table 5.8). Based on these results 10 mM Tris-saline was substituted by PBS in reaction cocktails used in subsequent studies (protocol #5; Figure 2.1).

Table 5.8: Hypoxia-selective labelling and RNA integrity in Super-DIPY labelled hypoxic cells in different buffer systems.

	10 mM Tris-saline (pH 7.4)	Culture medium (pH 7.4)	15 mM MOPS (pH 7.35)	PBS (pH 7.4)
Hypoxic/Oxic ratio	43.8	1.4	25.4	27.9
RIN	5.4	3.7	8.2	8.3

Note: Data are representative of 3 independent experiments.

The hypoxia-selective cell labelling with BODIPY-FL-azide following protocol #5 (Figure 2.1) was performed both in the tissue culture hood and in the anaerobic chamber. Compared with the flow cytometric histograms generated by cells labelled with BODIPY-FL-azide in the tissue culture hood (Figure 5.11B), the CuAAC-mediated cell labelling performed in the anaerobic chamber resulted in cells with relatively smaller variation in fluorescence intensity from the same sample as seen by the narrower bases (Figure 5.11A). Such difference in the distribution of cellular fluorescence intensity was especially obvious in hypoxic samples (dark green). There was a notable increase in hypoxic to oxic ratio when comparing the reaction in the tissue culture hood to the reaction in the anaerobic chamber. However, the integrity of RNA in cells incubated with the PBS-based reaction cocktail was higher when the CuAAC reaction was carried out in tissue culture hood, which was opposite to the previous results generated by using Super-DIPY and Tris-saline based reaction cocktail (see Figure 5.10).

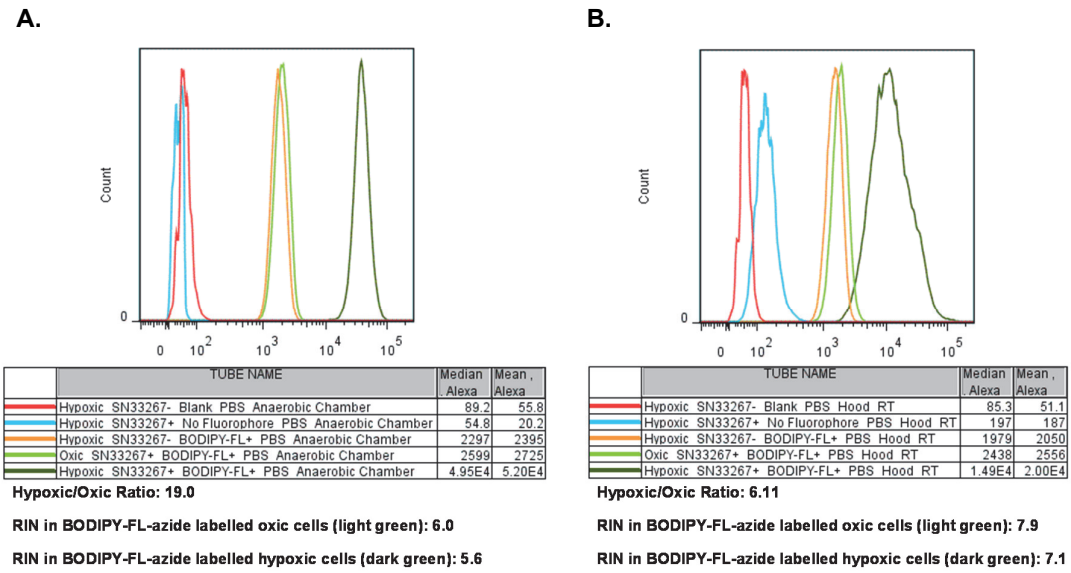

Figure 5.11: The effect of oxygen atmosphere on clicking cells with BODIPY-FL-azide in a hypoxia-selective manner.

Flow cytometric histograms of SiHa cells incubated under oxic or hypoxic conditions and clicked with BODIPY-FL-azide by following protocol #5 (Figure 2.1) and using reaction cocktail #7 (see Table 2.7) in a hypoxia-selective manner. (A) CuAAC-mediated cell labelling in an anaerobic chamber. (B) CuAAC-mediated cell labelling in a tissue culture hood. Data are representative of 3 independent experiments.

The same hypoxia-selective cell labelling experiments were repeated with Super-DIPY following protocol #5 (Figure 2.1) both in a tissue culture hood and in an anaerobic chamber. Compared to the flow cytometric histograms generated by cells labelled with BODIPY-FL-azide in the tissue culture hood (Figure 5.12B), the CuAAC-mediated cell labelling performed in the anaerobic chamber resulted in cells with relatively smaller variation in fluorescence intensity from the same sample, judged by the narrower bases (Figure 5.12A). Such difference in the distribution of cellular fluorescence intensity was especially obvious in hypoxic samples (dark green), which was also found in the previous experiment with BODIPY-FL-azide (see Figure 5.11). Unlike with BODIPY-FL-azide, there was no marked difference in hypoxic to oxic ratio between the reactions in the tissue culture hood and in the anaerobic chamber. The integrity of RNA in cells incubated with the PBS-based reaction cocktail was higher when the CuAAC reaction carried out in the tissue culture hood, which was similar to the results generated by CuAAC reactions with BODIPY-FL-azide and

PBS-based reaction cocktail (see Figure 5.11) but opposite to the results generated by CuAAC reactions deploying Super-DIPY and Tris-saline based reaction cocktail (see Figure 5.10).

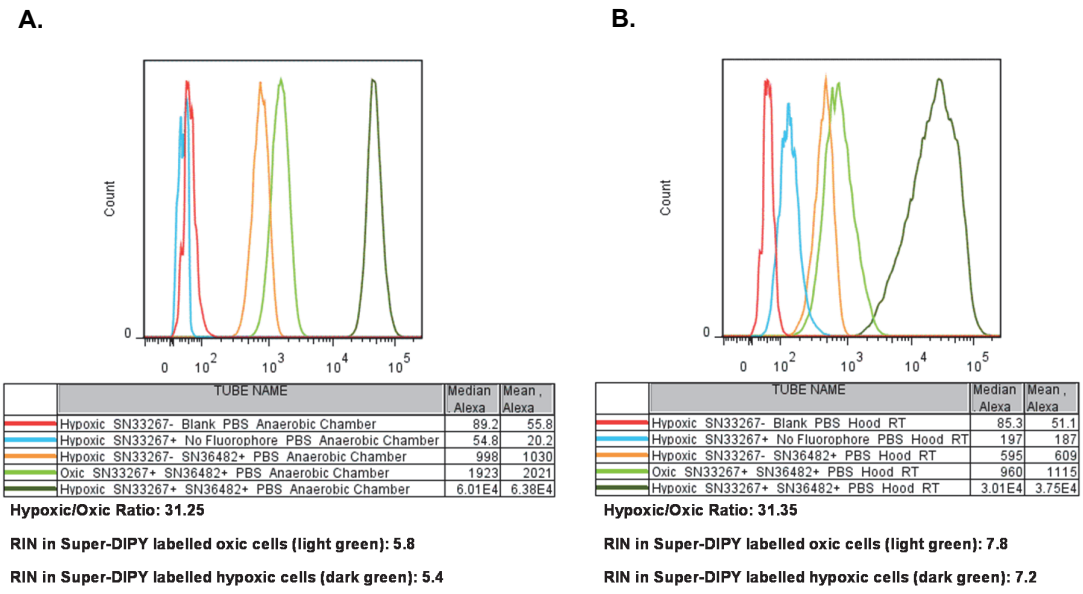

TUBE NAME	Median Alexa	Mean, Alexa
Hypoxic SN33267- Blank PBS Anaerobic Chamber	89.2	55.8
Hypoxic SN33267+ No Fluorophore PBS Anaerobic Chamber	54.8	20.2
Hypoxic SN33267- SN36482+ PBS Anaerobic Chamber	998	1030
Oxic SN33267+ SN36482+ PBS Anaerobic Chamber	1923	2021
Hypoxic SN33267+ SN36482+ PBS Anaerobic Chamber	6.01E4	6.38E4

Hypoxic/Oxic Ratio: 31.25

RIN in Super-DIPY labelled oxic cells (light green): 5.8

RIN in Super-DIPY labelled hypoxic cells (dark green): 5.4

TUBE NAME	Median Alexa	Mean, Alexa
Hypoxic SN33267- Blank PBS Hood RT	85.3	51.1
Hypoxic SN33267+ No Fluorophore PBS Hood RT	197	187
Hypoxic SN33267- SN36482+ PBS Hood RT	595	609
Oxic SN33267+ SN36482+ PBS Hood RT	960	1115
Hypoxic SN33267+ SN36482+ PBS Hood RT	3.01E4	3.75E4

Hypoxic/Oxic Ratio: 31.35

RIN in Super-DIPY labelled oxic cells (light green): 7.8

RIN in Super-DIPY labelled hypoxic cells (dark green): 7.2

Figure 5.12: The effect of oxygen atmosphere on clicking cells with Super-DIPY in a hypoxia-selective manner.

Flow cytometric histograms of SiHa cells incubated under oxic or hypoxic conditions and labelled with Super-DIPY by following protocol #5 (Figure 2.1) and using reaction cocktail #7 (see Table 2.7) in a hypoxia-selective manner. (A) CuAAC-mediated cell labelling in an anaerobic chamber. (B) CuAAC-mediated cell labelling in a tissue culture hood. Data are representative of 3 independent experiments.

Besides shortening the exposure time to reaction cocktail, the reduction in temperature may also slow down the copper-mediated generation of ROS from O_2 to maintain the RNA integrity in the treated cells as the general role of temperature in mediating chemical reaction rate (Levine, 2005). Moreover, the rate of CuAAC reaction may also be influenced by a change of temperature. To determine the effects of lower temperature in CuAAC-mediated hypoxia-selective cell labelling, SiHa cells were clicked with selected BODIPY-based azides following protocol #5 (Figure 2.1) using reaction cocktail #7 (see Table 2.7) at RT or 4°C following the incubation with 100 µM SN33267 for 2 h at 37°C under oxic or hypoxic conditions.

At RT, hypoxic cells had high fluorescence intensity than oxic cells independent of the selection of BODIPY-based azide (Hypoxic/Oxic ratio: 6.1 by BODIPY-FL-azide, 31.4 by Super-DIPY),

which was consistent with previous findings. In contrast, there was no noticeable difference in fluorescence intensity between oxic and hypoxic cells after SN33267-treated cells were incubated with reaction cocktail containing BODIPY-FL-azide at 4°C (Hypoxic/Oxic ratio: 1.5; Figure 5.13A). When Super-DIPY was used, the CuAAC reaction of SN33267-treated cells at 4°C resulted in a slight increase in fluorescence intensity of hypoxic compared oxic cells (Hypoxic/Oxic ratio: 3.0; Figure 5.13B). The rate of CuAAC reaction thus strongly depended on temperature, as expected. Reducing the temperature to 4°C might improve compatibility of CuAAC reaction with high-quality RNA.

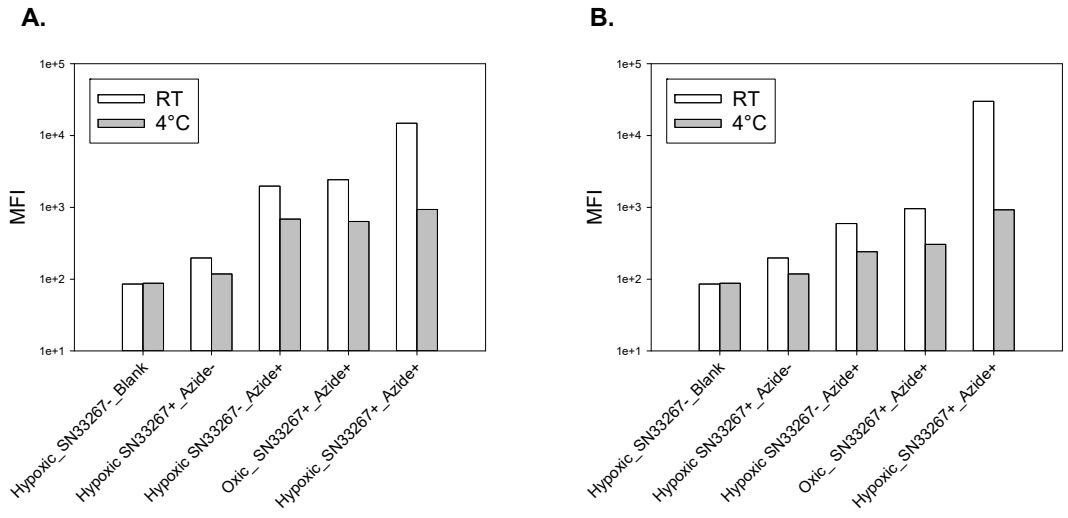

Figure 5.13: CuAAC-mediated labelling in SiHa cells at different temperatures.

SiHa cells incubated under oxic or hypoxic conditions and clicked with azide-modified fluorophore following protocol #5 (Figure 2.1) and using reaction cocktail #7 (see Table 2.7) at RT or 4°C in a hypoxia-dependent manner. (A) BODIPY-FL-azide; (B) Super-DIPY. Each bar represents the MFI derived from the corresponding flow cytometry histogram. Data are representative of 3 independent experiments.

5.3.3 Clicking mixed oxic and hypoxic cells

Mixtures of cells consisting of hypoxic and oxic populations in a 1:1 ratio were employed to assess the capability of the method in separating these two cell populations based on fluorescence intensity as a marker of hypoxic stress by flow cytometry.

The oxygen tension in cell cultures (19.95%) is usually close to the ambient atmospheric oxygen tension, which is higher than the levels of oxygen found *in vivo* (1–11% oxygen) due to the diffusion and tissue consumption of oxygen (Carreau, El Hafny-Rahbi, Matejuk, Grillon, & Kieda, 2011). In order to closer mimic physiological oxygen concentrations, the atmospheric conditions used in oxic incubation were changed from an atmosphere of 5% CO_2 : 95% O_2 to ambient conditions. In all following *in vitro* experiments in this thesis, the oxic cells were pre-incubated 1.5-h under ambient conditions followed by 2-h incubation with 100 μM SN33267 under the same oxygen tension.

Based on protocol #5 (Figure 2.1), oxic and hypoxic SiHa cells were mixed in a 1:1 ratio at three different points of the labelling procedure (underlined in Figure 5.14). Following the CuAAC-based hypoxia-dependent fluorescence labelling process using reaction cocktail #7 (Table 2.7), the fluorescence profiles of the mixed cells were analysed by flow cytometry. The unmixed oxic and hypoxic cells were used as controls to detect any changes in the fluorescence intensity of cells induced by mixing cells that were exposed to SN33267 under different oxygen tensions.

When oxic and hypoxic cells were mixed before the incubation with reaction cocktail to enable the CuAAC reaction, an obvious right-shift (i.e. to higher fluorescence intensity) was detected in the fluorescence intensity of oxic population in the mixed cells (the left-side peak of the orange histogram) compared with the fluorescence intensity of unmixed oxic cells (red histogram). Additionally, the right-side peak of the orange histogram representing the fluorescence intensity of hypoxic population in the mixed cells slightly shifted left-ward in comparison to the fluorescence intensity of unmixed hypoxic cells (blue histogram; Figure 5.14A).

When oxic and hypoxic cells were incubated with reaction cocktail separately *prior* to mixing, there was no noticeable change in fluorescence intensity of hypoxic population in mixed cells (the right-side peak of the orange histogram; Figure 5.14B and C) in comparison to the fluorescence intensity of unmixed hypoxic cells (blue histogram). Using the fluorescence intensity of unmixed oxic cells (red histogram) as a reference, a very slight shift towards the right (i.e. to higher fluorescence intensity) was detected in the fluorescence intensity of oxic population in the mixed

cells (the left-side peak of the orange histogram) in both cases when the two populations of cells were mixed after the CuAAC reactions (Figure 5.14B and C).

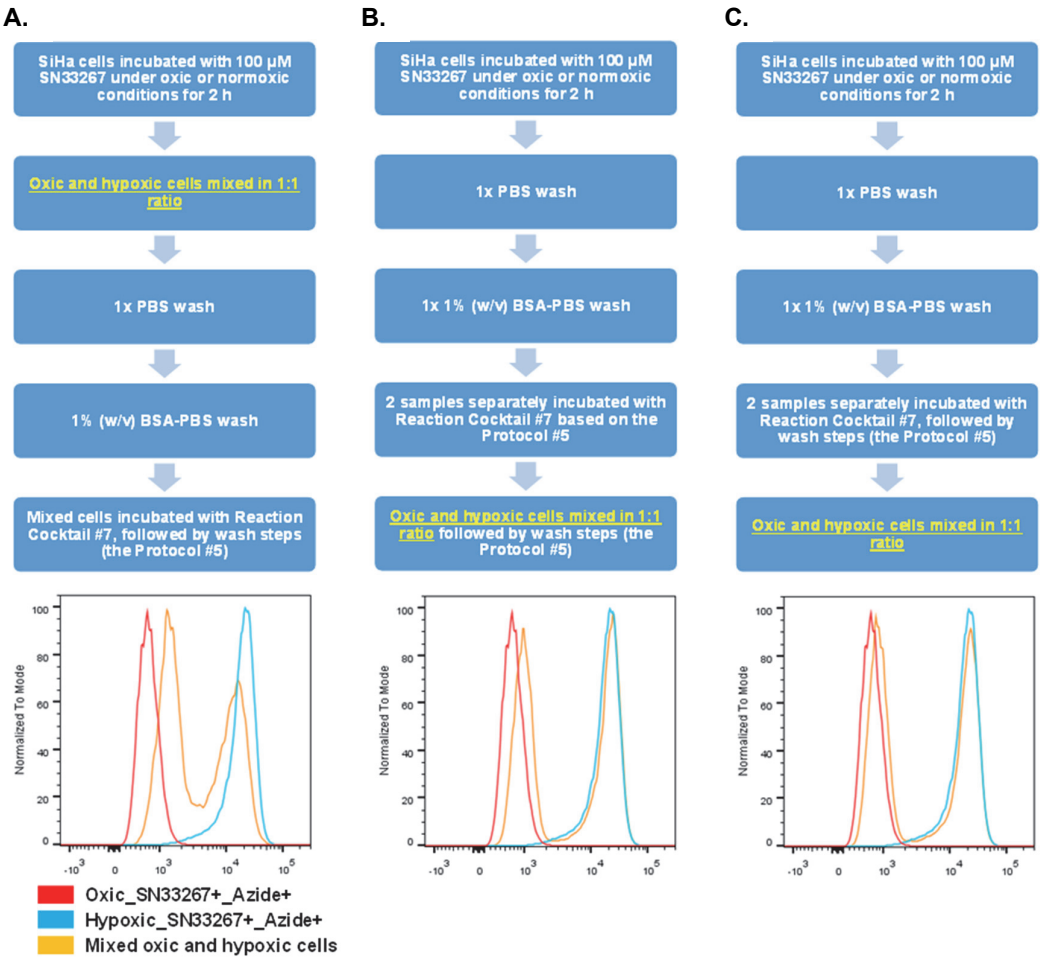

Figure 5.14: The effect of mixing cells at various stages of the experimental procedure on clicking cells with Super-DIPY in a hypoxia-selective manner.

(A) Oxic and hypoxic cells were mixed prior to the incubation with reaction cocktail. (B) Oxic and hypoxic cells were mixed at the end of the incubation with reaction cocktail followed by wash steps. (C) Oxic and hypoxic cells were incubated with reaction cocktail and went through wash steps separately. They were mixed prior to the flow cytometric analysis. Flow cytometric histograms of SiHa cells incubated under oxic or hypoxic conditions and labelled with Super-DIPY using reaction cocktail #7 (see Table 2.7) in a hypoxia-selective manner. Data are representative of 3 independent experiments.

To figure out the reason for the shift in fluorescence intensity associated with the CuAAC-mediated fluorescence labelling of pre-mixed cells exposed to SN33267 under different oxygen tensions, oxic and hypoxic cells were also incubated without SN33267, named “Oxic_DMSO” and “Hypoxic_DMSO”, respectively, were investigated.

Without SN33267, there was no matching alkyne reactant for the azide in the cells due to its bioorthogonality and Super-DIPY in the reaction cocktail might only bind to cells in a nonspecific manner, which would show up as background fluorescence. As expected, no change in fluorescence intensity was identified between oxic and hypoxic cells (Figure 5.15A). Oxic cells formed few covalent adducts with SN33267, which made the cells exhibit a low level of fluorescence upon CuAAC with Super-DIPY (red histogram in Figure 5.15B). Without SN33267, hypoxic cells alone displayed a very low level of background fluorescence after the CuAAC-mediated labelling procedure (blue histogram in Figure 5.15B). It was very hard to detect any change in fluorescence intensity based on the comparison of histograms when these two types of cells were pre-mixed together and then incubated with Super-DIPY in the reaction cocktail because of the low level of fluorescent intensities of all three samples (Figure 5.15B).

When SN33267-free oxic cells were mixed with SN33267-incubated hypoxic cells *prior* to the incubation with reaction cocktail, the histogram generated by the mixed cells exhibited two well-separated peaks (orange histogram in Figure 5.15C). Interestingly, the left peak, representing the fluorescence intensity of the oxic cell population with lower level of incorporated SN33267 adducts, markedly shifted towards the right (higher fluorescence intensity) compared to the histogram (red) representing the fluorescence intensity of unmixed SN33267-free oxic cells.

Similar shifts were observed in the histogram of mixed cells consisting SN33267-incubated oxic cells and hypoxic cells (Figure 5.15D). In Figure 5.15C and D, the fluorescence intensities of oxic samples were increased to a very similar level when they mixed with SN33267-incubated hypoxic cell sample *prior* to the clicking procedure.

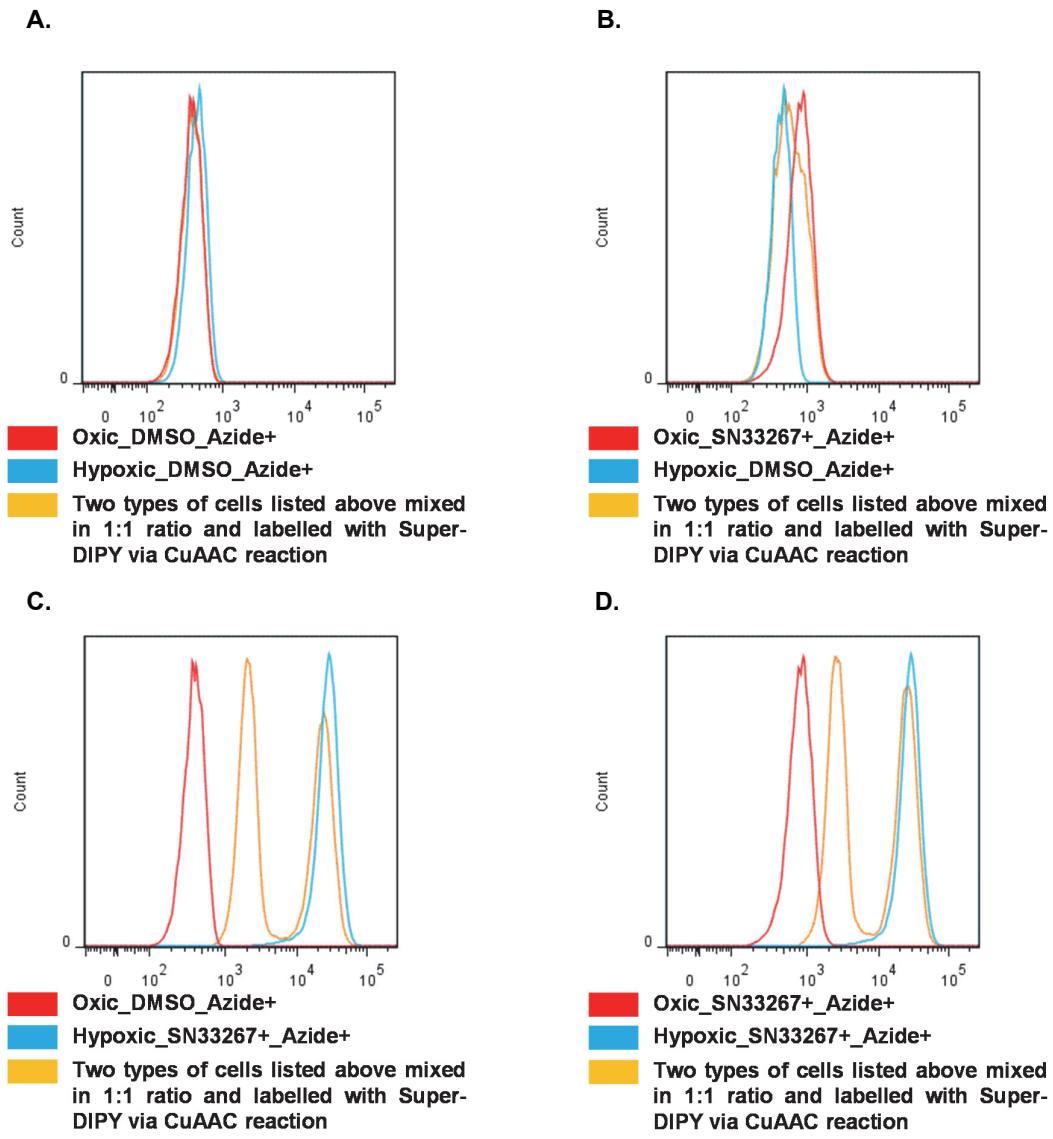

Figure 5.15: The effect of mixing two cell populations labelled with distinct levels of SN33267 adducts on simultaneously clicking with Super-DIPY in a single CuAAC reaction.

Flow cytometric analysis of mixed oxic and hypoxic SiHa cells (1:1 ratio) labelled via the CuAAC reaction between cell-incorporated SN33267 (100 μM) and Super-DIPY following protocol #5 (Figure 2.1) with reaction cocktail #7 (Table 2.7) in comparison to the histograms generated by the corresponding unmixed cells labelled via the same procedures. (A) Oxic and hypoxic cells without SN33267. (B) SN33267-incubated oxic cells and hypoxic cells without SN33267. (C) Oxic cells without SN33267 and SN33267-incubated hypoxic cells. (D) SN33267-incubated oxic and hypoxic cells. Data are representative of 3 independent experiments.

Reaction media that had been used to click hypoxic cells were employed to determine if any SN33267-derivatives were released from hypoxic cells that contributed to the increase in fluorescence intensity of the oxic cells in the cell mixture during the CuAAC reaction.

SN33267-incubated hypoxic SiHa cells and DMSO-incubated hypoxic cells were incubated with Super-DIPY using reaction cocktail #7 (Table 2.7) following protocol #5 (Figure 2.1). At the end of incubation, the reaction medium was carefully separated from the cells and collected, followed by a double-spin to remove any remaining cells. Oxic cells incubated with and without 100 μM SN33267 were then exposed to these two types of reaction medium for 1 h with gentle agitation, followed by wash steps as per protocol #5 (Figure 2.1).

A 1-h incubation of the DMSO-treated oxic cells with the reaction medium that had been used to label SN33267-treated hypoxic cells generated a histogram (orange) with two peaks, indicating that a fraction of the cells exhibited an elevated fluorescence intensity (Figure 5.16A).

In SN33267-treated oxic cells, both previously-used reaction media resulted in an increase of the fluorescence intensity in a fraction of the cells (Figure 5.16B). The reaction medium that had been used to label SN33267-treated hypoxic cells demonstrated a stronger effect on labelling SN33267-treated oxic cells (orange histogram) than the one that had been used to incubate DMSO-treated hypoxic cells (blue histogram).

In both cases, only a fraction of the cells in the sample clicked with the reaction medium that had been used by Hypoxic_SN33267+ cells (orange) were labelled with higher fluorescence intensity in comparison to cells clicked with fresh reaction medium (red).

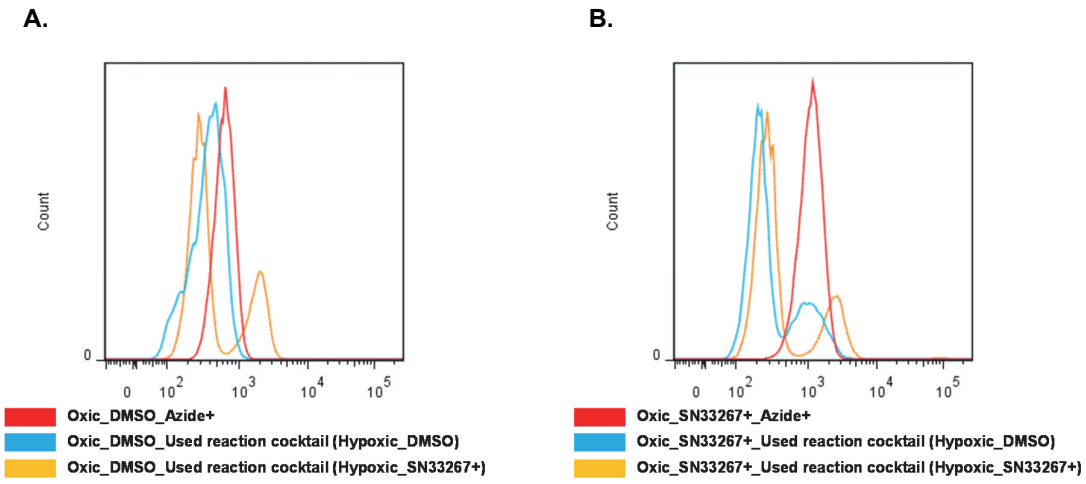

Figure 5.16: Flow cytometric analysis of oxic cells incubated with previously-used reaction cocktails.

Flow cytometric analysis of the oxic SiHa cells incubated with the supernatants from reaction media that had been used to incubate hypoxic SiHa cells. (A) DMSO-treated oxic cells. (B) SN33267-treated oxic cells. Data are representative of 3 independent experiments.

To determine the minimum required CuAAC reaction time, SN33267-treated oxic and hypoxic SiHa cells were mixed in a 1:1 ratio and labelled with Super-DIPY using reaction cocktail #7 (Table 2.7) following protocol #5 (Figure 2.1) with modified incubation times. Based on the histograms generated by flow cytometric analysis, poor peak resolution and the appearance of a third peak was associated with shorter clicking times (Figure 5.17A). In contrast, a baseline separation was almost achieved at longer clicking times (Figure 5.17F). The procedure using 10-min + 10-min double click (protocol #6 in Figure 2.1) was sufficient to separate the two mixed populations according to the fluorescence intensity of the cells (Figure 5.17B).

Cells were sampled immediately after the double-click (time point 1) and after the last wash step (time point 2). RNA was extracted from each cell sample.

RNA in cells taken immediately at the end of the CuAAC reaction gave a RIN score in a range between 7.9 and 8.9. In general, the integrity of RNA was inversely correlated with the total time of the CuAAC reaction step. Shortening the exposure time to reaction cocktail led to the higher integrity of RNA extracted from cells. Compared with the RNA scores at time point 1, RNA integrity

in cells was decreased after the final wash step. The RIN scores were reduced to values between 7.4 and 7.5 (Table 5.9).

To study the changes in RNA integrity in cells through the entire multiple-step washing procedure, mixed (1:1 ratio) SN33267-treated oxic and hypoxic SiHa cells were labelled via the CuAAC reaction between the cell-incorporated SN33267 and Super-DIPY supplied in reaction cocktail #7 (Table 2.7) via either 30-min + 30-min or 10-min + 10-min double click, followed by the multiple-step washing procedure.

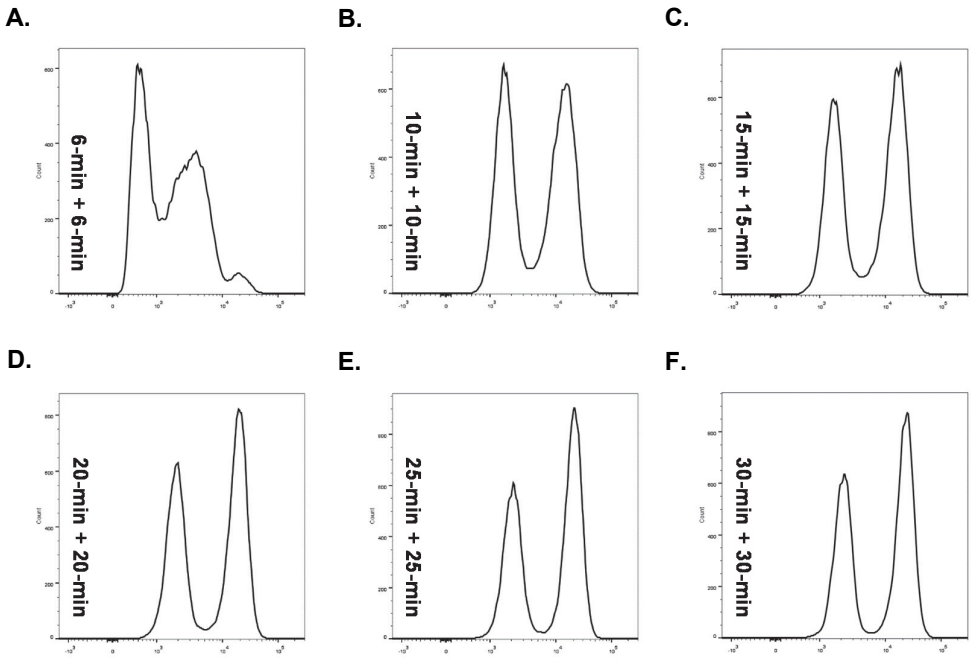

Figure 5.17: The effect of click reaction time on labelling cells with Super-DIPY in a hypoxia-selective manner.

SiHa cells were incubated with 100 μM SN33267 for 2 h under oxic or hypoxic conditions. Subsequently, the two types of cells were mixed in 1:1 ratio. Flow cytometric analysis was performed on the mixed cells labelled with Super-DIPY following protocol #5 (Figure 2.1) with modified incubation times with reaction cocktail #7 (Table 2.7). The incubation times with reaction cocktail were indicated in the corresponding histograms. Representative flow cytometric data from 3 independent experiments are shown.

Table 5.9: Integrity of RNA in cells labelled with Super-DIPY as a function of different incubation times with reaction cocktail and subsequent wash steps.

Super-DIPY	RIN	
	Time point 1 (After the double-click)	Time point 2 (After the last wash step)
6-min + 6-min	8.9	7.5
10-min + 10-min	8.5	7.5
15-min + 15-min	8.2	7.4
20-min + 20-min	8.0	7.4
25-min + 25-min	8.3	7.4
30-min + 30-min	7.9	7.4

Note: Data are representative of 3 independent experiments.

No RNA degradation was identified at the end of the 2-h SN33267 incubation. Following the PBS wash step with a couple of centrifugation steps to remove the remaining SN33267, there was only slight degradation of cellular RNA (RIN 9.8) before the click reaction.

Immediately after the CuAAC reaction, cells were sampled at each individual subsequent wash step. The integrity of RNA dropped considerably during the incubation with reaction cocktail (Figure 5.18).

Independent of incubation time with reaction cocktail, the integrity of RNA in cells was slightly higher after the wash step with 50% (v/v) ethanol-PBS, which was followed by a slight decrease in RNA integrity in the subsequent two PBS wash steps. The third PBS wash step resulted in a marked reduction in RNA integrity compared to the previous wash steps (Figure 5.18). The 10-min + 10-min double click procedure was slightly better than the 30-min + 30-min one in preserving the integrity of RNA in cells through all steps.

There were two peaks visible in all histograms in all histograms generated by flow cytometric analysis, indicating that the tested cells comprised of two cell populations with distinct intensities of fluorescence generated by the labelled fluorophores via the CuAAC reaction. At the end of the CuAAC reaction, the difference in fluorescence intensity between these two populations in the cell sample was relatively small. The separation of the two peaks was improved when more wash

steps were applied because increasingly non-specifically-bound fluorophore was removed. Based on the separation of the two peaks in each histogram, the wash step with 50% (v/v) ethanol-PBS and the subsequent PBS wash removed the majority of non-specific fluorescence (Figure 5.18).

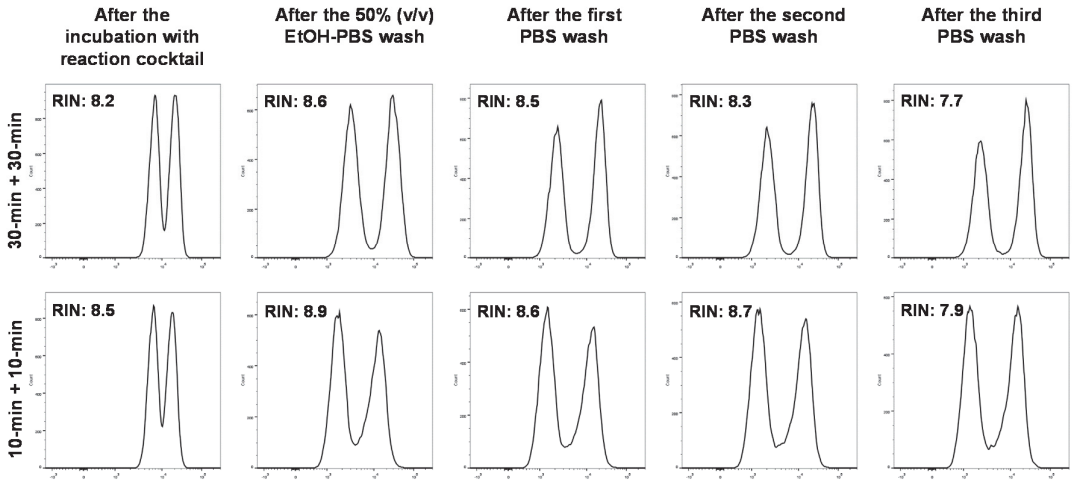

Figure 5.18: Flow cytometry analysis of mixed oxic and hypoxic SiHa cells at each wash step following the incubation with reaction cocktail.

SiHa cells were incubated with 100 μM SN33267 for 2 h under oxic or hypoxic conditions. Subsequently, the two types of cells were mixed in 1:1 ratio. Flow cytometric analysis was performed on mixed cells labelled with Super-DIPY in reaction cocktail #7 (Table 2.7) following protocol #5 or protocol #6 (Figure 2.1) modified by one additional PBS wash step at the end of the original wash procedure. Cells were sampled after each individual subsequent wash step immediately following the click reaction step. Representative flow cytometric data from 3 independent experiments are shown.

5.3.4 FACS trials with mixed cell suspensions

Considering the minimal interference with RNA integrity and with efficient removal of non-specific background fluorescent signal, protocol #7 was established by leaving out the second PBS wash step in protocol #6 (Figure 2.1). To confirm the effect of protocol #7 on RNA integrity, cells were sampled at the end of selected steps during the whole experimental labelling procedure.

Throughout the whole incubation and CuAAC-mediated hypoxia-dependent cell labelling process, the RIN score of cells only decreased from 10 at the very beginning to 8.8 immediately prior to the FACS step (Figure 5.19).

At the core of the design of the CuAAC-mediated hypoxia-dependent cell labelling methodology was the goal to utilise FACS of azide-modified fluorophore-stained cells to identify genes differentially regulated in oxic and hypoxic tumour compartments. To further investigate the compatibility with high-quality RNA the newly modified version of the protocol #7 (Figure 2.1) was used in conjunction with FACS. As shown in Figure 5.20, mixed oxic and hypoxic SiHa cells were sorted based on Super-DIPY fluorescence into quartiles of approximately equal cell numbers and collected into 5 mL polystyrene round-bottom tubes containing 2 mL of collection solution kept at 4 °C (Figure 5.20).

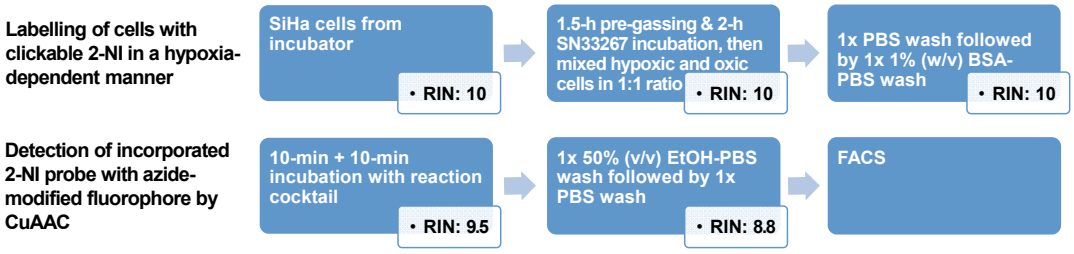

Figure 5.19: Changes in RNA integrity in cells throughout the whole labelling procedure of protocol #7.

SiHa cells were incubated with 100 µM SN33267 for 2 h under oxic or hypoxic conditions. Subsequently, the two types of cells were mixed in 1:1 ratio and clicked with Super-DIPY by using reaction cocktail #7 (Table 2.7) and following protocol #7 (Figure 2.1) in a hypoxia-selective manner. Cells were sampled after each selected step and RNA was extracted to determine a RIN score. Data are representative of 3 independent experiments.

The effects of four different collections solutions on RNA integrity were assessed. The RNA samples extracted from sorted cells collected into TRIzol® LS solution demonstrated the highest level of integrity (Table 5.10).

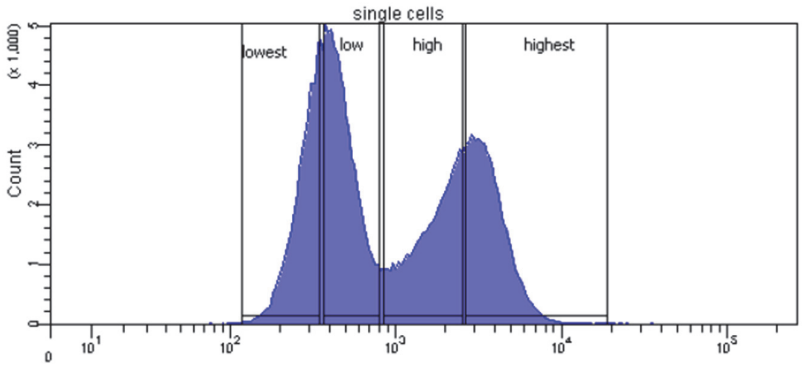

Figure 5.20: FACS analysis and separation of mixed oxic and hypoxic SN33267-labelled SiHa cells on the basis of Super-DIPY fluorescence.

SiHa cells were incubated with 100 μM SN33267 for 2 h under oxic or hypoxic conditions. Subsequently, the two types of cells were mixed in 1:1 ratio and clicked with Super-DIPY by using reaction cocktail #7 (Table 2.7) and following protocol #7 (Figure 2.1) in a hypoxia-selective manner. According to the fluorescence profile, cells were sorted into four fractions of equivalent cell numbers. Data are representative of 3 independent experiments.

Table 5.10: Integrity of RNA extracted from sorted SiHa cells collected into different solutions.

Solution used to collect sorted cells from FACS	RIN			
	1st Quartile	2nd Quartile	3rd Quartile	4th Quartile
2 mL PBS	2.2	2.3	2.3	2.3
2 mL RNAlater®	1.0	1.6	1.0	1.0
2 mL culture medium	1.8	1.6	1.5	2.0
2 mL TRIzol® LS	9.1	9.0	8.7	8.4

Note: Data are representative of 3 independent experiments.

5.3.5 Application of protocol #7 to other cell lines

Based on the histograms generated by flow cytometry analysis, the 15-min + 15-min double click procedure was the minimum total time required with the reaction cocktail to sufficiently separate mixed oxic and hypoxic FaDu cell populations (Figure 5.21A). In both HT-29 cells (Figure 5.21B) and HCT116 cells (Figure 5.21C), 20-min + 20-min double click procedure or a longer click time was necessary to separate the two mixed populations.

Three human cancer cell lines, FaDu, HT-29, and HCT116, were incubated with 100 μM SN33267 for 2 h under oxic or hypoxic conditions. For each line, the two types of cells were mixed in 1:1 ratio. To determine compatibility of the CuAAC-labelling methodology with good-quality RNA, the cells were sorted by clicked fluorescence intensity into quartiles of approximately equal cell numbers and collected in 5 mL polystyrene round-bottom tubes containing 2 mL TRIzol® LS solution at 4°C subsequent to the CuAAC-mediated hypoxia-selective clicking with Super-DIPY according to protocol #7 (Figure 2.1) modified with the click time determined in Figure 5.21 (FaDu, 15-min + 15-min; HT-29 and HCT116, 20-min + 20-min; Figure 5.22).

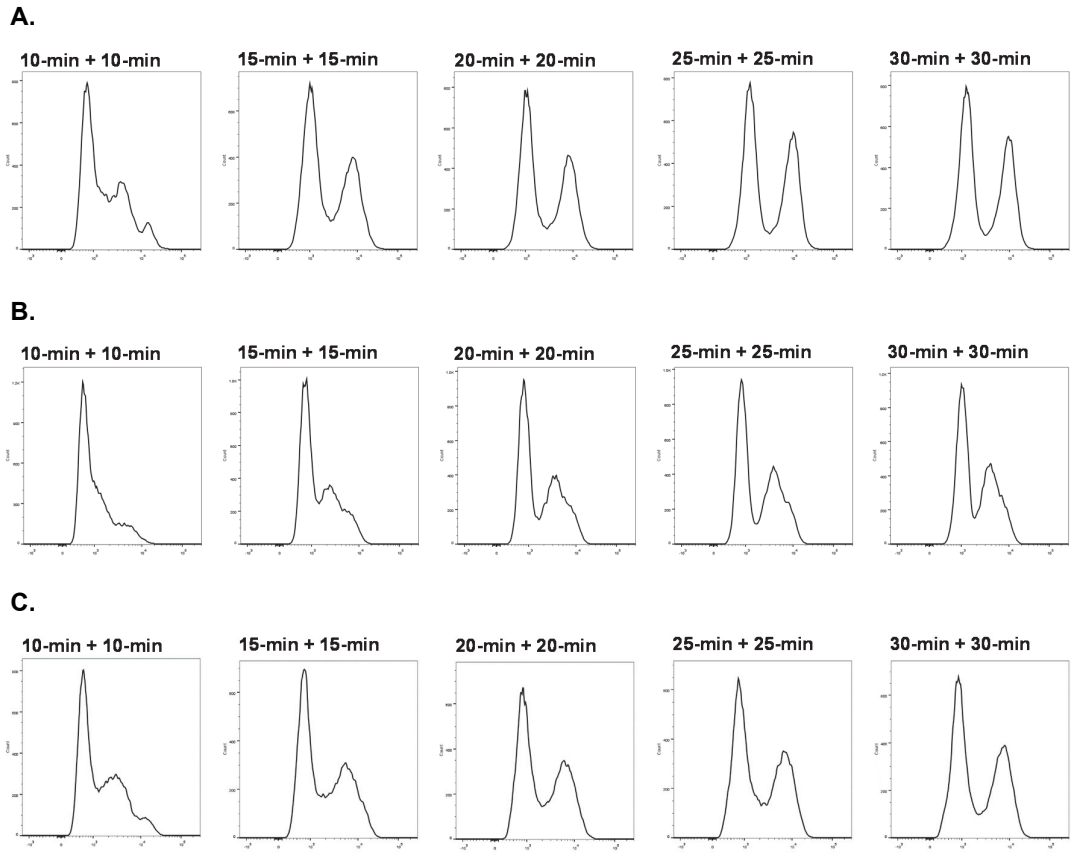

Figure 5.21: The effect of click reaction time on labelling with Super-DIPY in a hypoxia-selective manner in mixtures (1 : 1) of oxic and hypoxic cells of three human cancer cell lines.

Three human cancer cell lines, (A) FaDu, (B) HT-29, and (C) HCT116, were incubated with 100 μM SN33267 for 2 h under oxic or hypoxic conditions. For each line, the two types of cells were mixed in 1:1 ratio and clicked with Super-DIPY by using reaction cocktail #7 (Table 2.7) and based on protocol #7 (Figure 2.1) with different click times in a hypoxia-selective manner. The incubation time with reaction cocktail was indicated in the corresponding histogram. Data of each cell line are representative of 3 independent experiments.

A.

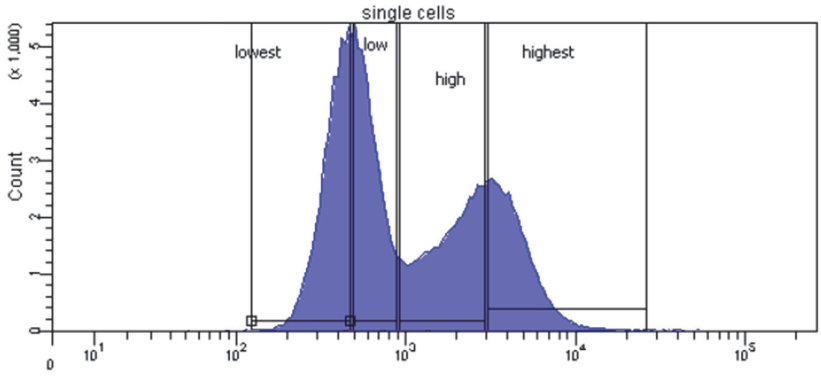

B.

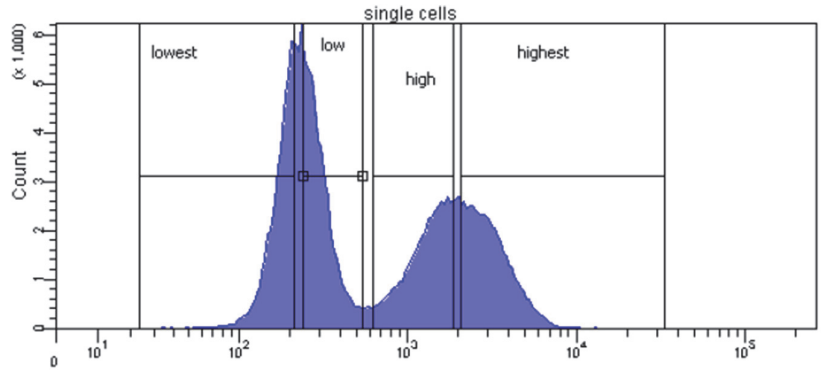

C.

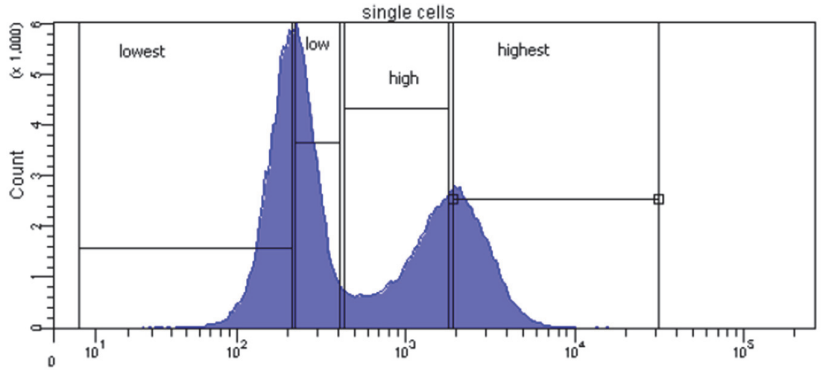

Figure 5.22: FACS analysis and separation of SN33267-labelled cells on the basis of Super-DIPY fluorescence.

(A) FaDu, (B) HT-29, and (C) HCT116 cells were incubated with 100 μM SN33267 for 2 h under oxic or hypoxic conditions. For each cell line, the two types of cells were mixed in 1:1 ratio and clicked with Super-DIPY by using reaction cocktail #7 (Table 2.7) and following protocol #7 (Figure 2.1) with the click time determined in Figure 5.21 (FaDu, 15-min + 15-min; HT-29 and HCT116, 20-min + 20-min) in a hypoxia-selective manner. According to the fluorescence profile, cells were sorted into four fractions with roughly equivalent cell number. For each cell type, representative flow cytometric data from 3 independent experiments are shown.

The RIN scores of RNA extracted from the sorted cells were all above 6. Among the three cell lines, FaDu and HCT116 cells generated RNA with slightly higher integrity than HT-29 cells (Table 5.11. No association between the order of quartile and RIN score was detected.

Table 5.11: RIN scores of RNA extracted from sorted cells.

	FaDu	HT-29	HCT116
1st Quartile (Lowest)	8.3	7.0	8.4
2nd Quartile (Low)	9.0	6.1	8.0
3rd Quartile (High)	8.7	7.2	8.8
4th Quartile (Highest)	8.7	7.2	8.4

Note: Data are representative of 3 independent experiments.

5.4 Discussion

RNA is labile and prone to hydrolysis, which is likely to be a large obstacle to applying CuAAC reactions on RNA (Paredes & Das, 2011; Shukla, 2014). The first application of CuAAC on RNA itself as the target biomolecule was reported by Salic *et al.* (Jao & Salic, 2008). In that study, the integrity of RNA was not a concern. Cells were exposed to 5-ethynyluridine *in vivo*, which was followed by fixation. Azide conjugated dye was utilised to visualise cellular transcripts randomly incorporated with 5-ethynyluridine in fixed cells via the CuAAC reaction. Subsequently, Brown and co-workers deployed CuAAC to generate a functional RNA by creating DNA–RNA hybrids crosslinked through nucleobases and also backbone ligation of two strands (El-Sagheer & Brown, 2010b). Different to previous applications of CuAAC with RNA, this thesis aimed to acquire untransformed RNA with adequate integrity for expression analysis using RT-qPCR from FACS-sorted cells labelled via CuAAC reactions.

It has been shown that use of intact RNA is critical to the successful application of modern molecular biological methods (Fleige & Pfaffl, 2006). Purity and integrity of RNA are critical for the overall success of RNA-based analyses. It is preferable to initiate molecular biological applications with high-quality, intact RNA because the accuracy of evaluation of gene expression is directly associated with the quantity and quality of the starting RNA (Imbeaud et al., 2005). On the other hand, working with low-quality RNA may strongly compromise the experimental results of

downstream applications (Fleige & Pfaffl, 2006; Fleige et al., 2006; Jahn et al., 2008; Miller, Diglisic, Leister, Webster, & Yolken, 2004).

Quantification of messenger RNA (mRNA) is typically undertaken via a two-step procedure, including cDNA synthesis via reverse transcription, and subsequent nucleic acid amplification usually via polymerase chain reaction (PCR), which is widely performed by deploying RT-qPCR, the results of which are very dependent on the quality of the RNA (Brisco & Morley, 2012). The use of RT-qPCR to study transcripts providing a snapshot of gene expression has demonstrated numerous advantages, such as high sensitivity, good reproducibility, and a wide dynamic quantification range (Grube et al., 2015; Ogata, Matsuda, Tsuji, & Nomoto, 2015).

To date, several approaches have been developed with the purpose of assessing RNA quality (Brisco & Morley, 2012). Nanodrop is the most widely used microvolume spectrophotometer for assessment of nuclear acid quantity and purity (Desjardins & Conklin, 2001). In RNA samples, Nanodrop is able to detect whether small DNA contaminants are present but is limited in indicating intactness of RNA (Schroeder et al., 2006). The Agilent 2100 Bioanalyzer provides an unambiguous assessment of RNA integrity with a sensitivity that is superior to alternative methods (Brisco & Morley, 2012).

Compared with spectrophotometry, analysis of 18S and 28S rRNA by electrophoresis, the 5'–3' assay (Nolan, Hands, & Bustin, 2006), as well as PCR amplification of different target lengths of complementary DNA (cDNA) (Bauer, Polzin, & Patzelt; Gong, Tao, & Li, 2006), the RIN software algorithm based on the analysis of the complete RNA pattern on electrophoresis provides a solution to estimate the integrity of RNA starting materials in an unambiguous way by removing user-dependent interpretation of RNA quality (Schroeder et al., 2006).

RNA degradation is a common concern in gene expression analysis. The RNA integrity, in general, affects RT-qPCR performance but not PCR efficiency. The increase in RIN score of RNA sample resulted in the reduced variability of the RT-qPCR results (Fleige & Pfaffl, 2006). Yolken and co-workers reported a study of brain tissue samples from 105 individuals and revealed a correlation between RIN scores and the outcome of a real-time PCR experiment of 4 different housekeeping genes (Miller et al., 2004). RNA integrity exerted a critical influence on downstream experiments.

In comparison to ribosomal ratio, it provided a straightforward means for controlling reliability of data generated in downstream real-time PCR analysis by a meaningful threshold value of RIN (Miller et al., 2004; Schroeder et al., 2006).

Assuming that RNA will be degraded to the extent at which fragments are too small to analyse reliably at a certain point on the RIN scale, RT-qPCR analysis, to some extent, can tolerate moderately degraded RNA samples and may still result in a reasonable expression profile (Fleige & Pfaffl, 2006; Fleige et al., 2006). Nevertheless, all efforts should be made to achieve high quality in RNA samples and thus more reliably representing the natural state (Imbeaud et al., 2005). Thus, this Chapter focused on maximising the compatibility of the CuAAC-based method with the integrity of RNA in FACS-sorted azide-modified fluorophore-clicked cells. To the best of our knowledge, no systematic studies have been published on how to improve the integrity of RNA extracted from FACS-sorted cells and applied to transcript measurements.

In the study of *in vivo* hypoxic gene expression profiling in gliomas reported by Koumenis and co-workers, a RIN score of 7 was deemed of sufficient quality for the study of RNA transcripts and used as the standard in qPCR and array analyses (Marotta et al., 2011). The same RIN score was accepted by Cerca et al. as appropriate for qPCR analysis in their study of prokaryotic RNA. They observed that RNA samples with a RIN value below 7 yielded high variation in reference transcript C_t values and loss of statistical significance when gene expression was analysed by real-time RT-qPCR (Jahn et al., 2008).

A RIN score higher than 8 indicated perfect total RNA competent to serve as template in downstream application in the study performed by Pfaffl *et al.*. A RIN score between 5 and 8 was suggested to represent the RNA quality resulting in suboptimal RT-qPCR expression results. The importance of RNA quality has been shown to increase with increasing length of the amplified product in PCR (Fleige et al., 2006). In mammalian RNA samples, values of RIN above 5 have been suggested as a minimum for reliable mRNA measurements (Fleige et al., 2006; Jung et al., 2010). It even has been suggested that the required quality for amplification of shorter RT-qPCR products, such as amplicons in TaqMan® assay mostly used with a length between 70-250 bp, were somewhat independent to the RNA integrity (Fleige & Pfaffl, 2006; Fleige et al., 2006; Li et

al., 2008). According to these previously used RNA integrity cut-off values for meaningful expression assessment by RT-qPCR, this Chapter aimed to at least achieve the RIN score of 5 by further optimising the click chemistry-based method on the basis of good hypoxia-mediated clicking selectivity.

Concerning the compatibility with RNA, a study of total eight combinations of copper source, reducing agent, and ligand (two candidates each) was performed to find a combination(s) that gives rise to both good hypoxia-selective click and intactness of RNA. The CuAAC reaction using CuOAc as copper source, reduced by TCEP, and stabilised by either TBTA or THPTA demonstrated the best RNA integrity in fluorophore-labelled cells in addition to an acceptable hypoxia-mediated clicking selectivity (Table 5.1).

Despite the wide application of CuAAC reaction in various fields of biological study, the *in vivo* approaches based on this most effective click reaction are considerably limited due to the major concern of the cytotoxicity caused by the copper(I)-mediated generation of ROS from O_2 (Brewer, 2010; Hong et al., 2010; Wang et al., 2003). Under physiological conditions, catalytically active copper(I) is easily oxidised by either O_2 or H_2O_2 to the +2 oxidation state via Fenton processes with the production of superoxide or hydroxyl radicals, respectively (Biaglow et al., 1997). The presence of ROS is able to induce the damages in structure and functional integrity of biomolecules, which has been detected under CuAAC conditions (Hong et al., 2009; Kennedy et al., 2011).

In addition to the degradation of proteins, it has been reported that copper-mediated production of ROS is able to induce strand scission of nucleic acids through both metal-assisted and free radical mechanisms (Burrows & Muller, 1998). Liu and co-workers observed that about 50% of nucleic acids underwent degradation when CuAAC was applied for only 10 min at RT (Gartner, Grubina, Calderone, & Liu, 2003; Kanan et al., 2004). Thus, reduction of the click reaction time may improve intactness of RNA in cells by decreasing the length of time that cells are exposed to ROS.

The double click incubation with reaction cocktail was critical to achieving a sufficient CuAAC reaction (Figure 5.3 and Figure 5.4). Interestingly, the sufficient reaction was more dependent on the copper-source, the reducing agent, as well as the stabilising ligand, rather than on the azide-

modified fluorophore in the second dose of the reaction cocktail (Figure 5.2). This observation indicated the important roles of ligand-stabilised copper(I)-mediated catalysis in the click reaction. To achieve a sufficient click reaction, any changes made in the click reaction time have to be based on the format of a double-click. The shortening of the total exposure time to the reaction cocktail was associated with higher RNA integrity in cells at the end of the labelling procedure (BODIPY-FL-azide, Table 5.2; Super-DIPY, Table 5.4 and Table 5.5). Even though this improvement in RNA integrity was not considerable, it was consistent in click reactions mediated by two different azide-modified fluorophores and supported by data of three independent experiments (with Super-DIPY only). The protocol was thus optimised by shortening the click reaction time.

It has been suggested that the ligand plays the role of sacrificial reductant in CuAAC to protect the substrate from oxidation by interrupting the *in situ* generated ROS in the coordination sphere of the copper. An excess of copper-binding ligand (five equivalents in tris(triazolyl)methylamine ligands) was used as additive and functional as the scavenger of ROS to minimise cytotoxicity (Hong et al., 2009). At least five equivalents of THPTA with respect to copper was suggested necessary in order to rapidly remove locally generated reactive oxygen species without markedly compromising the rate of CuAAC reaction (Hong et al., 2009).

However, an excess of copper-source, generally ten equivalents with respect to the copper-binding ligand, has been shown to consistently bring the best selectivity in hypoxia-mediated labelling based on the data generated by multiple experiments independent of the selection of either copper source or stabilising ligand in this thesis (Figure 4.3, Figure 4.4, Figure 4.5, Figure 5.3 bottom row, Figure 5.7A, B, and C). According to the data presented in Figure 5.3 (bottom row), an increase in ligand to copper ratio was associated with a decrease in the integrity of RNA extracted from azide-clicked hypoxic cells. However, this was the only experiment in which the effect of varying the ligand to copper ratio on the integrity of RNA in clicked cells was observed. Therefore, it is not possible to draw a firm conclusion about the relationship between ligand to copper ratio and RNA integrity.

Significant degradation of unmodified RNA species has been observed under various copper-catalysed click conditions, which previously limited studies of click reactions with RNA sequences when integrity became a concern (Paredes & Das, 2011). A pioneering study observed that in the presence of a large excess of copper(I) ions generated by *in situ* reduction of $CuSO_4$ with sodium ascorbate both DNA and RNA remained intact over 5 h in 100 mM degassed Tris buffer (pH 7.5) to remove dissolved oxygen and reduced the risk of oxidative degradation of the oligonucleotides (Paredes & Das, 2011).

As mentioned previously, the presence of atmospheric oxygen is able to induce degradation or aggregation of target biomolecules including RNA by mediating the generation of oxygen radicals or other reactive species during the maintenance of copper ions in the active +1 oxidation state in CuAAC (Hong et al., 2010; Houseley & Tollervey, 2009; Temple et al., 2005). Removal of atmospheric oxygen may provide another solution to preserving intactness of RNA. Therefore, click reaction and its following wash steps were moved from tissue culture hood into an anaerobic chamber. The reduced oxygen tension may also benefit CuAAC reaction by facilitating the generation of catalytically active copper(I) and stabilising this oxidation state (Chan et al., 2004). Consequently, the CuAAC reaction performed in the anaerobic chamber may result in a more efficient fluorophore-labelling with a relatively smaller variation of fluorescence intensity among cells in hypoxic sample presented as a sharper peak in the histogram (Figure 5.10 and Figure 5.11). However, conducting part of the procedure in an anaerobic chamber was impractical and inconvenient, led to some operating difficulties and, most importantly, did not induce any improvement in RIN scores. As a result, the intention of moving click reaction into an anaerobic chamber was terminated.

By using a standard azide, BODIPY-FL-azide, only a limited improvement in RIN could be achieved without compromising the hypoxia-selective labelling specificity. The RIN score of the RNA extracted from the labelled cells was increased from 4.1 to 4.6 when the 15-min + 15-min double click procedure was employed during the step of reaction cocktail incubation to replace the 30-min + 30-min double click procedure in the previously modified protocol (Figure 5.4 and Table 5.2). According to the experimental data from published literature and from this study, a faster CuAAC labelling protocol with a decreased requirement for copper concentration may benefit both

the detection of 2-NI metabolically tagged protein by azide-modified fluorophores and the compatibility with high-quality RNA (Uttamapinant et al., 2012).

Attempts to completely eliminate oligonucleotide degradation, compulsory exclusion of atmospheric oxygen has even been suggested (Géci, Filichev, & Pedersen, 2007). As an alternative approach to overcome these limitations mainly induced by ROS-mediated damage, extensive efforts have been devoted to the development of catalytic systems incorporating copper(I)-chelating ligands. The employment of stabilising ligands showed beneficial effects in maintaining the integrity of nucleic acids, which paved the way for CuAAC utilised as a reliable approach in nucleic acids modification.

The use of chelation-assisted CuAAC allows the concentration of copper to be decreased by virtue of raising the effective copper concentration at the reaction site (Uttamapinant et al., 2012). The application of copper-chelating azides can work complementarily with ligand design to dramatically benefit the CuAAC reaction rate and biocompatibility (Besanceney-Webler et al., 2011; Hong et al., 2010). It has been demonstrated in pioneering work from multiple research laboratories that the CuAAC reaction stabilised via a tris(triazolylmethyl)-amine-based ligand can be accelerated 4- to 6-fold by 2-(azidomethyl)pyridine derivatives in comparison to reactions using azides without copper-chelating functionality in *in vitro* model systems (Brotherton et al., 2009; Kuang et al., 2011; Kuang et al., 2010; Michaels & Zhu, 2011).

The successful application of chelation-assisted CuAAC in site-specific labelling of protein on the surface of living cells demonstrated 2.7- to 25-fold increase in labelling yields compared with conventional CuAAC (Uttamapinant et al., 2012). However, the utilisation of CuAAC in the cellular context was still limited to the surface of cells. The majority of applications based on click chemistry in living cells or organisms is still in favour of copper-free click reactions (Jewett et al., 2010; Lallana et al., 2011; Ning, Guo, Wolfert, & Boons, 2008).

Wu and co-workers used an electron-donating picolyl azide to label newly synthesised cell-surface glycans *in vivo* via ligand BTTPS-accelerated CuAAC reaction without apparent toxicity. The successful application of chelation-assisted CuAAC allowed scholars to monitor dynamic

biosynthesis of interested molecules in mammalian cells and early zebrafish embryogenesis (Jiang et al., 2014).

In comparison to the standard BODIPY-FL-azide, the use of a chelation-assisted version of BODIPY-based azide, Super-DIPY, in this thesis markedly increased the hypoxic to oxic ratio by nearly doubling the fluorescence intensity in hypoxic cells via the CuAAC reaction with SN33267 derivatives incorporated into cells.

Similar to what Ting and co-workers found in their study to site-specifically label membrane proteins and RNA molecules via CuAAC by a copper-chelating picolyl azide in fixed cells (Uttamapinant et al., 2012), the Super-DIPY effect was so strong that it more than compensated for the effect of omitting TBTA ligand (Figure 5.6 and Figure 5.7). But the expected decrease in the required concentration of copper in chelation-assisted CuAAC was not shown when Super-DIPY was used according to the data generated in SiHa cells in this Chapter. The CuAAC reactions mediating the hypoxia-dependent cell labelling were maximally favoured by a ligand to copper ration of 1:10 independent of the selection of azide-modified fluorophore. To achieve the best hypoxic to oxic ratio, 1 mM of either CuOAc or $CuSO_4$ was still required by the CuAAC reactions to coordinate with 100 μM TBTA (Figure 5.7). This was probably partially caused by limited transport of copper ions into the cytosol to reach the intracellularly localised SN33267 adducts and/or the presence of intracellular binding sites/sequestration of copper (Bertinato & L'Abbe, 2004; Leone & Mercer, 2012).

The CuAAC reaction demonstrated a broad-spectrum compatibility with aqueous buffers in the pH range between 6.5 and 8.0 as long as copper-binding species were absent (Hong et al., 2009; Presolski et al., 2011). It has been suggested that very high concentrations of chloride ion (greater than 0.2 M) should be avoided in buffer since it was capable to compete for copper and slow down the reaction rate (Presolski et al., 2011). Additionally, it has been pointed out that Tris buffer cannot be utilised in CuAAC because the tris(hydroxymethyl)aminomethane molecule may function as a competitive and inhibitory ligand for copper (Hong et al., 2009; Presolski et al., 2011). However, such inhibitory function of Tris buffer was not identified in this thesis. Reaction cocktail prepared

in 10 mM Tris-buffered saline worked well in the CuAAC reactions between clickable 2-NI and azide-modified fluorophores.

With the employment of Super-DIPY, the CuAAC reaction carried out in 10 mM Tris-buffered saline (pH 7.4) was clearly superior to PBS (pH 7.4) and resulted in an improved hypoxia-selectivity. The substitution of PBS for 10 mM Tris-buffered saline was made during the optimisation of methodology primarily in consideration of the integrity of RNA extracted from the labelled cells (Table 5.8). In order to evade the formation of insoluble copper-phosphate complexes, the copper source was recommended to be premixed with the ligand when phosphate was present in the reaction cocktail (Presolski et al., 2011). In addition, the data presented here indicated that the presence of ligand was associated with a slightly higher integrity of RNA in labelled cells (Table 5.3). It has been documented that the omission of ligand may induce enhanced membrane permeability contributing to the effects on cell damage (Hong et al., 2010). Thus, ligand was kept in the recipe of PBS-based reaction cocktail (reaction cocktail #7 in Table 2.7), despite the near-zero ligand dependency of chelation-assisted CuAAC (Figure 5.6 and Figure 5.7).

The use of a mixture of two cell populations exposed to SN33267 under different oxygen concentrations provided a more realistic case to validate the methodology in terms of the two main criteria of selectivity to hypoxia and biocompatibility with RNA. Oxic cells had higher fluorescence intensity when they were incubated with the reaction cocktail in the presence of hypoxic cells, i.e. as a mixture (Figure 5.14 and Figure 5.15). The study with reaction media that had been previously-used to incubate hypoxic cells in separate CuAAC reactions suggested that some fluorescence-labelled molecules were released from the hypoxic cells during the click reaction.

Investigations of model reduction systems indicate that the four-electron reduction product (hydroxylamine) of 2-NI is the primary adduct-forming species that is capable to covalently bind to the macromolecules, mainly thiol-containing proteins, with high efficiency in the cellular milieu (Koch & Raleigh, 1991; Raleigh & Koch, 1990). The covalent association between reactive intermediates generated by the bioreduction of nitroheterocyclic compounds and cellular molecules is extremely stable due to the build-up of electron density between the nuclei. The formation of covalent associations involved in both binding of cellular adducts of 2-NI and CuAAC

is irreversible (Petrucci, Herring, Madura, & Bissonnette, 2010). Thus it seems unlikely that these macromolecule covalently associated adducts of SN33267 in hypoxic cells were released and somehow taken up by the pre-mixed oxic cells.

Besides thiol side chains of cysteine residues in macromolecules, cysteine residues may also exist as free thiols in cytoplasm (Trivedi, Laurence, & Siahaan, 2009). In hypoxic cells, these free thiols can also be involved in the reductive formation and covalent association of cellular adducts of SN33267. These adducts will further covalently bind to azide-modified fluorophores via CuAAC and may be released out of hypoxic cells. The oxic cells that are pre-mixed with hypoxic cells or incubated with previously-used reaction medium may somehow take up these fluorophore-labelled molecules and therefore show elevated fluorescence intensity (Figure 5.15 and Figure 5.16). The mechanism behind this process still needs to be further investigated.

With the use of the optimised protocol, the click chemistry-base method successfully demonstrated the capability of separating pre-mixed cell populations in a hypoxia-selective manner (Figure 5.14 and Figure 5.15).

Moreover, the click reaction time was further tailored to four human cancer cell lines to achieve both hypoxia-mediated selectivity of CuAAC-labelling and compatibility with RNA intactness in FACS-sorted clicked cells (Figure 5.21). Consequently, the final protocol (protocol #7 in Figure 2.1) was optimised by shortening the incubation time with reaction cocktail and removing redundant wash step(s) without compromising the gradient of the azide-modified fluorophores clicked with cells in a hypoxia-selective fashion deployed by FACS. The CuAAC-mediated cell labelling method was validated *in vitro* with four different human cancer cell lines. Cells were successfully sorted into four fractions according to their fluorescence intensity by chelation-assisted CuAAC reaction (Figure 5.22), which demonstrated the potential of this method for clicking of dissociated tumours in Chapter 6.

Last but not least, the RNA quality is dependent on the choice of RNA extraction method (Fleige & Pfaffl, 2006; Fleige et al., 2006). When RNA is extracted from FACS-sorted cells, the selection of solution used to collect the cells from the sorter is also critical to the RIN score of the final extracted RNA (Nilsson, Krawczyk, & Johansson, 2014). In this thesis, the collection of sorted

cells in TRIzol® LS reagent followed directly by the extraction of total cellular RNA using a method combining the strong lysis capability of TRIzol® LS reagent and silica-cartridge purification gave rise to RNA with RIN values above 6 in general (Table 5.9 and Table 5.11). Human cancer cell lines used in this Chapter are derived from different types of tumour tissue. RNA samples extracted from FACS-sorted fractions demonstrated slight differences in RIN score among the four cell lines due to the tissue- and organ-dependent features in RNA integrity (Jung et al., 2010).

The click chemistry-based methodology was successfully optimised in this Chapter. The protocol of this method had even been customised for four human cancer cell lines. With the optimised method, pre-mixed cells were able to be clicked with azide fluorophores in a hypoxia-selective manner and be sorted by FACS. More excitingly, RNA extracted from FACS-sorted had a RIN score above 6, which was sufficiently high to be used in the assessment of mRNA transcripts according to RIN cut-off values reported in the literature. At this stage, the optimised methodology was deemed suitable for application in human tumour xenografts, which is described in the next chapter.

Chapter 6. Validation of the click chemistry-based method for labelling of hypoxic cells using a hypoxia gene signature

6.1 Introduction

Hypoxia is a well characterised feature of the microenvironment of solid tumours. The hypoxia status of tumours is directly associated with the resistance to radiotherapy and chemotherapy (Tatum et al., 2006; Vaupel et al., 2004). Both laboratory and clinical studies have provided evidence that hypoxia is a critical determinant of tumour aggressiveness, which has stimulated the development of accurate assessment approaches to quantify tumour hypoxia in patients (Marotta et al., 2011; Semenza, 2010; Semenza, 2012).

Ideally, tumour hypoxia should be evaluated by a noninvasive approach that accounts for spatial differences in the distribution of hypoxia without inducing alterations of the underlying physiology. The assessment of tumour hypoxia should be usable both in the laboratory and clinic, which should be not only repeatable over time but also achieve high sensitivity, specificity, as well as spatial resolution (Dhani & Milosevic, 2012; Höckel & Vaupel, 2001; Wong, Fyles, Milosevic, Pintilie, & Hill, 1997).

Noninvasive approaches of tumour hypoxia measurement have demonstrated advantages over oxygen sensor-based invasive techniques. With the use of noninvasive approaches, for example, the necrotic tissue can be distinguished from tumour areas with viable hypoxic cells and information about the microscopic distribution of hypoxia can also be obtained (Dhani & Milosevic, 2012; Harris, Barberis, West, & Buffa, 2015). The selection of hypoxia marker(s) is critical in sensitivity and reliability of noninvasive approaches (Burtness & Golemis, 2014).

Although the time-dependence of expression can sometimes be an obstacle to interpretation, the employment of endogenous biomarkers in the evaluation of tumour hypoxia is still particularly attractive. Measurement of cellular adaption provides an indirect measure of hypoxia. HIF, mammalian target of rapamycin (mTOR), and unfolded protein response (UPR) signalling pathways jointly influence many of the cellular consequences of hypoxia involved in tumour

metabolism, autophagy and ER homeostasis (Wouters & Koritzinsky, 2008). Genes regulated in response to hypoxia reflect the hypoxic phenotype and can provide insight into the biological consequences of the hypoxia at the cellular level (Dhani & Milosevic, 2012; Winter et al., 2007). Their expression can be evaluated at either the transcription level using RT-qPCR or at the protein level by use of immunohistochemistry (IHC) (Buffa et al., 2010; Ghazoui et al., 2011). HIF-1α is one of the key regulators responsible for the induction of genes facilitating adaptation to hypoxic stress (Semenza, 2010). Expression of HIF-1α and its downstream target CAIX have been intensively investigated (Schrijvers et al., 2008). However, expression of HIF-1α can also be under the regulation of other oncogene-mediated mechanisms independent to hypoxia and therefore may not always specifically reflect hypoxic status across tumours (Favaro, Lord, Harris, & Buffa, 2011; Moon, Brizel, Chi, & Dewhirst, 2007). The assessment of tumour hypoxia by noninvasive approaches is predominantly limited by a dependence on a specific gene or even a group of genes involved in a single mechanism (Le & Courter, 2008).

Recently, a global transcriptional response to hypoxia has been identified in several studies by use of gene expression microarrays (Harris et al., 2015). To take advantage of the excess of information in microarray data, genes observed in significant response to hypoxia are typically grouped together and termed hypoxia gene expression signature or hypoxia signature. Gene expression signatures can be used as strong predictors of clinical outcome with considerable reliability (van't Veer & Bernards, 2008). On the basis of combinations of hypoxia-responsive genes, their combined expression pattern is exclusively characteristic of a biological phenotype (Brown; de Cecco et al., 2015; Dhani & Milosevic, 2012). The assessment of tumour hypoxia by use of a hypoxia gene expression signature incorporates multiple endogenous hypoxia biomarkers into a single assay, which is highly enriched for hypoxia-regulated pathways and prognostic in multivariate analyses (Buffa et al., 2010; Melillo, 2013).

A 15-gene hypoxia gene expression signature developed in squamous cell carcinomas by Toustrup *et al*. was the first signature that could predict beneficial treatment strategies and consequently has been implemented in the clinic (Toustrup et al., 2011). Being a novel predictive hypoxia biomarker signature, this 15-gene signature has been applied both retrospectively and prospectively and shown to be of prognostic significance in non-squamous cell carcinomas,

including breast and lung cancer (Starmans et al., 2012; Toustrup, Sørensen, Alsner, et al., 2012; Toustrup, Sørensen, Lassen, et al., 2012).

Understanding gene expression patterns is essential to provide insight into complex regulatory networks, which most probably contributes to the identification of genes related to new biological processes or implicated in the development of physiological disorders. Assessment of mRNA transcript level of an interested gene in cells generally starts by converting the mRNA to cDNA via reverse transcription that is followed by polymerase chain reactions (PCR) to amplify the cDNA in an exponential manner (Huggett, Dheda, Bustin, & Zumla, 2005; Sun, Li, Luo, & Liao, 2012). Being one of the most sensitive methods commonly used for the quantification of low-abundance mRNA transcription, RT-qPCR has become the method of choice for high-throughput and accurate expression profiling of selected genes, including hypoxia gene expression signatures (Weis, Tan, Martin, & Wittwer, 1992).

6.2 Aims

The key task of this Chapter was to validate the methodology in labelling and sorting tumour cells in a hypoxia-dependent manner by measuring expression via RT-qPCR analysis of the clinically validated hypoxia gene expression signature of 15 genes developed by Toustrup *et al*. (Toustrup et al., 2011).

The specific objectives are:

- To assess any impact of CuAAC-mediated hypoxia-dependent cell labelling on the 15-gene hypoxia gene expression signature;
- To identify appropriate endogenous control genes under hypoxic conditions for quantifying gene expression;
- To apply the optimised methodology *in vitro* to sort pre-mixed oxic and hypoxic cells into 2 fractions according to their cellular hypoxic stress for evaluation of the hypoxia gene signature;

- To apply the optimised methodology *ex vivo* to sort cells from dissociated tumour xenograft according to their cellular hypoxic stress for evaluation of the hypoxia gene signature.

6.3 Statistics

Pearson correlations were computed in SigmaPlot for Windows Version 11, 12, or 12.5 (Systat Software Inc., CA, USA). Two-way ANOVA with Bonferroni *posthoc* test was used to study the hypoxia-mediated expression of selected genes. Fold change in mRNA abundance was the dependent variable. A P value ≤ 0.05 was considered to be significant. Analysis was performed using GraphPad Prism 5 for Windows Version 5.01 (GraphPad Software, CA, USA).

6.4 Results

6.4.1 Selection of endogenous control genes

According to published literatures and qPCR technical information on the Gene Quantification platform related to investigations of gene expression under anoxia/hypoxia, eight genes (Table 2.9, in bold) were chosen as candidates of endogenous controls (Türkoğlu & Köçkar, 2012; Baddela, Baufeld, Yenuganti, Vanselow, & Singh, 2014; Caradec et al., 2010; Eisenberg & Levanon, 2013; Munk et al., 2012; Pfaffl, 2015; Tan et al., 2012; Yao et al., 2012). To identify the optimal endogenous control genes for use in the study of hypoxia-regulated gene expression, a geNorm analysis was performed on eight candidate genes for both SiHa and FaDu cells. RNA samples prepared by *in vitro* experiments described in Chapter 5 (SiHa, Table 5.10 bottom row; FaDu, Table 5.11 left column) were converted into cDNAs and used as templates. The analysis using geNorm generated a measure of gene stability (M-value), which can be used to rank the candidate reference genes. An M-value of less than 1.5 has been arbitrarily suggested to be a suitable cut-off for gene stability (Coulson et al., 2008; Julian, de Oliveira, Perry, Tufik, & Chagas, 2014; Vandesompele et al., 2002). According to the geNorm evaluation the best candidate was *RPLP0* followed by Beta-2-Microglobulin (*B2M*) and 18S Ribosomal RNA (rRNA; *18S*). In addition, the least stable gene was *YWHAZ*, which had the highest M-value that was still less than 0.7 (Figure 6.1A).

A pairwise stability measure (V-value) was generated by geNorm to determine the benefit of adding extra reference genes for the normalisation process. Again, a lower value indicates greater stability of the normalisation factor. An arbitrary cut-off value of 0.15 indicates acceptable stability of the reference gene combination (Coulson et al., 2008; Julian et al., 2014; Vandesompele et al., 2002). The optimal number of reference targets in this particular experiment was 2 (Figure 6.1B). As such, the optimal normalisation factor was suggested to be the geometric mean of the reference targets *B2M* and *RPLP0*.

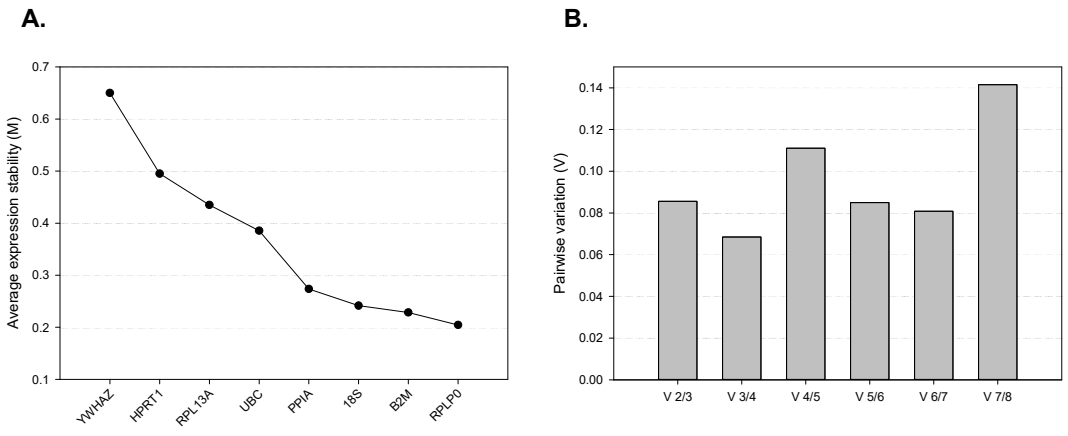

Figure 6.1: geNorm stability analysis of potential reference genes.

Evaluation of gene expression stability by geNorm for SiHa and FaDu cells by use of RNAs prepared in Chapter 5 (SiHa, Table 5.10 bottom row; FaDu, Table 5.11 left column). (A) Average expression stability values of eligible endogenous control genes. Expression stability of the reference gene candidates as calculated by geNorm. The stability value M is based on the average pair-wise variation between all candidates. The least stable gene with the highest M-value was excluded and the M-value was recalculated till it ended up with the most stable pair. (B) Determination of an optimal number of control genes for normalisation. The geNorm programme calculates a normalisation factor (NF) utilised to assess the optimal number of endogenous control genes required for accurate normalisation. The NF is calculated using the variable V as the pairwise variation (V_n/V_{n+1}) between two sequential NFs (NF_n and NF_{n+1}). The recommended cut-off V-value (V = 0.15) is the point at which it is unnecessary to include additional genes in a normalisation strategy. In this instance, the geNorm output file indicated that all tested candidates demonstrated high reference target stability (average geNorm M ≤ 0.5) and the optimal number of genes required for normalisation was two. Three independent experiments were performed.

All of the 8 candidate genes in all of the analyses gave M-values of less than 0.7, which was less than 50% of the cut-off for suitability (M = 1.5). The assessment of pairwise variation indicated that all tested conditions gave rise to V-values less than the cut-off value of 0.15. These data indicated

that all of the tested candidate genes were suitable for use according to the adopted cut-off values. For reasons of convenience *B2M* and *18S* were selected as endogenous control genes for subsequent RT-qPCR analyses.

6.4.2 Effect of the CuAAC-based procedure on gene expression

Similar to most applications of bioorthogonal reactions, the CuAAC-mediated methodology discussed in this thesis is based on a two-step bioorthogonal labelling strategy that requires introduction of exogenous functionality by chemical means followed by modification of the functionalised biomolecule(s) with a custom-designed highly specific bioorthogonal reaction. The intensity of fluorescence in labelled cells, by metabolically incorporating an alkyne-bearing 2-NI and reacting this with an azide-modified fluorophore via CuAAC, is the key to sorting them according to the hypoxia status. Before studying gene expression in cells labelled with fluorophores in a hypoxia-selective manner by use of this method, it was necessary to evaluate the effect of the whole click chemistry-based procedure on the expression of genes of interest.

To determine whether the entire CuAAC-mediated labelling methodology impacts on the hypoxia gene expression signature of 15 genes in response to hypoxic stress, hypoxia-induced fold change in gene expression in unlabelled SiHa cells was assessed by RT-qPCR analysis and compared with the expression data generated by qPCR from SiHa cells labelled with fluorophore (Super-DIPY) via the CuAAC-mediated methodology (Figure 6.2). No significant difference in transcription abundance of 15 hypoxia marker genes was detected in response to hypoxia ($P > 0.05$) when the click chemistry-based method was employed to label SiHa cells in a hypoxia-selective manner.

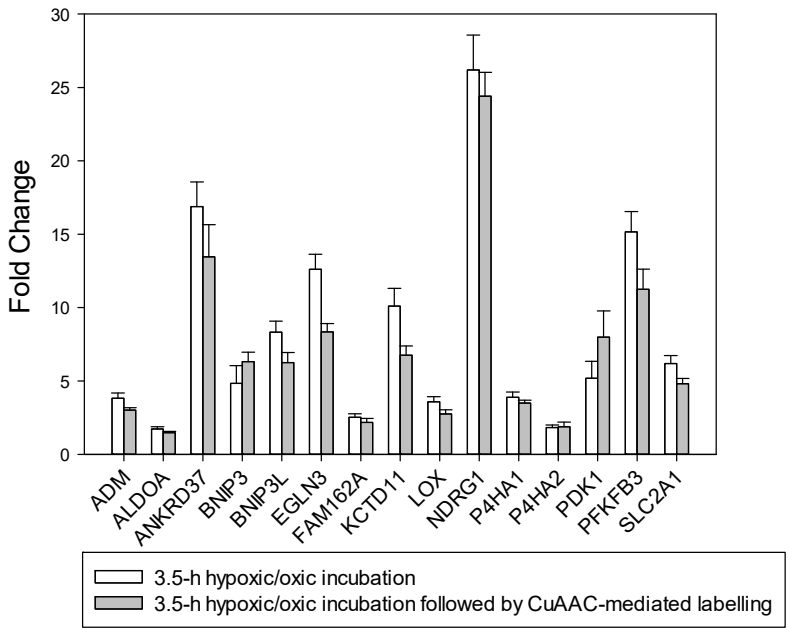

Figure 6.2: Effect of the CuAAC-mediated cell labelling procedure on the hypoxia-regulated expression of 15 hypoxia marker genes.

SiHa cells were pre-incubated for 1.5 h under ambient or hypoxic conditions followed by a 2-h incubation with 100 μM SN33267 under the same atmospheric conditions. These two cell samples were clicked with Super-DIPY using reaction cocktail #7 (Table 2.7) and following protocol #7 (Figure 2.1). RNA samples extracted from these two samples of clicked cells were converted into cDNA and used as templates for qPCR analysis by TaqMan gene expression assays to assess hypoxia-regulated fold change in transcript abundance of 15 hypoxia marker genes (grey bars). RNAs directly extracted from SiHa cells after 3.5-h incubation under same ambient or hypoxic conditions were converted into cDNA and used in qPCR analysis of hypoxia-regulated expression for control purposes (white bars). All investigated mRNA expression shows $P > 0.05$, compared to control as measured by two-way ANOVA with Bonferroni *posthoc* test. Errors are the standard error of the mean (SEM) from ≥ 2 qPCR experiments run with RNA isolated from two independent cultures.

6.4.3 Validating an additional cDNA clean-up procedure in gene expression study

Cells were pre-incubated for 1.5 h under ambient or hypoxic conditions followed by 2-h incubation with 100 μM SN33267 under the same atmospheric conditions and mixed together in 1:1 ratio. The click chemistry-based method was firstly applied in vitro to click mixed oxic and hypoxic cells with Super-DIPY in a hypoxia-selective manner following the experimental procedures described in Figure 6.3. To ensure a sufficient click with consideration of cellular RNA integrity, the second short click time, instead of the minimally required one, identified in Chapter 5 was used. The 15-min + 15-min double click and 20-min + 20-min double click procedures were selected for CuAAC reaction in SiHa and FaDu cells, respectively (Figure 6.3). The same click procedures were also used in cells dissociated from human tumour xenografts.

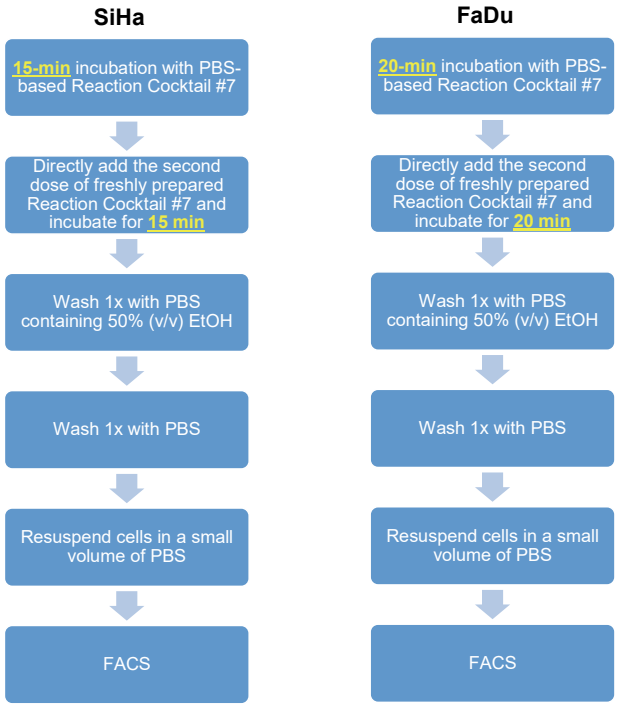

Figure 6.3: Schematic outlining the experimental procedures used to prepare cell samples for *in vitro* or *ex vivo* studies of gene expression in SiHa and FaDu cells.

Several pilot RT-qPCR experiments were performed to assess *ex vivo* expression of 15 hypoxia marker genes in clicked SiHa xenograft cell sorted by FACS. Since the click chemistry-based method was not completely optimised at that time, RNA samples extracted from clicked cells were heavily degraded. Use of those RNAs led to wells with missing values and considerable variations among technical replicates in RT-qPCR. According to some information from an online suggestion regarding a different question on ResearchGate, cDNA clean-up procedure might be helpful in solving problems with variation in technical replicates (Kirbach, 2013). This function of cDNA clean-up was still attractive even after the methodology had been optimised with much more improved RNA compatibility.

To determine the impact of cDNA clean-up on the expression of 15 hypoxia marker genes evaluated by RT-qPCR analysis, mixed oxic and hypoxic SiHa cells (in 1:1 ratio) were labelled with SN33267 and Super-DIPY following the procedures described in Figure 6.3. Cells were sorted into oxic and hypoxic fractions by FACS based on the fluorescence intensity and RNA was extracted from each fraction and converted into cDNA. Each cDNA sample was split into two aliquots. One aliquot was purified by an additional cDNA clean-up step using a Qiaquick® PCR purification kit (Qiagen GmbH, Hilden, Germany). Another aliquot without further cDNA clean-up was used as a control. These 2 groups of cDNA samples were used as templates to assess the expression of 15 hypoxia marker genes in response to hypoxia via RT-qPCR.

The C_t value of each hypoxia marker gene was significantly reduced ($P < 0.001$) when the cDNA samples with additional clean-up step were used as templates in RT-qPCR analysis (Figure 6.4). This change of C_t value was consistent across all tested genes but independent of hypoxia.

Based on the results of Bonferroni *posthoc* test for two-way ANOVA, there was no significant impact ($P > 0.05$) caused by the additional cDNA clean-up on the fold change in expression of all 15 hypoxia marker genes (Figure 6.5). In general, the intra-sample variance was smaller after cDNA clean-up as indicated by the smaller error bars for the 3 technical replicates. The cDNA clean-up procedure was added in the protocol *prior* to the PCR amplification and involved in all following experiments unless stated otherwise.

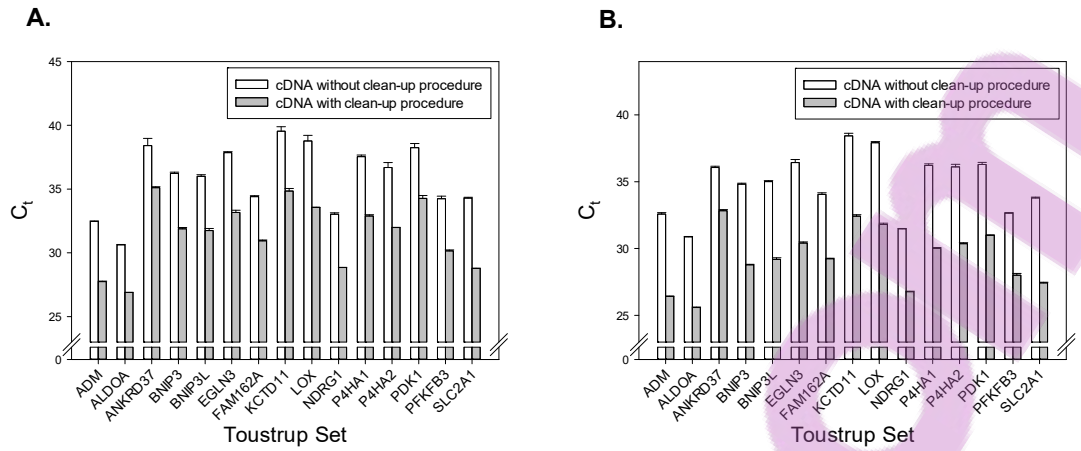

Figure 6.4: Effects of cDNA clean-up procedure on C_t value of hypoxia marker genes in RT-qPCR.

(A) Oxic samples. (B) Hypoxic samples. Mixed oxic and hypoxic SiHa cells (1:1 ratio) were labelled with fluorescence via the CuAAC reactions between cell-incorporated SN33267 derivatives and Super-DIPY following the procedures described in Figure 6.3. According to the fluorescence intensity, mixed cells were sorted into oxic and hypoxic fractions by FACS. RNA extracted from each fraction was converted into cDNA and split into two aliquots. An additional cDNA clean-up step was performed in one aliquot (grey bars). Another aliquot without cDNA clean-up was used for control purposes (white bars). Subsequently, RT-qPCR analyses were used to assess hypoxia-induced expression of 15 hypoxia marker genes and determine any alternations caused by the step of cDNA clean-up. All investigated mRNA expression shows $P < 0.001$, compared to control data generated from cDNA samples without clean-up procedure as measured by two-way ANOVA with Bonferroni *posthoc* test. Errors are SEM from 3 independent experiments.

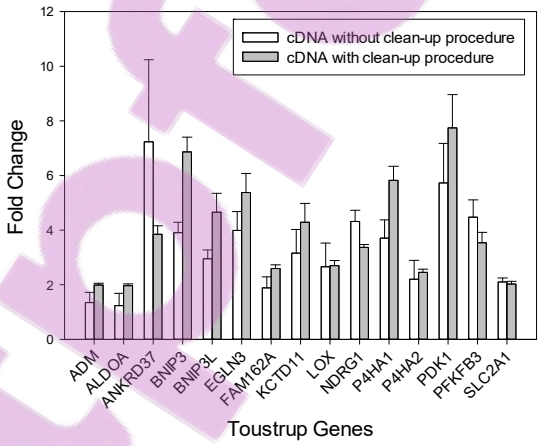

Figure 6.5: Effect of the cDNA clean-up procedure on the hypoxia-regulated expression of hypoxia marker genes.

The mixed oxic and hypoxic SiHa cells (1:1 ratio) were labelled with fluorescence via the CuAAC reactions between cell-incorporated SN33267 derivatives and Super-DIPY following the procedures described in Figure 6.3. According to the fluorescence intensity, mixed cells were sorted into oxic and hypoxic fractions by FACS. RNA extracted from each fraction was converted into cDNA and split into two aliquots. An additional cDNA clean-up step was performed in one aliquot (grey bars). Another aliquot without cDNA clean-up was used for control purposes (white bars). Subsequently, RT-qPCR analyses were used to assess hypoxia-induced expression of 15 hypoxia marker genes and determine any alternations caused by the step of cDNA clean-up. All investigated mRNA expression shows $P > 0.05$, compared to control as measured by two-way ANOVA with Bonferroni *posthoc* test. Errors are the SEM from ≥ 2 qPCR experiments run with RNA isolated from two independent experiments.

6.4.4 *In vitro* expression of 15 hypoxia marker genes

Mixed oxic and hypoxic cells (1:1 ratio) were clicked with fluorophores via the CuAAC-mediated methodology in a hypoxia-selective manner. Flow cytometric analysis revealed that the mixed cells were separated into 2 populations due to the distinct levels of labelled fluorescent signals, by which cells were sorted into two fractions. RNA samples were extracted from these 2 fractions and the expression of the hypoxia gene signature across 2 fractions was determined via RT-qPCR to validate if the methodology could isolate cells with known hypoxia status from the mixtures.

B2M and *18S* were selected from 8 candidates and used in this thesis as endogenous controls according to geNorm stability analysis (Figure 6.1). To further confirm that expression of both selected reference genes was independent to hypoxic stress, C_t values of *B2M* and *18S* generated from the RT-qPCR experiments that also produced *in vitro* expression data of hypoxia marker genes in SiHa and FaDu cells were plotted separately and reviewed first (Figure 6.6).

Among 3 independent RT-qPCR analyses, C_t values of the same reference gene, i.e. *B2M* or *18S*, showed random changes in response to hypoxic conditions in both SiHa and FaDu cells. According to the C_t values (i.e. the greater the abundance of mRNA, the smaller the C_t value), the transcript abundance of *18S* was notably higher than *B2M* gene in both cell lines. It was hard to compare the transcript level of the *B2M* gene between the two types of cells, but the transcript of *18S* in FaDu cells was more enriched than SiHa cells due to the smaller C_t values.

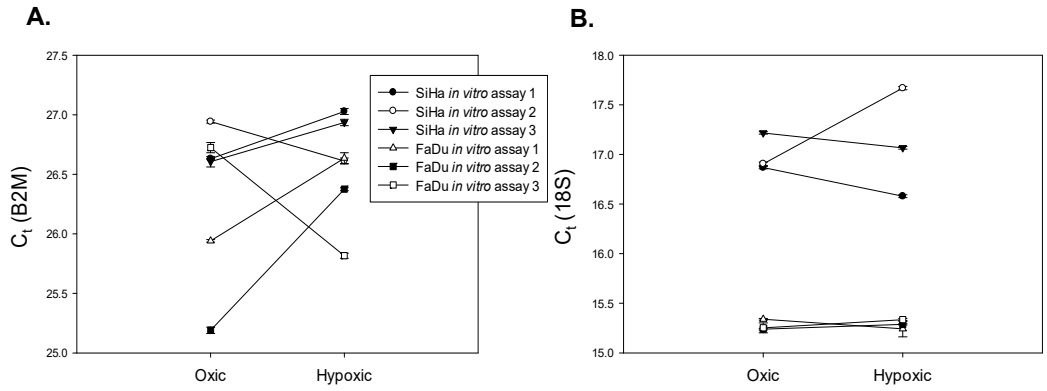

Figure 6.6: *B2M* and *18S* C_t variations in FACS-sorted *in vitro* fractions according to hypoxia status.

Cells were pre-incubated for 1.5 h under ambient or hypoxic conditions followed by a 2-h incubation with 100 μM SN33267 under the same atmospheric conditions. Mixed cells (1:1 ratio) were labelled with fluorescence via the CuAAC reactions between cell-incorporated SN33267 adducts and Super-DIPY following the procedures described in Figure 6.3. According to the fluorescence intensity, mixed cells were sorted into 2 fractions by FACS. RNA extracted from each fraction was converted into cDNA and used for RT-qPCR to assess hypoxia-induced expression of *B2M* (A) and *18S* (B). Error bars represent standard deviation (SD) from the mean of the technical replicates (n = 3). For each cell type, 3 independent experiments (assay 1–3) were performed.

In SiHa cells, the change in mRNA expression of all 15 genes demonstrated the same trend in response to hypoxic conditions (Figure 6.7). A total of 13 of 15 genes were significantly upregulated at their transcription level in the FACS-sorted fraction with higher level of fluorescence intensity, i.e. the hypoxic fraction. Although the changes in hypoxia-induced expression of *ADM* and *ALDOA* were not statistically significant, the hypoxia-induced upregulation of mRNA transcripts of all 15 genes was consistently shown in all 3 independent experiments. In general, the expression of *ANKRD37*, *BNIP3*, *BNIP3L*, *EGLN3*, *KCTD11*, *NDRG1*, *P4HA1*, and *PDK1* showed relatively larger responses to hypoxia in SiHa cells.

A.

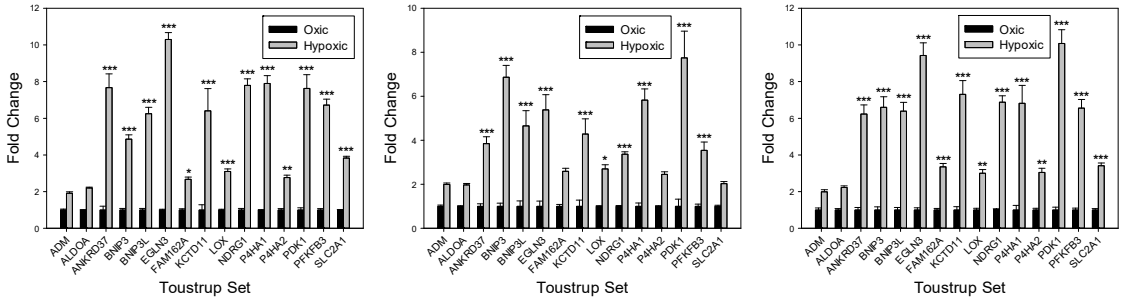

B.

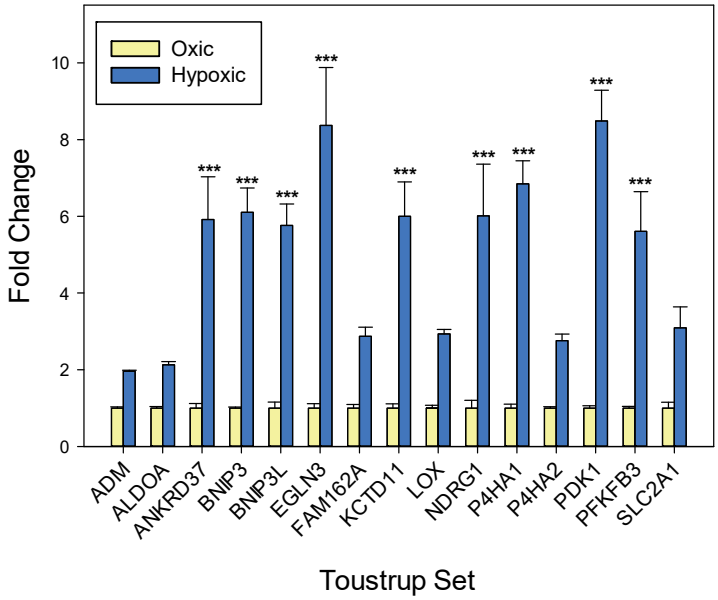

Figure 6.7: *In vitro* expression of hypoxia marker genes in SiHa cells in response to hypoxic stress.

The mixed oxic and hypoxic SiHa cells (1:1 ratio) were clicked with fluorescence via the CuAAC reactions between cell-incorporated SN33267 derivatives and Super-DIPY following the procedures described in Figure 6.3. According to the fluorescence intensity, mixed cells were sorted into oxic and hypoxic fractions by FACS. RNA extracted from each fraction was converted into cDNA. The hypoxia-induced expression of 15 hypoxia marker genes was evaluated by RT-qPCR analysis. (A) *In vitro* expression of hypoxia marker genes in 3 independent experiments. Error bars represent SD of the technical replicates (n = 3). (B) Averaged *in vitro* expression of hypoxia marker genes. Error bars indicate SEM (n = 9) derived from 3 biological replicates. * denotes $P < 0.05$, ** denotes $P < 0.01$, *** denotes $P < 0.001$, compared to oxic sample as measured by two-way ANOVA with Bonferroni *posthoc* test.

The mRNA expression of hypoxia marker genes demonstrated similar responses to hypoxic stress in FaDu cells (Figure 6.8). In FaDu cells 10 of 15 genes were significantly upregulated at their transcription levels in the FACS-sorted fraction with higher level of fluorescence intensity. Similar to SiHa cells, the mRNA level of *EGLN3*, *KCTD11*, *NDRG1*, and *PDK1* was also notably upregulated by hypoxia. In contrast, the hypoxia-induced regulation in the transcription of *LOX*, for example, was negligible in FaDu cells in all three independent experiments. On the other hand, the expression of *ADM* was significantly upregulated by hypoxia in FaDu cells.

A.

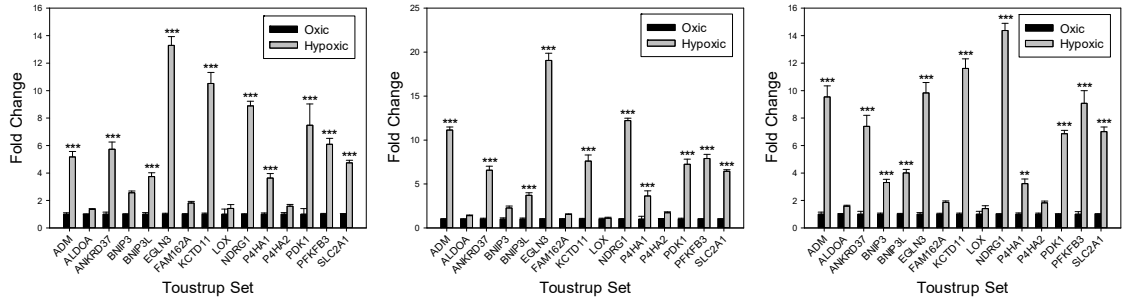

B.

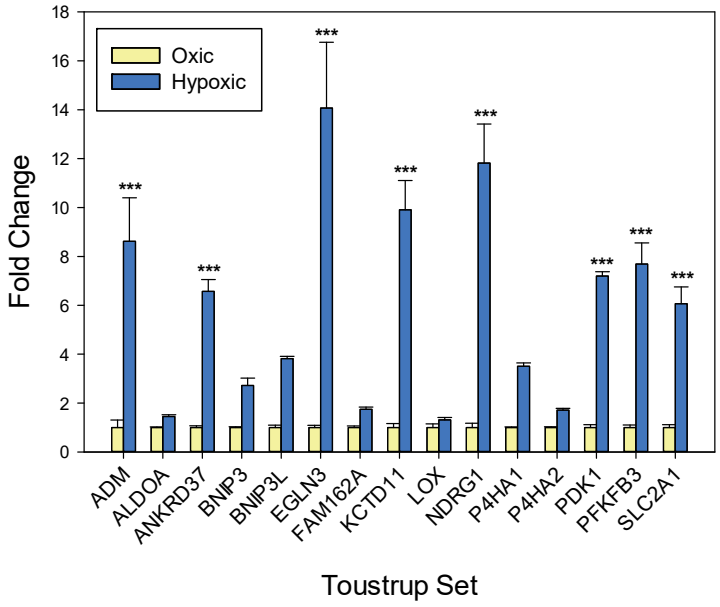

Figure 6.8: *In vitro* expression of hypoxia marker genes in FaDu cells in response to hypoxic stress.

The mixed oxic and hypoxic FaDu cells (1:1 ratio) were labelled with fluorescence via the CuAAC reactions between cell-incorporated SN33267 derivatives and Super-DIPY following the procedures described in Figure 6.3. According to the fluorescence intensity, mixed cells were sorted into oxic and hypoxic fractions by FACS. RNA extracted from each fraction was converted into cDNA. The hypoxia-induced expression of 15 hypoxia marker genes was evaluated by RT-qPCR analysis. (A) *In vitro* expression of hypoxia marker genes in 3 independent experiments. Error bars represent SD of the technical replicates (n = 3). (B) Averaged *in vitro* expression of hypoxia marker genes. Error bars indicate SEM (n = 9) derived from 3 biological replicates. * denotes $P < 0.05$, ** denotes $P < 0.01$, *** denotes $P < 0.001$, compared to oxic sample as measured by two-way ANOVA with Bonferroni *posthoc* test.

6.4.5 *Ex vivo* expression of 15 hypoxia marker genes

In each tested human cancer cell line, clicked cells were subsequently sorted into 2 fractions according to the fluorescence intensity by FACS. RNA samples extracted from both fractions were used in expression study of 15 hypoxia marker genes characterised by the feature of hypoxia-responsive expression (Toustrup et al., 2011). Since the entire CuAAC-mediated procedure did not impact on the expression, any differences in mRNA abundance of hypoxia marker genes detected between these two samples were caused by hypoxic stress, by which the methodology optimised in Chapter 5 could be validated. In two *in vitro* models, expression of all 15 hypoxia marker genes in SiHa and 11 in FaDu were consistently upregulated in the FACS-sorted fractions associated with higher level of fluorescence intensity, which indicated that the click chemistry-based methodology was capable of successfully labelling cells in a hypoxia-selective manner to provide a way for sorting cells actually according to the level of cellular hypoxia and compatible to downstream expression analysis by RT-qPCR.

To identify the susceptibility of the human TaqMan gene expression assay to cross-species contamination from mouse transcripts, cDNA prepared by mouse spleen RNA via reverse transcription was used as template for RT-qPCR. None of the human TaqMan gene expression assays for *18S*, *B2M*, as well as 15 hypoxia marker genes used in this Chapter amplified the cDNA template derived from mouse (Figure 6.9).

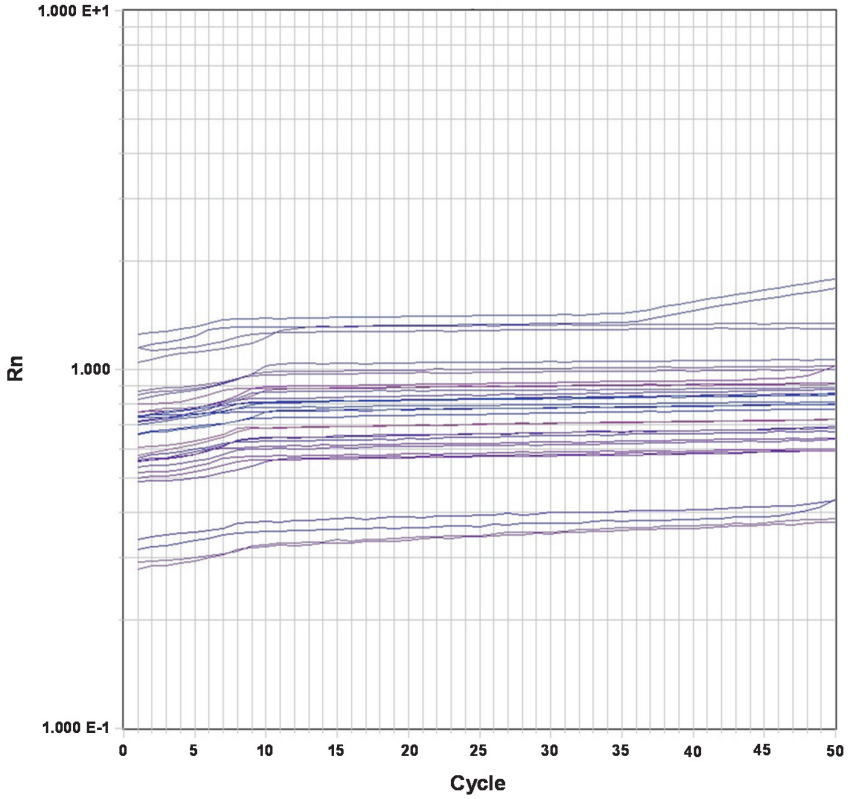

Figure 6.9: PCR amplification curves with TaqMan gene expression assays for *18S*, *B2M*, and 15 human hypoxia marker gene sequences in mouse spleen sample.

The plot indicates the normalised fluorescence (Rn) at the cycle number at which the C_t can be reached. There was no detectable amplification of mouse cDNA template. Three independent experiments were performed.

By ruling out the possibility of cross-species contamination from mouse transcripts, the validation of this click chemistry-based methodology was ready to move from cell line models to human tumour xenografts. Dissociated tumour xenograft cells were clicked with fluorophores via the CuAAC-mediated methodology in a hypoxia-selective manner. Clicked cells from each xenograft tumour were sorted into four fractions (quartiles) defined by equivalent cell number. The sorter used in this thesis can sort cells simultaneously into maximum 4 fractions. Sorting clicked cells in quartiles maximally avoids the overlapping of cell populations with closed levels of hypoxic stress. If sharp boundary of hypoxia status between samples was required, study could be done by investigating the first and the fourth quartiles. RNA sample was extracted from each fraction and the expression of the hypoxia gene signature across 4 fractions was determined via RT-qPCR to validate if the cells could be sorted according to the order of hypoxia status by use of this methodology.

B2M and *18S* were selected by geNorm stability analysis and used in this thesis as endogenous controls (see Figure 6.1). Similar to what had been done *in vitro* (see Figure 6.6), C_t values of *B2M* and *18S* in RT-qPCR experiments using *ex vivo* samples from 3 SiHa- and 3 FaDu xenografts were plotted separately to check if their expression was independent of the order of quartile in FACS.

In each type of human tumour xenograft, it was hard to find any consistent trends in the change of C_t values across 4 fractions among 3 independent RT-qPCR analyses (Figure 6.10). This indicated that the expression of both *B2M* and *18S* was not associated with what FACS relied on to sort clicked cells into quartiles. Similar to the in vitro expression of both endogenous genes (see Figure 6.6), the transcript abundance of *18S* was notably higher than *B2M* gene in both types of xenografts according to the C_t value. *B2M* and *18S* were also eligible to serve as endogenous control genes in the study of transcript abundance in SiHa and FaDu *ex vivo* samples.

Considerable effort had been devoted in Chapter 5 to optimising the click-based methodology to ensure that the integrity of RNA in cells labelled with fluorophores via CuAAC reactions and sorted by FACS was still acceptable for RT-qPCR analysis. According to the literature cited and discussed in Chapter 5, only RNA extracted from cells processed following the final version of

optimised protocol would be suitable to provide meaningful results from RT-qPCR analysis, i.e. RIN > 5.

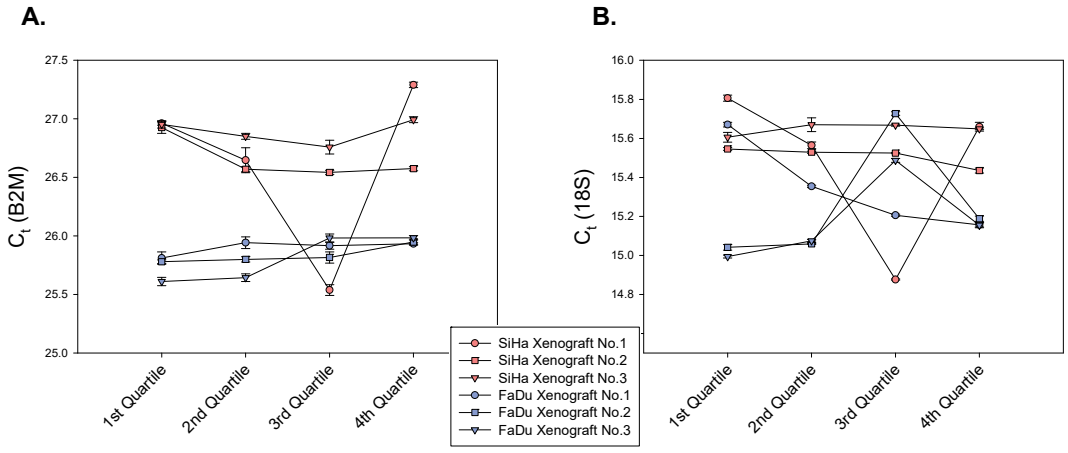

Figure 6.10: *B2M* and *18S* C_t variations in FACS-sorted *ex vivo* fractions over the increments of hypoxia status.

Dissociated SiHa and FaDu tumour xenograft cells were labelled with fluorescence via the CuAAC reactions between cell-incorporated SN33267 derivatives and Super-DIPY following the procedures described in Figure 6.3. According to the fluorescence intensity, cells were sorted into quartiles by FACS. An increased gradient of hypoxic stress in sorted fractions following the order from the 1st to the 4th Quartile. RNA extracted from each quartile was converted into cDNA and systematically used for RT-qPCR to assess the expression of selected endogenous control genes in response to hypoxia. Error bars represent SD of the technical replicates (n = 3). For each cell type, 3 independent experiments (assay 1–3) were performed.

To determine the influence of sample RNA integrity on subsequent RT-qPCR analysis of the hypoxia marker genes, RNA samples were compared from two SiHa xenograft tumours processed using different protocols, i.e. the semi-optimised protocol and the final version of optimised protocol.

After clicking dissociated tumour xenograft cells with BODIPY-FL-azide by the use of semi-optimised protocol (reaction cocktail #2 in Table 2.7; protocol #4 in Figure 2.1), four fractions of clicked cells sorted by FACS gave a rise to a group of RNA samples with RIN scores in the range between 1.0 and 2.1, which did not satisfy the requirement of qPCR to generate meaningful expression data when cDNAs converted from these RNA samples were used as templates (Coulson et al., 2008; Fleige & Pfaffl, 2006; Fleige et al., 2006). From another SiHa xenograft,

RNAs with RIN scores above 6 were extracted from dissociated cells processes with the fully optimised protocol (Super-DIPY; reaction cocktail #7 in Table 2.7; protocol #7 in Figure 2.1).

When these 2 groups of RNAs were converted into cDNAs to use as templates, the data generated by the RT-qPCR experiment using cDNA templates derived from low integrity RNAs showed a trend of elevated expression from the first to the fourth quartile, which was consistent in all 15 tested hypoxia marker genes (Figure 6.11A). According to the raw RT-qPCR data, use of degraded RNA as the starting material was associated with elevated C_t values (not shown). A similar expression pattern of 15 hypoxia marker genes across 4 quartiles was also observed in expression results generated by RT-qPCR using RNA samples above the suggested integrity cut-off (i.e. RIN > 5; Figure 6.11B).

It was quite hard to compare any specific level of mRNA expression fold change in a particular gene. Since the use of different reaction cocktails and different azide-modified fluorophores as well as the different SiHa xenografts, they might potentially contribute to the differences in final expression results. Expression results derived from highly degraded RNA in this particular case still provided meaningful results (Figure 6.11A). Meanwhile, the similar patterns of elevated transcript abundance of hypoxia marker genes in response to the increase in hypoxic stress from the first to the fourth quartile were observed between 2 experiments using different SiHa xenografts, reaction cocktails, levels of intactness in RNA samples. This, to some extent, also indicated the reproducibility of this click chemistry-based methodology.

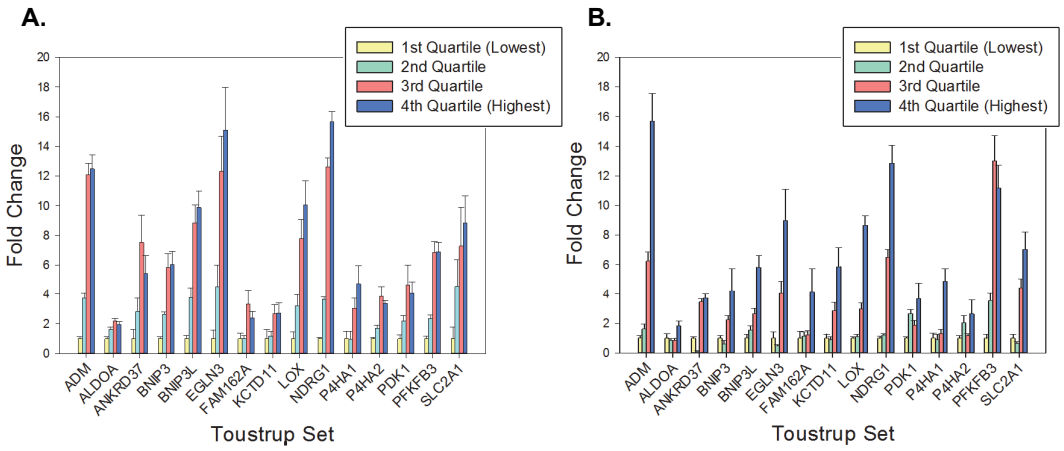

RNA Sample	RIN
1st Quartile	2.1
2nd Quartile	1.1
3rd Quartile	1.0
4th Quartile	1.8

RNA Sample	RIN
1st Quartile	6.1
2nd Quartile	6.8
3rd Quartile	6.4
4th Quartile	6.5

Figure 6.11: Influence of RNA integrity on *ex vivo* expression of hypoxia marker genes assessed by RT-qPCR.

(A) Expression of 15 hypoxia marker genes at their transcription levels evaluated by RT-qPCR using cDNAs converted from RNAs with low RIN scores. Cells were clicked with BODIPY-FL-azide in reaction cocktail #2 (Table 2.7) following protocol #4 (Figure 2.1). FACS-sorted fractions were collected into tubes with 2 mL PBS (pH 7.4). No clean-up step was applied to cDNA prior to PCR. (B) Expression of 15 hypoxia marker genes at their transcription levels evaluated by RT-qPCR using cDNAs converted from RNAs with intermediate RIN scores. Cells were labelled following the procedure described in Figure 6.3. FACS-sorted fractions were collected into tubes with 2 mL TRIzol LS reagent. No clean-up step was applied to cDNA prior to PCR. The dissociated SiHa tumour xenograft cells were labelled with Super-DIPY with the use of Reaction Cocktail #7 (Table 2.7). Errors are SEM (n = 9) from 3 independent experiments.

The click chemistry-based methodology was validated *ex vivo* by use of two types of human tumour xenograft models. Cells dissociated from three SiHa xenografts and labelled with Super-DIPY gave rise to three flow cytometric histograms with similar profiles, indicating the highly similar distributions of hypoxia among the three xenografts (Figure 6.12). All 15 Hypoxia marker genes showed a similar trend in response to elevated hypoxic stress from the first to the fourth quartile. In general, the mRNA transcript expression of 15 Hypoxia marker genes was upregulated with increasing hypoxia in each of the SiHa xenograft tumours (Figure 6.12). However, the exact upregulated level of transcript abundance in particular gene in response to the increase of hypoxic stress over 4 quartiles may be different among 3 SiHa xenografts.

A.

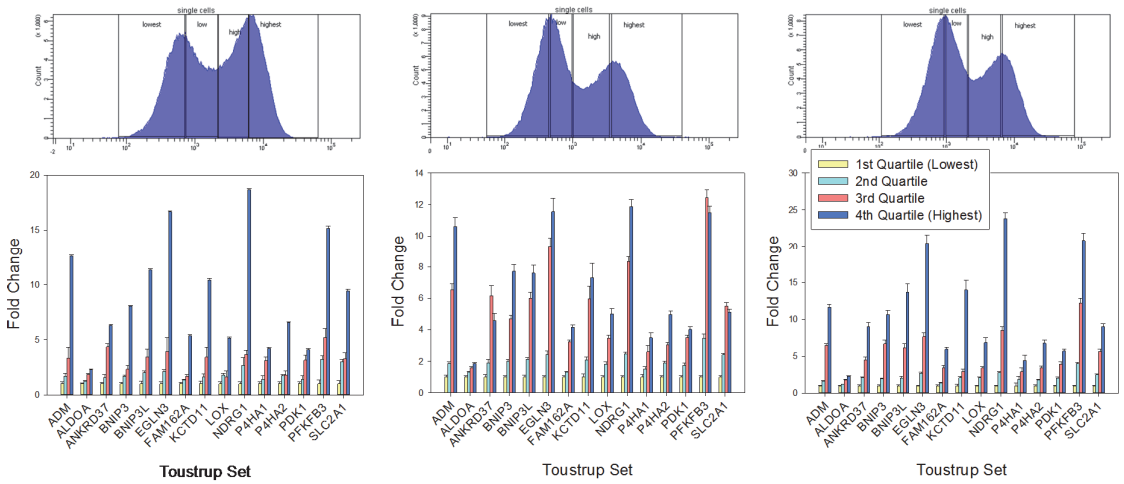

B.

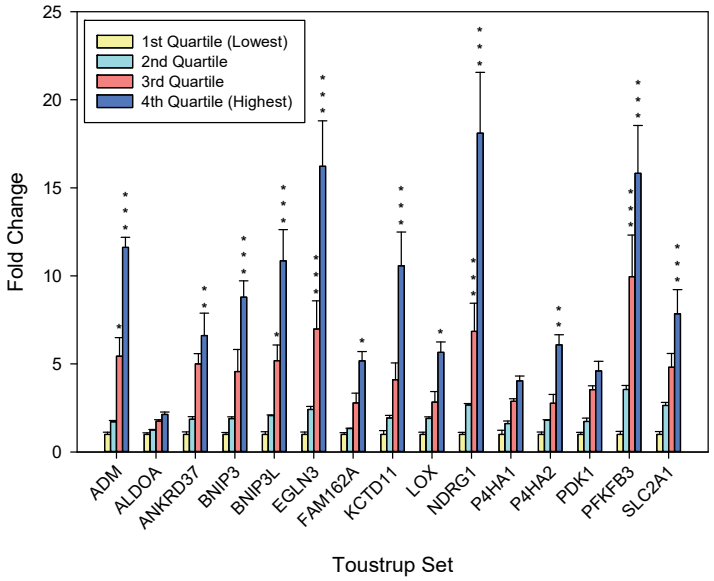

Figure 6.12: *Ex vivo* expression of hypoxia marker genes in SiHa xenografts in response to hypoxic stress.

Dissociated SiHa tumour xenograft cells were clicked with fluorescence via the CuAAC reactions between cell-incorporated SN33267 derivatives and Super-DIPY following the procedures described in Figure 6.3. Cells were sorted into quartiles by FACS according to the fluorescence intensity with the 1st quartile representing the cells with the lowest level of hypoxia status. RNA extracted from each quartile was converted into cDNA and used for RT-qPCR to assess the expression of 15 hypoxia marker genes. (A) *Ex vivo* expression of hypoxia marker genes in 3 xenografts. Each bar graph presents the data generated from an independent experiment. Error bars represent SD of the technical replicates (n = 3). (B) Averaged *ex vivo* expression of hypoxia marker genes. * denotes $P < 0.05$, ** denotes $P < 0.01$, *** denotes $P < 0.001$, compared to the first Quartile as measured by two-way ANOVA with Bonferroni *posthoc* test. Error bars indicate SEM (n = 9) derived from 3 biological replicates.

Flow cytometric histograms generated from dissociated FaDu xenografts were quite different to SiHa xenografts with a relatively long tail of cells with the brightest fluorescent cells in the 4th quartile (Figure 6.13).

Again, all 15 hypoxia marker genes showed a similar trend in response to hypoxic stress. For each particular gene, the level of hypoxia-mediated upregulation was not exactly identical among 3 independent experiments, which could be induced by the genetic heterogeneity among FaDu xenograft tumours. In general, the mRNA transcript expression of 15 hypoxia marker genes was upregulated across the increment of hypoxia in FaDu xenograft tumours (Figure 6.13).

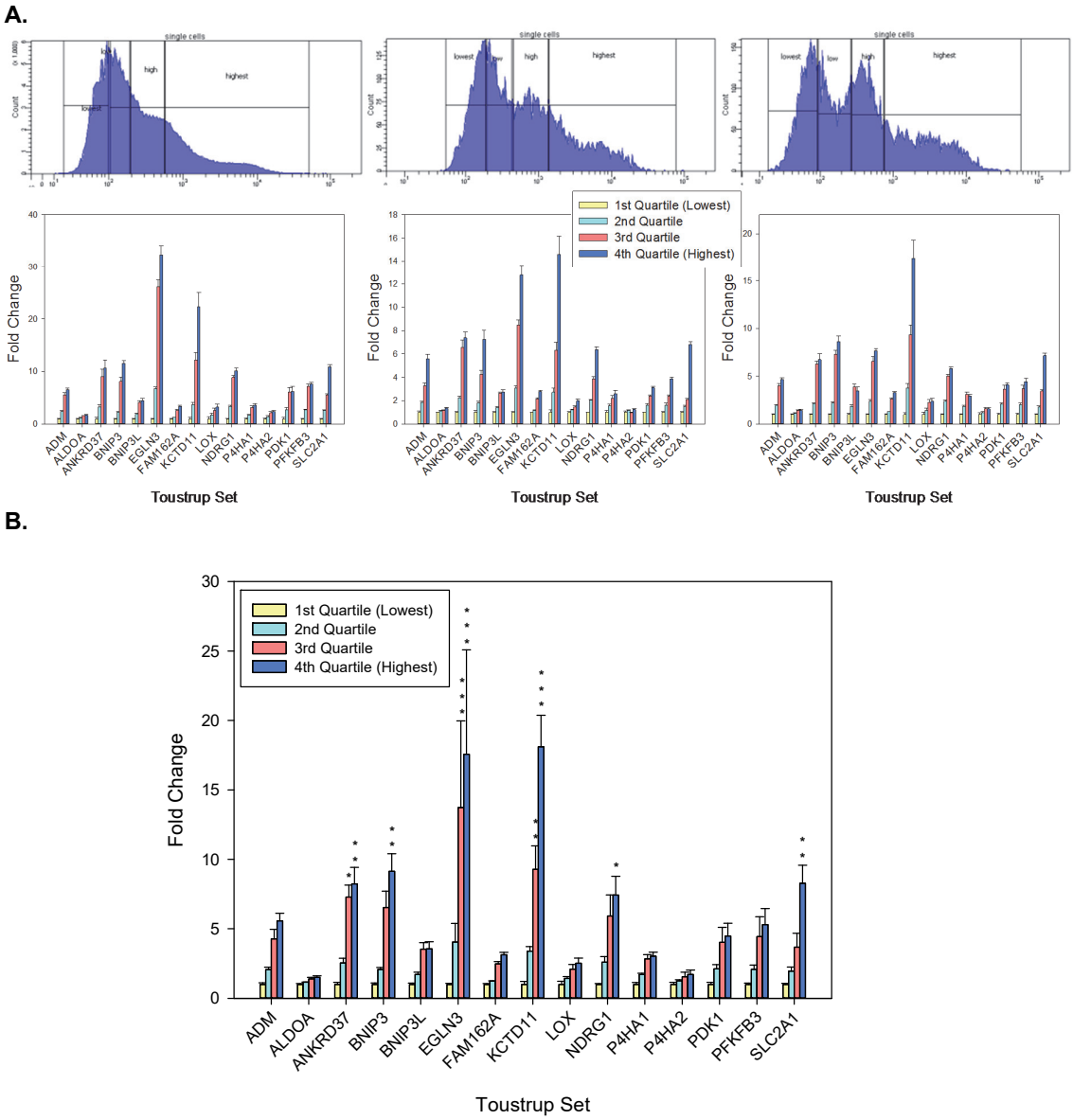

Figure 6.13: *Ex vivo* expression of hypoxia marker genes in FaDu xenografts in response to hypoxic stress.

The dissociated FaDu tumour xenograft cells were labelled with fluorescence via the CuAAC reactions between cell-incorporated SN33267 derivatives and Super-DIPY following the procedures described in Figure 6.3. Cells were sorted into quartiles by FACS according to the fluorescence intensity with the 1st quartile representing the cells with the lowest level of hypoxia status. RNA extracted from each quartile was converted into cDNA and systematically used for RT-qPCR to assess the expression of 15 hypoxia marker genes in response to the increment of hypoxia across 4 Quartiles. (A) *Ex vivo* expression of hypoxia marker genes in 3 xenografts. Each bar graph presents the data generated from an independent experiment. Error bars represent SD of the technical replicates (n = 3). (B) Averaged *ex vivo* expression of hypoxia marker genes. * denotes $P < 0.05$, ** denotes $P < 0.01$, *** denotes $P < 0.001$, compared to the first Quartile as measured by two-way ANOVA with Bonferroni *posthoc* test. Error bars indicate SEM (n = 9) derived from 3 biological replicates.

6.5 Discussion

In normal human tissues, the physiological pO_2 is usually in the range from 20 mm Hg in liver and brain to 70 mm Hg in kidney (Carreau et al., 2011; Vaupel et al., 1989). The upregulation of HIF1 and other adaptive molecular mechanisms are initiated by pO_2 below 10 mm Hg to retain cellular functions (Dhani et al., 2015). Further reduction of the oxygen tension, typically at pO_2 levels below 1 mm Hg, results in irreversible changes in the cellular genome (Bristow, Berlin, & Dal Pra, 2014).

The evaluation of tumour hypoxia can be performed via the more biology-driven approach characterized by the measurement of one or more endogenous genes being expressed under hypoxic conditions in the tumour (Moon et al., 2007; Vordermark & Brown, 2003). Therefore, the generally-deployed approach of measuring the expression of endogenous HIF-dependent biomarkers is able to assess tumour hypoxia at pO_2 levels below 10 mm Hg (Dhani et al., 2015). Whereas techniques to evaluate tumour hypoxia based on the use of exogenous 2-nitroimidazole probes show a distinct oxygen sensing range as these bioreductive probes typically initiate their activations at the oxygen tensions ($pO_2 < 1$ mm Hg) at least one order of magnitude lower (Dhani et al., 2015; Koch, 2002; Tuttle et al., 2007).

The methodology optimised in this thesis uses a cell labelling approach based on the enzymatic formation of cell-entrapped adducts of clickable 2-NI in a hypoxia-dependent manner. Thus, the sensitivity to oxygen of expression of hypoxia-mediated genes is suitable to validate the relative hypoxia status in cell samples sorted by FACS according to the cellular fluorescence intensity labelled via the click-based methodology.

Based on a subset of *in vitro* hypoxia-responsive genes identified using microarray in at least 4 tumour cell lines by Sørensen *et al*., Toustrup and co-workers generated a 15-gene hypoxia gene expression signature by means of comparison with another biomarker of hypoxia in xenograft tumours from human squamous cell carcinoma cell lines, including SiHa and FaDu, and subsequently quantified in head and neck squamous cell carcinoma (HNSCC) clinical samples by using oxygen electrode measurements (Sørensen et al., 2010; Toustrup et al., 2011). During the development phase of this hypoxia gene signature, hypoxia radiotracer ^{18}F-flouroazomycin arabinoside (FAZA) was used as an exogenous tracer to detect and isolate hypoxic and

nonhypoxic tumour tissue in xenograft tumour. Similar to SN33267, FAZA is also a 2-NI compound but with a sugar addition (Reischl et al., 2005). This 15-gene hypoxia signature derived on the basis of *in vitro* responses to hypoxia had demonstrated to serve as an independent prognostic factor with the capability to predict the therapeutic response for hypoxic modification of radiotherapy in a data set of 323 HNSCC patients (Toustrup et al., 2011). This clinically validated hypoxia gene signature was used in this thesis to validate the click chemistry-based methodology.

In this thesis, SiHa and FaDu cells are selected for use as both *in vitro* and *ex vivo* tumour models, in which the click chemistry-based methodology with the optimised protocol was validated. Toustrup *et al.* also started their work from *in vitro* experiments in cultured cells during the establishment of their hypoxia gene signature. Tumour xenografts derived from both SiHa and FaDu cells were employed during the development of this hypoxia gene expression signature by Toustrup *et al.* (Toustrup et al., 2011). Once hypoxia-selectively clicked with fluorophores, cells were sorted into fractions on the basis of cellular fluorescence intensity. The mRNA expression of this clinically validated hypoxia gene expression signature was assessed in these fractions by RT-qPCR, by which the performance of the optimised methodology was validated.

RT-qPCR is the most wildly used method with extremely high sensitivity for gene expression studies in both research and clinical diagnostics (Palmer et al., 2003). The reliability of this method greatly depends on the correct normalisation of the results based on the selection of stable endogenous control genes due to the same reason (Caradec et al., 2010; Zhang et al., 2015). The appropriate selection of an internal standard is crucial in quantitative RNA analyses since accurate normalisation is an absolute prerequisite for reliable results particularly in the study of biological significance mediated by subtle gene expression differences (Vandesompele et al., 2002).

It has been well documented that the expression levels of housekeeping genes vary between tissues and with treatments. The impact of hypoxia on expression of housekeeping genes was evaluated. Large variations of housekeeping gene transcripts were identified under hypoxic conditions dependent on the type of cell line and oxygen tension (Caradec et al., 2010). Thus, the selection of reference genes needs to be critically evaluated prior to any experiment for each situation (Zhong & Simons, 1999).

With the use of samples prepared from the experimental conditions in which hypoxia-mediated transcription effects were being examined, *B2M* and *18S* were selected as endogenous control genes in this thesis according to the geNorm stability analysis.

B2M is a component of MHC class I molecules presenting on all nucleated cells. It has been reported in some previous studies that the expression level of *B2M* RNA was constant in certain tested cell lines with chemically-induced hypoxic conditions (Türkoğlu & Köçkar, 2012). In different hypoxia-related studies, *B2M* sometimes appeared to be one of the least stable endogenous control genes (Türkoğlu & Köçkar, 2012; Schmittgen & Zakrajsek, 2000; Vandesompele et al., 2002).

Ribosomal RNA comprises 85–90% of total cellular RNA. The various rRNA transcripts are less likely to be impacted by the conditions that generally cause changes in the expression of mRNAs due to the employment of a distinct RNA polymerase (Bustin, 2000; Paule & White, 2000). Therefore, rRNAs are useful internal controls. The levels of rRNA transcription between samples, however, are not always representative of the mRNA fraction as they can be influenced by either biological factors or drugs (Spanakis, 1993; Vandesompele et al., 2002). Regarding the use of *18S* as an endogenous control gene, contradictory results have been reported. Fink *et al.* observed that *18S* was unsuitable for normalisation in the tested hypoxic condition (Fink et al., 2008). However, *18S* was also found to be constant and independent of hypoxia types in rat brain tissue and primary cultured neural cells (Yang et al., 2008).

According to previous studies, the expression of *B2M* and *18S* in response to hypoxia was highly dependent on the type of cells and hypoxic conditions used. The transcript abundance of *B2M* and *18S* were confirmed in both *in vitro* and *ex vivo* samples that were prepared under the exactly identical experimental conditions used in the evaluation of 15 hypoxia marker genes to validate the methodology. According to the results generated from 3 independent experiments in each type of model, *B2M* and *18S* were qualified to serve as endogenous controls in this study.

However, it was found consistently in all RT-qPCR experiments in this thesis that the transcript abundance of *18S* was notably higher than not only *B2M* but all hypoxia marker genes involved. The use of rRNAs as internal standards was suggested to be limited when there was a marked

difference in the level of expression between rRNA and target mRNA transcripts. In this case, it was difficult to accurately subtract the baseline value in RT-qPCR data analysis, which definitely resulted in a large normalisation error when used for standardisation (Vandesompele et al., 2002). Thus, an endogenous control should be expressed at roughly the same level as the RNA under study (Bustin, 2000). More recently, it has been suggested that a good reference gene does not have to be expressed at the same level as the gene of interest. The only concern in selecting a reference gene is the stable expression in the selected experimental conditions (D'haene, 2013).

To detect if there was any bias associated with the use of *18S* as a reference gene, all experimental results generated by RT-qPCR were analysed by normalising with either the geometric mean of *B2M* and *18S* data or *B2M* data alone. There was no noticeable difference in final fold change results of the both *in vitro* and *ex vivo* expression in hypoxia gene signature, which was probably caused by the capacity of RT-qPCR to measure gene expression levels with a very wide linear dynamic range of quantification. As a consequence, there is no need that the reference genes have similar expression levels as the genes of interest in this study.

As soon as the endogenous controls were selected by geNorm analysis, mRNA expression of 15 hypoxia marker genes in response to hypoxia was evaluated in cells clicked with azide-modified fluorophores by this CuAAC-mediated approach by RT-qPCR, which was compared with the same hypoxia-induced response in control samples without 2-NI incubation and clicking with azide. According to the results, the application of this click chemistry-based methodology did not influence the alternations in transcript abundance of tested hypoxia markers genes in response to hypoxic stress.

The majority of hypoxia gene expression signatures of the hypoxia response are established by *in vitro* estimates from hypoxic cells (Horsman, Mortensen, Petersen, Busk, & Overgaard, 2012). It has been documented that the *in vitro* transcriptional response to hypoxic stress is not capable to accurately represent the hypoxia phenotype observed in tumours (Marotta et al., 2011; Vordermark & Brown, 2003). Compared with cell line models, human tumour xenograft models more accurately reflect the biological characteristics of human tumours with three-dimensional growth associated with dynamic tumour microenvironment. Hypoxia in tumours also interacts

against an intricate background of additional physiological influences, including low nutrients, abnormal pH, and infiltrating immune cells. As a consequence, the gene *in vivo* expression profile cannot be faithfully represented by the corresponding *in vitro* one due to the presence of these additional parameters (Mayer, Hockel, & Vaupel, 2008).

On the other hand, a study using *ex vivo* samples may identify false-positive signals from pathways less relevant for tumours due to contamination caused by stromal tissue (Harris et al., 2015). In this study, genomic cross-contamination from mouse tissue potentially influenced the reliability of expression results if the primers were designed complementarily to the sequences with less human specificity. Before moving to *ex vivo* experiments, a quality control testing for the species specificity of Taqman gene expression assays was conducted by use of mouse RNA. No PCR product was detected even after 45+ cycles, indicating that the *ex vivo* expression study by using these TaqMan gene expression assays for 18S, B2M, and 15 human hypoxia marker gene sequences was capable of revealing transcript expression in dissociated human tumour xenograft cells without bias as a consequence of the contaminating mouse tissue.

In this thesis, the click chemistry-based methodology was firstly validated *in vitro* by assessing the mRNA expression of a hypoxia signature in 2 cell line models. With the optimised protocol, pre-mixed oxic and hypoxic cells were sorted into 2 fractions according to fluorescence signals clicked with cells via CuAAC. The expression of 15 hypoxia marker genes in 2 FACS-sorted fractions indicated that cells were clicked with azide-modified fluorophores in a hypoxia-selective manner as the consequence of the hypoxia-dependent formation of cellular SN33267 adducts. In other words, this method successfully clicked cells with fluorophores. The cellular fluorescence intensity of clicked cells indicated the relative level of hypoxic stress during the incubation with SN33267, by which cells could be sorted according to relative hypoxic stress.

In this Chapter, pre-mixed oxic and hypoxic SiHa cells were also used to check the effect of additional cDNA clean-up procedure on the final expression of hypoxia marker genes (Figure 6.5). The expression results from the sample with cDNA clean-up procedure were generally consistent with 3 separated experiments used to validate the methodology in SiHa cell line model (Figure 6.7). The same consistency from the expression of 15 hypoxia marker genes was also observed

in 3 independent experiments in FaDu *in vitro* model. There were also some slight differences in the fold change level of particular genes, which could be caused by gate settings during FACS.

After this methodology was validated *in vitro*, cells dissociated from human tumour xenografts were clicked with azide fluorophore and sorted into 4 fractions defined by equivalent cell number according to the density of clicked fluorescence signals in cells. The expression of a same hypoxia gene signature at transcription level was evaluated in each FACS-sorted fraction. The increase in intensity of fluorescence from fluorophores clicked with cells by CuAAC reactions followed the same order with the increase of transcription abundance in all 15 tested hypoxia marker genes. In this way, the click chemistry-based methodology was proven to be capable of clicking fluorophores with cells in a hypoxia-selective manner one the bases of hypoxia-dependent formation of SN33267 cellular adducts.

This validation was also conducted *ex vivo* in both SiHa and FaDu tumour xenografts. Within each model, the fluorescence profile of dissociated tumour cells clicked with azide fluorophores was very similar among three xenografts, indicating the reproducibility of the click chemistry-based method. Between two types of xenograft model, clicked xenograft cells showed different fluorescence profiles. Consequently, the expression pattern of this hypoxia gene signature in response to the elevated hypoxic stress was also quite different between 2 models as the FACS sorting of tumour cells defined by equivalent cell number. In each type of xenograft, three independent experiments demonstrated relative higher level of variations in mRNA expression in comparison to the experiments in corresponding *in vitro* models. Relatively large variations in mRNA expression of the same 15 hypoxia marker genes in response to hypoxia were also found in the study of SiHa and FaDu xenografts performed by Toustrup and co-workers (Toustrup et al., 2011).

The large variation in the expression of particular gene in response to hypoxia in xenograft tumours in comparison to corresponding *in vitro* model can be caused by the heterogeneity between xenograft tumours. Each human tumour xenograft used in this Chapter grew in a different mouse. Heterogeneity between tumour xenografts can be increased due to heterogeneity in the tumour microenvironment. The differences in the biological characteristics between individual mice may

impose different selective pressures on tumours, which is capable of inducing a wider spectrum of variations in gene expression profile between xenografts (Junttila & de Sauvage, 2013).

In vitro experiments in this Chapter used pre-mixed cells consisting of 2 cell populations with 2 distinct levels of hypoxic stress. During cell sorting, the middle area of the FACS profile in which two populations were overlapped each other was relatively easier to be gated out. In dissociated tumour xenograft cells, however, there was no boundary to clearly divide cells into populations according to the level of hypoxia due to the presence of intratumoral hypoxic gradient. As a result, the contamination induced by cells out of the gate was much harder to avoid unless to set two gates far from each other or only compare the first quartile with the fourth one as mentioned previously. Tumour cells in this thesis were sorted into four fractions defined by equivalent cell number. The four fractions interrogated different levels of hypoxic stress in each xenograft. This complexity induced by the intratumoral hypoxic gradient as well as gate setting also contributed to the variations in mRNA expression.

As mentioned in Chapter 5, there was certain cut-off of RNA integrity determined by previous studies. Only the RNA with integrity better than the cut-off was assumed to provide meaningful results in either RT-qPCR or microarray analysis. To achieve the integrity standard of RNA that is often reported in the literature, considerable effort was made to further optimise the methodology on the basis of good hypoxia-dependent cell labelling. Interestingly, the RT-qPCR analysis based on the RNA samples with extremely low RIN scores also successfully demonstrated the *ex vivo* expression of hypoxia marker genes in response to hypoxia in SiHa xenograft tumour. Pfaffl and Fleige indicated that normalisation using validated internal reference was capable of minimising the impact of RNA integrity on relative quantification of gene expression independent of gene or tissue (Fleige & Pfaffl, 2006; Fleige et al., 2006). This might be one of reasons why heavily degraded RNAs gave meaningful expression results in this case. Moreover, an additional cDNA clean-up procedure prior to qPCR was shown to reduce both C_t values without influence final results of hypoxia-regulated expression and diminish variations of technical replicates, which may result from in improvement in polymerase activity and template efficiency during the subsequent PCR amplification.

The click chemistry-based methodology was validated both in vitro and in vivo by use of a clinically validated hypoxia gene signature (Toustrup et al., 2011). The validation results indicate that this methodology could work with either cultured cells or cells dissociated from tumour xenograft and click them with azide fluorophores in a hypoxia-selective manner. The consistent expression results of 15 hypoxia marker genes from cell samples sorted by FACS according to the fluorescence signals clicked in cells by use of this CuAAC-mediated method in multiple independent experiments proved the reproducibility of this methodology. In all 15 hypoxia marker genes tested in both cell line and xenograft models, this methodology demonstrated its capability of actually measuring differences in gene expression, particularly of individual genes.

Chapter 7. The effect of hypoxia on the expression of oxidoreductases

7.1 Introduction

Regions of severe hypoxia generally develop in solid tumours as a consequence of an imbalance between oxygen supply and demand caused by a structurally and functionally defective microvascular system. As a prevalent feature, the involvement of hypoxia in multiple interrelated aspects of tumour progression has been extensively documented (Dewhirst, Cao, & Moeller, 2008; Secomb, Dewhirst, & Pries, 2012; Vaupel & Mayer, 2007; Wilson et al., 2014). To date, the existence of intratumoural hypoxia has been demonstrated in a broad spectrum of cancers (Tatum et al., 2006; Vaupel, 2008). Being a notable characteristic of tumours, hypoxia has long been considered for exploitation as an important target for therapeutic benefit and with the potential to overcome the resistance of hypoxic cells to radiotherapy and chemotherapy (Brown, 2010; Rohwer & Cramer, 2011; Wilson & Hay, 2011; Wilson et al., 2014).

One of the approaches to exploit hypoxia for therapeutic gain is to utilise prodrugs activated to generate active metabolites by endogenous enzymes only under the hypoxic conditions prevailing in tumours (Chen & Hu, 2009; Guise et al., 2014; Wilson & Hay, 2011). Since the first report of nitroaromatic-based prodrugs used to target hypoxic tumour cells, similar strategies have led to the rational development of hypoxia-activated prodrugs (HAP) (Teicher & Sartorelli, 1980). HAPs are typically metabolised by flavoenzyme-catalysed one-electron reduction to a prodrug radical intermediate. Under hypoxic conditions, fragmentation of the initial prodrug radical intermediate or its further reduction results in subsequent formation of cytotoxic species, generally DNA damaging agents. In the presence of oxygen at concentrations in the physiological range, this radical is rapidly back-oxidised to the parent prodrug (Mason & Holtzman, 1975; Wardman & Clarke, 1976). Consequently, the formation of cytotoxins downstream from the prodrug radical is suppressed by this futile redox cycling, by which HAPs exploit hypoxia to achieve selective cytotoxicity (Wardman et al., 1995).

Considering the potential to be enzymatically reduced under hypoxic conditions, the design of HAPs is based on five different chemical moieties including nitro groups, quinones, aromatic and aliphatic N-oxides, and transition metals (Wilson & Hay, 2011; Yeh & Kim, 2015). According to the hypoxic threshold required for the activation, HAPs can be broadly divided into two classes with different PK/PD features (Foehrenbacher, Secomb, Wilson, & Hicks, 2013). Class I HAPs, *e.g.* benzotriazine N-oxides tirapazamine (TPZ) and SN30000, are activated predominantly by 1-electron reduction under relatively mild hypoxia to generate an active metabolite with cytotoxicity restricted to the cell where it is formed without affecting adjacent cells in three-dimensional cell cultures (Shinde et al., 2010; Wilson et al., 2007; Yin, Glaser, & Gates, 2012). On the other hand, Class II HAPs, typified by nitro compounds such as PR-104A and TH-302, are maximally activated by 1-electron reduction only under extreme hypoxia to generate relatively stable effector molecules promoting the ability of active metabolites to diffuse locally from severely hypoxic zones to adjacent regions at intermediate oxygen concentrations, known as the bystander effect (Foehrenbacher et al., 2013; Meng et al., 2012; Patterson et al., 2007; Wilson et al., 2007; Yeh & Kim, 2015).

Among HAPs that have progressed to clinical trial, TPZ is the most extensively studied (Marcu & Olver, 2006). A second generation TPZ analogue, SN30000 (previously known as CEN-209), has been developed with improved extravascular diffusion properties which offer greater hypoxic cell killing activity in multiple human tumour xenografts (Hicks, 2006; Hicks, 2010). The nitroimidazole mustard evofosfamide (TH-302) is currently the most advanced HAP in clinical development and currently in phase III trials for pancreatic adenocarcinoma and soft tissue sarcoma (NCT01746979 and NCT01440088) (Borad et al., 2015; Chawla et al., 2014). Although there are so far still no bioreductive prodrugs approved for clinical use, studies of these candidate compounds have illustrated important concepts and provided valuable knowledge to modulate the ongoing development of the field (Wang et al., 2014; Wilson et al., 2014).

Except limited knowledge of reductases activating nitroCBIs, metabolic activation of other HAPs is predominantly mediated by flavoreductases (Hunter et al., 2014; Wilson et al., 2014). This family of enzymes is capable of catalysing two-electron transfer process between NAD(P)H donors to FAD and FMN cofactors subsequently mediating one-electron transfer to substrates. In this case,

small molecule HAPs serve as substrates and intercept single electrons from the reduced cofactors due to one-electron reduction potentials (E(1)) (Wardman, 2001).

NADPH:cytochrome P450 oxidoreductase (POR) is the best characterised 1-electron HAP oxidoreductase (Guise et al., 2007; Meng et al., 2012; Patterson, Saunders, Chinje, Patterson, & Stratford, 1998; Patterson et al., 1997; Wang et al., 2012). Besides being a useful biomarker of PR-104A activation (Guise et al., 2012), POR is considered one of the major enzymes responsible for HAP activation in an anoxia-specific manner according to studies of *in vitro* models. POR has been reported to metabolise other bioreductive prodrugs in recent or current clinical development for targeting hypoxia, such as TPZ, SN30000, PR-104A, TH-302, 2,5-di(aziridin-1-yl)-3-(hydroxymethyl)-6-methylcyclohexa-2,5-diene-1,4-dione (RH1), 4-[3-(2-nitro-1-imidazolyl)-propylamino]-7-chloroquinoline hydrochloride (NLCQ-1), and apaziquone (Bailey et al., 2001; Begleiter, Leith, Patel, & Hasinoff, 2007; Guise et al., 2012; Meng et al., 2012; Papadopoulou, Ji, Rao, & Bloomer, 2003; Patterson et al., 1998; Su et al., 2013; Wang et al., 2012; Weiss et al., 2011).

Methionine synthase reductase (MTRR), Diflavin oxidoreductase-1 (NDOR1), and nitric oxide synthase (NOS) isoforms also belong to the diflavin reductase family (Wilson & Hay, 2011). The close homology with the reductase domain of POR makes them capable of reducing HAP (Bredt et al., 1991; Leclerc et al., 1998; Paine et al., 2000). It has been demonstrated in HCT116 cells with overexpression of reductase that PR-104A is substrate of MTRR, NDOR1, and inducible nitric oxide synthase (NOS2A) under hypoxia (Guise et al., 2012). In addition, NOS isoforms are capable of activating CB1954 and TPZ under hypoxic conditions (Chandor et al., 2008; Chinje et al., 2003; Garner et al., 1999).

Other flavoproteins capable of one-electron prodrug activation include adrenodoxin reductase (FDXR) and NADH:ferricytochrome b_5 reductases 3 (CYB5R3). Studies of purified recombinant enzyme demonstrated the abilities of FDXR and CYB5R3 for the reductive activation of mitomycin C under anoxic conditions (Hodnick & Sartorelli, 1993; Jiang et al., 2001). CYB5R3 has also demonstrated to be capable of catalysing either one or two electron reduction under both aerobic and hypoxic conditions (Belcourt, Hodnick, Rockwell, & Sartorelli, 1998; Holtz, Rockwell, Tomasz,

& Sartorelli, 2003). Thioredoxin reductase (TXNRD1) shares the same one or two electron reduction feature with CYB5R3 but only catalyses the reduction of nitroaromatic compounds under aerobic conditions (Cenas, Prast, Nivinskas, Sarlauskas, & Arner, 2006). ER-luminal flavoprotein FAD-dependent oxidoreductase domain containing 2 (FOXRED2) has shown to oxygen-sensitively activate HAPs belonging to different chemical classes inside ER lumen and has been identified as a novel nitroCBI-activating flavoprotein (Hunter et al., 2014).

Generally, one-electron reductases are central players in hypoxia-selective bioreduction of prodrugs and appear to have much lower substrate specificity than their two-electron counterparts (Wardman, 2001; Wilson & Hay, 2011).

NAD(P)H:Quinone oxidoreductase (NQO) 1 is the most intensively studied two-electron oxidoreductase (Wilson et al., 2014). The two-electron reduction by NQO1 competes with the metabolism mediated by one-electron reductases and exhibits poor hypoxic selectivity by avoiding the formation of initial oxygen-sensitive prodrug radical (Patterson et al., 1998). NQO1 mediates aerobic activation of quinones, such as mitomycin (MMC), apaziquone, and RH1, by catalysing the facile two-electron reduction, (Beall et al., 1995; Ross et al., 1994; Winski et al., 2001). With dihydronicotinamide riboside (NRH) serving as a cofactor, NQO2 efficiently catalyses the aerobic reduction of CB1954 and RH1 (Knox & Chen, 2004; Yan, Kepa, Siegel, Stratford, & Ross, 2008). Aldo-keto reductase 1C3 (AKR1C3) is another oxygen-insensitive two-electron oxidoreductase. Study of HCT116 cells overexpressing AKR1C3 demonstrated that AKR1C3 mediated aerobic activation of PR-104A, indicating the limited selectivity of PR-104A for hypoxic tissues (Guise et al., 2010; Guise et al., 2007).

Exploiting hypoxia as a therapeutic target for selective activation of prodrugs is particularly attractive due to the prevalence of severe hypoxia in various tumour types (Vaupel & Mayer, 2007). The knowledge and identification of hypoxia, activating reductases, as well as the molecular determinants of sensitivity to the active metabolites are equally critical for the development of HAPs (Wilson et al., 2014). The mechanism by which most HAPs are selectively activated particularly relies on the endogenous expression in tumour cells of oxidoreductases. Thus, assessment of endogenous expression of enzymes responsible for prodrug activation during

hypoxia is essential and urgently required in identifying biomarkers for HAP sensitivity to ultimately benefit the development of HAPs (Hunter et al., 2015).

Recently, the 2-nitromidazole EF5, a hypoxia probe used in the clinic, was shown to be metabolically activated by the same reductases that activate SN30000 with high hypoxic potency and selectivity across multiple human cancer cell lines (Wang et al., 2012). In a subsequent study, a strong correlation between activation of the two compounds in an anoxia-specific manner was detected in various human cancer cell lines (Wang et al., 2014). Thus, EF5 was suggested to function as a dual reporter of both hypoxia and reductase activity in human tumours (Wang et al., 2012). This gives rise to the possibility that the metabolic activation of the hypoxia marker used in this thesis (i.e. SN33267) and the fluorescence signal intensity clicked in cells may be dependent on the expression of reductases.

To understand the relative contribution of oxidoreductases responsible for metabolic activation under hypoxic conditions in human tumours, it is necessary to identify these oxidoreductases and to assess their expression. This is also important in developing integrated clinical biomarker sets to assess HAP sensitivity of individual tumours. Previous studies of these prodrug-activating reductases in response to bioreductive agents under hypoxic conditions have been largely based on *in vitro* experiments using purified enzymes or forced expression to supraphysiological levels (Guise et al., 2014; Hunter et al., 2015; Wang et al., 2014; Wilson et al., 2014). A lack of information on the expression of these reductases in human cancers has become an obstacle to development, optimisation, and future clinical use of HAPs. Moreover, mRNA abundance barely represents protein expression in general, since gene expression is a multistep process and protein expression is predominantly regulated at the level of translation (Schwanhausser et al., 2011). Quantitation of gene expression at the protein level provides increased power to predict its biological functions in comparison to transcript abundance particularly with the involvement of hypoxic stress (Meng et al., 2005; Textoris et al., 2012).

In this Chapter, the mRNA expression of 10 reductases (indicated in bold, Table 7.1), including 3 two-electron reductases, were evaluated in both *in vitro* and *ex vivo* models as a function of hypoxia. Apart from the abundance of transcript, protein expression of *POR* was also investigated

in SiHa xenografts since POR has been indicated to activate EF5 and potentially serve as a predictive biomarker/determinant of HAP sensitivity (Hunter et al., 2015; Wang et al., 2012).

Table 7.1: Candidate enzymes involved in metabolism of bioreductive drugs.

Common Name	Symbol (EC)	Cofactor	1- or 2-e	References
Aldo-keto reductase 1C3	AKR1C3 (1.1.1.188)	NADH, NADPH	2e	(Guise et al., 2010)
NADH:ferricytochrome b_5 reductase 3	CYB5R3 (1.6.2.2)	FAD	1e, 2e	(Barham & Stratford, 1996; Hodnick & Sartorelli, 1993)
Adrenodoxin reductase	FDXR (1.18.1.2)	FAD	1e	(Miskiniene, Dickancaite, Nemeikaite, & Cenas, 1997)
FAD-dependent oxidoreductase domain containing 2	FOXRED2 (N/A)	FAD	1e	(Hunter et al., 2014)
Methionine synthase reductase	MTRR (1.16.1.8)	FAD, FMN	1e	(Olteanu & Banerjee, 2001)
Diflavin oxidoreductase-1	NDOR1 (1.6.2)	FAD, FMN	1e	(Guise et al., 2012)
Nitric oxide synthase, inducible	NOS2A (1.14.13.39)	FAD, FMN, heme	1e	(Chandor et al., 2008)
Nitric oxide synthase, endothelial	NOS3 (1.14.13.39)	FAD, FMN, heme	1e	(Chandor et al., 2008)
NAD(P)H:quinone oxidoreductase 1	NQO1 (1.6.5.2)	FAD	2e	(Seow et al., 2004)
NAD(P)H:quinone oxidoreductase 2	NQO2 (1.10.99.2)	FAD	2e	(Yan et al., 2008)
Thioredoxin reductase	TXNRD1 (1.8.1.9)	FAD	1e, 2e	(Cenas et al., 2006)
Cytochrome (c) P450 reductase	POR (1.6.2.4)	FAD, FMN	1e	(Patterson et al., 1997)

Note: EC, Enzyme Commission. Enzymes assessed in this Chapter are indicated in **bold**.

7.2 Aims

After the CuAAC-mediated hypoxia-dependent methodology for fluorescence-based detection and flow cytometric sorting of hypoxic cells was established, optimised, and validated, it was ready to be applied to the study of expression of genes of interest in tumour xenografts. Intratumoural hypoxia with both spatial and temporal heterogeneity makes interrogation of genes differentially regulated between the oxic and hypoxic compartments in the tumour microenvironment extremely challenging (Vaupel, 2008; Yeh & Kim, 2015). By applying the validated methodology for fluorescence-based detection of hypoxic cells followed by FACS to sort tumour cells in a hypoxia-

dependent manner, the major task of this Chapter was to evaluate the endogenous expression of selected prodrug-activating reductase genes in response to hypoxia status.

The specific objectives were:

- To apply the optimised methodology for fluorescence-based detection and flow cytometric sorting of hypoxic cells *in vitro* and to evaluate the effect of hypoxia in cell cultures on the expression of prodrug-activating reductase genes;
- To apply the optimised methodology for fluorescence-based detection and flow cytometric sorting of hypoxic cells *ex vivo* to sort cells dissociated from tumour xenografts into quartiles according to their cellular hypoxic stress and to evaluate the expression of prodrug-activating reductase genes across the gradient of hypoxia in tumour xenografts;
- To measure the expression of *BNIP3* and *POR* at both transcriptional and translational levels in response to cellular hypoxia status in SiHa xenografts.

7.3 Results

7.3.1 *In vitro* expression of oxidoreductase genes

Hypoxia-induced transcript expression of ten oxidoreductases was investigated in two *in vitro* models. Mixed oxic and hypoxic cells (1:1 ratio) were clicked with Super-DIPY via CuAAC reactions in a hypoxia-selective manner and sorted into 2 fractions due to the distinct levels of labelled fluorescent signals by FACS. RNA samples were extracted from these 2 fractions and the expression of these 10 oxidoreductases in 2 fractions was determined via RT-qPCR. For each cell line, three independent experiments were performed in triplicate.

In SiHa cells, *AKR1C3* transcript demonstrated a consistent pattern of upregulation in response to hypoxic stress among three independent *in vitro* experiments. In two of them, the hypoxia-mediated upregulation in mRNA transcript of *AKR1C3* was statistically significant. In contrast, the transcription of *NQO1* was downregulated in all three *in vitro* experiments as a result of increased cellular hypoxia status. Among them, two experiments showed statistical significance in hypoxia-mediated downregulation at the transcript level of *NQO1*. For *NDOR1*, only one *in vitro* experiment

demonstrated the statistically significant downregulation in response to elevated cellular hypoxic stress. None of the other seven genes showed statistical significance of gene expression changes observed as a consequence of alternations in cellular hypoxic stress. However, mRNA transcripts of *CYB5R3* as well as *NQO2* were consistently upregulated and the transcription of *MTRR* was consistently downregulated with the increase in cellular hypoxic stress among all three isolated *in vitro* experiments (Figure 7.1).

In FaDu cells, *TXNRD1* was the only gene of which mRNA transcripts were consistently upregulated in response to elevated cellular hypoxic stress with statistical significance in all three independent *in vitro* experiments. Even though without statistical significance, *CYB5R3*, *FDXR*, and *NQO2* demonstrated similar trends in hypoxia-mediated upregulation of mRNA transcripts. MTRR and NQO1, on the other hand, showed similar trends in hypoxia-mediated downregulation of mRNA transcripts in three separated experiments (Figure 7.1). In both cell lines *in vitro*, the hypoxia-mediated regulation of oxidoreductases at their transcription levels was not very large. *TXNRD1* in FaDu cells showed the most marked changes in expression of mRNA transcripts as a function of the tested hypoxic conditions, which was only slightly greater than 1.5-fold upregulation.

A.

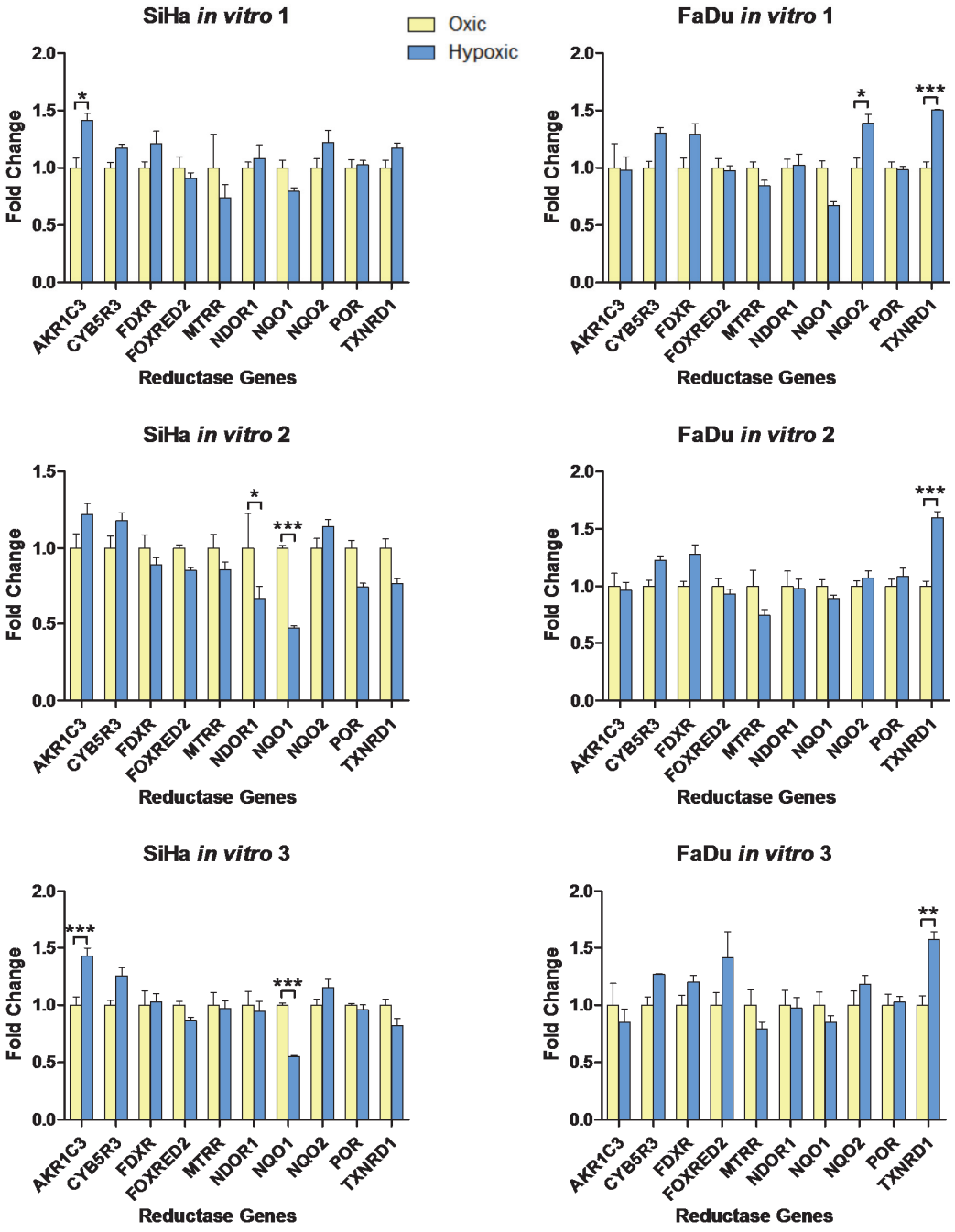

B.

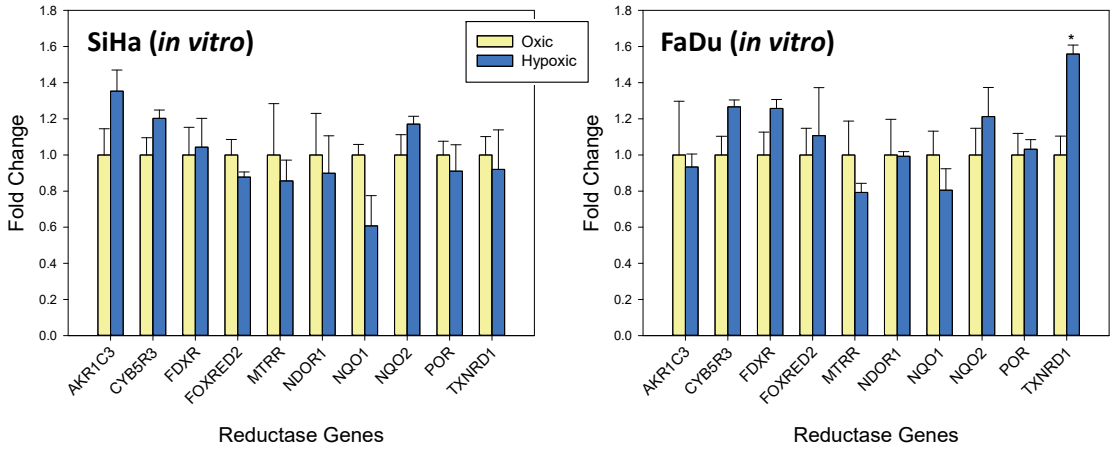

Figure 7.1: The effect of hypoxia on the *in vitro* expression of oxidoreductase genes.

Mixed oxic and hypoxic cells (1:1 ratio) were incubated with SN33267 and labelled with Super-Dipy via the CuAAC reactions following the procedures described in Figure 6.3. According to the fluorescence intensity, mixed cells were sorted into oxic and hypoxic fractions by FACS. RNA extracted from each fraction was converted into cDNA. The hypoxia-induced expression of ten oxidoreductase genes was evaluated by RT-qPCR analysis. (A) *In vitro* expression of oxidoreductase genes in 3 independent experiments. Error bars represent SD of the technical replicates (n = 3). (B) Averaged *in vitro* expression of oxidoreductase genes. Error bars indicate SEM (n = 9) derived from 3 biological replicates. * denotes $P < 0.05$, ** denotes $P < 0.01$, *** denotes $P < 0.001$, compared to oxic sample as measured by two-way ANOVA with Bonferroni *posthoc* test.

7.3.2 *Ex vivo* expression of oxidoreductase genes

Dissociated tumour xenograft cells were clicked with fluorescence via the CuAAC reactions between cell-incorporated SN33267 derivatives and Super-DIPY following the procedures described in Figure 6.3. Cells were sorted into quartiles by FACS according to the labelled fluorescence signals intensity. Expression of these ten oxidoreductases at their transcription levels responded to the increments of cellular hypoxic stress in very similar patterns in each of three SiHa tumour xenografts tested. In comparison to the first quartile consisting of cells with the lowest hypoxic stress, mRNA transcripts of oxidoreductases were upregulated to reach their maximum levels in either the second or the third quartile. The further elevated cellular hypoxic stress in the fourth quartile resulted in a downregulation of oxidoreductase mRNA transcripts. In most of the cases, there were no significant differences in mRNA expression between the first and the fourth quartiles. Among three SiHa tumour xenografts, xenografts 1 and 2 demonstrated very similar hypoxia-mediated expressions of oxidoreductases, which was however quite different to the third xenograft. Although mRNA transcripts of ten oxidoreductases showed very similar trends in response to the increase of cellular hypoxic stress in the SiHa tumour xenograft 3, there were no statistical differences in mRNA expressions of *FDXR*, *MTRR*, *NDOR1*, and *POR* across quartiles. The mRNA expression of *NQO1* was unchanged with the elevated hypoxic stress in the first three quartiles. In the fourth quartile, the further increased cellular hypoxic stress led to a significant downregulation in the *NQO1* transcript (Figure 7.2A).

Among the three investigated FaDu tumour xenografts, *AKR1C3*, *MTRR*, and *NQO1* did not show any statistical differences at their transcription levels in response to the increments of cellular hypoxia status across quartiles. In addition, mRNA transcripts of both *NQO2* and *TXNRD1* were consistently upregulated by the increased level of cellular hypoxic stress following the order quartiles. The mRNA transcripts of *CYB5R3*, *FOXRED2*, and *POR* were upregulated to reach the maximum levels in either the second or the third quartile in response to elevated cellular hypoxic stress. Further increase of hypoxic stress in cells resulted in a negative effect to reduce the transcription of three genes back to their baseline levels. This hypoxia-mediated upregulation followed by a downregulation was also observed in both *FDXR* and *NDOR1* mRNAs in only FaDu

xenograft 1. In the other two xenografts, there were no significant differences in both mRNAs across quartiles (Figure 7.2B).

A.

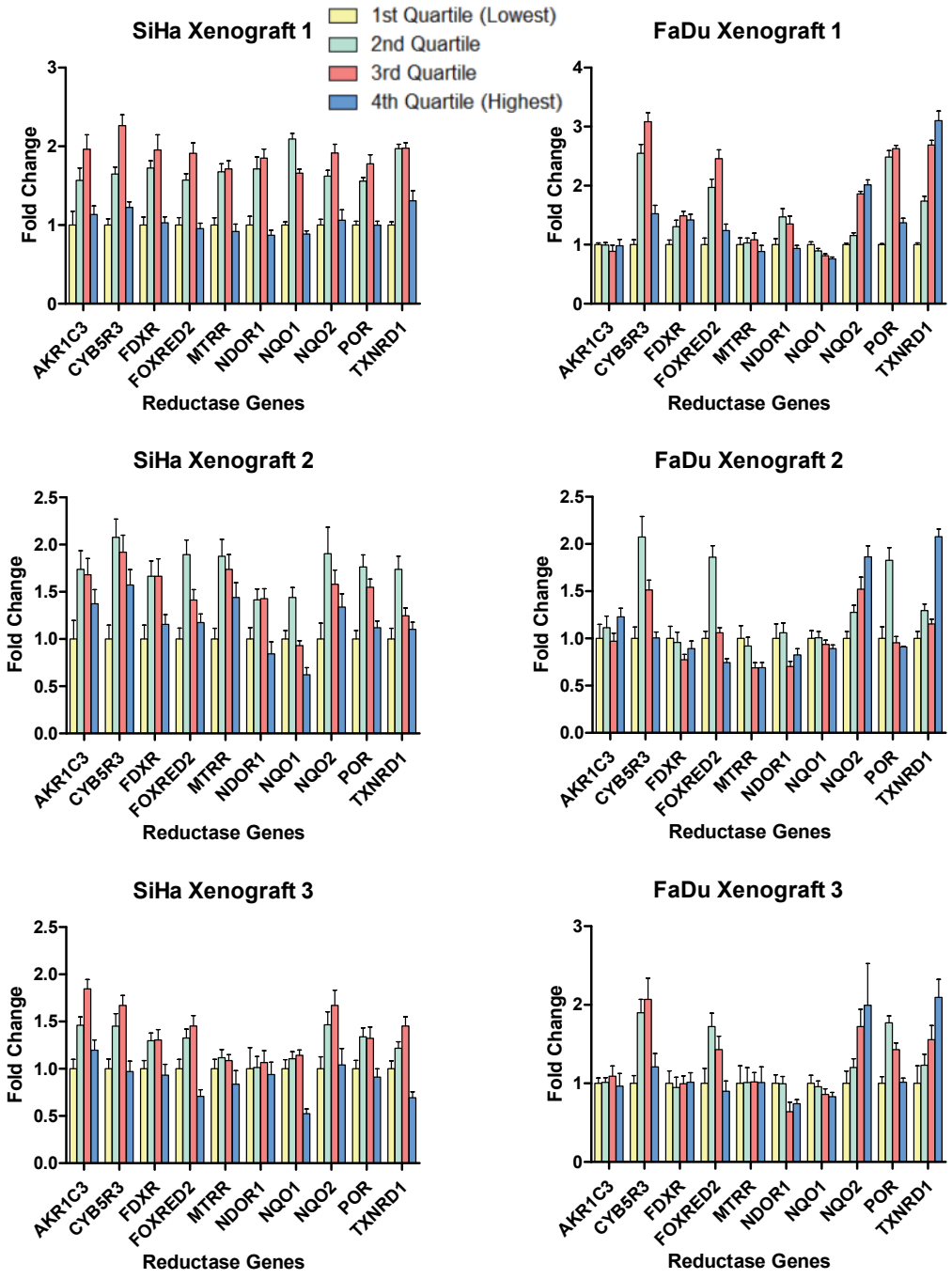
1st Quartile (Lowest)
2nd Quartile
3rd Quartile
4th Quartile (Highest)
SiHa Xenograft 1
FaDu Xenograft 1
SiHa Xenograft 2
FaDu Xenograft 2
SiHa Xenograft 3
FaDu Xenograft 3
Fold Change
Reductase Genes
AKR1C3
CYB5R3
FDXR
FOXRED2
MTRR
NDOR1
NQO1
NQO2
POR
TXNRD1

B.

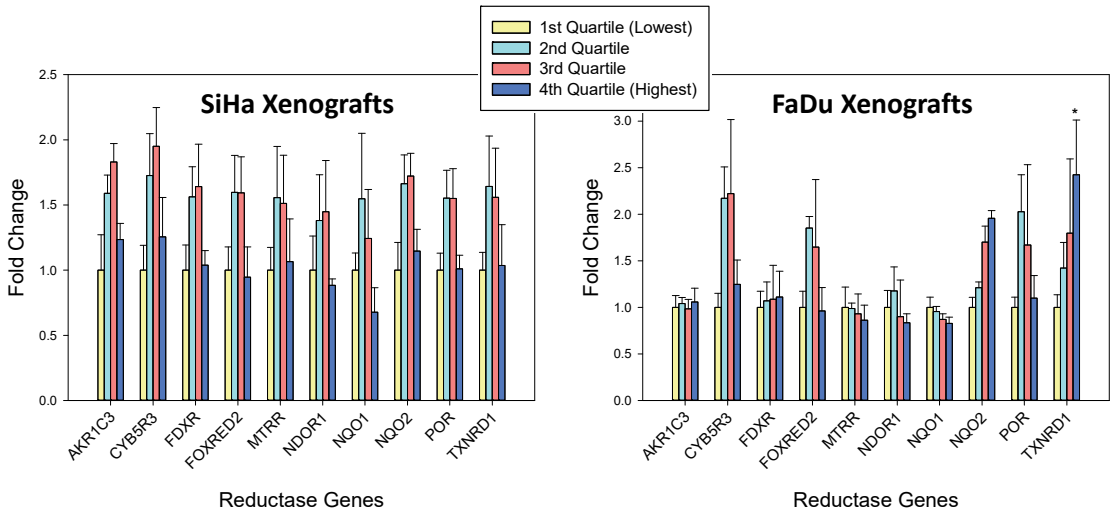

Figure 7.2: The effect of hypoxia on the *ex vivo* expression of oxidoreductase genes.

The dissociated tumour xenograft cells were labelled with fluorescence via the CuAAC reactions between cell-incorporated SN33267 derivatives and Super-DIPY following the procedures described in Figure 6.3. According to the fluorescence intensity, cells were sorted into quartiles by FACS. An increased gradient of hypoxic stress in sorted fractions following the order from the 1st to the 4th Quartile. RNA extracted from each quartile was converted into cDNA and systematically used for RT-qPCR to assess the expression of 10 oxidoreductase genes. (A) *Ex vivo* expression of oxidoreductase genes in 3 xenografts of each xenograft type. Each bar graph presents the data generated from an independent experiment. Error bars represent SD of the technical replicates (n = 3). (B) Averaged *ex vivo* expression of oxidoreductase genes. * denotes $P < 0.05$, compared to the first Quartile as measured by two-way ANOVA with Bonferroni *posthoc* test. Error bars indicate SEM (n = 9) derived from 3 biological replicates.

The mRNA expression of the ten oxidoreductases in SiHa tumour xenograft 3 was also evaluated by the same set of TaqMan® gene expression assays with the use of the same group of mRNA samples in two different qPCR platforms, conventional real-time PCR in 384-well plate and TaqMan® low-density array (TLDA) card. In comparison to the conventional real-time PCR performed in a 384-well plate, the TLDA card generally produced higher C_t values (not shown) with much larger variations among the three technical replicates. According to the mRNA expression results generated by conventional real-time PCR, hypoxia only slightly affected the transcription of the ten target genes in the SiHa tumour xenograft (Figure 7.3).

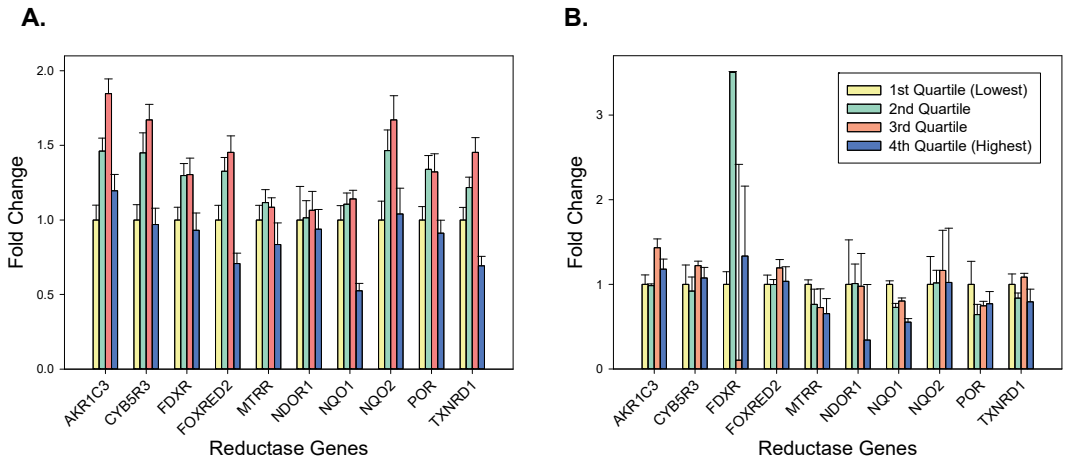

Figure 7.3: Assessment of oxidoreductase gene expression in response to hypoxic stress in different formats of TaqMan® gene expression assays.

(A) TaqMan® gene expression assays in a 384-well plate format. (B) TaqMan® gene expression assays in a low density array format. The cells dissociated from SiHa tumour xenograft 3 were labelled with fluorescence via the CuAAC reactions between cell-incorporated SN33267 derivatives and Super-DIPY following the procedures described in Figure 6.3. According to the fluorescence intensity, cells were sorted into quartiles by FACS. An increased gradient of hypoxic stress in sorted fractions following the order from the 1st to the 4th Quartile. RNA extracted from each quartile was converted into cDNA and systematically used for RT-qPCR to assess the expression of 10 oxidoreductase genes in response to the increment of hypoxia across 4 Quartiles. Each bar graph presents the data generated from an independent experiment. Error bars indicate SEM (n ≥ 6) derived from ≥ 2 independent experiments.

In order to interrogate both the hypoxia marker *BNIP3* and flavoreductase *POR* genes differentially regulated between the oxic and hypoxic compartments in the tumour microenvironment, two additional SiHa tumour xenografts were used. The expression of both genes was assessed at their levels of transcription and translation by RT-qPCR and Western blotting, respectively.

In comparison to the previous three SiHa tumour xenografts (SiHa tumour xenografts 1 to 3; Figure 6.12), both SiHa tumour xenografts 4 and 5 contained fewer cells with relatively high levels of hypoxic stress according to their FACS profiles (Figure 7.4). In both SiHa xenografts 4 and 5, mRNA transcript of *BNIP3* was significantly upregulated with the increments of cellular hypoxic stress across quartiles, which was consistent with the other three tested SiHa tumour xenografts. In contrast, there were no significant differences in *POR* mRNA transcript in response to the gradient of hypoxia status in SiHa tumour xenografts 4 and 5. Even though lack of statistical significance, the trend of *POR* mRNA expression across quartiles illustrated the identical pattern in all five tested SiHa tumour xenografts (Figure 7.4). The mRNA transcript of *POR* was slightly upregulated in the second and the third quartiles comparing to the first one, which was followed by the decrease in *POR* mRNA back to the baseline level in the fourth quartile.

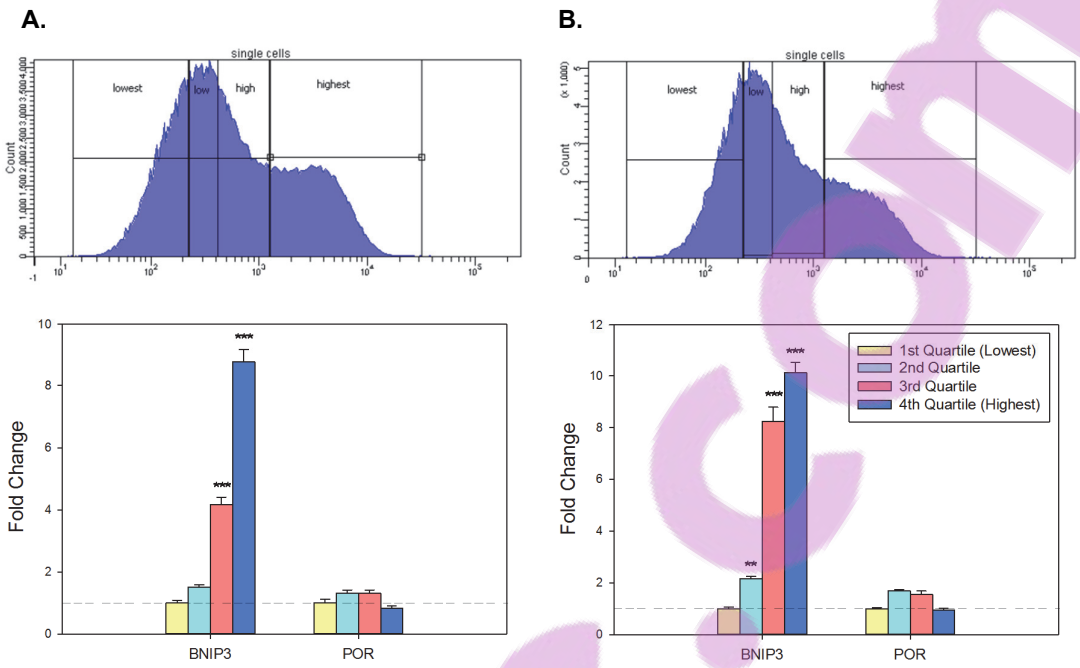

Figure 7.4: *Ex vivo* expression of *BNIP3* and *POR* transcripts in SiHa xenografts in response to hypoxic stress.

(A) FACS profile and mRNA transcript level of *BNIP3* and *POR* in SiHa tumour xenograft 4. (B) FACS profile and mRNA transcript level of BNIP3 and POR in SiHa tumour xenograft 5. The dissociated SiHa tumour xenograft cells were labelled with fluorescence via the CuAAC reactions between cell-incorporated SN33267 derivatives and Super-DIPY following the procedures described in Figure 6.3. According to the fluorescence intensity, cells were sorted into quartiles by FACS. An increased gradient of hypoxic stress in sorted fractions following the order from the 1st to the 4th Quartile. RNA extracted from each quartile was converted into cDNA and systematically used for RT-qPCR to assess the expression of *BNIP3* and *POR* as a function of increasing hypoxia across 4 Quartiles. Each bar graph presents the data generated from an independent experiment. * denotes $P < 0.05$, ** denotes $P < 0.01$, *** denotes $P < 0.001$, compared to the first Quartile as measured by two-way ANOVA with Bonferroni *posthoc* test. Error bars represent SD of the technical replicates (n = 3).

The expression of *BNIP3* and *POR* at their translational levels demonstrated very similar responses to the increments of hypoxic stress between SiHa tumour xenograft 4 and SiHa tumour xenograft 5. With both *BNIP3* and *POR*, the cellular hypoxic status mediated expression followed the same pattern in both transcription and translation levels in the tumour microenvironment. With the increase in cellular hypoxic stress, the protein expression of *BNIP3* was consistently increased, but the expression of *POR* at protein level was elevated initially to reach at a maximum level which was followed by a downregulation with further increase of hypoxic stress (Figure 7.5).

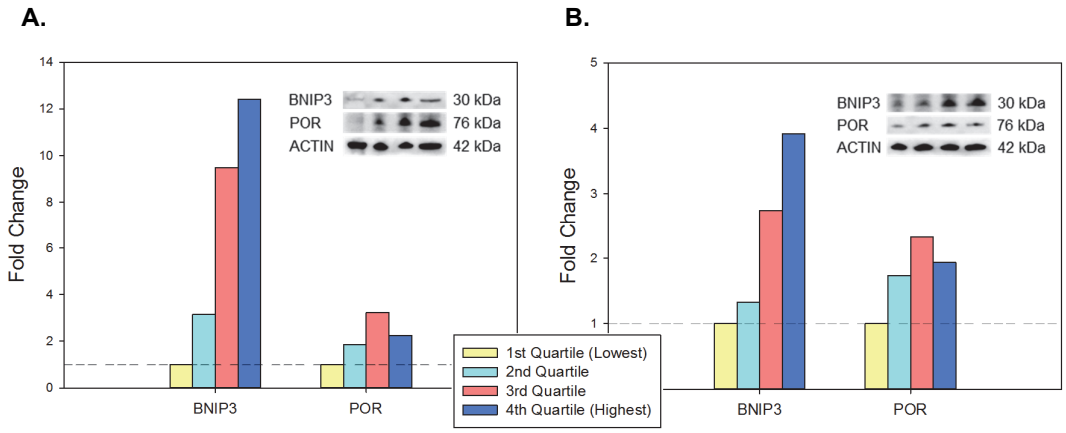

Figure 7.5: *Ex vivo* protein expression of *BNIP3* and *POR* in SiHa xenografts in response to hypoxic stress.

(A) Protein expression level of *BNIP3* and *POR* in SiHa tumour xenograft 4. (B) Protein expression level of BNIP3 and POR in SiHa tumour xenograft 5. The dissociated SiHa tumour xenograft cells were labelled with fluorescence via the CuAAC reactions between cell-incorporated SN33267 derivatives and Super-DIPY following the procedures described in Figure 6.3. According to the fluorescence intensity, cells were sorted into quartiles by FACS. An increased gradient of hypoxic stress in sorted fractions following the order from the 1st to the 4th Quartile. Total protein sample was prepared from each quartile and used for Western blotting to assess the protein expression of *BNIP3* and *POR* transcripts in response to the increment of hypoxia across 4 Quartiles. Each bar graph presents the data generated from an independent experiment.

7.4 Discussion

The majority of human tumours exhibit considerable heterogeneity in many morphological and physiological features between patients with the same clinical classification (Fisher, Pusztai, & Swanton, 2013; Marusyk & Polyak, 2010). When a ubiquitous feature, such as hypoxia, is selected as a target for therapeutic gain, assessment of the presence of the target in individual tumours will largely benefit the clinical outcome (Reddy & Williamson, 2009; Wilson & Hay, 2011). According to the results of this assessment, selection of tumour expressing the intended therapeutic target(s) is crucial for optimising the clinical application of HAPs.

The effect of HAP relies on reductive activation (Hunter et al., 2015). Unfortunately, the genetic determinants of sensitivity to HAPs are still poorly defined (Hunter et al., 2015; Wang et al., 2014; Wilson & Hay, 2011). Intratumoural hypoxia with both spatial and temporal heterogeneity makes the development of predictive biomarkers of HAP response extremely challenging (Vaupel, 2008; Yeh & Kim, 2015).

Enzymes responsible for prodrug activation in hypoxic tumour cells are potentially good candidates of predictive biomarkers for evaluating potential therapeutical responses of individual tumours to HAP (Su et al., 2013). Studies of pro-drug activating reductases are limited to *in vitro* models, which largely relied on the use of purified enzymes or panels of cancer cell lines with forced expression of individual candidates to supraphysiological levels (Hunter et al., 2015; Wilson & Hay, 2011; Wilson et al., 2014). Prior identification of the flavoprotein POR as the key determinant of sensitivity to SN30000 was performed by genome-scale shRNA screens and a high-representation library enriched for oxidoreductases, which was limited to *in vitro* studies in three different cancer cell lines (Hunter et al., 2015).

The CuAAC-mediated hypoxia-dependent cell labelling methodology optimised in this thesis provides an opportunity to interrogate the expression of genes differentially regulated in response to cellular hypoxia status in the tumour microenvironment. By use of this methodology, for the first time, to the best of our knowledge, the expression of oxidoreductases in response to cellular hypoxia stress in human tumour xenograft models was profiled. Quantitative data on expression of reductases along with their spatial relationship to regions of hypoxia are essential for identifying

tumour types and systematically evaluating clinical response of individual tumours to HAP, which is ultimately going to benefit clinic use of HAP in future.

The mRNA expressions of ten reductases, including three two-electron reductases, were evaluated in both *in vitro* and *ex vivo* models. The click chemistry-based methodology established, optimised, and validated in this thesis successfully sorted cells according to hypoxia status, which provided a powerful approach to analyse gene differentially regulated in response to intratumoral hypoxic stress in tumour microenvironment.

The CuAAC-based methodology established and optimised in this thesis employs a clickable 2-NI compound, SN33267, as a probe to initiate the whole CuAAC-mediated cell labelling process by tagging cells in a hypoxia-dependent fashion. The final cell labelling result is actually on the basis of the cellular incorporation of reduced SN33267.

If SN33267 was also metabolically activated by the same reductases as SN30000, the variation in fluorescence intensity between cells labelled by this CuAAC-mediated methodology will reflect differences in reductase activity as well as hypoxia. Therefore, the fluorescence intensity carried by cells may also be used to predict metabolic activation of SN30000. In addition to labelling cells in a hypoxia-dependent manner, this methodology may be an even more appropriate approach for investigating cells that respond differently to HAP.

One-electron oxidoreductases are ubiquitously expressed in tumour cells (Huang et al., 2012). The functional redundancy of oxidoreductases has also been confirmed in hypoxic human tumour cells (Su et al., 2013). Taken together, even though cellular incorporation of SN33267 relies on both hypoxic stress and expression of oxidoreductases in target cells, our methodology is still able to assess the expression of oxidoreductases in response to cellular hypoxia status.

In this Chapter, statistical significances in the expression of 10 oxidoreductase genes were hardly detected between individual FACS-sorted fractions. The same set of *ex vivo* RNA samples were used in both expression analysis of 15 hypoxia marker genes in Chapter 6 and the expression of 10 oxidoreductase genes in this Chapter. The expression patterns of the hypoxia gene signature (Toustrup et al., 2011) in FACS-sorted fractions from each individual xenograft involved in this

thesis indicated that the clickable 2-NI hypoxia marker SN33267 was reduced to form cellular adducts in response to hypoxia status. By the CuAAC-mediated procedure, any differences in the formation of cellular adducts were converted into different levels of intensity of fluorescence signals clicked with cells that FACS sorted based on. Another compound from the same 2-NI family, EF5, was suggested to reflect both hypoxia and reductase activity in human tumours (Wang et al., 2012). So differences in reductase activity could also be shown between FACS-sorted fractions. However, there were no significant changes in mRNA abundance of tested oxidoreductases among sorted quartiles of dissociated xenograft cells. The expression of reductase does not constantly associate with hypoxia status (Naranjo-Suarez et al., 2012). Other reductase(s) characterised by the feature of hypoxia-mediated expression but not identified yet may be present in cells and involved in the reduction of 2-NI as functional redundancy of oxidoreductases in hypoxic human tumour cells (Su et al., 2013). Unlike FaDu xenografts, a similar pattern in the expression of oxidoreductases was shown in SiHa xenografts, which might indicate the existence of an upstream regulating mechanism shared by these oxidoreductases.

In HCT116 cells, forced expression of *POR* significantly increased the anoxic metabolism of EF5, SN30000, and PR-104A (Guise et al., 2012; Wang et al., 2014). According to public domain mRNA expression data, little variation was observed in endogenous transcript abundance of *POR* among different tumour types (Wang et al., 2014). Different to the ubiquitous mRNA expression, investigation of *POR in vivo* protein expression in a set of surgical tumour samples covering 19 common cancers demonstrated heterogeneous patterns of expression (Guise et al., 2012).

However, there is still a lack of evidence for a role of POR in HAP activation in hypoxic tumour cells at endogenous levels of expression (Su et al., 2013). Given that gene expression is often more strongly regulated at the level of translation than transcription under hypoxic stress (Magagnin et al., 2007; Sørensen et al., 2009), the hypoxia-mediated expression of *POR* was investigated at both mRNA and protein levels in human SiHa tumour xenografts. Due to the use of this novel methodology based on click chemistry, the results generated here reflected the expression of *POR* in response to cellular hypoxic stress in the tumour microenvironment. In both xenografts, mRNA expression and protein expression demonstrated a very similar manner of adaptation to the increments of hypoxic stress in tumour. Although lacking statistical significance,

two independent experiments showed consistent trends in hypoxia-mediated *POR* expression both at transcriptional and translational levels.

Bcl-2⁄E1B-19K-interacting protein 3 (BNIP3) is a death-inducing mitochondrial protein belonging to the Bcl-2 protein family (Chen et al., 1997). BNIP3 was initially described as a proapoptotic protein. Subsequent studies indicated that it was implicated in necrotic cell death in various human and animal cell lines (Bruick, 2000). Among the members of Bcl-2 family, *BNIP3* and its homologue, BNIP3-like (*BNIP3L*), are the only members induced in response to hypoxia (Namas et al., 2011). The expression of *BNIP3* can be initiated by a classical HIF-1 element and consensus sequences for the transcription factor nuclear factor-κB (NF-κB) and/or E2F-1 (Guo et al., 2001; Yurkova et al., 2008).

Due to the presence of functional hypoxia-response element (HRE) in promoter, mRNA and protein expression of *BNIP3* are dramatically increased in multiple cell types in response to hypoxia (Bruick, 2000; Guo et al., 2001; Kim et al., 1997; Kothari et al., 2003; Sowter, Ratcliffe, Watson, Greenberg, & Harris, 2001; Zhang et al., 2008). For the same reason, *BNIP3* was selected by Toustrup et al. as a member of hypoxia gene expression classifier (Toustrup et al., 2011). The hypoxia-mediated upregulation in expression of *BNIP3* mRNA transcript was clearly demonstrated in Chapter 5 with two cell lines using *in vitro* and *in vivo* models. The expression of BNIP3 protein in response to the elevated cellular hypoxic stress illustrated the trend as same as its mRNA transcripts in both SiHa and FaDu tumour xenografts.

The FACS-sorted xenograft cells in the fourth quartile suffered the most severe hypoxic stresses in tumours, which could be confirmed by the highest expression of *BNIP3* gene at both transcription and translation levels. Upregulated levels of *BNIP3* expression are correlated with cell death in caspase-independent apoptosis (Li et al., 2013; Velde et al., 2000). In addition, oxygen deprivation can activate autophagic degradation of intracellular macromolecules to initiate type 2 programmed cell death via the activity of 5'-AMP-activated protein kinase (AMPK), independent of HIF-1, BNIP3, and BNIP3L particularly in SiHa cells (Papandreou, Lim, Laderoute, & Denko, 2008). Taken together, it is quite possible that the fourth quartile cells might under such high hypoxic stress that they started to switch off transcription and translation of all genes not

involved in cell survival (Wouters & Koritzinsky, 2008). This may explain the concordant down-regulation of mRNA expression in all ten tested reductase genes in the last quartile of FACS-sorted SiHa xenograft cells.

On the basis of singleplex qPCR assays, TaqMan® low density array (TLDA) is a novel microfluidic-technology format that has provided a convenient platform and utilised extensively in cancer research for quantitative analysis of multiple gene expression (Sanchez-Espiridion et al., 2009; Steg et al., 2006). It is an efficient tool for rapid screening of multiple mRNA transcripts simultaneously especially suitable for large-scale experiments (Keys, Au-Young, & Fekete, 2010). Similar to the conventional real-time PCR performed in optical reaction plates, each well provides a real-time semiquantitative readout in both platforms. As a closed system incorporating validated singleplex PCR methodology, the reagents for each TaqMan® gene expression assay are preallocated to the reaction chambers in TLDA card. Such feature makes the cDNA template need to be added only once, which reduces the amount of handling required and the chance for human error (Devonshire, Elaswarapu, & Foy, 2011; Steg et al., 2006).

Due to all these advantages, TLDA card approach for real-time qPCR detection was selected in the study of oxidoreductases for rapid and simultaneous identification of multiple genes for systematic surveillance and investigation of their transcription. The reaction volume of each TaqMan® gene expression assay is reduced from 20 µL in the conventional platform to 1 µL in TLDA. Consequently, much smaller amount of cDNA templates is needed when real-time PCR is performed in a TLDA card, which may lead to a requirement of higher concentration of cDNA templates by TLDA.

In this study, the performance of TLDA was compared to the conventional real-time qPCR in 384-well plate with the same TaqMan® gene expression assays using an identical set of cDNAs. Despite less amount of cDNA template required, the results of TLDA card showed much higher levels of variability among technically replicates in comparison to real-time qPCR performed on the conventional platform and even missing readouts from several wells. On both platforms, qPCR data analyses were conducted via multi-step comparative C_t method with the concern of propagation of uncertainty. The increased variability was associated with low abundance of the

transcripts in both microfluidic and standard real-time PCR approaches (Devonshire et al., 2011). It has been reported that TLDA cards are about 10-fold less sensitive than conventional real-time PCR assays (Kodani et al., 2011). Moreover, at least 10-fold more concentrated cDNA templates are required by real-time PCR performed in TLDA card compared with the conventional platform (Kodani et al., 2011). This may explain the reason why the same set of cDNA templates well amplified by conventional real-time PCR in 384-well plates but not TLDA card.

In *ex vivo* studies, RNA sample extracted from FACS-sorted fractions following the click procedure was generally limited in the amount. The assessment of gene transcription by TLDA card was predominantly limited by the low RNA quantity obtained from FACS-sorted cell fractions. An additional procedure of pre-amplification prior to mRNA quantification is suggested to add in the protocol when the starting material is limited (Keys et al., 2010; Li et al., 2008; Vermeulen et al., 2009). Depending on the target to be amplified, pre-amplification can be performed either before the step of reverse transcription by linear amplification of RNA or after it by the PCR-based exponential amplification of cDNA (Eberwine et al., 1992; Iscove et al., 2002; Kurn et al., 2005). During development of the hypoxia gene expression signature, which was used to validate the CuAAC-mediated hypoxia-dependent cell labelling methodology in this thesis, pre-amplification of cDNA targets was also employed before real time qPCR to provide a sufficient amount of specific amplicons for quantification of hypoxia-mediated expression by Overgaard *et al.* (Toustrup et al., 2011).

Concerns have been raised as to whether pre-amplification of cDNA templates by exponential amplification introduces bias in expression levels between genes (Ginsberg, 2005). By running with a limited number of cycles (in general less than 14 cycles) with optimised conditions, artefacts induced by nonspecific amplification and target specific bias during the pre-amplification process can be minimised, which has been shown to improve both the accuracy and precision of the transcript quantification using microfluidic arrays (Devonshire et al., 2011; Keys et al., 2010).

Owing to the nature of template amplification by PCR, any difference of less than a single cycle is above the resolution of this method. A 2-fold cut-off was widely cited as a limit to the resolving power of conventional PCR (Lo et al., 2007). In this study, the mRNA expression of

oxidoreductases fluctuated within a 2-fold range in response to cellular hypoxic stress both in *in vitro* cell models and tumour microenvironments. These hypoxia-mediated expressions were confirmed by at least three independent experiments and demonstrated relatively consistent patterns. The inclusion of technical and biological replicates enhanced the confidence dependability of the observations in hypoxia-mediated mRNA expression of oxidoreductases. The reliability of these experimental results was further supported by the findings of Foy *et al.* that both microfluidic and standard real-time PCR platforms were capable to accurately identify a 1.5-fold change in mRNA expression (Devonshire et al., 2011). Additionally, with the larger number of technical replicates involved to achieve greater levels of precision, the resolution of qPCR analysis was even increased to detect a 1.25-fold difference in DNA copy number (Weaver et al., 2010). Meanwhile, the consistent expression results from individual experiments, to some context reflected, the reproducibility of this click chemistry-based methodology.

Enzymes catalysing one-electron transfer to prodrugs play critical roles in hypoxia-selective bioreduction (Wilson & Hay, 2011). The click chemistry-based methodology allows the profiling of their expression corresponding to cellular hypoxia status in individual tumours. In this Chapter, the mRNA expression of ten reductases was evaluated in both *in vitro* and *ex vivo* models. The protein expression of the most extensively studied one-electron oxidoreductase POR, for the first time, was investigated in compartments of human xenograft with different levels of hypoxic stress indicated by the expression of a hypoxia marker gene, *BNIP3*. The consistent results generated from 2 SiHa xenografts further confirmed the capability of this approach in accurately and precisely measuring gene and/or protein expression in tumours. The application of this novel methodology will predominantly benefit the identification of prodrug-activating reductases based on the enzymology of HAP activation at their endogenous levels of expression in human malignancy and assessment of their potential as sensitivity biomarkers. Moreover, studies in variation of their expression in tumours as well as the correlation between hypoxia status and *in vivo* expression of those enzymes can also take great advantage of this novel methodology.

Chapter 8. Future directions and concluding remarks

The general aim of this thesis was to establish and optimise a novel click chemistry-based methodology to fluorescently label cells according to hypoxic stress and use it to study genes differentially expressed in regions with different hypoxic stress in the tumour microenvironment.

The majority of previous studies in hypoxia-mediated gene expression were performed using (2D) cultures of human tumour cell lines under hypoxic conditions. Very limited information on gene expression in the tumour microenvironment was available from few published studies that relied on immune-laser capture microdissection (Marotta et al., 2011). As a major technical breakthrough, click chemistry brought a solution to targeting biomolecules via a single covalent reaction among complementary functional groups with exquisite selectivity comparable with antibody-antigen interaction (Boyce & Bertozzi, 2011).

8.1 Future directions

8.1.1 Further improvement and optimisation of click methodology

8.1.1.1 Deployment of a fluorogenic strategy in designing azide-modified fluorophores

The transfer of electrons between nonplanar parts of a fluorescent molecule results in quenching of fluorescence in a fluorophore. This intramolecular photo-induced electron transfer (PeT) has been adopted to develop a new generation of fluorophores with fluorescence ON−OFF switching mechanism (de Silva et al., 1997).

Different to traditional fluorescent probes exhibiting an “always on” fluorescence, fluorogenic probes have weak or undetectable fluorescence at the wavelength of detection. Their fluorescence is dramatically boosted when these “latent” fluorophores react with molecules of interest (Jewett & Bertozzi, 2011; Nadler & Schultz, 2013; Qi, Han, Chang, & Tung, 2011). The phenomenon of fluorogenic reaction has been utilised as a powerful approach in diverse chemical contexts. The application of fluorogenic probes is associated with an improved signal-to-noise ratio. The fact that these switchable labels/probes are introduced as derivatives without detectable fluorescence eliminates the concern of the non-specific labelling induced by excessive reagents without

compromising sensitivity (Herner et al., 2013; Shieh, Hangauer, & Bertozzi, 2012). It also has been suggested that fluorogenic tags are remarkably suitable for bioorthogonal tagging schemes (Herner et al., 2013).

Although their inherently advantageous features, applying fluorogenic reagents to covalently modify biomatter are rarely reported due to the design difficulties (Shieh et al., 2012). The design of fluorogenic probes for the CuAAC reaction is accomplished by the construction of either an azide or alkyne modified with a pro-fluorophore to provide the quenched state. The reaction between the probe and a cycloaddition partner produces a triazole compound with strong fluorescence (Chauhan, Saha, Lahiri, & Talukdar, 2014).

On the basis of this fluorogenic concept, a panel of azido quenched fluorescent tags has been developed since the first fluorogenic coumarin derivatives-based CuAAC reaction was reported by two groups simultaneously (Sivakumar et al., 2004; Zhou & Fahrni, 2004). In Chapter 4 of this thesis, an additional wash step with 50% ethanol-PBS (pH7.4) was employed following the incubation with reaction cocktail to remove the non-specifically bound fluorescent label resulting in background fluorescence staining and compromising the sensitivity of detection. Fluorogenic probes allow the targets labelled with the clicked triazole congener to show intense fluorescence because of a very large stokes shift and at the same time suppress the background fluorescence when the azide function is intact (Herner et al., 2013). The recruitment of this new strategy may provide an alternative solution to overcome this issue of background staining, resulting in low signal-to-noise ratio without introducing ethanol into the system.

The elimination of the cytotoxic copper catalyst allows a copper-free click reaction to be performed in living cells without obvious toxicity. The potential of SPAAC-mediated hypoxia-dependent cell labelling has been briefly demonstrated in Chapter 4 of this thesis. However, the previous investigation demonstrated that high background fluorescence and unspecific staining generally hampered the application of copper-free click reactions in labelling target proteins in live mammalian cells (Beatty et al., 2010). Subsequent studies of SPAAC-mediated labelling in living cells indicated that the background fluorescence signals were largely attributed to the nonspecific relativity of the cyclooctyne probe toward free thiols or cysteine-containing proteins (Chang et al.,

2010; Hao, Hong, Chen, & Chen, 2011). Introducing the concept of fluorogenic probes into the strain-promoted azide-alkyne cycloaddition may further improve the biocompatibility of click chemistry-based methodology and expand the options of downstream analysis to viable cells (Le Droumaguet, Wang, & Wang, 2010).

8.1.1.2 Assessment of hypoxia-regulated gene expression by high-throughput approaches

In this thesis, evaluation of mRNA abundance was limited in the platform of TLDA primarily due to the restricted amount of cDNA templates. When the starting material is limited, an additional procedure of pre-amplification prior to mRNA quantification is necessary to ensure confidence in results of gene expression (Keys et al., 2010; Li et al., 2008; Vermeulen et al., 2009).

It will be worthwhile to determine if the amplification of cDNA templates can provide a sufficient amount of specific amplicons for quantification of hypoxia-mediated expression of those reductases in TLDA cards. In order to amplify cDNA templates without inducing nonspecific amplification and target-specific bias during the pre-amplification process and bias in expression levels between tested genes, fewer cycles of pre-amplification (10–14) may allow the assessment of transcript quantification in TLDA cards with improved accuracy and precision. (Devonshire et al., 2011; Keys et al., 2010).

Acetonitrile has been suggested by Paredes and Das to use as co-solvent in CuAAC reaction to stabilise copper(I) ions and confer additional benefit in RNA integrity in cells labelled with fluorophores via CuAAC reactions (Paredes & Das, 2012). Recent work has demonstrated that trace amounts of acetonitrile served as pseudo-ligand to stabilise free copper(I) ions in aqueous solution while still facilitating efficient cycloaddition catalysis (Paredes & Das, 2011; Paredes & Das, 2012). In addition, Viljoen and Blackburn proposed an investigation of the relationship between RNA integrity and array quality on the commonly used Affymetrix Gene 1.0 ST array platform, indicating a direct association between RINs and array quality in the majority of cases. According to their study, the widely used RIN cut-off of 7 for microarray analysis can be decreased with the use of appropriate effective array-quality assessment strategy (Viljoen & Blackburn, 2013). With the employment of both acetonitrile as co-solvent during CuAAC reaction and pre-

amplification of the template, the samples prepared from FACS-sorted cells labelled with fluorophores in a hypoxia-dependent manner via this click chemistry-based methodology may be eligible for large-scale expression screening of genes differentially regulated by hypoxia in tumour microenvironment on a microarray platform.

8.1.2 Useful applications and extensions of the click methodology

8.1.2.1 Analysis of hypoxia-regulated protein expression by mass spectrometry-based proteomics

In this thesis, the differences in protein expression of *BNIP3* and *POR* corresponding to the hypoxic stress were assessed by Western blotting in two types of human tumour xenografts. To our knowledge, this was the first time that protein expression of genes differentially regulated among compartments with different hypoxic stress was determined in tumour microenvironment by use of click chemistry-based approach without the requirement of cell fixation and permeabilization. However, the use of immunoassay-based targeted approaches, such as Western blotting or enzyme-linked immunosorbent assay (ELISA), heavily relies on the availability of high quality antibodies and requires a significant investment in time and resources (Pan et al., 2009; Wilhelm et al., 2014). A universal approach to perform quantitative assays for a wide spectrum of proteins with the capability of multiplexed interrogations in a single measurement will be advantageous.

To date, mass spectrometry (MS)-based proteomics has matured into an attractive technology for the unbiased analysis of protein composition, modifications, as well as dynamics in a systematic way (Walther & Mann, 2010). Using LC-MS/MS for the analysis of complex peptide mixtures is the core of MS-based proteomics (Hunt et al., 1992).

Recently, our group has been devoting efforts to the development of an MS-based absolute quantification strategy of protein expression of pre-defined target proteins, also known as targeted proteomics. This application has been reported for measuring concentrations of specific tryptic peptides (PTP) for POR in tumour lysates (Su et al., 2013). This MS-based methodology for targeted protein quantification is potentially compatible with systematic analysis downstream of

the click chemistry-based methodology established in this thesis to evaluate hypoxia-regulated expression of proteins of interest in tumour microenvironment.

8.1.2.2 Study of DNA methylation in the tumour microenvironment

Tumour cell adaptations to hypoxia are driven by both genetic and epigenetic alternations. Both of them have significant downstream effects physiologically in the transition from normal to cancerous tissue and in the progression of solid tumours (Ramachandran, Ient, Gottgens, Krieg, & Hammond, 2015).

Through changes in DNA methylation at promoter regions and satellite repeats, histone modifications, and micro-RNAs, hypoxia-mediated epigenetic modifications result in transcriptional changes and chromosomal instability as the consequence of gene amplification and DNA strand breaks at fragile sites alongside disruption of DNA repair in cancer (Coquelle, Toledo, Stern, Bieth, & Debatisse, 1998; Hoshino & Matsubara, 2013; Pal et al., 2010; Xia et al., 2009). The role of hypoxic stress in genome-wide DNA methylation has been indicated in previous *in vitro* studies, postulating a mechanism for the global hypomethylation and consequently elevated genomic instability and aneuploidy in response to chronic hypoxia during tumourigenesis (Pal et al., 2010; Shahrzad, Bertrand, Minhas, & Coomber, 2007).

Besides genetic events, hypoxia-mediated epigenetic modifications have also demonstrated potential in the development of new tumour biomarkers in diagnosis as well as prognosis and treatment strategies (Thirlwell, Schulz, Dibra, & Beck, 2011). The click chemistry-based methodology established in this thesis makes the investigation of DNA methylation in response to hypoxic stress in real tumour microenvironment possible, which will definitely extend our understanding of hypoxia-mediated effects on the epigenome and considerably contribute to the identification of novel clinical biomarkers and therapeutic targets.

8.2 Concluding remarks

The work for this thesis began by optimising the click chemistry-based methodology to label cells with fluorescence signals via CuAAC reactions in a hypoxia-dependent manner. When both high

level of hypoxia-specificity in cell labelling and minimum CuAAC-induced interference with RNA integrity had been achieved simultaneously, the methodology was validated by assessment of mRNA expression of a clinically-validated hypoxia gene expression signature (15 hypoxia marker genes) in cell fractions sorted by FACS according to the labelled fluorescence intensity representing relative level of cellular hypoxic stress (Toustrup et al., 2011). Finally, the methodology was used to investigate the transcript abundance of ten reductases genes in response to hypoxic stress in cell cultures and human tumour xenografts of two human cancer cell lines. The hypoxia-mediated *ex vivo* expression of *BNIP3* and *POR* was evaluated both at transcriptional and translational levels. This novel click chemistry-based methodology is at least as sensitive but also much faster and more versatile than the established antibody-based hypoxic cell detection techniques. It provides a powerful approach to study a variety of molecular responses to hypoxia in tumour microenvironment. The application of this novel methodology will extend our understanding of the role of hypoxia in tumourigenesis, by which to facilitate the identification of novel clinical biomarkers and therapeutic targets.

REFERENCES

Accurso, A. A., Delaney, M., O'Brien, J., Kim, H., Iovine, P. M., Diaz Diaz, D., & Finn, M. G. (2014). Improved metal-adhesive polymers from copper(I)-catalyzed azide-alkyne cycloaddition. *Chemistry-A European Journal, 20*(34), 10710-10719.

Ackermann, L., & Potukuchi, H. K. (2010). Regioselective syntheses of fully-substituted 1,2,3-triazoles: the CuAAC/C-H bond functionalization nexus. *Organic & Biomolecular Chemistry, 8*(20), 4503-4513.

Adams, G. E., & Cooke, M. S. (1969). Electron-affinic sensitization. I. A structural basis for chemical radiosensitizers in bacteria. *International journal of radiation biology and related studies in physics, chemistry, and medicine, 15*(5), 457-471.

Adams, S. R., Campbell, R. E., Gross, L. A., Martin, B. R., Walkup, G. K., Yao, Y., . . . Tsien, R. Y. (2002). New biarsenical ligands and tetracysteine motifs for protein labeling in vitro and in vivo: synthesis and biological applications. *Journal of the American Chemical Society, 124*(21), 6063-6076.

Agard, N. J., Baskin, J. M., Prescher, J. A., Lo, A., & Bertozzi, C. R. (2006). A comparative study of bioorthogonal reactions with azides. *ACS Chemical Biology [Electronic Resource], 1*(10), 644-648.

Agard, N. J., Prescher, J. A., & Bertozzi, C. R. (2004). A strain-promoted [3 + 2] azide−alkyne cycloaddition for covalent modification of biomolecules in living systems. *Journal of the American Chemical Society, 126*(46), 15046-15047.

Ahn, G. O., & Brown, M. (2007). Targeting tumors with hypoxia-activated cytotoxins. *Frontiers in Bioscience, 12*, 3483-3501.

Al-Waili, N. S., Butler, G. J., Beale, J., Hamilton, R. W., Lee, B. Y., & Lucas, P. (2005). Hyperbaric oxygen and malignancies: A potential role in radiotherapy, chemotherapy, tumor surgery and phototherapy. *Medical Science Monitor, 11*(9), RA279-RA289.

Alvarez-Tejado, M., Naranjo-Suárez, S., Jiménez, C., Carrera, A. C., Landázuri, M. O., & Del Peso, L. (2001). Hypoxia induces the activation of the phosphatidylinositol 3-kinase/Akt cell survival pathway in PC12 cells. Protective role in apoptosis. *Journal of Biological Chemistry, 276*(25), 22368-22374.

Amblard, F., Cho, J. H., & Schinazi, R. F. (2009). Cu(I)-catalyzed Huisgen azide−alkyne 1,3-dipolar cycloaddition reaction in nucleoside, nucleotide, and oligonucleotide chemistry. *Chemical Reviews, 109*(9), 4207-4220.

AnaSpec. (2013a). DEAC, SE. In *Reactive fluorescent dyes.* Retrieved Nov 10, 2015, from http://www.anaspec.com/products/product.asp?id=28812&productid=10050

AnaSpec. (2013b). DMACA, SE. In *Reactive fluorescent dyes.* Retrieved Nov 10, 2015, from http://www.anaspec.com/products/product.asp?id=28814&productid=10052

Antica, M., Paradzik, M., Novak, S., Dzebro, S., & Dominis, M. (2010). Gene expression in formalin-fixed paraffin-embedded lymph nodes. *Journal of Immunological Methods, 359*(1–2), 42-46.

Arlen, M., Arlen, P., Coppa, G., Crawford, J., Wang, X., Saric, O., . . . Molmenti, E. (2014). Monoclonal antibodies that target the immunogenic proteins expressed in colorectal cancer. *World Journal of Gastrointestinal Oncology, 6*(6), 170-176.

Arteel, G. E., Thurman, R. G., & Raleigh, J. A. (1998). Reductive metabolism of the hypoxia marker pimonidazole is regulated by oxygen tension independent of the pyridine nucleotide redox state. *European Journal of Biochemistry, 253*(3), 743-750.

Aydoğan Türkoğlu, S., & Köçkar, F. (2012). Expression Of Gapdh, B-Actin And B-2-Microglobulin genes under chemically induced hypoxic conditions In Hep3b And Pc3 cells. *Journal of Applied Biological Sciences, 6*(3), 1-6.

Bacon, A. L., & Harris, A. L. (2004). Hypoxia-inducible factors and hypoxic cell death in tumour physiology. *Annals of Medicine, 36*(7), 530-539.

Baddela, V. S., Baufeld, A., Yenuganti, V. R., Vanselow, J., & Singh, D. (2014). Suitable housekeeping genes for normalization of transcript abundance analysis by real-time RT-PCR in cultured bovine granulosa cells during hypoxia and differential cell plating density. *Reproductive Biology and Endocrinology : RB&E, 12*, 118.

Bae, S. H., Jeong, J. W., Park, J. A., Kim, S. H., Bae, M. K., Choi, S. J., & Kim, K. W. (2004). Sumoylation increases HIF-1α stability and its transcriptional activity. *Biochemical and Biophysical Research Communications, 324*(1), 394-400.

Bailey, S. M., Lewis, A. D., Patterson, L. H., Fisher, G. R., Knox, R. J., & Workman, P. (2001). Involvement of NADPH:cytochrome P450 reductase in the activation of indoloquinone EO9 to free radical and DNA damaging species. *Biochemical Pharmacology, 62*(4), 461-468.

Bar, T., Ståhlberg, A., Muszta, A., & Kubista, M. (2003). Kinetic Outlier Detection (KOD) in real-time PCR. *Nucleic Acids Research, 31*(17), e105-e105.

Barbet, J., Bardies, M., Bourgeois, M., Chatal, J. F., Cherel, M., Davodeau, F., . . . Kraeber-Bodere, F. (2012). Radiolabeled antibodies for cancer imaging and therapy. *Methods in Molecular Biology, 907*, 681-697.

Barham, H. M., & Stratford, I. J. (1996). Enzymology of the reduction of the novel fused pyrazine mono-n-oxide bioreductive drug, RB90740 roles for P450 reductase and cytochrome b5 reductase. *Biochemical Pharmacology, 51*(6), 829-837.

Baskin, J. M., Prescher, J. A., Laughlin, S. T., Agard, N. J., Chang, P. V., Miller, I. A., . . . Bertozzi, C. R. (2007). Copper-free click chemistry for dynamic in vivo imaging. *Proceedings of the National Academy of Sciences of the United States of America, 104*(43), 16793-16797.

Batchelder, R. M., Wilson, W. R., Hay, M. P., & Denny, W. A. (1996). Oxygen dependence of the cytotoxicity of the enediyne anti-tumour antibiotic esperamicin A1. *British Journal of Cancer - Supplement, 27*, S52-56.

Bauer, M., Polzin, S., & Patzelt, D. Quantification of RNA degradation by semi-quantitative duplex and competitive RT-PCR: a possible indicator of the age of bloodstains? *Forensic Science International, 138*(1), 94-103.

Beall, H. D., Murphy, A. M., Siegel, D., Hargreaves, R. H., Butler, J., & Ross, D. (1995). Nicotinamide adenine dinucleotide (phosphate): quinone oxidoreductase (DT-diaphorase) as a target for bioreductive antitumor quinones: quinone cytotoxicity and selectivity in human lung and breast cancer cell lines. *Molecular Pharmacology, 48*(3), 499-504.

Beatty, K. E., Fisk, J. D., Smart, B. P., Lu, Y. Y., Szychowski, J., Hangauer, M. J., . . . Tirrell, D. A. (2010). Live-cell imaging of cellular proteins by a strain-promoted azide–alkyne cycloaddition. *Chembiochem, 11*(15), 2092-2095.

Becer, C. R., Hoogenboom, R., & Schubert, U. S. (2009). Click chemistry beyond metal-catalyzed cycloaddition. *Angewandte Chemie International Edition, 48*(27), 4900-4908.

Begleiter, A., Leith, M. K., Patel, D., & Hasinoff, B. B. (2007). Role of NADPH cytochrome P450 reductase in activation of RH1. *Cancer Chemotherapy & Pharmacology, 60*(5), 713-723.

Belcourt, M. F., Hodnick, W. F., Rockwell, S., & Sartorelli, A. C. (1998). The intracellular location of NADH:cytochromeb 5 reductase modulates the cytotoxicity of the mitomycins to Chinese hamster ovary cells. *Journal of Biological Chemistry, 273*(15), 8875-8881.

Benjamin, L. E., Golijanin, D., Itin, A., Pode, D., & Keshet, E. (1999). Selective ablation of immature blood vessels in established human tumors follows vascular endothelial growth factor withdrawal. *Journal of Clinical Investigation, 103*(2), 159-165.

Berg, R., & Straub, B. F. (2013). Advancements in the mechanistic understanding of the copper-catalyzed azide–alkyne cycloaddition. *Beilstein Journal of Organic Chemistry, 9*, 2715-2750.

Berta, M. A., Mazure, N., Hattab, M., Pouysségur, J., & Brahimi-Horn, M. C. (2007). SUMOylation of hypoxia-inducible factor-1α reduces its transcriptional activity. *Biochemical and Biophysical Research Communications, 360*(3), 646-652.

Bertinato, J., & L'Abbe, M. R. (2004). Maintaining copper homeostasis: regulation of copper-trafficking proteins in response to copper deficiency or overload. *Journal of Nutritional Biochemistry, 15*(6), 316-322.

Besanceney-Webler, C., Jiang, H., Zheng, T., Feng, L., Soriano del Amo, D., Wang, W., . . . Wu, P. (2011). Increasing the efficacy of bioorthogonal click reactions for bioconjugation: A comparative study. *Angewandte Chemie, 123*(35), 8201-8206.

Best, M. D. (2009). Click chemistry and bioorthogonal reactions: unprecedented selectivity in the labeling of biological molecules. *Biochemistry, 48*(28), 6571-6584.

Best, M. D., Rowland, M. M., & Bostic, H. E. (2011). Exploiting bioorthogonal chemistry to elucidate protein–lipid binding interactions and other biological roles of phospholipids. *Accounts of Chemical Research, 44*(9), 686-698.

Bevilacqua, V., King, M., Chaumontet, M., Nothisen, M., Gabillet, S., Buisson, D., . . . Taran, F. (2014). Copper-chelating azides for efficient click conjugation reactions in complex media. *Angewandte Chemie. International Ed. in English, 53*(23), 5872-5876.

Biaglow, J. E., Manevich, Y., Uckun, F., & Held, K. D. (1997). Quantitation of hydroxyl radicals produced by radiation and copper-linked oxidation of ascorbate by 2-deoxy-D-ribose method. *Free Radical Biology & Medicine, 22*(7), 1129-1138.

Biaglow, J. E., Varnes, M. E., Clark, E. P., & Epp, E. R. (1983). The role of thiols in cellular response to radiation and drugs. *Radiation Research, 95*(3), 437-455.

Blavier, L., Lazaryev, A., Dorey, F., Shackleford, G. M., & DeClerck, Y. A. (2006). Matrix metalloproteinases play an active role in Wnt1-induced mammary tumorigenesis. *Cancer Research, 66*(5), 2691-2699.

Bock, V. D., Hiemstra, H., & van Maarseveen, J. H. (2006). Cu(I)-catalyzed alkyne–azide “click” cycloadditions from a mechanistic and synthetic perspective. *European Journal of Organic Chemistry, 2006*(1), 51-68.

Boens, N., Leen, V., & Dehaen, W. (2012). Fluorescent indicators based on BODIPY. *Chemical Society Reviews, 41*(3), 1130-1172.

Borad, M. J., Reddy, S. G., Bahary, N., Uronis, H. E., Sigal, D., Cohn, A. L., . . . Ryan, D. P. (2015). Randomized phase II trial of gemcitabine plus TH-302 versus gemcitabine in patients with advanced pancreatic cancer. *Journal of Clinical Oncology, 33*(13), 1475-1481.

Boyce, M., & Bertozzi, C. R. (2011). Bringing chemistry to life. *Nat Meth, 8*(8), 638-642.

Bredt, D. S., Hwang, P. M., Glatt, C. E., Lowenstein, C., Reed, R. R., & Snyder, S. H. (1991). Cloned and expressed nitric oxide synthase structurally resembles cytochrome P-450 reductase. *Nature, 351*(6329), 714-718.

Breinbauer, R., & Köhn, M. (2003). Azide–alkyne coupling: A powerful reaction for bioconjugate chemistry. *Chembiochem, 4*(11), 1147-1149.

Brewer, G. J. (2010). Risks of copper and iron toxicity during aging in humans. *Chemical Research in Toxicology, 23*(2), 319-326.

Brisco, M. J., & Morley, A. A. (2012). Quantification of RNA integrity and its use for measurement of transcript number. *Nucleic Acids Research, 40*(18), e144.

Bristow, R. G., Berlin, A., & Dal Pra, A. (2014). An arranged marriage for precision medicine: hypoxia and genomic assays in localized prostate cancer radiotherapy. *British Journal of Radiology, 87*(1035), 20130753.

Brizel, D. M., Dodge, R. K., Clough, R. W., & Dewhirst, M. W. (1999). Oxygenation of head and neck cancer: Changes during radiotherapy and impact on treatment outcome. *Radiotherapy and Oncology, 53*(2), 113-117.

Brotherton, W. S., Guha, P. M., Phan, H., Clark, R. J., Shatruk, M., & Zhu, L. (2011). Tridentate complexes of 2,6-bis(4-substituted-1,2,3-triazol-1-ylmethyl)pyridine and its organic azide precursors: an application of the copper(ii) acetate-accelerated azide-alkyne cycloaddition. *Dalton Transactions, 40*(14), 3655-3665.

Brotherton, W. S., Michaels, H. A., Simmons, J. T., Clark, R. J., Dalal, N. S., & Zhu, L. (2009). Apparent copper(II)-accelerated azide−alkyne cycloaddition. *Organic Letters, 11*(21), 4954-4957.

Brown, J. M. (2007). Tumor hypoxia in cancer therapy. *Methods in Enzymology, 435*, 297-321.

Brown, J. M., & Giaccia, A. J. (1998). The unique physiology of solid tumors: opportunities (and problems) for cancer therapy. *Cancer Research, 58*(7), 1408-1416.

Brown, J. M., & Wilson, W. R. (2004). Exploiting tumour hypoxia in cancer treatment. *Nature Reviews. Cancer, 4*(6), 437-447.

Brown, M. Oncology scan—Biology. *International Journal of Radiation Oncology • Biology • Physics, 84*(5), 1045-1047.

Brown, M. (2010). Henry S. Kaplan Distinguished Scientist Award Lecture 2007. The remarkable yin and yang of tumour hypoxia. *International Journal of Radiation Biology, 86*(11), 907-917.

Bruick, R. K. (2000). Expression of the gene encoding the proapoptotic Nip3 protein is induced by hypoxia. *Proceedings of the National Academy of Sciences of the United States of America, 97*(16), 9082-9087.

Buckanovich, R. J., Sasaroli, D., O'Brien-Jenkins, A., Botbyl, J., Conejo-Garcia, J. R., Benencia, F., . . . Coukos, G. (2006). Use of immuno-LCM to identify the in situ expression profile of cellular constituents of the tumor microenvironment. *Cancer Biology & Therapy, 5*(6), 635-642.

Buffa, F. M., Harris, A. L., West, C. M., & Miller, C. J. (2010). Large meta-analysis of multiple cancers reveals a common, compact and highly prognostic hypoxia metagene.[Erratum appears in Br J Cancer. 2010 Sep 7;103(6):929]. *British Journal of Cancer, 102*(2), 428-435.

Bump, E. A., Cerce, B. A., al-Sarraf, R., Pierce, S. M., & Koch, C. J. (1992). Radioprotection of DNA in isolated nuclei by naturally occurring thiols at intermediate oxygen tension. *Radiation Research, 132*(1), 94-104.

Burrows, C. J., & Muller, J. G. (1998). Oxidative nucleobase modifications leading to strand scission. *Chemical Reviews, 98*(3), 1109-1152.

Burtness, B., & Golemis, E. A. (2014). *Molecular determinants of head and neck cancer*: Springer New York.

Busk, M., Horsman, M. R., Jakobsen, S., Keiding, S., van der Kogel, A. J., Bussink, J., & Overgaard, J. (2008). Imaging hypoxia in xenografted and murine tumors with 18F-fluoroazomycin arabinoside: A comparative study involving microPET, autoradiography, Po2-polarography, and fluorescence microscopy. *International Journal of Radiation Oncology Biology Physics, 70*(4), 1202-1212.

Busk, M., Toustrup, K., Sørensen, B. S., Alsner, J., Horsman, M. R., Jakobsen, S., & Overgaard, J. (2011). In vivo identification and specificity assessment of mRNA markers of hypoxia in human and mouse tumors. *BMC Cancer, 11*, 63.

Bustin, S. A. (2000). Absolute quantification of mRNA using real-time reverse transcription polymerase chain reaction assays. *Journal of Molecular Endocrinology, 25*(2), 169-193.

Caradec, J., Sirab, N., Keumeugni, C., Moutereau, S., Chimingqi, M., Matar, C., . . . Loric, S. (2010). 'Desperate house genes': the dramatic example of hypoxia. *British Journal of Cancer, 102*(6), 1037-1043.

Carbia-Nagashima, A., Gerez, J., Perez-Castro, C., Paez-Pereda, M., Silberstein, S., Stalla, G. K., . . . Arzt, E. (2007). RSUME, a small RWD-containing protein, enhances SUMO conjugation and stabilizes HIF-1α during hypoxia. *Cell, 131*(2), 309-323.

Carmeliet, P., & Jain, R. K. (2000). Angiogenesis in cancer and other diseases. *Nature, 407*(6801), 249-257.

Carreau, A., El Hafny-Rahbi, B., Matejuk, A., Grillon, C., & Kieda, C. (2011). Why is the partial oxygen pressure of human tissues a crucial parameter? Small molecules and hypoxia. *Journal of Cellular & Molecular Medicine, 15*(6), 1239-1253.

Casas-Solvas, J. M., Ortiz-Salmerón, E., Fernández, I., García-Fuentes, L., Santoyo-González, F., & Vargas-Berenguel, A. (2009). Ferrocene–β-cyclodextrin conjugates: Synthesis, supramolecular behavior, and use as electrochemical sensors. *Chemistry – A European Journal, 15*(33), 8146-8162.

Casazza, A., Di Conza, G., Wenes, M., Finisguerra, V., Deschoemaeker, S., & Mazzone, M. (2014). Tumor stroma: a complexity dictated by the hypoxic tumor microenvironment. *Oncogene, 33*(14), 1743-1754.

Cenas, N., Prast, S., Nivinskas, H., Sarlauskas, J., & Arner, E. S. (2006). Interactions of nitroaromatic compounds with the mammalian selenoprotein thioredoxin reductase and the relation to induction of apoptosis in human cancer cells. *Journal of Biological Chemistry, 281*(9), 5593-5603.

Chan, T. R., & Fokin, V. V. (2007). Polymer-supported copper(I) catalysts for the experimentally simplified azide–alkyne cycloaddition. *Qsar & Combinatorial Science, 26*(11-12), 1274-1279.

Chan, T. R., Hilgraf, R., Sharpless, K. B., & Fokin, V. V. (2004). Polytriazoles as copper(I)-stabilizing ligands in catalysis. *Organic Letters, 6*(17), 2853-2855.

Chandor, A., Dijols, S., Ramassamy, B., Frapart, Y., Mansuy, D., Stuehr, D., . . . Boucher, J. L. (2008). Metabolic activation of the antitumor drug 5-(Aziridin-1-yl)-2,4-dinitrobenzamide (CB1954) by NO synthases. *Chemical Research in Toxicology, 21*(4), 836-843.

Chang, P. V., Prescher, J. A., Sletten, E. M., Baskin, J. M., Miller, I. A., Agard, N. J., . . . Bertozzi, C. R. (2010). Copper-free click chemistry in living animals. *Proceedings of the National Academy of Sciences of the United States of America, 107*(5), 1821-1826.

Chao, K. S. C., Bosch, W. R., Mutic, S., Lewis, J. S., Dehdashti, F., Mintun, M. A., . . . Welch, M. J. (2001). A novel approach to overcome hypoxic tumor resistance: Cu-ATSM-guided intensity-modulated radiation therapy. *International Journal of Radiation Oncology Biology Physics, 49*(4), 1171-1182.

Chaplin, D. J., Olive, P. L., & Durand, R. E. (1987). Intermittent blood flow in a murine tumor: radiobiological effects. *Cancer Research, 47*(2), 597-601.

Chapman, J. D. (1979). Hypoxic sensitizers — Implications for radiation therapy. *New England Journal of Medicine, 301*(26), 1429-1432.

Chapman, J. D. (1991). Measurement of tumor hypoxia by invasive and non-invasive procedures: a review of recent clinical studies. *Radiotherapy & Oncology, 20 Suppl 1*, 13-19.

Chassaing, S., Kumarraja, M., Sani Souna Sido, A., Pale, P., & Sommer, J. (2007). Click chemistry in Cu(I)-zeolites: The Huisgen [3 + 2]-cycloaddition. *Organic Letters, 9*(5), 883-886.

Chaudary, N., & Hill, R. P. (2007). Hypoxia and metastasis. *Clinical Cancer Research, 13*(7), 1947-1949.

Chauhan, D. P., Saha, T., Lahiri, M., & Talukdar, P. (2014). BODIPY based 'click on' fluorogenic dyes: Application in live cell imaging. *Tetrahedron Letters, 55*(1), 244-247.

Chawla, S. P., Cranmer, L. D., Van Tine, B. A., Reed, D. R., Okuno, S. H., Butrynski, J. E., . . . Ganjoo, K. N. (2014). Phase II study of the safety and antitumor activity of the hypoxia-activated prodrug TH-302 in combination with doxorubicin in patients with advanced soft tissue sarcoma. *Journal of Clinical Oncology, 32*(29), 3299-3306.

Chen, E. A., Souaiaia, T., Herstein, J. S., Evgrafov, O. V., Spitsyna, V. N., Rebolini, D. F., & Knowles, J. A. (2014). Effect of RNA integrity on uniquely mapped reads in RNA-Seq. *BMC Research Notes, 7*, 753.

Chen, G., Ray, R., Dubik, D., Shi, L., Cizeau, J., Bleackley, R. C., . . . Greenberg, A. H. (1997). The E1B 19K/Bcl-2-binding protein Nip3 is a dimeric mitochondrial protein that activates apoptosis. *Journal of Experimental Medicine, 186*(12), 1975-1983.

Chen, Y., & Hu, L. (2009). Design of anticancer prodrugs for reductive activation. *Medicinal Research Reviews, 29*(1), 29-64.

Cheng, J., Kang, X., Zhang, S., & Yeh, E. T. H. (2007). SUMO-specific protease 1 is essential for stabilization of HIF1α during hypoxia. *Cell, 131*(3), 584-595.

Cherk, M. H., Foo, S. S., Poon, A. M. T., Knight, S. R., Murone, C., Papenfuss, A. T., . . . Scott, A. M. (2006). Lack of correlation of hypoxic cell fraction and angiogenesis with glucose metabolic rate in non-small cell lung cancer assessed by 18F- fluoromisonidazole and 18F-FDG PET. *Journal of Nuclear Medicine, 47*(12), 1921-1926.

Chesterman, F. C. (1959). Heterotransplantation of human tumours and tissues: Based on an imperial cancer research fund lecture delivered at the Royal College of Surgeons of England on 10th February 1959. *Annals of The Royal College of Surgeons of England, 25*(1), 39-60.

Chi, J.-T., Wang, Z., Nuyten, D. S. A., Rodriguez, E. H., Schaner, M. E., Salim, A., . . . Brown, P. O. (2006). Gene expression programs in response to hypoxia: cell type specificity and prognostic significance in human cancers. *PLoS Medicine / Public Library of Science, 3*(3), e47.

Chilov, D., Camenisch, G., Kvietikova, I., Ziegler, U., Gassmann, M., & Wenger, R. H. (1999). Induction and nuclear translocation of hypoxia-inducible factor-1 (HIF-1): heterodimerization with ARNT is not necessary for nuclear accumulation of HIF-1alpha. *Journal of Cell Science, 112*(Pt 8), 1203-1212.

Chinje, E. C., Cowen, R. L., Feng, J., Sharma, S. P., Wind, N. S., Harris, A. L., & Stratford, I. J. (2003). Non-nuclear localized human NOSII enhances the bioactivation and toxicity of tirapazamine (SR4233) in vitro. *Molecular Pharmacology, 63*(6), 1248-1255.

Cockman, M. E., Masson, N., Mole, D. R., Jaakkola, P., Chang, G.-W., Clifford, S. C., . . . Maxwell, P. H. (2000). Hypoxia inducible factor-α binding and ubiquitylation by the von Hippel-Lindau tumor suppressor protein. *Journal of Biological Chemistry, 275*(33), 25733-25741.

Comerford, K. M., Wallace, T. J., Karhausen, J., Louis, N. A., Montalto, M. C., & Colgan, S. P. (2002). Hypoxia-inducible factor-1-dependent regulation of the multidrug resistance (MDR1) gene. *Cancer Research, 62*(12), 3387-3394.

Cooper, R. A., Carrington, B. M., Loncaster, J. A., Todd, S. M., Davidson, S. E., Logue, J. P., . . . West, C. M. L. (2000). Tumour oxygenation levels correlate with dynamic contrast-enhanced magnetic resonance imaging parameters in carcinoma of the cervix. *Radiotherapy and Oncology, 57*(1), 53-59.

Coquelle, A., Toledo, F., Stern, S., Bieth, A., & Debatisse, M. (1998). A new role for hypoxia in tumor progression: induction of fragile site triggering genomic rearrangements and formation of complex DMs and HSRs. *Molecular Cell, 2*(2), 259-265.

Coralli, C., Cemazar, M., Kanthou, C., Tozer, G. M., & Dachs, G. U. (2001). Limitations of the reporter green fluorescent protein under simulated tumor conditions. *Cancer Research, 61*(12), 4784-4790.

Coulson, D., Brockbank, S., Quinn, J., Murphy, S., Ravid, R., Irvine, G. B., & Johnston, J. (2008). Identification of valid reference genes for the normalization of RT qPCR gene expression data in human brain tissue. *BMC Molecular Biology, 9*(1), 46.

Cox, M. L., Schray, C. L., Luster, C. N., Stewart, Z. S., Korytko, P. J., KN, M. K., . . . Dunstan, R. W. (2006). Assessment of fixatives, fixation, and tissue processing on morphology and RNA integrity. *Experimental & Molecular Pathology, 80*(2), 183-191.

Cunningham, C. W., Mukhopadhyay, A., Lushington, G. H., Blagg, B. S., Prisinzano, T. E., & Krise, J. P. (2010). Uptake, distribution and diffusivity of reactive fluorophores in cells: implications toward target identification. *Molecular Pharmaceutics, 7*(4), 1301-1310.

D'haene, B. (2013). Four tips for RT-qPCR data normalization using reference genes. In *Knowledge center.* Retrieved from https://www.biogazelle.com/four-tips-rt-qpcr-data-normalization-using-reference-genes

de Cecco, L., Nicolau, M., Giannoccaro, M., Daidone, M. G., Bossi, P., Locati, L., . . . Canevari, S. (2015). Head and neck cancer subtypes with biological and clinical relevance: Meta-analysis of gene-expression data. *Oncotarget, 6*(11), 9627-9642.

de Silva, A. P., Gunaratne, H. Q. N., Gunnlaugsson, T., Huxley, A. J. M., McCoy, C. P., Rademacher, J. T., & Rice, T. E. (1997). Signaling recognition events with fluorescent sensors and switches. *Chemical Reviews, 97*(5), 1515-1566.

Debets, M. F., van der Doelen, C. W., Rutjes, F. P., & van Delft, F. L. (2010). Azide: a unique dipole for metal-free bioorthogonal ligations. *Chembiochem, 11*(9), 1168-1184.

DeForest, C. A., Polizzotti, B. D., & Anseth, K. S. (2009). Sequential click reactions for synthesizing and patterning three-dimensional cell microenvironments. *Nat Mater, 8*(8), 659-664.

Dehdashti, F., Grigsby, P. W., Mintun, M. A., Lewis, J. S., Siegel, B. A., & Welch, M. J. (2003). Assessing tumor hypoxia in cervical cancer by positron emission tomography with 60Cu-ATSM: Relationship to therapeutic response - A preliminary report. *International Journal of Radiation Oncology Biology Physics, 55*(5), 1233-1238.

Dehdashti, F., Mintun, M. A., Lewis, J. S., Bradley, J., Govindan, R., Laforest, R., . . . Siegel, B. A. (2003). In vivo assessment of tumor hypoxia in lung cancer with 60Cu-ATSM. *European Journal of Nuclear Medicine and Molecular Imaging, 30*(6), 844-850.

Denekamp, J., & Stewart, F. A. (1978). Sensitization of mouse tumours using fractionated X-irradiation. *British Journal of Cancer, 37*(SUPPL.3), 259-263.

Denko, N. C., Fontana, L. A., Hudson, K. M., Sutphin, P. D., Raychaudhuri, S., Altman, R., & Giaccia, A. J. (2003). Investigating hypoxic tumor physiology through gene expression patterns. *Oncogene, 22*(37), 5907-5914.

Devaraj, N. K., Miller, G. P., Ebina, W., Kakaradov, B., Collman, J. P., Kool, E. T., & Chidsey, C. E. D. (2005). Chemoselective covalent coupling of oligonucleotide probes to self-assembled monolayers. *Journal of the American Chemical Society, 127*(24), 8600-8601.

Devonshire, A., Elaswarapu, R., & Foy, C. (2011). Applicability of RNA standards for evaluating RT-qPCR assays and platforms. *BMC Genomics, 12*(1), 118.

Dewhirst, M. W., Cao, Y., & Moeller, B. (2008). Cycling hypoxia and free radicals regulate angiogenesis and radiotherapy response. *Nat Rev Cancer, 8*(6), 425-437.

Dhani, N., Fyles, A., Hedley, D., & Milosevic, M. (2015). The clinical significance of hypoxia in human cancers. *Seminars in Nuclear Medicine, 45*(2), 110-121.

Dhani, N., & Milosevic, M. (2012). Targeting tumoral hypoxia: Finding opportunity in complexity. *Future Oncology, 8*(9), 1065-1068.

Diaz, D. D., Rajagopal, K., Strable, E., Schneider, J., & Finn, M. G. (2006). "Click" chemistry in a supramolecular environment: stabilization of organogels by copper(I)-catalyzed azide-alkyne [3 + 2] cycloaddition. *Journal of the American Chemical Society, 128*(18), 6056-6057.

Diez-Gonzalez, S. (2011). Well-defined copper(i) complexes for Click azide-alkyne cycloaddition reactions: one Click beyond. *Catalysis Science & Technology, 1*(2), 166-178.

Dlugokencky, E., & Tans, P. (2015). Trends in atmospheric carbon dioxide. Retrieved November 15, 2015, from www.esrl.noaa.gov/gmd/ccgg/trends/

Dolbier, W. R., Jr., Li, A. R., Koch, C. J., Shiue, C. Y., & Kachur, A. V. (2001). [18F]-EF5, a marker for PET detection of hypoxia: synthesis of precursor and a new fluorination procedure. *Applied Radiation & Isotopes, 54*(1), 73-80.

Drummen, G. P. (2012). Fluorescent probes and fluorescence (microscopy) techniques--illuminating biological and biomedical research. *Molecules, 17*(12), 14067-14090.

Dunn, J. F., O'Hara, J. A., Zaim-Wadghiri, Y., Lei, H., Meyerand, M. E., Grinberg, O. Y., . . . Swartz, H. M. (2002). Changes in oxygenation of intracranial tumors with carbogen: A BOLD MRI and EPR oximetry study. *Journal of Magnetic Resonance Imaging, 16*(5), 511-521.

Eberwine, J., Yeh, H., Miyashiro, K., Cao, Y., Nair, S., Finnell, R., . . . Coleman, P. (1992). Analysis of gene expression in single live neurons. *Proceedings of the National Academy of Sciences of the United States of America, 89*(7), 3010-3014.

Edgar, L. J., Vellanki, R. N., Halupa, A., Hedley, D., Wouters, B. G., & Nitz, M. (2014). Identification of hypoxic cells using an organotellurium tag compatible with mass cytometry. *Angewandte Chemie. International Ed. in English, 53*(43), 11473-11477.

Eisenberg, E., & Levanon, E. Y. (2013). Human housekeeping genes, revisited.[Erratum appears in Trends Genet. 2014 Mar;30(3):119-20]. *Trends in Genetics, 29*(10), 569-574.

Eisold, U., Sellrie, F., Schenk, J., Lenz, C., Stöcklein, W. M., & Kumke, M. (2015). Bright or dark immune complexes of anti-TAMRA antibodies for adapted fluorescence-based bioanalysis. *Analytical and Bioanalytical Chemistry, 407*(12), 3313-3323.

El-Sagheer, A. H., & Brown, T. (2008). Synthesis, serum stability and cell uptake of cyclic and hairpin decoy oligonucleotides for TCF/LEF and GLI transcription factors. *International Journal of Peptide Research and Therapeutics, 14*(4), 367-372.

El-Sagheer, A. H., & Brown, T. (2010a). Click chemistry with DNA. *Chemical Society Reviews, 39*(4), 1388-1405.

El-Sagheer, A. H., & Brown, T. (2010b). New strategy for the synthesis of chemically modified RNA constructs exemplified by hairpin and hammerhead ribozymes. *Proceedings of the National Academy of Sciences, 107*(35), 15329-15334.

El-Sagheer, A. H., Kumar, R., Findlow, S., Werner, J. M., Lane, A. N., & Brown, T. (2008). A very stable cyclic DNA miniduplex with just two base pairs. *Chembiochem, 9*(1), 50-52.

Evans, R. A. (2007). The rise of azide–alkyne 1,3-dipolar 'click' cycloaddition and its application to polymer science and surface modification. *Australian Journal of Chemistry, 60*(6), 384-395.

Evans, S. M., Fraker, D., Hahn, S. M., Gleason, K., Jenkins, W. T., Jenkins, K., . . . Koch, C. J. (2006). EF5 binding and clinical outcome in human soft tissue sarcomas. *International Journal of Radiation Oncology, Biology, Physics, 64*(3), 922-927.

Evans, S. M., Judy, K. D., Dunphy, I., Jenkins, W. T., Nelson, P. T., Collins, R., . . . Koch, C. J. (2004). Comparative measurements of hypoxia in human brain tumors using needle electrodes and EF5 binding. *Cancer Research, 64*(5), 1886-1892.

Evans, S. M., Kachur, A. V., Shiue, C. Y., Hustinx, R., Jenkins, W. T., Shive, G. G., . . . Koch, C. J. (2000). Noninvasive detection of tumor hypoxia using the 2-nitroimidazole [18F]EF1. *Journal of Nuclear Medicine, 41*(2), 327-336.

Fardin, P., Barla, A., Mosci, S., Rosasco, L., Verri, A., & Varesio, L. (2009). The l1-l2 regularization framework unmasks the hypoxia signature hidden in the transcriptome of a set of heterogeneous neuroblastoma cell lines. *BMC Genomics, 10*, 474.

Fardin, P., Barla, A., Mosci, S., Rosasco, L., Verri, A., Versteeg, R., . . . Varesio, L. (2010). A biology-driven approach identifies the hypoxia gene signature as a predictor of the outcome of neuroblastoma patients. *Molecular Cancer, 9*, 185.

Favaro, E., Lord, S., Harris, A., & Buffa, F. (2011). Gene expression and hypoxia in breast cancer. *Genome Medicine, 3*(8), 55.

Fekner, T., Li, X., Lee, M. M., & Chan, M. K. (2009). A pyrrolysine analogue for protein click chemistry. *Angewandte Chemie, 121*(9), 1661-1663.

Fens, M. H. A. M., Storm, G., & Schiffelers, R. M. (2010). Tumor vasculature as target for therapeutic intervention. *Expert Opinion on Investigational Drugs, 19*(11), 1321-1338.

Ferlay, J., Shin, H.-R., Bray, F., Forman, D., Mathers, C., & Parkin, D. M. (2010a). Estimates of worldwide burden of cancer in 2008: GLOBOCAN 2008. *International Journal of Cancer, 127*(12), 2893-2917.

Ferlay, J., Shin, H.-R., Bray, F., Forman, D., Mathers, C., & Parkin, D. M. (2010b). Globocan 2008: Cancer Incidence and Mortality Worldwide: IARC CancerBase No. 10 [Internet]. Retrieved 03/05/2012, from Lyon, France: International Agency for Research on Cancer

Festa, R. A., & Thiele, D. J. (2011). Copper: An essential metal in biology. *Current Biology, 21*(21), R877-883.

Fili, N., & Toseland, C. P. (2014). Fluorescence and labelling: How to choose and what to do. *EXS, 105*, 1-24.

Fink, T., Lund, P., Pilgaard, L., Rasmussen, J., Duroux, M., & Zachar, V. (2008). Instability of standard PCR reference genes in adipose-derived stem cells during propagation, differentiation and hypoxic exposure. *BMC Molecular Biology, 9*(1), 98.

Finn, M. G., & Fokin, V. V. (2010). Click chemistry: Function follows form. *Chemical Society Reviews, 39*(4), 1231-1232.

Fisher, R., Pusztai, L., & Swanton, C. (2013). Cancer heterogeneity: Implications for targeted therapeutics. *British Journal of Cancer, 108*(3), 479-485.

Fleige, S., & Pfaffl, M. W. (2006). RNA integrity and the effect on the real-time qRT-PCR performance. *Molecular Aspects of Medicine, 27*(2-3), 126-139.

Fleige, S., Walf, V., Huch, S., Prgomet, C., Sehm, J., & Pfaffl, M. W. (2006). Comparison of relative mRNA quantification models and the impact of RNA integrity in quantitative real-time RT-PCR. *Biotechnology Letters, 28*(19), 1601-1613.

Foehrenbacher, A., Patel, K., Abbattista, M. R., Guise, C. P., Secomb, T. W., Wilson, W. R., & Hicks, K. O. (2013). The role of bystander effects in the antitumor activity of the hypoxia-activated prodrug PR-104. *Frontiers in Oncology, 3*, 263.

Foehrenbacher, A., Secomb, T. W., Wilson, W. R., & Hicks, K. O. (2013). Design of optimized hypoxia-activated prodrugs using pharmacokinetic/pharmacodynamic modeling. *Frontiers in Oncology, 3*, 314.

Folkman, J. (1971). Tumor angiogenesis: therapeutic implications. *New England Journal of Medicine, 285*(21), 1182-1186.

Folkman, J. (2001). Angiogenesis-dependent diseases. *Seminars in Oncology, 28*(6), 536-542.

Folkman, J. (2003). Fundamental concepts of the angiogenic process. *Current Molecular Medicine, 3*(7), 643-651.

Foo, S. S., Abbott, D. F., Lawrentschuk, N., & Scott, A. M. (2004). Functional imaging of intratumoral hypoxia. *Molecular Imaging & Biology, 6*(5), 291-305.

Franko, A. J., & Chapman, J. D. (1982). Binding of 14C-misonidazole to hypoxic cells in V79 spheroids. *British Journal of Cancer, 45*(5), 694-699.

Fritzsche, M., & Mandenius, C. F. (2010). Fluorescent cell-based sensing approaches for toxicity testing. *Analytical & Bioanalytical Chemistry, 398*(1), 181-191.

Fujibayashi, Y., Taniuchi, H., Yonekura, Y., Ohtani, H., Konishi, J., & Yokoyama, A. (1997). Copper-62-ATSM: A new hypoxia imaging agent with high membrane permeability and low redox potential. *Journal of Nuclear Medicine, 38*(7), 1155-1160.

Fukumura, D., Duda, D. G., Munn, L. L., & Jain, R. K. (2010). Tumor microvasculature and microenvironment: Novel insights through intravital imaging in pre-clinical models. *Microcirculation, 17*(3), 206-225.

Fukumura, D., & Jain, R. K. (2007). Tumor microvasculature and microenvironment: Targets for anti-angiogenesis and normalization. *Microvascular Research, 74*(2-3), 72-84.

Furuya, M., & Yonemitsu, Y. (2008). Cancer neovascularization and proinflammatory microenvironments. *Current Cancer Drug Targets, 8*(4), 253-265.

Furuya, M., Yonemitsu, Y., & Aoki, I. (2009). III. Angiogenesis: Complexity of tumor vasculature and microenvironment. *Current Pharmaceutical Design, 15*(16), 1854-1867.

Garner, A. P., Paine, M. J. I., Rodriguez-Crespo, I., Chinje, E. C., De Montellano, P. O., Stratford, I. J., . . . Wolf, C. R. (1999). Nitric oxide synthases catalyze the activation of redox cycling and bioreductive anticancer agents. *Cancer Research, 59*(8), 1929-1934.

Gartner, Z. J., Grubina, R., Calderone, C. T., & Liu, D. R. (2003). Two enabling architectures for DNA-templated organic synthesis. *Angewandte Chemie International Edition, 42*(12), 1370-1375.

Gatenby, R. A., & Gillies, R. J. (2004). Why do cancers have high aerobic glycolysis? *Nature Reviews, Cancer. 4*(11), 891-899.

Gatenby, R. A., Kessler, H. B., Rosenblum, J. S., Coia, L. R., Moldofsky, P. J., Hartz, W. H., & Broder, G. J. (1988). Oxygen distribution in squamous cell carcinoma metastases and its relationship to outcome of radiation therapy. *International Journal of Radiation Oncology, Biology, Physics, 14*(5), 831-838.

Géci, I., Filichev, V. V., & Pedersen, E. B. (2007). Stabilization of parallel triplexes by twisted intercalating nucleic acids (TINAs) incorporating 1,2,3-triazole units and prepared by microwave-accelerated click chemistry. *Chemistry – A European Journal, 13*(22), 6379-6386.

GenomeMedicine. (2012). Target genes transcriptionally activated by HIF-1α. Retrieved 2013, from http://www.genomemedicine.com/content/figures/gm271-1-l.jpg

Ghazoui, Z., Buffa, F. M., Dunbier, A. K., Anderson, H., Dexter, T., Detre, S., . . . Dowsett, M. (2011). Close and stable relationship between proliferation and a hypoxia metagene in aromatase inhibitor-treated ER-positive breast cancer.[Erratum appears in Clin Cancer Res. 2011 Jul 15;17(14):4915], [Erratum appears in Clin Cancer Res. 2011 May 1;17(9). doi:10.1158/1078-0432.CCR-11-1325]. *Clinical Cancer Research, 17*(9), 3005-3012.

Gierlich, J., Burley, G. A., Gramlich, P. M. E., Hammond, D. M., & Carell, T. (2006). Click chemistry as a reliable method for the high-density postsynthetic functionalization of alkyne-modified DNA. *Organic Letters, 8*(17), 3639-3642.

Gierlich, J., Gutsmiedl, K., Gramlich, P. M. E., Schmidt, A., Burley, G. A., & Carell, T. (2007). Synthesis of highly modified DNA by a combination of PCR with alkyne-bearing triphosphates and click chemistry. *Chemistry-A European Journal, 13*(34), 9486-9494.

Gillespie, J. W., Best, C. J., Bichsel, V. E., Cole, K. A., Greenhut, S. F., Hewitt, S. M., . . . Emmert-Buck, M. R. (2002). Evaluation of non-formalin tissue fixation for molecular profiling studies. *American Journal of Pathology, 160*(2), 449-457.

Gillies, R. J., Schornack, P. A., Secomb, T. W., & Raghunand, N. (1999). Causes and effects of heterogeneous perfusion in tumors. *Neoplasia, 1*(3), 197-207.

Ginsberg, S. D. (2005). RNA amplification strategies for small sample populations. *Methods (Duluth), 37*(3), 229-237.

Goebl, N., Berridge, B., Wroblewski, V. J., & Brown-Augsburger, P. L. (2007). Development of a sensitive and specific in situ hybridization technique for the cellular localization of antisense oligodeoxynucleotide drugs in tissue sections. *Toxicologic Pathology, 35*(4), 541-548.

Golas, P. L., Tsarevsky, N. V., Sumerlin, B. S., & Matyjaszewski, K. (2006). Catalyst performance in “click” coupling reactions of polymers prepared by ATRP: Ligand and metal effects. *Macromolecules, 39*(19), 6451-6457.

Gonçalves, M. S. T. (2009). Fluorescent labeling of biomolecules with organic probes. *Chemical Reviews, 109*(1), 190-212.

Gong, X., Tao, R., & Li, Z. (2006). Quantification of RNA damage by reverse transcription polymerase chain reactions. *Analytical Biochemistry, 357*(1), 58-67.

Graeber, T. G., Osmanian, C., Jacks, T., Housman, D. E., Koch, C. J., Lowe, S. W., & Giaccia, A. J. (1996). Hypoxia-mediated selection of cells with diminished apoptotic potential in solid tumours. *Nature, 379*(6560), 88-91.

Gramlich, P. M. E., Wirges, C. T., Manetto, A., & Carell, T. (2008). Postsynthetic DNA modification through the copper-catalyzed azide–alkyne cycloaddition reaction. *Angewandte Chemie International Edition, 47*(44), 8350-8358.

Grammel, M., & Hang, H. C. (2013). Chemical reporters for biological discovery. *Nature Chemical Biology, 9*(8), 475-484.

Gratzner, H. (1982). Monoclonal antibody to 5-bromo- and 5-iododeoxyuridine: A new reagent for detection of DNA replication. *Science, 218*(4571), 474-475.

Graves, E. E., Maity, A., & Le, Q. T. (2010). The tumor microenvironment in non-small-cell lung cancer. *Seminars in Radiation Oncology, 20*(3), 156-163.

Gray, L. H., Conger, A. D., Ebert, M., Hornsey, S., & Scott, O. C. A. (1953). The concentration of oxygen dissolved in tissues at the time of irradiation as a factor in radiotherapy. *British Journal of Radiology, 26*(312), 638-648.

Green, S. L., & Giaccia, A. J. (1998). Tumor hypoxia and the cell cycle: implications for malignant progression and response to therapy. *The Cancer Journal from Scientific American, 4*(4), 218-223.

Griffin, B. A., Adams, S. R., & Tsien, R. Y. (1998). Specific covalent labeling of recombinant protein molecules inside live cells. *Science, 281*(5374), 269-272.

Griffin, R. J. (1994). The medicinal chemistry of the azido group. *Progress in Medicinal Chemistry, 31*, 121-232.

Grube, S., Gottig, T., Freitag, D., Ewald, C., Kalff, R., & Walter, J. (2015). Selection of suitable reference genes for expression analysis in human glioma using RT-qPCR. *Journal of Neuro-Oncology, 123*(1), 35-42.

Guise, C. P., Abbattista, M. R., Singleton, R. S., Holford, S. D., Connolly, J., Dachs, G. U., . . . Patterson, A. V. (2010). The bioreductive prodrug PR-104A is activated under aerobic conditions by human aldo-keto reductase 1C3. *Cancer Research, 70*(4), 1573-1584.

Guise, C. P., Abbattista, M. R., Tipparaju, S. R., Lambie, N. K., Su, J., Li, D., . . . Patterson, A. V. (2012). Diflavin oxidoreductases activate the bioreductive prodrug PR-104A under hypoxia. *Molecular Pharmacology, 81*(1), 31-40.

Guise, C. P., Mowday, A. M., Ashoorzadeh, A., Yuan, R., Lin, W. H., Wu, D. H., . . . Ding, K. (2014). Bioreductive prodrugs as cancer therapeutics: targeting tumor hypoxia. *Chinese Journal of Cancer, 33*(2), 80-86.

Guise, C. P., Wang, A. T., Theil, A., Bridewell, D. J., Wilson, W. R., & Patterson, A. V. (2007). Identification of human reductases that activate the dinitrobenzamide mustard prodrug PR-104A: A role for NADPH:cytochrome P450 oxidoreductase under hypoxia. *Biochemical Pharmacology, 74*(6), 810-820.

Guo, K., Searfoss, G., Krolikowski, D., Pagnoni, M., Franks, C., Clark, K., . . . Ivashchenko, Y. (2001). Hypoxia induces the expression of the pro-apoptotic gene BNIP3. *Cell Death & Differentiation, 8*(4), 367-376.

Guzy, R. D., Hoyos, B., Robin, E., Chen, H., Liu, L., Mansfield, K. D., . . . Schumacker, P. T. (2005). Mitochondrial complex III is required for hypoxia-induced ROS production and cellular oxygen sensing. *Cell Metabolism, 1*(6), 401-408.

Guzy, R. D., & Schumacker, P. T. (2006). Oxygen sensing by mitochondria at complex III: the paradox of increased reactive oxygen species during hypoxia. *Experimental Physiology, 91*(5), 807-819.

Hanahan, D., & Weinberg, R. A. (2011). Hallmarks of cancer: the next generation. *Cell, 144*(5), 646-674.

Hang, H. C., Yu, C., Kato, D. L., & Bertozzi, C. R. (2003). A metabolic labeling approach toward proteomic analysis of mucin-type O-linked glycosylation. *Proceedings of the National Academy of Sciences of the United States of America, 100*(25), 14846-14851.

Hanna, E., Quick, J., & Libutti, S. K. (2009). The tumour microenvironment: A novel target for cancer therapy. *Oral Diseases, 15*(1), 8-17.

Hanson, S. R., Hsu, T.-L., Weerapana, E., Kishikawa, K., Simon, G. M., Cravatt, B. F., & Wong, C.-H. (2007). Tailored glycoproteomics and glycan site mapping using saccharide-selective bioorthogonal probes. *Journal of the American Chemical Society, 129*(23), 7266-7267.

Hao, Z., Hong, S., Chen, X., & Chen, P. R. (2011). Introducing bioorthogonal functionalities into proteins in living cells. *Accounts of Chemical Research, 44*(9), 742-751.

Harris, B. H. L., Barberis, A., West, C. M. L., & Buffa, F. M. (2015). Gene expression signatures as biomarkers of tumour hypoxia. *Clinical Oncology, 27*(10), 547-560.

Harris, E. D. (2001). Copper homeostasis: The role of cellular transporters. *Nutrition Reviews, 59*(9), 281-285.

Harrison, L. B., Chadha, M., Hill, R. J., Hu, K., & Shasha, D. (2002). Impact of tumor hypoxia and anemia on radiation therapy outcomes. *Oncologist, 7*(6), 492-508.

Hashizume, H., Baluk, P., Morikawa, S., McLean, J. W., Thurston, G., Roberge, S., . . . McDonald, D. M. (2000). Openings between defective endothelial cells explain tumor vessel leakiness. *American Journal of Pathology, 156*(4), 1363-1380.

He, F., Deng, X., Wen, B., Liu, Y., Sun, X., Xing, L., . . . Li, G. C. (2008). Noninvasive molecular imaging of hypoxia in human xenografts: Comparing hypoxia-induced gene expression with endogenous and exogenous hypoxia markers. *Cancer Research, 68*(20), 8597-8606.

Hein, C. D., Liu, X.-M., & Wang, D. (2008). Click chemistry, a powerful tool for pharmaceutical sciences. *Pharmaceutical Research, 25*(10), 2216-2230.

Hein, J. E., & Fokin, V. V. (2010). Copper-catalyzed azide-alkyne cycloaddition (CuAAC) and beyond: new reactivity of copper(I) acetylides. *Chemical Society Reviews, 39*(4), 1302-1315.

Hein, J. E., Krasnova, L. B., Iwasaki, M., & Fokin, V. V. (2011). Cu-catalyzed azide-alkyne cycloaddition: Preparation of tris((1-benzyl-1H-1,2,3-triazolyl)mehtyl)amine. *Organic Syntheses, 88*, 238-247.

Helmlinger, G., Yuan, F., Dellian, M., & Jain, R. K. (1997). Interstitial pH and pO2 gradients in solid tumors in vivo: high-resolution measurements reveal a lack of correlation. *Nature Medicine, 3*(2), 177-182.

Hensley, K., Robinson, K. A., Gabbita, S. P., Salsman, S., & Floyd, R. A. (2000). Reactive oxygen species, cell signaling, and cell injury. *Free Radical Biology & Medicine, 28*(10), 1456-1462.

Herner, A., Nikic, I., Kallay, M., Lemke, E. A., & Kele, P. (2013). A new family of bioorthogonally applicable fluorogenic labels. *Organic & Biomolecular Chemistry, 11*(20), 3297-3306.

Hicks, K. O. (2006). Use of three-dimensional tissue cultures to model extravascular transport and predict in vivo activity of hypoxia-targeted anticancer drugs. *J. Natl Cancer Inst., 98*, 1118-1128.

Hicks, K. O. (2010). Pharmacokinetic/pharmacodynamic modeling identifies SN30000 and SN29751 as tirapazamine analogues with improved tissue penetration and hypoxic cell killing in tumors. *Clin. Cancer Res., 16*, 4946-4957.

Hicks, K. O., Pruijn, F. B., Secomb, T. W., Hay, M. P., Hsu, R., Brown, J. M., . . . Wilson, W. R. (2006). Use of three-dimensional tissue cultures to model extravascular transport and predict in vivo activity of hypoxia-targeted anticancer drugs. *Journal of the National Cancer Institute, 98*(16), 1118-1128.

Hill, R. P., & Bush, R. S. (1978). The effect of misonidazole in combination with radiation dose fractionation. *British Journal of Cancer, 37*(SUPPL.3), 255-258.

Himo, F., Lovell, T., Hilgraf, R., Rostovtsev, V. V., Noodleman, L., Sharpless, K. B., & Fokin, V. V. (2004). Copper(I)-catalyzed synthesis of azoles. DFT study predicts unprecedented reactivity and intermediates. *Journal of the American Chemical Society, 127*(1), 210-216.

Hirst, D. G., & Denekamp, J. (1979). Tumour cell proliferation in relation to the vasculature. *Cell & Tissue Kinetics, 12*(1), 31-42.

Höckel, M., & Vaupel, P. (2001). Tumor hypoxia: Definitions and current clinical, biologic, and molecular aspects. *Journal of the National Cancer Institute, 93*(4), 266-276.

Hodnick, W. F., & Sartorelli, A. C. (1993). Reductive activation of mitomycin C by NADH:cytochrome b5 reductase. *Cancer Research, 53*(20), 4907-4912.

Holmquist, L., Lofstedt, T., & Pahlman, S. (2006). Effect of hypoxia on the tumor phenotype: The neuroblastoma and breast cancer models. *Advances in Experimental Medicine & Biology, 587*, 179-193.

Holtz, K. M., Rockwell, S., Tomasz, M., & Sartorelli, A. C. (2003). Nuclear overexpression of NADH:cytochrome b5 reductase activity increases the cytotoxicity of mitomycin C (MC) and the total number of MC-DNA adducts in Chinese hamster ovary cells. *Journal of Biological Chemistry, 278*(7), 5029-5034.

Hong, V., Presolski, S. I., Ma, C., & Finn, M. G. (2009). Analysis and optimization of copper-catalyzed azide-alkyne cycloaddition for bioconjugation. *Angewandte Chemie. International Ed. in English, 48*(52), 9879-9883.

Hong, V., Steinmetz, N. F., Manchester, M., & Finn, M. G. (2010). Labeling live cells by copper-catalyzed alkyne--azide click chemistry. *Bioconjugate Chemistry, 21*(10), 1912-1916.

Hong, V., Udit, A. K., Evans, R. A., & Finn, M. G. (2008). Electrochemically protected copper(I)-catalyzed azide-alkyne cycloaddition. *Chembiochem, 9*(9), 1481-1486.

Horan, A. D., & Koch, C. J. (2001). The K(m) for radiosensitization of human tumor cells by oxygen is much greater than 3 mmHg and is further increased by elevated levels of cysteine. *Radiation Research, 156*(4), 388-398.

Horsman, M. R., Mortensen, L. S., Petersen, J. B., Busk, M., & Overgaard, J. (2012). Imaging hypoxia to improve radiotherapy outcome. *Nature Reviews Clinical Oncology, 9*(12), 674-687.

Hoshino, I., & Matsubara, H. (2013). MicroRNAs in cancer diagnosis and therapy: From bench to bedside. *Surgery Today, 43*(5), 467-478.

Houseley, J., & Tollervey, D. (2009). The many pathways of RNA degradation. *Cell, 136*(4), 763-776.

Howes, A. L., Arthur, J. F., Zhang, T., Miyamoto, S., Adams, J. W., Dorn Ii, G. W., . . . Brown, J. H. (2003). Akt-mediated cardiomyocyte survival pathways are compromised by Gα q-induced phosphoinositide 4,5-bisphosphate depletion. *Journal of Biological Chemistry, 278*(41), 40343-40351.

Hu, M., & Polyak, K. (2008). Molecular characterisation of the tumour microenvironment in breast cancer. *European Journal of Cancer, 44*(18), 2760-2765.

Hu, Z., Fan, C., Livasy, C., He, X., Oh, D. S., Ewend, M. G., . . . Perou, C. M. (2009). A compact VEGF signature associated with distant metastases and poor outcomes. *BMC Medicine, 7*, 9.

Huang, G., & Chen, L. (2008). Tumor vasculature and microenvironment normalization: a possible mechanism of antiangiogenesis therapy. *Cancer Biotherapy & Radiopharmaceuticals, 23*(5), 661-667.

Huang, H. L., Hsing, H. W., Lai, T. C., Chen, Y. W., Lee, T. R., Chan, H. T., . . . Chan, H. L. (2010). Trypsin-induced proteome alteration during cell subculture in mammalian cells. *Journal of Biomedical Science, 17*, 36.

Huang, L. E., Arany, Z., Livingston, D. M., & Franklin Bunn, H. (1996). Activation of hypoxia-inducible transcription factor depends primarily upon redox-sensitive stabilization of its α subunit. *Journal of Biological Chemistry, 271*(50), 32253-32259.

Huang, L. E., & Bunn, H. F. (2003). Hypoxia-inducible factor and its biomedical relevance. *Journal of Biological Chemistry, 278*(22), 19575-19578.

Huang, X., Dong, Y., Bey, E. A., Kilgore, J. A., Bair, J. S., Li, L. S., . . . Boothman, D. A. (2012). An NQO1 substrate with potent antitumor activity that selectively kills by PARP1-induced programmed necrosis. *Cancer Research, 72*(12), 3038-3047.

Huggett, J., Dheda, K., Bustin, S., & Zumla, A. (2005). Real-time RT-PCR normalisation; strategies and considerations. *Genes Immun, 6*(4), 279-284.

Huisgen, R. (1961). Proceedings of the Chemical Society. October 1961. *Proceedings of the Chemical Society*(October), 357-396.

Hung, J.-J., Yang, M.-H., Hsu, H.-S., Hsu, W.-H., Liu, J.-S., & Wu, K.-J. (2009). Prognostic significance of hypoxia-inducible factor-1α, TWIST1 and Snail expression in resectable non-small cell lung cancer. *Thorax, 64*(12), 1082-1089.

Hunt, D. F., Henderson, R. A., Shabanowitz, J., Sakaguchi, K., Michel, H., Sevilir, N., . . . Engelhard, V. H. (1992). Characterization of peptides bound to the class I MHC molecule HLA-A2.1 by mass spectrometry. *Science, 255*(5049), 1261-1263.

Hunter, F. W., Jaiswal, J. K., Hurley, D. G., Liyanage, H. D., McManaway, S. P., Gu, Y., . . . Pruijn, F. B. (2014). The flavoprotein FOXRED2 reductively activates nitro-chloromethylbenzindolines and other hypoxia-targeting prodrugs. *Biochemical Pharmacology, 89*(2), 224-235.

Hunter, F. W., Young, R. J., Shalev, Z., Vellanki, R. N., Wang, J., Gu, Y., . . . Wouters, B. G. (2015). Identification of P450 Oxidoreductase as a Major Determinant of Sensitivity to Hypoxia-Activated Prodrugs. *Cancer Research, 75*(19), 4211-4223.

Hur, E., Chang, K. Y., Lee, E., Lee, S. K., & Park, H. (2001). Mitogen-activated protein kinase kinase inhibitor PD98059 blocks the trans-activation but not the stabilization or DNA binding ability of Hypoxia-inducible factor-1α. *Molecular Pharmacology, 59*(5), 1216-1224.

Iha, R. K., Wooley, K. L., Nyström, A. M., Burke, D. J., Kade, M. J., & Hawker, C. J. (2009). Applications of Orthogonal "Click" Chemistries in the Synthesis of Functional Soft Materials. *Chemical Reviews, 109*(11), 5620-5686.

Ilie, M., Mazure, N. M., Hofman, V., Ammadi, R. E., Ortholan, C., Bonnetaud, C., . . . Hofman, P. (2010). High levels of carbonic anhydrase IX in tumour tissue and plasma are biomarkers of poor prognostic in patients with non-small cell lung cancer. *Br J Cancer, 102*(11), 1627-1635.

Imbeaud, S., Graudens, E., Boulanger, V., Barlet, X., Zaborski, P., Eveno, E., . . . Auffray, C. (2005). Towards standardization of RNA quality assessment using user-independent classifiers of microcapillary electrophoresis traces. *Nucleic Acids Research, 33*(6), e56.

International Human Genome Sequencing, C. (2004). Finishing the euchromatic sequence of the human genome. *Nature, 431*(7011), 931-945.

Iscove, N. N., Barbara, M., Gu, M., Gibson, M., Modi, C., & Winegarden, N. (2002). Representation is faithfully preserved in global cDNA amplified exponentially from sub-picogram quantities of mRNA. *Nature Biotechnology, 20*(9), 940-943.

Jahan-Tigh, R. R., Ryan, C., Obermoser, G., & Schwarzenberger, K. (2012). Flow cytometry. *Journal of Investigative Dermatology, 132*(10), e1.

Jahn, C. E., Charkowski, A. O., & Willis, D. K. (2008). Evaluation of isolation methods and RNA integrity for bacterial RNA quantitation. *Journal of Microbiological Methods, 75*(2), 318-324.

Jain, R. K. (1988). Determinants of tumor blood flow: a review. *Cancer Research, 48*(10), 2641-2658.

Jao, C. Y., & Salic, A. (2008). Exploring RNA transcription and turnover in vivo by using click chemistry. *Proceedings of the National Academy of Sciences, 105*(41), 15779-15784.

Jemal, A., Bray, F., Center, M. M., Ferlay, J., Ward, E., & Forman, D. (2011). Global cancer statistics. *CA: A Cancer Journal for Clinicians, 61*(2), 69-90.

Jewett, J. C., & Bertozzi, C. R. (2010). Cu-free click cycloaddition reactions in chemical biology. *Chemical Society Reviews, 39*(4), 1272-1279.

Jewett, J. C., & Bertozzi, C. R. (2011). Synthesis of a fluorogenic cyclooctyne activated by Cu-free click chemistry. *Organic Letters, 13*(22), 5937-5939.

Jewett, J. C., Sletten, E. M., & Bertozzi, C. R. (2010). Rapid Cu-free click chemistry with readily synthesized biarylazacyclooctynones. *Journal of the American Chemical Society, 132*(11), 3688-3690.

Jiang, H., Zheng, T., Lopez-Aguilar, A., Feng, L., Kopp, F., Marlow, F. L., & Wu, P. (2014). Monitoring dynamic glycosylation in vivo using supersensitive click chemistry. *Bioconjugate Chemistry, 25*(4), 698-706.

Jiang, H. B., Ichikawa, M., Furukawa, A., Tomita, S., Ohnishi, T., & Ichikawa, Y. (2001). Metabolic activation of mitomycin C by NADPH-ferredoxin reductase in vitro. *Life Sciences, 68*(14), 1677-1685.

Jiang, X., Khan, M. A., Tian, W., Beilke, J., Natarajan, R., Kosek, J., . . . Nicolls, M. R. (2011). Adenovirus-mediated HIF-1α gene transfer promotes repair of mouse airway allograft microvasculature and attenuates chronic rejection. *Journal of Clinical Investigation, 121*(6), 2336-2349.

Jones, D. T., Lechertier, T., Mitter, R., Herbert, J. M., Bicknell, R., Jones, J. L., . . . Hodivala-Dilke, K. (2012). Gene expression analysis in human breast cancer associated blood vessels. *PLoS ONE [Electronic Resource], 7*(10), e44294.

Joyce, J. A. (2005). Therapeutic targeting of the tumor microenvironment. *Cancer Cell, 7*(6), 513-520.

Julian, G. S., de Oliveira, R. W., Perry, J. C., Tufik, S., & Chagas, J. R. (2014). Validation of housekeeping genes in the brains of rats submitted to chronic intermittent hypoxia, a sleep apnea model. *PLoS ONE [Electronic Resource], 9*(10), e109902.

Jung, M., Schaefer, A., Steiner, I., Kempkensteffen, C., Stephan, C., Erbersdobler, A., & Jung, K. (2010). Robust microRNA stability in degraded RNA preparations from human tissue and cell samples. *Clinical Chemistry, 56*(6), 998-1006.

Junttila, M. R., & de Sauvage, F. J. (2013). Influence of tumour micro-environment heterogeneity on therapeutic response. *Nature, 501*(7467), 346-354.

Juricek, M., Kouwer, P. H. J., & Rowan, A. E. (2011). ChemInform abstract: Triazole: A unique building block for the construction of functional materials. *ChemInform, 42*(47), no-no.

Kaelin Jr, W. G., & Ratcliffe, P. J. (2008). Oxygen sensing by metazoans: The central role of the HIF hydroxylase pathway. *Molecular Cell, 30*(4), 393-402.

Kanan, M. W., Rozenman, M. M., Sakurai, K., Snyder, T. M., & Liu, D. R. (2004). Reaction discovery enabled by DNA-templated synthesis and in vitro selection. *Nature, 431*(7008), 545-549.

Kap, M., Sieuwerts, A. M., Kubista, M., Oomen, M., Arshad, S., & Riegman, P. (2015). The influence of tissue procurement procedures on RNA integrity, gene expression, and morphology in porcine and human liver tissue. *Biopreservation and Biobanking, 13*(3), 200-206.

Kennedy, A. S., Raleigh, J. A., Perez, G. M., Calkins, D. P., Thrall, D. E., Novotny, D. B., & Varia, M. A. (1997). Proliferation and hypoxia in human squamous cell carcinoma of the cervix: first report of combined immunohistochemical assays. *International Journal of Radiation Oncology, Biology, Physics, 37*(4), 897-905.

Kennedy, D. C., McKay, C. S., Legault, M. C., Danielson, D. C., Blake, J. A., Pegoraro, A. F., . . . Pezacki, J. P. (2011). Cellular consequences of copper complexes used to catalyze

bioorthogonal click reactions. *Journal of the American Chemical Society, 133*(44), 17993-18001.

Keys, D. N., Au-Young, J. K., & Fekete, R. A. (2010). TaqMan Array Cards in pharmaceutical research. *Methods in Molecular Biology, 632*, 87-97.

Kiaune, L., & Singhasemanon, N. (2011). Pesticidal copper (I) oxide: environmental fate and aquatic toxicity. *Reviews of Environmental Contamination & Toxicology, 213*, 1-26.

Kim, C. Y., Tsai, M. H., Osmanian, C., Graeber, T. G., Lee, J. E., Giffard, R. G., . . . Giaccia, A. J. (1997). Selection of human cervical epithelial cells that possess reduced apoptotic potential to low-oxygen conditions. *Cancer Research, 57*(19), 4200-4204.

Kimura, H., Braun, R. D., Ong, E. T., Hsu, R., Secomb, T. W., Papahadjopoulos, D., . . . Dewhirst, M. W. (1996). Fluctuations in red cell flux in tumor microvessels can lead to transient hypoxia and reoxygenation in tumor parenchyma. *Cancer Research, 56*(23), 5522-5528.

Kirbach, B. B. (2013). Can any one tell me the best way to purify cDNA? Is it by column or precipitation with sodium acetate and ethanol? Retrieved 2014, from http://www.researchgate.net/post/Can_any_one_tell_me_the_best_way_to_purify_cDNA_Is_it_by_column_or_precipitation_with_sodium_acetate_and_ethanol

Knox, R. J., & Chen, S. (2004). Quinone reductase-mediated nitro-reduction: clinical applications. *Methods in Enzymology, 382*, 194-221.

Kocalka, P., El-Sagheer, A. H., & Brown, T. (2008). Rapid and efficient DNA strand cross-linking by click chemistry. *Chembiochem, 9*(8), 1280-1285.

Koch, C. J. (2002). Measurement of absolute oxygen levels in cells and tissues using oxygen sensors and 2-nitroimidazole EF5. *Methods in Enzymology, 352*, 3-31.

Koch, C. J. (2008). Importance of antibody concentration in the assessment of cellular hypoxia by flow cytometry: EF5 and pimonidazole. *Radiation Research, 169*(6), 677-688.

Koch, C. J., Jenkins, W. T., Jenkins, K. W., Yang, X. Y., Shuman, A. L., Pickup, S., . . . Evans, S. M. (2013). Mechanisms of blood flow and hypoxia production in rat 9L-epigastric tumors. *Tumor microenvironment and therapy, 1*, 1-13.

Koch, C. J., & Raleigh, J. A. (1991). Radiolytic reduction of protein and nonprotein disulfides in the presence of formate: A chain reaction. *Archives of Biochemistry and Biophysics, 287*(1), 75-84.

Kodani, M., Yang, G., Conklin, L. M., Travis, T. C., Whitney, C. G., Anderson, L. J., . . . Fields, B. S. (2011). Application of TaqMan Low-Density Arrays for simultaneous detection of multiple respiratory pathogens. *Journal of Clinical Microbiology, 49*(6), 2175-2182.

Koh, M. Y., Darnay, B. G., & Powis, G. (2008). Hypoxia-associated factor, a novel E3-ubiquitin ligase, binds and ubiquitinates hypoxia-inducible factor 1α, leading to its oxygen-independent degradation. *Molecular and Cellular Biology, 28*(23), 7081-7095.

Koh, W. J., Rasey, J. S., Evans, M. L., Grierson, J. R., Lewellen, T. K., Graham, M. M., . . . Griffin, T. W. (1992). Imaging of hypoxia in human tumors with [F-18]Fluoromisonidazole. *International Journal of Radiation Oncology Biology Physics, 22*(1), 199-212.

Kolb, H. C., Finn, M. G., & Sharpless, K. B. (2001). Click chemistry: diverse chemical function from a few good geactions. *Angewandte Chemie International Edition, 40*(11), 2004-2021.

Kolb, H. C., & Sharpless, K. B. (2003). The growing impact of click chemistry on drug discovery. *Drug Discovery Today, 8*(24), 1128-1137.

Kothari, S., Cizeau, J., McMillan-Ward, E., Israels, S. J., Bailes, M., Ens, K., . . . Gibson, S. B. (2003). BNIP3 plays a role in hypoxic cell death in human epithelial cells that is inhibited by growth factors EGF and IGF. *Oncogene, 22*(30), 4734-4744.

Krause, B. J., Beck, R., Souvatzoglou, M., & Piert, M. (2006). PET and PET/CT studies of tumor tissue oxygenation. *Quarterly Journal of Nuclear Medicine and Molecular Imaging, 50*(1), 28-43.

Krogh, A. (1922). *The anatomy and physiology of capillaries*. New York: New Haven, Yale University Press.

Kuang, G. C., Guha, P. M., Brotherton, W. S., Simmons, J. T., Stankee, L. A., Nguyen, B. T., . . . Zhu, L. (2011). Experimental investigation on the mechanism of chelation-assisted, copper(II) acetate-accelerated azide-alkyne cycloaddition. *Journal of the American Chemical Society, 133*(35), 13984-14001.

Kuang, G. C., Michaels, H. A., Simmons, J. T., Clark, R. J., & Zhu, L. (2010). Chelation-assisted, copper(II)-acetate-accelerated azide-alkyne cycloaddition. *Journal of Organic Chemistry, 75*(19), 6540-6548.

Kumar, A., Li, K., & Cai, C. Z. (2011). Anaerobic conditions to reduce oxidation of proteins and to accelerate the copper-catalyzed "Click" reaction with a water-soluble bis(triazole) ligand. *Chemical Communications, 47*(11), 3186-3188.

Kumar, P., Stypinski, D., Xia, H., McEwan, A. J. B., Machulla, H. J., & Wiebe, L. I. (1999). Fluoroazomycin arabinoside (FAZA): synthesis, 2H and 3H-labelling and preliminary biological evaluation of a novel 2-nitroimidazole marker of tissue hypoxia. *Journal of Labelled Compounds and Radiopharmaceuticals, 42*(1), 3-16.

Kumar, R., El-Sagheer, A., Tumpane, J., Lincoln, P., Wilhelmsson, L. M., & Brown, T. (2007). Template-directed oligonucleotide strand ligation, covalent intramolecular DNA circularization and catenation using click chemistry. *Journal of the American Chemical Society, 129*(21), 6859-6864.

Kurn, N., Chen, P., Heath, J. D., Kopf-Sill, A., Stephens, K. M., & Wang, S. (2005). Novel isothermal, linear nucleic acid amplification systems for highly multiplexed applications. *Clinical Chemistry, 51*(10), 1973-1981.

Kuzmin, A., Poloukhtine, A., Wolfert, M. A., & Popik, V. V. (2010). Surface functionalization using catalyst-free azide−alkyne cycloaddition. *Bioconjugate Chemistry, 21*(11), 2076-2085.

Kyle, A. H., Huxham, L. A., Yeoman, D. M., & Minchinton, A. I. (2007). Limited tissue penetration of taxanes: a mechanism for resistance in solid tumors. *Clinical Cancer Research, 13*(9), 2804-2810.

Lacroix, M. (2008). Persistent use of "false" cell lines. *International Journal of Cancer, 122*(1), 1-4.

Lakowicz, J. R. (2007). *Principles of fluorescence spectroscopy*: Springer.

Lallana, E., Riguera, R., & Fernandez-Megia, E. (2011). Reliable and efficient procedures for the conjugation of biomolecules through Huisgen azide-alkyne cycloadditions. *Angewandte Chemie. International Ed. in English, 50*(38), 8794-8804.

Lam, M. H.-W., Law, G.-L., Lee, C.-S., & Wong, K.-L. (2014). Organic molecules for optical imaging *The Chemistry of Molecular Imaging* (pp. 245-274): John Wiley & Sons, Inc.

Lando, D., Peet, D. J., Gorman, J. J., Whelan, D. A., Whitelaw, M. L., & Bruick, R. K. (2002). FIH-1 is an asparaginyl hydroxylase enzyme that regulates the transcriptional activity of hypoxia-inducible factor. *Genes and Development, 16*(12), 1466-1471.

Lando, D., Peet, D. J., Whelan, D. A., Gorman, J. J., & Whitelaw, M. L. (2002). Asparagine hydroxylation of the HIF transactivation domain: A hypoxic switch. *Science, 295*(5556), 858-861.

Landuyt, W., Hermans, R., Bosmans, H., Sunaert, S., Beatse, E., Farina, D., . . . Marchal, G. (2001). BOLD contrast fMRI of whole rodent tumour during air or carbogen breathing using echo-planar imaging at 1.5 T. *European Radiology, 11*(11), 2332-2340.

Lang, K., & Chin, J. W. (2014). Bioorthogonal reactions for labeling proteins. *ACS Chemical Biology [Electronic Resource], 9*(1), 16-20.

Larsson, T., Wedborg, M., & Turner, D. (2007). Correction of inner-filter effect in fluorescence excitation-emission matrix spectrometry using Raman scatter. *Analytica Chimica Acta, 583*(2), 357-363.

Laughlin, S. T., Baskin, J. M., Amacher, S. L., & Bertozzi, C. R. (2008). In vivo imaging of membrane-associated glycans in developing zebrafish. *Science, 320*(5876), 664-667.

Laughlin, S. T., & Bertozzi, C. R. (2009). Imaging the glycome. *Proceedings of the National Academy of Sciences, 106*(1), 12-17.

Le, A., Stine, Z. E., Nguyen, C., Afzal, J., Sun, P., Hamaker, M., . . . Dang, C. V. (2014). Tumorigenicity of hypoxic respiring cancer cells revealed by a hypoxia-cell cycle dual reporter. *Proceedings of the National Academy of Sciences of the United States of America, 111*(34), 12486-12491.

Le Droumaguet, C., Wang, C., & Wang, Q. (2010). Fluorogenic click reaction. *Chemical Society Reviews, 39*(4), 1233-1239.

Le, Q. T., Chen, E., Salim, A., Cao, H., Kong, C. S., Whyte, R., . . . Giaccia, A. J. (2006). An evaluation of tumor oxygenation and gene expression in patients with early stage non-small cell lung cancers. *Clinical Cancer Research, 12*(5), 1507-1514.

Le, Q. T., & Courter, D. (2008). Clinical biomarkers for hypoxia targeting. *Cancer metastasis reviews, 27*(3), 351-362.

Leclerc, D., Wilson, A., Dumas, R., Gafuik, C., Song, D., Watkins, D., . . . Gravel, R. A. (1998). Cloning and mapping of a cDNA for methionine synthase reductase, a flavoprotein defective in patients with homocystinuria. *Proceedings of the National Academy of Sciences of the United States of America, 95*(6), 3059-3064.

Lee, J. H., So, J.-H., Jeon, J. H., Choi, E. B., Lee, Y.-R., Chang, Y.-T., . . . Ahn, J. H. (2011). Synthesis of a new fluorescent small molecule probe and its use for in vivolipid imaging. *Chemical Communications, 47*(26), 7500-7502.

Lee, L. V., Mitchell, M. L., Huang, S.-J., Fokin, V. V., Sharpless, K. B., & Wong, C.-H. (2003). A Potent and highly selective inhibitor of human α-1,3-fucosyltransferase via click chemistry. *Journal of the American Chemical Society, 125*(32), 9588-9589.

Leone, A., & Mercer, J. F. B. (2012). *Copper transport and its disorders: Molecular and cellular aspects*: Springer US.

Levine, R. D. (2005). *Molecular reaction dynamics*: Cambridge University Press.

Lewis, J. S., McCarthy, D. W., McCarthy, T. J., Fujibayashi, Y., & Welch, M. J. (1999). Evaluation of 64Cu-ATSM in vitro and in vivo in a hypoxic tumor model. *Journal of Nuclear Medicine, 40*(1), 177-183.

Lewis, W. G., Green, L. G., Grynszpan, F., Radic, Z., Carlier, P. R., Taylor, P., . . . Sharpless, K. B. (2002). Click chemistry in situ: acetylcholinesterase as a reaction vessel for the

selective assembly of a femtomolar inhibitor from an array of building blocks. *Angewandte Chemie-International Edition, 41*(6), 1053-1057.

Lewis, W. G., Magallon, F. G., Fokin, V. V., & Finn, M. G. (2004). Discovery and characterization of catalysts for azide−alkyne cycloaddition by fluorescence quenching. *Journal of the American Chemical Society, 126*(30), 9152-9153.

Li, C., Guan, T., Chen, X., Li, W., Cai, Q., Niu, J., . . . Kong, J. (2013). BNIP3 mediates pre-myelinating oligodendrocyte cell death in hypoxia and ischemia. *Journal of Neurochemistry, 127*(3), 426-433.

Li, C. Y., Shan, S., Huang, Q., Braun, R. D., Lanzen, J., Hu, K., . . . Dewhirst, M. W. (2000). Initial stages of tumor cell-induced angiogenesis: evaluation via skin window chambers in rodent models. *Journal of the National Cancer Institute, 92*(2), 143-147.

Li, J., Smyth, P., Cahill, S., Denning, K., Flavin, R., Aherne, S., . . . Sheils, O. (2008). Improved RNA quality and TaqMan Pre-amplification method (PreAmp) to enhance expression analysis from formalin fixed paraffin embedded (FFPE) materials. *BMC Biotechnology, 8*, 10.

Lim, R. K. V., & Lin, Q. (2010). Bioorthogonal chemistry: Recent progress and future directions. *Chemical Communications, 46*(10), 1589-1600.

Lim, S. I., Mizuta, Y., Takasu, A., Kim, Y. H., & Kwon, I. (2014). Site-specific bioconjugation of a murine dihydrofolate reductase enzyme by copper(I)-catalyzed azide-alkyne cycloaddition with retained activity. *PLoS ONE [Electronic Resource], 9*(6), e98403.

Lin, A., & Hahn, S. M. (2012). Hypoxia imaging markers and applications for radiation treatment planning. *Seminars in Nuclear Medicine, 42*(5), 343-352.

Little, J. B., & Williams, J. R. (2010). Effects of ionizing radiation on mammalian cells *Comprehensive Physiology*: John Wiley & Sons, Inc.

Liu, Y. V., Baek, J. H., Zhang, H., Diez, R., Cole, R. N., & Semenza, G. L. (2007). RACK1 competes with HSP90 for binding to HIF-1α and is required for O2-independent and HSP90 inhibitor-induced degradation of HIF-1α. *Molecular Cell, 25*(2), 207-217.

Liu, Y. V., Hubbi, M. E., Pan, F., McDonald, K. R., Mansharamani, M., Cole, R. N., . . . Semenza, G. L. (2007). Calcineurin promotes jypoxia-inducible factor 1α expression by dephosphorylating RACK1 and blocking RACK1 dimerization. *Journal of Biological Chemistry, 282*(51), 37064-37073.

Livak, K. J., & Schmittgen, T. D. (2001). Analysis of relative gene expression data using real-time quantitative PCR and the 2(-Delta Delta C(T)) Method. *Methods (Duluth), 25*(4), 402-408.

Ljungkvist, A. S. E., Bussink, J., Kaanders, J. H. A. M., & van der Kogel, A. J. (2007). Dynamics of tumor hypoxia measured with bioreductive hypoxic cell markers. *Radiation Research, 167*(2), 127-145.

Lo, Y. M., Lun, F. M., Chan, K. C., Tsui, N. B., Chong, K. C., Lau, T. K., . . . Chiu, R. W. (2007). Digital PCR for the molecular detection of fetal chromosomal aneuploidy. *Proceedings of the National Academy of Sciences of the United States of America, 104*(32), 13116-13121.

Lo, Y. M. D., Chiu, R. W. K., & Chan, K. C. A. (2006). *Clinical applications of PCR*: Humana Press.

Loboda, A., Jozkowicz, A., & Dulak, J. (2010). HIF-1 and HIF-2 transcription factors--similar but not identical. *Molecules & Cells, 29*(5), 435-442.

Loenarz, C., Coleman, M. L., Boleininger, A., Schierwater, B., Holland, P. W. H., Ratcliffe, P. J., & Schofield, C. J. (2011). The hypoxia-inducible transcription factor pathway regulates

oxygen sensing in the simplest animal, Trichoplax adhaerens. *EMBO Reports, 12*(1), 63-70.

Lord, E. M., Harwell, L., & Koch, C. J. (1993). Detection of hypoxic cells by monoclonal antibody recognizing 2-nitroimidazole adducts. *Cancer Research, 53*(23), 5721-5726.

Luo, W., Zhong, J., Chang, R., Hu, H., Pandey, A., & Semenza, G. L. (2010). Hsp70 and CHIP selectively mediate ubiquitination and degradation of hypoxia-inducible factor (HIF)-1α but not HIF-2α. *Journal of Biological Chemistry, 285*(6), 3651-3663.

Lutz, J.-F. (2007). 1,3-Dipolar cycloadditions of azides and alkynes: A universal ligation tool in polymer and materials science. *Angewandte Chemie International Edition, 46*(7), 1018-1025.

Lwowski, W. (1984). *1,3-Dipolar cycloaddition chemistry* (Vol. 1). New York: Wiley.

Lyden, D., Hattori, K., Dias, S., Costa, C., Blaikie, P., Butros, L., . . . Rafii, S. (2001). Impaired recruitment of bone-marrow-derived endothelial and hematopoietic precursor cells blocks tumor angiogenesis and growth. *Nature Medicine, 7*(11), 1194-1201.

Mack, P. C., Redman, M. W., Chansky, K., Williamson, S. K., Farneth, N. C., Lara Jr, P. N., . . . Gandara, D. R. (2008). Lower osteopontin plasma levels are associated with superior outcomes in advanced non-small-cell lung cancer patients receiving platinum-based chemotherapy: SWOG study S0003. *Journal of Clinical Oncology, 26*(29), 4771-4776.

Magagnin, M. G., Sergeant, K., van den Beucken, T., Rouschop, K. M., Jutten, B., Seigneuric, R., . . . Wouters, B. G. (2007). Proteomic analysis of gene expression following hypoxia and reoxygenation reveals proteins involved in the recovery from endoplasmic reticulum and oxidative stress. *Radiotherapy & Oncology, 83*(3), 340-345.

Marcu, L., & Olver, I. (2006). Tirapazamine: from bench to clinical trials. *Current Clinical Pharmacology, 1*(1), 71-79.

Marks, I. S., Kang, J. S., Jones, B. T., Landmark, K. J., Cleland, A. J., & Taton, T. A. (2011). Strain-promoted "click" chemistry for terminal labeling of DNA. *Bioconjugate Chemistry, 22*(7), 1259-1263.

Marotta, D., Karar, J., Jenkins, W. T., Kumanova, M., Jenkins, K. W., Tobias, J. W., . . . Koumenis, C. (2011). In vivo profiling of hypoxic gene expression in gliomas using the hypoxia marker EF5 and laser-capture microdissection. *Cancer Research, 71*(3), 779-789.

Martin, B. R., Giepmans, B. N., Adams, S. R., & Tsien, R. Y. (2005). Mammalian cell-based optimization of the biarsenical-binding tetracysteine motif for improved fluorescence and affinity. *Nature Biotechnology, 23*(10), 1308-1314.

Marusyk, A., & Polyak, K. (2010). Tumor heterogeneity: Causes and consequences. *Biochimica et Biophysica Acta, 1805*(1), 105.

Mason, R. P., & Holtzman, J. L. (1975). The role of catalytic superoxide formation in the O2 inhibition of nitroreductase. *Biochemical and Biophysical Research Communications, 67*(4), 1267-1274.

Masters, J. R., Thomson, J. A., Daly-Burns, B., Reid, Y. A., Dirks, W. G., Packer, P., . . . Debenham, P. G. (2001). Short tandem repeat profiling provides an international reference standard for human cell lines. *Proceedings of the National Academy of Sciences of the United States of America, 98*(14), 8012-8017.

Matsumoto, K. I., Szajek, L., Krishna, M. C., Cook, J. A., Seidel, J., Grimes, K., . . . Mitchell, J. B. (2007). The influence of tumor oxygenation on hypoxia imaging in murine squamous cell

carcinoma using [64Cu]Cu-ATSM or [18F] Fluoromisonidazole positron emission tomography. *International Journal of Oncology, 30*(4), 873-881.

Maxwell, P. H., Wiesener, M. S., Chang, G.-W., Clifford, S. C., Vaux, E. C., Cockman, M. E., . . . Ratcliffe, P. J. (1999). The tumour suppressor protein VHL targets hypoxia-inducible factors for oxygen-dependent proteolysis. *Nature, 399*(6733), 271-275.

Mayer, A., Hockel, M., & Vaupel, P. (2008). Endogenous hypoxia markers: case not proven! *Advances in Experimental Medicine & Biology, 614*, 127-136.

Mayrhofer, C., Krieger, S., Allmaier, G., & Kerjaschki, D. (2006). DIGE compatible labelling of surface proteins on vital cells in vitro and in vivo. *Proteomics, 6*(2), 579-585.

Mbua, N. E., Guo, J., Wolfert, M. A., Steet, R., & Boons, G.-J. (2011). Strain-promoted alkyne–azide cycloadditions (SPAAC) reveal new features of glycoconjugate biosynthesis. *Chembiochem, 12*(12), 1912-1921.

McKay, C. S., & Finn, M. G. (2014). Click chemistry in complex mixtures: bioorthogonal bioconjugation. *Chemistry & Biology, 21*(9), 1075-1101.

McNulty, J., Keskar, K., & Vemula, R. (2011). The first well-defined silver(I)-complex-catalyzed cycloaddition of azides onto terminal alkynes at room temperature. *Chemistry – A European Journal, 17*(52), 14727-14730.

Mees, G., Dierckx, R., Vangestel, C., & Van De Wiele, C. (2009). Molecular imaging of hypoxia with radiolabelled agents. *European Journal of Nuclear Medicine and Molecular Imaging, 36*(10), 1674-1686.

Meldal, M. (2008). Polymer “clicking” by CuAAC reactions. *Macromolecular Rapid Communications, 29*(12-13), 1016-1051.

Meldal, M., & Tornoe, C. W. (2008). Cu-catalyzed azide-alkyne cycloaddition. *Chemical Reviews, 108*(8), 2952-3015.

Melillo, G. (2013). *Hypoxia and cancer: Biological implications and therapeutic opportunities*: Springer New York.

Meng, A. X., Jalali, F., Cuddihy, A., Chan, N., Bindra, R. S., Glazer, P. M., & Bristow, R. G. (2005). Hypoxia down-regulates DNA double strand break repair gene expression in prostate cancer cells. *Radiotherapy & Oncology, 76*(2), 168-176.

Meng, F., Evans, J. W., Bhupathi, D., Banica, M., Lan, L., Lorente, G., . . . Hart, C. P. (2012). Molecular and cellular pharmacology of the hypoxia-activated prodrug TH-302. *Molecular Cancer Therapeutics, 11*(3), 740-751.

Meng, X., Kong, F.-M. S., & Yu, J. (2012). Implementation of hypoxia measurement into lung cancer therapy. *Lung Cancer, 75*(2), 146-150.

Menon, C., & Fraker, D. L. (2005). Tumor oxygenation status as a prognostic marker. *Cancer Letters, 221*(2), 225-235.

Michaels, H. A., & Zhu, L. (2011). Ligand-assisted, copper(II) acetate-accelerated azide–alkyne cycloaddition. *Chemistry – An Asian Journal, 6*(10), 2825-2834.

Mihich, E., & Kaelin, W. (2004). Fifteenth annual Pezcoller symposium: Molecular in vivo visualization of cancer cells. *Cancer Research, 64*(8), 2929-2933.

Milcheva, R., Janega, P., Celec, P., Russev, R., & Babal, P. (2013). Alcohol based fixatives provide excellent tissue morphology, protein immunoreactivity and RNA integrity in paraffin embedded tissue specimens. *Acta Histochemica, 115*(3), 279-289.

Miller, C. L., Diglisic, S., Leister, F., Webster, M., & Yolken, R. H. (2004). Evaluating RNA status for RT-PCR in extracts of postmortem human brain tissue. *Biotechniques, 36*(4), 628-633.

Milosevic, M., Fyles, A., Hedley, D., & Hill, R. (2004). The human tumor microenvironment: invasive (needle) measurement of oxygen and interstitial fluid pressure. *Seminars in Radiation Oncology, 14*(3), 249-258.

Minchinton, A. I., & Tannock, I. F. (2006). Drug penetration in solid tumours. *Nature Reviews Cancer, 6*(8), 583-592.

Miskiniene, V., Dickancaite, E., Nemeikaite, A., & Cenas, N. (1997). Nitroaromatic betulin derivatives as redox cycling agents. *Biochemistry & Molecular Biology International, 42*(2), 391-397.

Mitchell, J. B., Biaglow, J. E., & Russo, A. (1988). Role of glutathione and other endogenous thiols in radiation protection. *Pharmacology & Therapeutics, 39*(1–3), 269-274.

Moeller, B. J., Richardson, R. A., & Dewhirst, M. W. (2007). Hypoxia and radiotherapy: opportunities for improved outcomes in cancer treatment. *Cancer & Metastasis Reviews, 26*(2), 241-248.

MolecularDevices. (2006). SpectraMax M2 & SpectraMax M2e Multi-mode Plate Readers User Guide. California, U.S.A.: Molecular Devices Corporation.

Monici, M. (2005). Cell and tissue autofluorescence research and diagnostic applications. *Biotechnology Annual Review, 11*, 227-256.

Moon, E. J., Brizel, D. M., Chi, J. T., & Dewhirst, M. W. (2007). The potential role of intrinsic hypoxia markers as prognostic variables in cancer. *Antioxidants & Redox Signaling, 9*(8), 1237-1294.

Moorhouse, A. D., Santos, A. M., Gunaratnam, M., Moore, M., Neidle, S., & Moses, J. E. (2006). Stabilization of G-quadruplex DNA by highly selective ligands via click chemistry. *Journal of the American Chemical Society, 128*(50), 15972-15973.

Mortensen, L. S., Buus, S., Nordsmark, M., Bentzen, L., Munk, O. L., Keiding, S., & Overgaard, J. (2010). Identifying hypoxia in human tumors: A correlation study between 18F-FMISO PET and the Eppendorf oxygen-sensitive electrode. *Acta Oncologica, 49*(7), 934-940.

Moses, J. E., & Moorhouse, A. D. (2007). The growing applications of click chemistry. *Chemical Society Reviews, 36*(8), 1249-1262.

Mueller, O., Hahnenberger, K., Dittmann, M., Yee, H., Dubrow, R., Nagle, R., & Ilsley, D. (2000). A microfluidic system for high-speed reproducible DNA sizing and quantitation. *ELECTROPHORESIS, 21*(1), 128-134.

Munk, M., Memon, A. A., Goetze, J. P., Nielsen, L. B., Nexo, E., & Sørensen, B. S. (2012). Hypoxia changes the expression of the epidermal growth factor (EGF) system in human hearts and cultured cardiomyocytes. *PLoS ONE [Electronic Resource], 7*(7), e40243.

Nadler, A., & Schultz, C. (2013). The power of fluorogenic probes. *Angewandte Chemie International Edition, 52*(9), 2408-2410.

Namas, R. A., Metukuri, M. R., Dhupar, R., Velosa, C., Jefferson, B. S., Myer, E., . . . Zamora, R. (2011). Hypoxia-induced overexpression of BNIP3 is not dependent on hypoxia-inducible factor 1alpha in mouse hepatocytes. *Shock, 36*(2), 196-202.

Naranjo-Suarez, S., Carlson, B. A., Tsuji, P. A., Yoo, M. H., Gladyshev, V. N., & Hatfield, D. L. (2012). HIF-independent regulation of thioredoxin reductase 1 contributes to the high

levels of reactive oxygen species induced by hypoxia. *PLoS ONE [Electronic Resource], 7*(2), e30470.

Neef, A. B., & Schultz, C. (2009). Selective fluorescence labeling of lipids in living cells. *Angewandte Chemie International Edition, 48*(8), 1498-1500.

Nilsson, H., Krawczyk, K. M., & Johansson, M. E. (2014). High salt buffer improves integrity of RNA after fluorescence-activated cell sorting of intracellular labeled cells. *Journal of Biotechnology, 192 Pt A*, 62-65.

Ning, X., Guo, J., Wolfert, M. A., & Boons, G.-J. (2008). Visualizing metabolically labeled glycoconjugates of living cells by copper-free and fast Huisgen cycloadditions. *Angewandte Chemie International Edition, 47*(12), 2253-2255.

Nolan, T., Hands, R. E., & Bustin, S. A. (2006). Quantification of mRNA using real-time RT-PCR. *Nat. Protocols, 1*(3), 1559-1582.

Nordsmark, M., Bentzen, S. M., Rudat, V., Brizel, D., Lartigau, E., Stadler, P., . . . Overgaard, J. (2005). Prognostic value of tumor oxygenation in 397 head and neck tumors after primary radiation therapy. An international multi-center study. *Radiotherapy and Oncology, 77*(1), 18-24.

O'Brien, M. A., Costin, B. N., & Miles, M. F. (2012). Using genome-wide expression profiling to define gene networks relevant to the study of complex traits: from RNA integrity to network topology. *International Review of Neurobiology, 104*, 91-133.

Ogata, K., Matsuda, K., Tsuji, H., & Nomoto, K. (2015). Sensitive and rapid RT-qPCR quantification of pathogenic Candida species in human blood. *Journal of Microbiological Methods, 117*, 128-135.

Olive, P. L., & Aquino-Parsons, C. (2004). Measurement of tumor hypoxia using single-cell methods. *Seminars in Radiation Oncology, 14*(3), 241-248.

Olive, P. L., Banath, J. P., & Aquino-Parsons, C. (2001). Measuring hypoxia in solid tumours--is there a gold standard? *Acta Oncologica, 40*(8), 917-923.

Olive, P. L., Luo, C.-M., & Banáth, J. P. (2002). Local hypoxia is produced at sites of intratumour injection. *British Journal of Cancer, 86*, 7.

Olteanu, H., & Banerjee, R. (2001). Human methionine synthase reductase, a soluble P-450 reductase-like dual flavoprotein, is sufficient for NADPH-dependent methionine synthase activation. *Journal of Biological Chemistry, 276*(38), 35558-35563.

Orgueira, H. A., Fokas, D., Isome, Y., Chan, P. C. M., & Baldino, C. M. (2005). Regioselective synthesis of [1,2,3]-triazoles catalyzed by Cu(I) generated in situ from Cu(0) nanosize activated powder and amine hydrochloride salts. *Tetrahedron Letters, 46*(16), 2911-2914.

Padera, T. P., Stoll, B. R., Tooredman, J. B., Capen, D., di Tomaso, E., & Jain, R. K. (2004). Pathology: cancer cells compress intratumour vessels. *Nature, 427*(6976), 695.

Padhani, A. R. (2005). Where are we with imaging oxygenation in human tumours? *Cancer Imaging, 5*, 128-130.

Padhani, A. R., Krohn, K. A., Lewis, J. S., & Alber, M. (2007). Imaging oxygenation of human tumours. *European Radiology, 17*(4), 861-872.

Paine, M. J., Garner, A. P., Powell, D., Sibbald, J., Sales, M., Pratt, N., . . . Wolf, C. R. (2000). Cloning and characterization of a novel human dual flavin reductase. *Journal of Biological Chemistry, 275*(2), 1471-1478.

Pal, A., Srivastava, T., Sharma, M. K., Mehndiratta, M., Das, P., Sinha, S., & Chattopadhyay, P. (2010). Aberrant methylation and associated transcriptional mobilization of Alu elements contributes to genomic instability in hypoxia. *Journal of Cellular & Molecular Medicine, 14*(11), 2646-2654.

Palazon, A., Aragones, J., Morales-Kastresana, A., de Landazuri, M. O., & Melero, I. (2012). Molecular pathways: hypoxia response in immune cells fighting or promoting cancer. *Clinical Cancer Research, 18*(5), 1207-1213.

Palmer, S., Wiegand, A. P., Maldarelli, F., Bazmi, H., Mican, J. M., Polis, M., . . . Coffin, J. M. (2003). New real-time reverse transcriptase-initiated PCR assay with single-copy sensitivity for human immunodeficiency virus type 1 RNA in plasma. *Journal of Clinical Microbiology, 41*(10), 4531-4536.

Pan, S., Aebersold, R., Chen, R., Rush, J., Goodlett, D. R., McIntosh, M. W., . . . Brentnall, T. A. (2009). Mass spectrometry based targeted protein quantification: methods and applications. *Journal of Proteome Research, 8*(2), 787-797.

Pandey, M., & Mahadevan, D. (2014). Monoclonal antibodies as therapeutics in human malignancies. *Future Oncology, 10*(4), 609-636.

Papadopoulou, M. V., Ji, M., Rao, M. K., & Bloomer, W. D. (2003). Reductive metabolism of the nitroimidazole-based hypoxia-selective cytotoxin NLCQ-1 (NSC 709257). *Oncology Research, 14*(1), 21-29.

Papandreou, I., Lim, A. L., Laderoute, K., & Denko, N. C. (2008). Hypoxia signals autophagy in tumor cells via AMPK activity, independent of HIF-1, BNIP3, and BNIP3L. *Cell Death & Differentiation, 15*(10), 1572-1581.

Paredes, E., & Das, S. R. (2011). Click chemistry for rapid labeling and ligation of RNA. *Chembiochem, 12*(1), 125-131.

Paredes, E., & Das, S. R. (2012). Optimization of acetonitrile co-solvent and copper stoichiometry for pseudo-ligandless click chemistry with nucleic acids. *Bioorganic & Medicinal Chemistry Letters, 22*(16), 5313-5316.

Patterson, A. V., Ferry, D. M., Edmunds, S. J., Gu, Y., Singleton, R. S., Patel, K., . . . Wilson, W. R. (2007). Mechanism of action and preclinical antitumor activity of the novel hypoxia-activated DNA cross-linking agent PR-104. *Clinical Cancer Research, 13*(13), 3922-3932.

Patterson, A. V., Saunders, M. P., Chinje, E. C., Patterson, L. H., & Stratford, I. J. (1998). Enzymology of tirapazamine metabolism: A review. *Anti-Cancer Drug Design, 13*(6), 541-573.

Patterson, A. V., Saunders, M. P., Chinje, E. C., Talbot, D. C., Harris, A. L., & Strafford, I. J. (1997). Overexpression of human NADPH:cytochrome c (P450) reductase confers enhanced sensitivity to both tirapazamine (SR 4233) and RSU 1069. *British Journal of Cancer, 76*(10), 1338-1347.

Patterson, D. M., Nazarova, L. A., & Prescher, J. A. (2014). Finding the right (bioorthogonal) chemistry. *ACS Chemical Biology [Electronic Resource], 9*(3), 592-605.

Paule, M. R., & White, R. J. (2000). Survey and summary: Transcription by RNA polymerases I and III. *Nucleic Acids Research, 28*(6), 1283-1298.

Peralta Soler, A., Knudsen, K. A., Tecson-Miguel, A., McBrearty, F. X., Han, A. C., & Salazar, H. (1997). Expression of E-cadherin and N-cadherin in surface epithelial-stromal tumors of the ovary distinguishes mucinous from serous and endometrioid tumors. *Human Pathology, 28*(6), 734-739.

Petrucci, R. H., Herring, F. G., Madura, J. D., & Bissonnette, C. (2010). *General chemistry principles and modern applications: Pearson Etext Student Access Kit*: Pearson College Division.

Pfaffl, M. W. (2015). Reference genes / Housekeeping genes. In *The Reference in qPCR - Academic & Industrial Information Platform.* Retrieved from http://normalisation.gene-quantification.info/

Pitsillides, C. M., Runnels, J. M., Spencer, J. A., Zhi, L., Wu, M. X., & Lin, C. P. (2011). Cell labeling approaches for fluorescence-based in vivo flow cytometry. *Cytometry Part A: The Journal of the International Society for Analytical Cytology, 79*(10), 758-765.

Plass, T., Milles, S., Koehler, C., Schultz, C., & Lemke, E. A. (2011). Genetically encoded copper-free click chemistry. *Angewandte Chemie International Edition, 50*(17), 3878-3881.

Prabhakar, N. R. (2013). Sensing hypoxia: physiology, genetics and epigenetics. *Journal of Physiology, 591*(Pt 9), 2245-2257.

Prescher, J. A., & Bertozzi, C. R. (2005). Chemistry in living systems. *Nat Chem Biol, 1*(1), 13-21.

Prescher, J. A., Dube, D. H., & Bertozzi, C. R. (2004). Chemical remodelling of cell surfaces in living animals. *Nature, 430*(7002), 873-877.

Presolski, S. I., Hong, V., Cho, S.-H., & Finn, M. G. (2010). Tailored ligand acceleration of the Cu-catalyzed azide−alkyne cycloaddition reaction: Practical and mechanistic implications. *Journal of the American Chemical Society, 132*(41), 14570-14576.

Presolski, S. I., Hong, V. P., & Finn, M. G. (2011). Copper-catalyzed azide–alkyne click chemistry for bioconjugation. *Current protocols in chemical biology, 3*(4), 153-162.

Pugh, C. W., & Ratcliffe, P. J. (2003). Regulation of angiogenesis by hypoxia: role of the HIF system. *Nature Medicine, 9*(6), 677-684.

Qi, J., Han, M.-S., Chang, Y.-C., & Tung, C.-H. (2011). Developing visible fluorogenic 'click-on' dyes for cellular imaging. *Bioconjugate Chemistry, 22*(9), 1758-1762.

R. Desjardins, P., & Conklin, D. S. (2001). Microvolume quantitation of nucleic acids *Current Protocols in Molecular Biology*: John Wiley & Sons, Inc.

Raleigh, J. A., & Koch, C. J. (1990). Importance of thiols in the reductive binding of 2-nitroimidazoles to macromolecules. *Biochemical Pharmacology, 40*(11), 2457-2464.

Ramachandran, S., Ient, J., Gottgens, E. L., Krieg, A. J., & Hammond, E. M. (2015). Epigenetic therapy for solid tumors: Highlighting the impact of tumor hypoxia. *Genes (Basel), 6*(4), 935-956.

Rasey, J. S., Koh, W. J., Evans, M. L., Peterson, L. M., Lewellen, T. K., Graham, M. M., & Krohn, K. A. (1996). Quantifying regional hypoxia in human tumors with positron emission tomography of [18F]fluoromisonidazole: A pretherapy study of 37 patients. *International Journal of Radiation Oncology Biology Physics, 36*(2), 417-428.

Ravi, R., Mookerjee, B., Bhujwalla, Z. M., Sutter, C. H., Artemov, D., Zeng, Q., . . . Bedi, A. (2000). Regulation of tumor angiogenesis by p53-induced degradation of hypoxia- inducible factor 1α. *Genes and Development, 14*(1), 34-44.

Reddy, S. B., & Williamson, S. K. (2009). Tirapazamine: a novel agent targeting hypoxic tumor cells. *Expert Opinion on Investigational Drugs, 18*(1), 77-87.

Reischl, G., Ehrlichmann, W., Bieg, C., Solbach, C., Kumar, P., Wiebe, L. I., & Machulla, H. J. (2005). Preparation of the hypoxia imaging PET tracer [18F]FAZA: reaction parameters and automation. *Applied Radiation & Isotopes, 62*(6), 897-901.

Revesz, L. (1985). The role of endogenous thiols in intrinsic radioprotection. *International Journal of Radiation Biology & Related Studies in Physics, Chemistry & Medicine, 47*(4), 361-368.

Richard, D. E., Berra, E., Gothié, E., Roux, D., & Pouysségur, J. (1999). p42/p44 mitogen-activated protein kinases phosphorylate hypoxia- reducible factor (HIF-1α) and enhance the transcriptional activity of HIF-1. *Journal of Biological Chemistry, 274*(46), 32631-32637.

Rodionov, V. O., Fokin, V. V., & Finn, M. G. (2005). Mechanism of the ligand-free CuI-catalyzed azide–alkyne cycloaddition reaction. *Angewandte Chemie International Edition, 44*(15), 2210-2215.

Rodionov, V. O., Presolski, S. I., Diaz, D. D., Fokin, V. V., & Finn, M. G. (2007). Ligand-accelerated Cu-catalyzed azide-alkyne cycloaddition: a mechanistic report. *Journal of the American Chemical Society, 129*(42), 12705-12712.

Rodrigues, L. M., Howe, F. A., Griffiths, J. R., & Robinson, S. P. (2004). Tumor R2* is a prognostic indicator of acute radiotherapeutic response in rodent tumors. *Journal of Magnetic Resonance Imaging, 19*(4), 482-488.

Rofstad, E. K., Galappathi, K., Mathiesen, B., & Ruud, E.-B. M. (2007). Fluctuating and diffusion-limited hypoxia in hypoxia-induced metastasis. *Clinical Cancer Research, 13*(7), 1971-1978.

Rohwer, N., & Cramer, T. (2011). Hypoxia-mediated drug resistance: novel insights on the functional interaction of HIFs and cell death pathways. *Drug Resistance Updates, 14*(3), 191-201.

Rolls, G. (2012). Fixation and fixatives (3) – Fixing agents other than the common aldehydes. Retrieved November 13, 2015, from http://www.leicabiosystems.com/pathologyleaders/fixation-and-fixatives-3-fixing-agents-other-than-the-common-aldehydes/

Ronnov-Jessen, L., Petersen, O. W., & Bissell, M. J. (1996). Cellular changes involved in conversion of normal to malignant breast: importance of the stromal reaction. *Physiological Reviews, 76*(1), 69-125.

Roots, R., & Smith, K. C. (1974). On the nature of the oxygen effect on x-ray-induced DNA single-strand breaks in mammalian cells. *International Journal of Radiation Biology & Related Studies in Physics, Chemistry & Medicine, 26*(5), 467-480.

Ross, D., Beall, H., Traver, R. D., Siegel, D., Phillips, R. M., & Gibson, N. W. (1994). Bioactivation of quinones by DT-diaphorase, molecular, biochemical, and chemical studies. *Oncology Research, 6*(10-11), 493-500.

Rostovtsev, V. V., Green, L. G., Fokin, V. V., & Sharpless, K. B. (2002). A stepwise Huisgen cycloaddition process: Copper(I)-catalyzed regioselective “ligation” of azides and terminal alkynes. *Angewandte Chemie International Edition, 41*(14), 2596-2599.

Rudolf, G. C., & Sieber, S. A. (2013). Copper-assisted click reactions for activity-based proteomics: fine-tuned ligands and refined conditions extend the scope of application. *Chembiochem, 14*(18), 2447-2455.

Salic, A., & Mitchison, T. J. (2008). A chemical method for fast and sensitive detection of DNA synthesis in vivo. *Proceedings of the National Academy of Sciences of the United States of America, 105*(7), 2415-2420.

Sanchez-Espiridion, B., Sanchez-Aguilera, A., Montalban, C., Martin, C., Martinez, R., Gonzalez-Carrero, J., . . . Spanish Hodgkin's Lymphoma Study, G. (2009). A TaqMan low-density array to predict outcome in advanced Hodgkin's lymphoma using paraffin-embedded samples. *Clinical Cancer Research, 15*(4), 1367-1375.

Sang, N., Stiehl, D. P., Bohensky, J., Leshchinsky, I., Srinivas, V., & Caro, J. (2003). MAPK signaling up-regulates the activity of hypoxia-inducible factors by its effects on p300. *Journal of Biological Chemistry, 278*(16), 14013-14019.

Satchi-Fainaro, R. (2002). Targeting tumor vasculature: reality or a dream? *Journal of Drug Targeting, 10*(7), 529-533.

Schilling, C., Jung, N., & Bräse, S. (2010). Cycloaddition Reactions with Azides: An Overview *Organic Azides* (pp. 269-284): John Wiley & Sons, Ltd.

Schmittgen, T. D., & Livak, K. J. (2008). Analyzing real-time PCR data by the comparative C(T) method. *Nature Protocols, 3*(6), 1101-1108.

Schmittgen, T. D., & Zakrajsek, B. A. (2000). Effect of experimental treatment on housekeeping gene expression: validation by real-time, quantitative RT-PCR. *Journal of Biochemical and Biophysical Methods, 46*(1–2), 69-81.

Schnell, U., Dijk, F., Sjollema, K. A., & Giepmans, B. N. (2012). Immunolabeling artifacts and the need for live-cell imaging. *Nature Methods, 9*(2), 152-158.

Schrijvers, M. L., van der Laan, B. F. A. M., de Bock, G. H., Pattje, W. J., Mastik, M. F., Menkema, L., . . . van der Wal, J. E. (2008). Overexpression of intrinsic hypoxia markers HIF1α and CA-IX predict for local recurrence in stage T1-T2 glottic laryngeal carcinoma treated with radiotherapy. *International Journal of Radiation Oncology*Biology*Physics, 72*(1), 161-169.

Schroeder, A., Mueller, O., Stocker, S., Salowsky, R., Leiber, M., Gassmann, M., . . . Ragg, T. (2006). The RIN: An RNA integrity number for assigning integrity values to RNA measurements. *BMC Molecular Biology, 7*(1), 3.

Schwanhausser, B., Busse, D., Li, N., Dittmar, G., Schuchhardt, J., Wolf, J., . . . Selbach, M. (2011). Global quantification of mammalian gene expression control.[Erratum appears in Nature. 2013 Mar 7;495(7439):126-7; PMID: 23407496]. *Nature, 473*(7347), 337-342.

Secomb, T. W., Dewhirst, M. W., & Pries, A. R. (2012). Structural adaptation of normal and tumour vascular networks. *Basic & Clinical Pharmacology & Toxicology, 110*(1), 63-69.

Seigneuric, R., Starmans, M. H. W., Fung, G., Krishnapuram, B., Nuyten, D. S. A., van Erk, A., . . . Lambin, P. (2007). Impact of supervised gene signatures of early hypoxia on patient survival. *Radiotherapy & Oncology, 83*(3), 374-382.

Semenza, G. L. (2010). Defining the role of hypoxia-inducible factor 1 in cancer biology and therapeutics. *Oncogene, 29*(5), 625-634.

Semenza, G. L. (2010). HIF-1: upstream and downstream of cancer metabolism. *Current Opinion in Genetics & Development, 20*(1), 51-56.

Semenza, G. L. (2012). Hypoxia-inducible factors: mediators of cancer progression and targets for cancer therapy. *Trends in Pharmacological Sciences, 33*(4), 207-214.

Semenza, G. L., Jiang, B. H., Leung, S. W., Passantino, R., Concordet, J. P., Maire, P., & Giallongo, A. (1996). Hypoxia response elements in the aldolase A, enolase 1, and lactate dehydrogenase A gene promoters contain essential binding sites for hypoxia- inducible factor 1. *Journal of Biological Chemistry, 271*(51), 32529-32537.

Seow, H. A., Penketh, P. G., Belcourt, M. F., Tomasz, M., Rockwell, S., & Sartorelli, A. C. (2004). Nuclear overexpression of NAD(P)H:quinone oxidoreductase 1 in Chinese hamster ovary cells increases the cytotoxicity of mitomycin C under aerobic and hypoxic conditions. *Journal of Biological Chemistry, 279*(30), 31606-31612.

Serdiuk, T., Alekseev, S., Lysenko, V., Skryshevsky, V., & Geloen, A. (2014). Trypsinization-dependent cell labeling with fluorescent nanoparticles. *Nanoscale Research Letters, 9*(1), 568.

Sevick, E. M., & Jain, R. K. (1989). Geometric resistance to blood flow in solid tumors perfused ex vivo: Effects of tumor size and perfusion pressure. *Cancer Research, 49*(13), 3506-3512.

Sevick, E. M., & Jain, R. K. (1991). Effect of red blood cell rigidity on tumor blood flow: increase in viscous resistance during hyperglycemia. *Cancer Research, 51*(10), 2727-2730.

Shahrzad, S., Bertrand, K., Minhas, K., & Coomber, B. L. (2007). Induction of DNA hypomethylation by tumor hypoxia. *Epigenetics: Official Journal of the DNA Methylation Society, 2*(2), 119-125.

Sharpless, K. B., & Manetsch, R. (2006). In situ click chemistry: a powerful means for lead discovery. *Expert Opinion on Drug Discovery, 1*(6), 525-538.

Shekhar, M. P., Werdell, J., Santner, S. J., Pauley, R. J., & Tait, L. (2001). Breast stroma plays a dominant regulatory role in breast epithelial growth and differentiation: implications for tumor development and progression. *Cancer Research, 61*(4), 1320-1326.

Sheldon, P. W., & Fowler, J. F. (1978). Radiosensitization by misonidazole (Ro-07-0582) of fractionated X-rays in murine tumour. *Br J Cancer, 37*, 243-245.

Shieh, P., Hangauer, M. J., & Bertozzi, C. R. (2012). Fluorogenic azidofluoresceins for biological imaging. *Journal of the American Chemical Society, 134*(42), 17428-17431.

Shinde, S. S., Maroz, A., Hay, M. P., Patterson, A. V., Denny, W. A., & Anderson, R. F. (2010). Characterization of radicals formed following enzymatic reduction of 3-substituted analogues of the hypoxia-selective cytotoxin 3-amino-1,2,4-benzotriazine 1,4-dioxide (tirapazamine). *Journal of the American Chemical Society, 132*(8), 2591-2599.

Shukla, R. N. (2014). *Analysis of chromosome*: AGROTECH PRESS.

Siegel, R., Naishadham, D., & Jemal, A. (2012). Cancer statistics, 2012. *CA: A Cancer Journal for Clinicians, 62*(1), 10-29.

Siemann, D. W. (2006). Tumor vasculature: A target for anticancer therapies *Vascular-Targeted Therapies in Oncology* (pp. 1-8): John Wiley & Sons, Ltd.

Sivakumar, K., Xie, F., Cash, B. M., Long, S., Barnhill, H. N., & Wang, Q. (2004). A fluorogenic 1,3-dipolar cycloaddition reaction of 3-azidocoumarins and acetylenes. *Organic Letters, 6*(24), 4603-4606.

Sletten, E. M., & Bertozzi, C. R. (2009). Bioorthogonal chemistry: Fishing for selectivity in a sea of functionality. *Angewandte Chemie International Edition, 48*(38), 6974-6998.

Sletten, E. M., & Bertozzi, C. R. (2011). From mechanism to mouse: A tale of two bioorthogonal reactions. *Accounts of Chemical Research, 44*(9), 666-676.

Sloka, J. S., Hollett, P. D., & Mathews, M. (2007). A quantitative review of the use of FDG-PET in the axillary staging of breast cancer. *Medical Science Monitor, 13*(3), RA37-RA46.

Smith, P. K., Krohn, R. I., Hermanson, G. T., Mallia, A. K., Gartner, F. H., Provenzano, M. D., . . . Klenk, D. C. (1985). Measurement of protein using bicinchoninic acid.[Erratum appears in Anal Biochem 1987 May 15;163(1):279]. *Analytical Biochemistry, 150*(1), 76-85.

Sodhi, A., Montaner, S., Patel, V., Zohar, M., Bais, C., Mesri, E. A., & Gutkind, J. S. (2000). The Kaposi's sarcoma-associated herpes virus G protein-coupled receptor up-regulates vascular endothelial growth factor expression and secretion through mitogen-activated protein kinase and p38 pathways acting on hypoxia-inducible factor 1α. *Cancer Research, 60*(17), 4873-4880.

Soh, N. (2008). Selective chemical labeling of proteins with small fluorescent molecules based on metal-chelation methodology. *Sensors (Basel, Switzerland), 8*(2), 1004-1024.

Sørensen, B. S., Alsner, J., Overgaard, J., & Horsman, M. R. (2007). Hypoxia induced expression of endogenous markers in vitro is highly influenced by pH. *Radiotherapy and Oncology, 83*(3), 362-366.

Sørensen, B. S., Hao, J., Overgaard, J., Vorum, H., Honoré, B., Alsner, J., & Horsman, M. R. (2005). Influence of oxygen concentration and pH on expression of hypoxia induced genes. *Radiotherapy and Oncology, 76*(2), 187-193.

Sørensen, B. S., Horsman, M. R., Vorum, H., Honore, B., Overgaard, J., & Alsner, J. (2009). Proteins upregulated by mild and severe hypoxia in squamous cell carcinomas in vitro identified by proteomics. *Radiotherapy & Oncology, 92*(3), 443-449.

Sørensen, B. S., Toustrup, K., Horsman, M. R., Overgaard, J., & Alsner, J. (2010). Identifying pH independent hypoxia induced genes in human squamous cell carcinomas in vitro. *Acta Oncologica, 49*(7), 895-905.

Soriano del Amo, D., Wang, W., Jiang, H., Besanceney, C., Yan, A. C., Levy, M., . . . Wu, P. (2010). Biocompatible copper(I) catalysts for in vivo imaging of glycans. *Journal of the American Chemical Society, 132*(47), 16893-16899.

Souvatzoglou, M., Grosu, A. L., Roper, B., Krause, B. J., Beck, R., Reischl, G., . . . Piert, M. (2007). Tumour hypoxia imaging with [18F]FAZA PET in head and neck cancer patients: a pilot study. *European Journal of Nuclear Medicine & Molecular Imaging, 34*(10), 1566-1575.

Sowter, H. M., Ratcliffe, P. J., Watson, P., Greenberg, A. H., & Harris, A. L. (2001). HIF-1-dependent regulation of hypoxic induction of the cell death factors BNIP3 and NIX in human tumors. *Cancer Research, 61*(18), 6669-6673.

Spanakis, E. (1993). Problems related to the interpretation of autoradiographic data on gene expression using common constitutive transcripts as controls. *Nucleic Acids Res, 21*, 3809 - 3819.

Speers, A. E., Adam, G. C., & Cravatt, B. F. (2003). Activity-based protein profiling in vivo using a copper(I)-catalyzed azide-alkyne [3 + 2] cycloaddition. *Journal of the American Chemical Society, 125*(16), 4686-4687.

Speers, A. E., & Cravatt, B. F. (2004). Profiling enzyme activities in vivo using click chemistry methods. *Chemistry & Biology, 11*(4), 535-546.

Spiteri, C., & Moses, J. E. (2010). Copper-catalyzed azide–alkyne cycloaddition: Regioselective synthesis of 1,4,5-trisubstituted 1,2,3-triazoles. *Angewandte Chemie International Edition, 49*(1), 31-33.

Stadtman, E. R. (2006). Protein oxidation and aging. *Free Radical Research, 40*(12), 1250-1258.

Stadtman, E. R., & Berlett, B. S. (1998). Reactive oxygen-mediated protein oxidation in aging and disease. *Drug Metabolism Reviews, 30*(2), 225-243.

Stany, M. P., Vathipadiekal, V., Ozbun, L., Stone, R. L., Mok, S. C., Xue, H., . . . Birrer, M. J. (2011). Identification of novel therapeutic targets in microdissected clear cell ovarian cancers. *PLoS ONE [Electronic Resource], 6*(7), e21121.

Starmans, M. H. W., Chu, K. C., Haider, S., Nguyen, F., Seigneuric, R., Magagnin, M. G., . . . Lambin, P. (2012). The prognostic value of temporal in vitro and in vivo derived hypoxia gene-expression signatures in breast cancer. *Radiotherapy and Oncology, 102*(3), 436-443.

Steg, A., Wang, W., Blanquicett, C., Grunda, J. M., Eltoum, I. A., Wang, K., . . . Johnson, M. R. (2006). Multiple gene expression analyses in paraffin-embedded tissues by TaqMan low-density array: Application to hedgehog and Wnt pathway analysis in ovarian endometrioid adenocarcinoma. *Journal of Molecular Diagnostics, 8*(1), 76-83.

Stewart, G. D., Ross, J. A., McLaren, D. B., Parker, C. C., Habib, F. K., & Riddick, A. C. P. (2010). The relevance of a hypoxic tumour microenvironment in prostate cancer. *BJU International, 105*(1), 8-13.

Struthers, H., Mindt, T. L., & Schibli, R. (2010). Metal chelating systems synthesized using the copper(I) catalyzed azide-alkyne cycloaddition. *Dalton Transactions, 39*(3), 675-696.

Su, J., Gu, Y., Pruijn, F. B., Smaill, J. B., Patterson, A. V., Guise, C. P., & Wilson, W. R. (2013). Zinc finger nuclease knock-out of NADPH:cytochrome P450 oxidoreductase (POR) in human tumor cell lines demonstrates that hypoxia-activated prodrugs differ in POR dependence. *Journal of Biological Chemistry, 288*(52), 37138-37153.

Sun, W., Shen, Z. Y., Zhang, H., Fan, Y. Z., Zhang, W. Z., Zhang, J. T., . . . Ye, C. (2012). Overexpression of HIF-1alpha in primary gallbladder carcinoma and its relation to vasculogenic mimicry and unfavourable prognosis. *Oncology Reports, 27*(6), 1990-2002.

Sun, Y., Li, Y., Luo, D., & Liao, D. J. (2012). Pseudogenes as weaknesses of ACTB (Actb) and GAPDH (Gapdh) used as reference genes in reverse transcription and polymerase chain reactions. *PLoS ONE, 7*(8), e41659.

Suzuki, Y., Nakano, T., Ohno, T., Kato, S., Niibe, Y., Morita, S., & Tsujii, H. (2006). Oxygenated and reoxygenated tumors show better local control in radiation therapy for cervical cancer. *International Journal of Gynecological Cancer, 16*(1), 306-311.

Tabbi, G., Fry, S. C., & Bonomo, R. P. (2001). ESR study of the non-enzymic scission of xyloglucan by an ascorbate-H2O2-copper system: the involvement of the hydroxyl radical and the degradation of ascorbate. *Journal of Inorganic Biochemistry, 84*(3-4), 179-187.

Tabrizi, M., Bornstein, G. G., & Suria, H. (2010). Biodistribution mechanisms of therapeutic monoclonal antibodies in health and disease. *AAPS Journal, 12*(1), 33-43.

Takahashi, N., Fujibayashi, Y., Yonekura, Y., Welch, M. J., Waki, A., Tsuchida, T., . . . Itoh, H. (2000). Evaluation of 62Cu labeled diacetyl-bis(N4-methylthiosemicarbazone) as a hypoxic tissue tracer in patients with lung cancer. *Annals of Nuclear Medicine, 14*(5), 323-328.

Tan, S. C., Carr, C. A., Yeoh, K. K., Schofield, C. J., Davies, K. E., & Clarke, K. (2012). Identification of valid housekeeping genes for quantitative RT-PCR analysis of cardiosphere-derived cells preconditioned under hypoxia or with prolyl-4-hydroxylase inhibitors. *Molecular Biology Reports, 39*(4), 4857-4867.

Tannock, I. F. (1968). The relation between cell proliferation and the vascular system in a transplanted mouse mammary tumour. *British Journal of Cancer, 22*(2), 258-273.

Tannock, I. F., Lee, C. M., Tunggal, J. K., Cowan, D. S. M., & Egorin, M. J. (2002). Limited penetration of anticancer drugs through tumor tissue: a potential cause of resistance of solid tumors to chemotherapy. *Clinical Cancer Research, 8*(3), 878-884.

Tannock, I. F., & Rotin, D. (1989). Acid pH in tumors and its potential for therapeutic exploitation. *Cancer Research, 49*(16), 4373-4384.

Taraska, J. W., & Zagotta, W. N. (2010). Fluorescence applications in molecular neurobiology. *Neuron, 66*(2), 170-189.

Tatum, J. L., Kelloff, G. J., Gillies, R. J., Arbeit, J. M., Brown, J. M., Chao, K. S. C., . . . Sullivan, D. (2006). Hypoxia: importance in tumor biology, noninvasive measurement by imaging, and value of its measurement in the management of cancer therapy. *International Journal of Radiation Biology, 82*(10), 699-757.

Teicher, B. A., Lazo, J. S., & Sartorelli, A. C. (1981). Classification of antineoplastic agents by their selective toxicities toward oxygenated and hypoxic tumor cells. *Cancer Research, 41*(1), 73-81.

Teicher, B. A., & Sartorelli, A. C. (1980). Nitrobenzyl halides and carbamates as prototype bioreductive alkylating agents. *Journal of Medicinal Chemistry, 23*(8), 955-960.

Temple, M. D., Perrone, G. G., & Dawes, I. W. (2005). Complex cellular responses to reactive oxygen species. *Trends in Cell Biology, 15*(6), 319-326.

Tercel, M., & Pruijn, F. B. (2011). WO2011145957A1.

Textoris, J., Beaufils, N., Quintana, G., Ben Lassoued, A., Zieleskiewicz, L., Wiramus, S., . . . Leone, M. (2012). Hypoxia-inducible factor (HIF1α) gene expression in human shock states. *Critical Care, 16*(4), R120-R120.

Thermofisher. (2013). Amine-reactive probes. *Molecular Probes*. Retrieved from https://tools.thermofisher.com/content/sfs/manuals/mp00143.pdf

Thirlwell, C., Schulz, L., Dibra, H., & Beck, S. (2011). Suffocating cancer: Hypoxia-associated epimutations as targets for cancer therapy. *Clinical Epigenetics, 3*, 9.

Thomlinson, R. H., & Gray, L. H. (1955). The histological structure of some human lung cancers and the possible implications for radiotherapy. *British Journal of Cancer, 9*(4), 539-549.

Tornøe, C. W., Christensen, C., & Meldal, M. (2002). Peptidotriazoles on solid phase: [1,2,3]-triazoles by regiospecific copper(I)-catalyzed 1,3-dipolar cycloadditions of terminal alkynes to azides. *The Journal of organic chemistry, 67*(9), 3057-3064.

Toustrup, K., Sørensen, B. S., Alsner, J., & Overgaard, J. (2012). Hypoxia gene expression signatures as prognostic and predictive markers in head and neck radiotherapy. *Seminars in Radiation Oncology, 22*(2), 119-127.

Toustrup, K., Sørensen, B. S., Lassen, P., Wiuf, C., Alsner, J., & Overgaard, J. (2012). Gene expression classifier predicts for hypoxic modification of radiotherapy with nimorazole in squamous cell carcinomas of the head and neck. *Radiotherapy and Oncology, 102*(1), 122-129.

Toustrup, K., Sørensen, B. S., Nordsmark, M., Busk, M., Wiuf, C., Alsner, J., & Overgaard, J. (2011). Development of a hypoxia gene expression classifier with predictive impact for hypoxic modification of radiotherapy in head and neck cancer. *Cancer Research, 71*(17), 5923-5931.

Tredan, O., Galmarini, C. M., Patel, K., & Tannock, I. F. (2007). Drug resistance and the solid tumor microenvironment. *Journal of the National Cancer Institute, 99*(19), 1441-1454.

Trinkaus, M. E., Blum, R., Rischin, D., Callahan, J., Bressel, M., Segard, T., . . . Hicks, R. J. (2013). Imaging of hypoxia with 18F-FAZA PET in patients with locally advanced non-small cell lung cancer treated with definitive chemoradiotherapy. *Journal of Medical Imaging & Radiation Oncology, 57*(4), 475-481.

Trivedi, M. V., Laurence, J. S., & Siahaan, T. J. (2009). The role of thiols and disulfides in protein chemical and physical stability. *Current protein & peptide science, 10*(6), 614-625.

Tuttle, S. W., Maity, A., Oprysko, P. R., Kachur, A. V., Ayene, I. S., Biaglow, J. E., & Koch, C. J. (2007). Detection of reactive oxygen species via endogenous oxidative pentose phosphate cycle activity in response to oxygen concentration: Implications for the mechanism of HIF-1α stabilization under moderate hypoxia. *Journal of Biological Chemistry, 282*(51), 36790-36796.

Uttamapinant, C., Sanchez, M. I., Liu, D. S., Yao, J. Z., & Ting, A. Y. (2013). Site-specific protein labeling using PRIME and chelation-assisted click chemistry. *Nature Protocols, 8*(8), 1620-1634.

Uttamapinant, C., Tangpeerachaikul, A., Grecian, S., Clarke, S., Singh, U., Slade, P., . . . Ting, A. Y. (2012). Fast, cell-compatible click chemistry with copper-chelating azides for biomolecular labeling. *Angewandte Chemie. International Ed. in English, 51*(24), 5852-5856.

Vaapil, M., Helczynska, K., Villadsen, R., Petersen, O. W., Johansson, E., Beckman, S., . . . Jögi, A. (2012). Hypoxic conditions induce a cancer-like phenotype in human breast epithelial cells. *PLoS ONE, 7*(9), e46543.

Valeur, B., & Berberan-Santos, M. N. (2012). Introduction *Molecular Fluorescence* (pp. 1-30): Wiley-VCH Verlag GmbH & Co. KGaA.

van't Veer, L. J., & Bernards, R. (2008). Enabling personalized cancer medicine through analysis of gene-expression patterns. *Nature, 452*(7187), 564-570.

van de Linde, S., Aufmkolk, S., Franke, C., Holm, T., Klein, T., Löschberger, A., Proppert, S., . . . Sauer, M. (2013). Investigating cellular structures at the nanoscale with organic fluorophores. *Chemistry & Biology, 20*(1), 8-18.

van Dijk, M., Rijkers, D. T. S., Liskamp, R. M. J., van Nostrum, C. F., & Hennink, W. E. (2009). Synthesis and applications of biomedical and pharmaceutical polymers via click chemistry methodologies. *Bioconjugate Chemistry, 20*(11), 2001-2016.

van Geel, R., Pruijn, G. J. M., van Delft, F. L., & Boelens, W. C. (2012). Preventing thiol-yne addition improves the specificity of strain-promoted azide–alkyne cycloaddition. *Bioconjugate Chemistry, 23*(3), 392-398.

van Hagen, M., Overmeer, R. M., Abolvardi, S. S., & Vertegaal, A. C. O. (2010). RNF4 and VHL regulate the proteasomal degradation of SUMO-conjugated Hypoxia-Inducible Factor-2alpha. *Nucleic Acids Research, 38*(6), 1922-1931.

Vande Velde, C., Cizeau, J., Dubik, D., Alimonti, J., Brown, T., Israels, S., . . . Greenberg, A. H. (2000). BNIP3 and genetic control of necrosis-like cell death through the mitochondrial permeability transition pore. *Molecular & Cellular Biology, 20*(15), 5454-5468.

Vandesompele, J., De Preter, K., Pattyn, F., Poppe, B., Van Roy, N., De Paepe, A., & Speleman, F. (2002). Accurate normalization of real-time quantitative RT-PCR data by geometric averaging of multiple internal control genes. *Genome Biology, 3*(7), research0034.0031 - research0034.0011.

Vaupel, P. (2004). Tumor microenvironmental physiology and its implications for radiation oncology. *Seminars in Radiation Oncology, 14*(3), 198-206.

Vaupel, P. (2008). Hypoxia and aggressive tumor phenotype: implications for therapy and prognosis. *Oncologist, 13 Suppl 3*, 21-26.

Vaupel, P., & Harrison, L. (2004). Tumor hypoxia: Causative factors, compensatory mechanisms, and cellular response. *Oncologist, 9*(SUPPL. 5), 4-9.

Vaupel, P., Kallinowski, F., & Okunieff, P. (1989). Blood flow, oxygen and nutrient supply, and metabolic microenvironment of human tumors: a review. *Cancer Research, 49*(23), 6449-6465.

Vaupel, P., & Mayer, A. (2007). Hypoxia in cancer: Significance and impact on clinical outcome. *Cancer & Metastasis Reviews, 26*(2), 225-239.

Vaupel, P., Mayer, A., & Höckel, M. (2004). Tumor hypoxia and malignant progression. *Methods in Enzymology, 381*, 335-354.

Vermeulen, J., Derveaux, S., Lefever, S., De Smet, E., De Preter, K., Yigit, N., . . . Vandesompele, J. (2009). RNA pre-amplification enables large-scale RT-qPCR gene-expression studies on limiting sample amounts. *BMC Research Notes, 2*, 235.

Vikram, D. S., Zweier, J. L., & Kuppusamy, P. (2007). Methods for noninvasive imaging of tissue hypoxia. *Antioxidants and Redox Signaling, 9*(10), 1745-1756.

Viljoen, K. S., & Blackburn, J. M. (2013). Quality assessment and data handling methods for Affymetrix Gene 1.0 ST arrays with variable RNA integrity. *BMC Genomics, 14*, 14.

von Prowazek, S. (1914). Über fluorescenz der zellen. *Kleinwelt, 6*, 37-40.

Vordermark, D., & Brown, J. M. (2003). Endogenous markers of tumor hypoxia: Predictors of clinical radiation resistance? *Strahlentherapie und Onkologie, 179*(12), 801-811.

Vordermark, D., Shibata, T., & Brown, J. M. (2001). Green fluorescent protein is a suitable reporter of tumor hypoxia despite an oxygen requirement for chromophore formation. *Neoplasia (New York), 3*(6), 527-534.

Walther, T. C., & Mann, M. (2010). Mass spectrometry-based proteomics in cell biology. *Journal of Cell Biology, 190*(4), 491-500.

Wang, A., Winblade Nairn, N., Johnson, R. S., Tirrell, D. A., & Grabstein, K. (2008). Processing of N-terminal unnatural amino acids in recombinant human interferon-β in Escherichia coli. *Chembiochem, 9*(2), 324-330.

Wang, J., Foehrenbacher, A., Su, J., Patel, R., Hay, M. P., Hicks, K. O., & Wilson, W. R. (2012). The 2-nitroimidazole EF5 is a biomarker for oxidoreductases that activate the bioreductive prodrug CEN-209 under hypoxia. *Clinical Cancer Research, 18*(6), 1684-1695.

Wang, J., Guise, C. P., Dachs, G. U., Phung, Y., Hsu, A. H. L., Lambie, N. K., . . . Wilson, W. R. (2014). Identification of one-electron reductases that activate both the hypoxia prodrug SN30000 and diagnostic probe EF5. *Biochemical Pharmacology, 91*(4), 436-446.

Wang, Q., Chan, T. R., Hilgraf, R., Fokin, V. V., Sharpless, K. B., & Finn, M. G. (2003). Bioconjugation by copper(I)-catalyzed azide-alkyne [3 + 2] cycloaddition. *Journal of the American Chemical Society, 125*(11), 3192-3193.

Wardman, P. (2001). Electron transfer and oxidative stress as key factors in the design of drugs selectively active in hypoxia. *Current Medicinal Chemistry, 8*(7), 739-761.

Wardman, P., & Clarke, E. D. (1976). Oxygen inhibition of nitroreductase: electron transfer from nitro radical-anions to oxygen. *Biochemical & Biophysical Research Communications, 69*(4), 942-949.

Wardman, P., Dennis, M. F., Everett, S. A., Patel, K. B., Stratford, M. R., & Tracy, M. (1995). Radicals from one-electron reduction of nitro compounds, aromatic N-oxides and quinones: the kinetic basis for hypoxia-selective, bioreductive drugs. *Biochemical Society Symposia, 61*, 171-194.

Weaver, S., Dube, S., Mir, A., Qin, J., Sun, G., Ramakrishnan, R., . . . Livak, K. J. (2010). Taking qPCR to a higher level: Analysis of CNV reveals the power of high throughput qPCR to enhance quantitative resolution. *Methods (Duluth), 50*(4), 271-276.

Weis, J. H., Tan, S. S., Martin, B. K., & Wittwer, C. T. (1992). Detection of rare mRNAs via quantitative RT-PCR. *Trends in Genetics, 8*(8), 263-264.

Weiss, G. J., Infante, J. R., Chiorean, E. G., Borad, M. J., Bendell, J. C., Molina, J. R., . . . Burris Iii, H. A. (2011). Phase 1 study of the safety, tolerability, and pharmacokinetics of TH-302, a hypoxia-activated prodrug, in patients with advanced solid malignancies. *Clinical Cancer Research, 17*(9), 2997-3004.

Weller, R. L., & Rajski, S. R. (2005). DNA methyltransferase-moderated click chemistry. *Organic Letters, 7*(11), 2141-2144.

WHO. (2008). *The Global Burden of Disease: 2004 Update*. Geneva: World Health Organization.

WHO. (2010). *WHO Statistical Information System*. Geneva: World Health Organization Databank.

Wikipedia. (2015). Azide-alkyne Huisgen cycloaddition. Retrieved 2012, from https://en.wikipedia.org/wiki/Azide-alkyne_Huisgen_cycloaddition

Wilhelm, M., Schlegl, J., Hahne, H., Moghaddas Gholami, A., Lieberenz, M., Savitski, M. M., . . . Kuster, B. (2014). Mass-spectrometry-based draft of the human proteome. *Nature, 509*(7502), 582-587.

Wilson, W. R., & Hay, M. P. (2011). Targeting hypoxia in cancer therapy. *Nature Reviews, Cancer. 11*(6), 393-410.

Wilson, W. R., Hicks, K. O., Pullen, S. M., Ferry, D. M., Helsby, N. A., & Patterson, A. V. (2007). Bystander effects of bioreductive drugs: Potential for exploiting pathological tumor hypoxia with dinitrobenzamide mustards. *Radiation Research, 167*(6), 625-636.

Wilson, W. R., Hicks, K. O., Wang, J., & Pruijn, F. B. (2014). Prodrug strategies for targeting tumour hypoxia. In G. Melillo (Ed.), *Hypoxia and Cancer* (pp. 283-328): Springer New York.

Winski, S. L., Swann, E., Hargreaves, R. H., Dehn, D. L., Butler, J., Moody, C. J., & Ross, D. (2001). Relationship between NAD(P)H:quinone oxidoreductase 1 (NQO1) levels in a series of stably transfected cell lines and susceptibility to antitumor quinones. *Biochemical Pharmacology, 61*(12), 1509-1516.

Winter, G., & Milstein, C. (1991). Man-made antibodies. *Nature, 349*(6307), 293-299.

Winter, S. C., Buffa, F. M., Silva, P., Miller, C., Valentine, H. R., Turley, H., . . . Harris, A. L. (2007). Relation of a hypoxia metagene derived from head and neck cancer to prognosis of multiple cancers. *Cancer Res, 67*(7), 3441-3449.

Wirges, C. T., Gramlich, P. M. E., Gutsmiedl, K., Gierlich, J., Burley, G. A., & Carell, T. (2007). Pronounced effect of DNA hybridization on click reaction efficiency. *Qsar & Combinatorial Science, 26*(11-12), 1159-1164.

Wong, R. K., Fyles, A., Milosevic, M., Pintilie, M., & Hill, R. P. (1997). Heterogeneity of polarographic oxygen tension measurements in cervix cancer: an evaluation of within and between tumor variability, probe position, and track depth. *International Journal of Radiation Oncology, Biology, Physics, 39*(2), 405-412.

Worrell, B. T., Malik, J. A., & Fokin, V. V. (2013). Direct evidence of a dinuclear copper intermediate in Cu(I)-catalyzed azide-alkyne cycloadditions. *Science, 340*(6131), 457-460.

Wouters, B. G., & Koritzinsky, M. (2008). Hypoxia signalling through mTOR and the unfolded protein response in cancer. *Nature Reviews, Cancer. 8*(11), 851-864.

Wu, P., & Fokin, V. V. (2007). Catalytic azide-alkyne cycloaddition: Reactivity and applications. *ChemInform, 38*(36), no-no.

Xia, X., Lemieux, M. E., Li, W., Carroll, J. S., Brown, M., Liu, X. S., & Kung, A. L. (2009). Integrative analysis of HIF binding and transactivation reveals its role in maintaining histone methylation homeostasis. *Proceedings of the National Academy of Sciences of the United States of America, 106*(11), 4260-4265.

Yan, C., Kepa, J. K., Siegel, D., Stratford, I. J., & Ross, D. (2008). Dissecting the role of multiple reductases in bioactivation and cytotoxicity of the antitumor agent 2,5-diaziridinyl-3-(hydroxymethyl)-6-methyl- 1,4-benzoquinone (RH1). *Molecular Pharmacology, 74*(6), 1657-1665.

Yang, L., DeBusk, L. M., Fukuda, K., Fingleton, B., Green-Jarvis, B., Shyr, Y., . . . Lin, P. C. (2004). Expansion of myeloid immune suppressor Gr+CD11b+ cells in tumor-bearing host directly promotes tumor angiogenesis. *Cancer Cell, 6*(4), 409-421.

Yang, Y.-Y., Ascano, J. M., & Hang, H. C. (2010). Bioorthogonal chemical reporters for monitoring protein acetylation. *Journal of the American Chemical Society, 132*(11), 3640-3641.

Yang, Y., Fan, W., Zhu, L., Zhao, T., Ma, L., Wu, Y., . . . Fan, M. (2008). Effects of hypoxia on mRNA expression of housekeeping genes in rat brain tissue and primary cultured neural cells. *Frontiers of Medicine in China, 2*(3), 239-243.

Yao, J. Z., Uttamapinant, C., Poloukhtine, A., Baskin, J. M., Codelli, J. A., Sletten, E. M., . . . Ting, A. Y. (2012). Fluorophore targeting to cellular proteins via enzyme-mediated azide ligation and strain-promoted cycloaddition. *Journal of the American Chemical Society, 134*(8), 3720-3728.

Yao, L., Chen, X., Tian, Y., Lu, H., Zhang, P., Shi, Q., . . . Liu, Y. (2012). Selection of housekeeping genes for normalization of RT-PCR in hypoxic neural stem cells of rat in vitro. *Molecular Biology Reports, 39*(1), 569-576.

Yapp, D. T. T., Woo, J., Kartono, A., Sy, J., Oliver, T., Skov, K. A., . . . Gleave, M. (2007). Non-invasive evaluation of tumour hypoxia in the Shionogi tumour model for prostate cancer with 18F-EF5 and positron emission tomography. *BJU International, 99*(5), 1154-1160.

Yeh, J. J., & Kim, W. Y. (2015). Targeting tumor hypoxia with hypoxia-activated prodrugs. *Journal of Clinical Oncology, 33*(13), 1505-1508.

Yin, J., Glaser, R., & Gates, K. S. (2012). On the reaction mechanism of tirapazamine reduction chemistry: unimolecular N-OH homolysis, stepwise dehydration, or triazene ring-opening. *Chemical Research in Toxicology, 25*(3), 634-645.

Young, S. D., & Hill, R. P. (1989). Radiation sensitivity of tumour cells stained in vitro or in vivo with the bisbenzimide fluorochrome Hoechst 33342. *British Journal of Cancer, 60*(5), 715-721.

Young, S. D., & Hill, R. P. (1990). Effects of reoxygenation on cells from hypoxic regions of solid tumors: anticancer drug sensitivity and metastatic potential. *Journal of the National Cancer Institute, 82*(5), 371-380.

Yuan, G., Khan, S. A., Luo, W., Nanduri, J., Semenza, G. L., & Prabhakar, N. R. (2011). Hypoxia-inducible factor 1 mediates increased expression of NADPH oxidase-2 in response to intermittent hypoxia. *Journal of Cellular Physiology, 226*(11), 2925-2933.

Yuan, Z., Kuang, G.-C., Clark, R. J., & Zhu, L. (2012). Chemoselective sequential “click” ligation using unsymmetrical bisazides. *Organic Letters, 14*(10), 2590-2593.

Yurkova, N., Shaw, J., Blackie, K., Weidman, D., Jayas, R., Flynn, B., & Kirshenbaum, L. A. (2008). The cell cycle factor E2F-1 activates Bnip3 and the intrinsic death pathway in ventricular myocytes. *Circulation Research, 102*(4), 472-479.

Zhan, W.-h., Barnhill, H. N., Sivakumar, K., Tian, H., & Wang, Q. (2005). Synthesis of hemicyanine dyes for ‘click’ bioconjugation. *Tetrahedron Letters, 46*(10), 1691-1695.

Zhang, H., Bosch-Marce, M., Shimoda, L. A., Tan, Y. S., Baek, J. H., Wesley, J. B., . . . Semenza, G. L. (2008). Mitochondrial autophagy is an HIF-1-dependent adaptive metabolic response to hypoxia. *Journal of Biological Chemistry, 283*(16), 10892-10903.

Zhang, L., Gao, L., Liu, Q., Yang, F., & Fang, Y. (2012). A novel surfactant-like fluorophore and its probing ability to the aggregation of amphiphilic compounds. *Journal of Photochemistry and Photobiology A: Chemistry, 245*, 58-65.

Zhang, Q., Wang, J., Deng, F., Yan, Z., Xia, Y., Wang, Z., . . . Jiang, L. (2015). TqPCR: A touchdown qPCR assay with significantly improved detection sensitivity and amplification efficiency of SYBR green qPCR. *PLoS ONE [Electronic Resource], 10*(7), e0132666.

Zhang, Y., Li, M., Yao, Q., & Chen, C. (2007). Recent advances in tumor hypoxia: Tumor progression, molecular mechanisms, and therapeutic implications. *Medical Science Monitor, 13*(10), RA175-RA180.

Zheng, Y., Ni, Y., Huang, X., Wang, Z., & Han, W. E. I. (2013). Overexpression of HIF-1α indicates a poor prognosis in tongue carcinoma and may be associated with tumour metastasis. *Oncology Letters, 5*(4), 1285-1289.

Zhong, H., De Marzo, A. M., Laughner, E., Lim, M., Hilton, D. A., Zagzag, D., . . . Simons, J. W. (1999). Overexpression of hypoxia-inducible factor 1α in common human cancers and their metastases. *Cancer Research, 59*(22), 5830-5835.

Zhong, H., & Simons, J. W. (1999). Direct comparison of GAPDH, beta-actin, cyclophilin, and 28S rRNA as internal standards for quantifying RNA levels under hypoxia. *Biochemical & Biophysical Research Communications, 259*(3), 523-526.

Zhou, Z., & Fahrni, C. J. (2004). A fluorogenic probe for the copper(I)-catalyzed azide-alkyne ligation reaction: modulation of the fluorescence emission via 3(n,pi)-1(pi,pi) inversion. *Journal of the American Chemical Society, 126*(29), 8862-8863.

Zhu, P., Ning, Y., Yao, L., Chen, M., & Xu, C. (2010). The proliferation, apoptosis, invasion of endothelial-like epithelial ovarian cancer cells induced by hypoxia. *Journal of Experimental & Clinical Cancer Research, 29*, 124.

Zhuang, X., Ha, T., Kim, H. D., Centner, T., Labeit, S., & Chu, S. (2000). Fluorescence quenching: A tool for single-molecule protein-folding study. *Proceedings of the National Academy of Sciences, 97*(26), 14241-14244.

11200 Rockville Pike
Suite 302
Rockville, Maryland 20852

August 19, 2011

American Society for Biochemistry and Molecular Biology

To whom it may concern,

It is the policy of the American Society for Biochemistry and Molecular Biology to allow reuse of any material published in its journals (the Journal of Biological Chemistry, Molecular & Cellular Proteomics and the Journal of Lipid Research) in a thesis or dissertation at no cost and with no explicit permission needed. Please see our copyright permissions page on the journal site for more information.

Best wishes,

Sarah Crespi

American Society for Biochemistry and Molecular Biology
11200 Rockville Pike, Rockville, MD
Suite 302
240-283-6616
JBC | MCP | JLR

NATURE PUBLISHING GROUP LICENSE
TERMS AND CONDITIONS

Oct 31, 2016

This Agreement between Alec Hou ("You") and Nature Publishing Group ("Nature Publishing Group") consists of your license details and the terms and conditions provided by Nature Publishing Group and Copyright Clearance Center.

License Number	3744710293846
License date	Nov 09, 2015
Licensed Content Publisher	Nature Publishing Group
Licensed Content Publication	Nature Reviews Cancer
Licensed Content Title	Targeting hypoxia in cancer therapy
Licensed Content Author	William R. Wilson and Michael P. Hay
Licensed Content Date	Jun 1, 2011
Licensed Content Volume Number	11
Licensed Content Issue Number	6
Type of Use	reuse in a dissertation / thesis
Requestor type	academic/educational
Format	print and electronic
Portion	figures/tables/illustrations
Number of figures/tables/illustrations	1
High-res required	no
Figures	Figure 1 Oxygen dependence of hypoxia-responsive processes in tumours.
Author of this NPG article	no
Your reference number	
Title of your thesis / dissertation	Novel Click Chemistry Probes to Target Hypoxic Tumour Cells and Characterise Their Gene Expression
Expected completion date	Nov 2015
Estimated size (number of pages)	200
Requestor Location	Alec Hou 4/99 Mountain Rd Auckland, 1023 New Zealand Attn: Alec Hou
Billing Type	Invoice
Billing Address	Alec Hou 4/99 Mountain Rd Auckland, New Zealand 1023 Attn: Alec Hou
Total	0.00 USD

Total 0.00 USD

Terms and Conditions

Terms and Conditions for Permissions

Nature Publishing Group hereby grants you a non-exclusive license to reproduce this material for this purpose, and for no other use,subject to the conditions below:

1. NPG warrants that it has, to the best of its knowledge, the rights to license reuse of this material. However, you should ensure that the material you are requesting is original to Nature Publishing Group and does not carry the copyright of another entity (as credited in the published version). If the credit line on any part of the material you have requested indicates that it was reprinted or adapted by NPG with permission from another source, then you should also seek permission from that source to reuse the material.

2. Permission granted free of charge for material in print is also usually granted for any electronic version of that work, provided that the material is incidental to the work as a whole and that the electronic version is essentially equivalent to, or substitutes for, the print version.Where print permission has been granted for a fee, separate permission must be obtained for any additional, electronic re-use (unless, as in the case of a full paper, this has already been accounted for during your initial request in the calculation of a print run).NB: In all cases, web-based use of full-text articles must be authorized separately through the 'Use on a Web Site' option when requesting permission.

3. Permission granted for a first edition does not apply to second and subsequent editions and for editions in other languages (except for signatories to the STM Permissions Guidelines, or where the first edition permission was granted for free).

4. Nature Publishing Group's permission must be acknowledged next to the figure, table or abstract in print. In electronic form, this acknowledgement must be visible at the same time as the figure/table/abstract, and must be hyperlinked to the journal's homepage.

5. The credit line should read:
   Reprinted by permission from Macmillan Publishers Ltd: [JOURNAL NAME] (reference citation), copyright (year of publication)
   For AOP papers, the credit line should read:
   Reprinted by permission from Macmillan Publishers Ltd: [JOURNAL NAME], advance online publication, day month year (doi: 10.1038/sj.[JOURNAL ACRONYM].XXXXX)

   Note: For republication from the *British Journal of Cancer*, the following credit lines apply.
   Reprinted by permission from Macmillan Publishers Ltd on behalf of Cancer Research UK: [JOURNAL NAME] (reference citation), copyright (year of publication)For AOP papers, the credit line should read:
   Reprinted by permission from Macmillan Publishers Ltd on behalf of Cancer Research UK: [JOURNAL NAME], advance online publication, day month year (doi: 10.1038/sj.[JOURNAL ACRONYM].XXXXX)

6. Adaptations of single figures do not require NPG approval. However, the adaptation should be credited as follows:

   Adapted by permission from Macmillan Publishers Ltd: [JOURNAL NAME] (reference citation), copyright (year of publication)

   Note: For adaptation from the *British Journal of Cancer*, the following credit line applies.
   Adapted by permission from Macmillan Publishers Ltd on behalf of Cancer Research UK: [JOURNAL NAME] (reference citation), copyright (year of publication)

7. Translations of 401 words up to a whole article require NPG approval. Please visit http://www.macmillanmedicalcommunications.com for more information.Translations of up to a 400 words do not require NPG approval. The translation should be credited as follows:

   Translated by permission from Macmillan Publishers Ltd: [JOURNAL NAME] (reference citation), copyright (year of publication).

   Note: For translation from the *British Journal of Cancer*, the following credit line applies.

Translated by permission from Macmillan Publishers Ltd on behalf of Cancer Research UK: [JOURNAL NAME] (reference citation), copyright (year of publication)

We are certain that all parties will benefit from this agreement and wish you the best in the use of this material. Thank you.
Special Terms:
v1.1

NATURE PUBLISHING GROUP LICENSE
TERMS AND CONDITIONS

Oct 31, 2016

This Agreement between Alec Hou ("You") and Nature Publishing Group ("Nature Publishing Group") consists of your license details and the terms and conditions provided by Nature Publishing Group and Copyright Clearance Center.

License Number	3744710459253
License date	Nov 09, 2015
Licensed Content Publisher	Nature Publishing Group
Licensed Content Publication	Nature Reviews Cancer
Licensed Content Title	Exploiting tumour hypoxia in cancer treatment
Licensed Content Author	J. Martin BrownandWilliam R. Wilson
Licensed Content Date	Jun 1, 2004
Licensed Content Volume Number	4
Licensed Content Issue Number	6
Type of Use	reuse in a dissertation / thesis
Requestor type	academic/educational
Format	print and electronic
Portion	figures/tables/illustrations
Number of figures/tables/illustrations	1
High-res required	no
Figures	Box 1 | Radiation resistance of hypoxic cells
Author of this NPG article	no
Your reference number	
Title of your thesis / dissertation	Novel Click Chemistry Probes to Target Hypoxic Tumour Cells and Characterise Their Gene Expression
Expected completion date	Nov 2015
Estimated size (number of pages)	200
Requestor Location	Alec Hou 4/99 Mountain Rd Auckland, 1023 New Zealand Attn: Alec Hou
Billing Type	Invoice
Billing Address	Alec Hou 4/99 Mountain Rd Auckland, New Zealand 1023 Attn: Alec Hou
Total	0.00 USD
Total	0.00 USD

Terms and Conditions

Terms and Conditions for Permissions

Nature Publishing Group hereby grants you a non-exclusive license to reproduce this material for this purpose, and for no other use,subject to the conditions below:

1. NPG warrants that it has, to the best of its knowledge, the rights to license reuse of this material. However, you should ensure that the material you are requesting is original to Nature Publishing Group and does not carry the copyright of another entity (as credited in the published version). If the credit line on any part of the material you have requested indicates that it was reprinted or adapted by NPG with permission from another source, then you should also seek permission from that source to reuse the material.

2. Permission granted free of charge for material in print is also usually granted for any electronic version of that work, provided that the material is incidental to the work as a whole and that the electronic version is essentially equivalent to, or substitutes for, the print version.Where print permission has been granted for a fee, separate permission must be obtained for any additional, electronic re-use (unless, as in the case of a full paper, this has already been accounted for during your initial request in the calculation of a print run).NB: In all cases, web-based use of full-text articles must be authorized separately through the 'Use on a Web Site' option when requesting permission.

3. Permission granted for a first edition does not apply to second and subsequent editions and for editions in other languages (except for signatories to the STM Permissions Guidelines, or where the first edition permission was granted for free).

4. Nature Publishing Group's permission must be acknowledged next to the figure, table or abstract in print. In electronic form, this acknowledgement must be visible at the same time as the figure/table/abstract, and must be hyperlinked to the journal's homepage.

5. The credit line should read:
   Reprinted by permission from Macmillan Publishers Ltd: [JOURNAL NAME] (reference citation), copyright (year of publication)
   For AOP papers, the credit line should read:
   Reprinted by permission from Macmillan Publishers Ltd: [JOURNAL NAME], advance online publication, day month year (doi: 10.1038/sj.[JOURNAL ACRONYM].XXXXX)

   Note: For republication from the *British Journal of Cancer*, the following credit lines apply.
   Reprinted by permission from Macmillan Publishers Ltd on behalf of Cancer Research UK: [JOURNAL NAME] (reference citation), copyright (year of publication)For AOP papers, the credit line should read:
   Reprinted by permission from Macmillan Publishers Ltd on behalf of Cancer Research UK: [JOURNAL NAME], advance online publication, day month year (doi: 10.1038/sj.[JOURNAL ACRONYM].XXXXX)

6. Adaptations of single figures do not require NPG approval. However, the adaptation should be credited as follows:

   Adapted by permission from Macmillan Publishers Ltd: [JOURNAL NAME] (reference citation), copyright (year of publication)

   Note: For adaptation from the *British Journal of Cancer*, the following credit line applies.
   Adapted by permission from Macmillan Publishers Ltd on behalf of Cancer Research UK: [JOURNAL NAME] (reference citation), copyright (year of publication)

7. Translations of 401 words up to a whole article require NPG approval. Please visit http://www.macmillanmedicalcommunications.com for more information.Translations of up to a 400 words do not require NPG approval. The translation should be credited as follows:

   Translated by permission from Macmillan Publishers Ltd: [JOURNAL NAME] (reference citation), copyright (year of publication).

   Note: For translation from the *British Journal of Cancer*, the following credit line applies.

Translated by permission from Macmillan Publishers Ltd on behalf of Cancer Research UK: [JOURNAL NAME] (reference citation), copyright (year of publication)

We are certain that all parties will benefit from this agreement and wish you the best in the use of this material. Thank you.
Special Terms:
v1.1

SPRINGER LICENSE
TERMS AND CONDITIONS

Oct 31, 2016

This Agreement between Alec Hou ("You") and Springer ("Springer") consists of your license details and the terms and conditions provided by Springer and Copyright Clearance Center.

License Number	3744711030653
License date	Nov 09, 2015
Licensed Content Publisher	Springer
Licensed Content Publication	Molecules and Cells
Licensed Content Title	HIF-1 and HIF-2 transcription factors — Similar but not identical
Licensed Content Author	Agnieszka Loboda
Licensed Content Date	Jan 1, 2010
Licensed Content Volume Number	29
Licensed Content Issue Number	5
Type of Use	Thesis/Dissertation
Portion	Figures/tables/illustrations
Number of figures/tables/illustrations	1
Author of this Springer article	No
Order reference number	
Original figure numbers	Fig. 1. Structure of hypoxia inducible factor-1α and 2α
Title of your thesis / dissertation	Novel Click Chemistry Probes to Target Hypoxic Tumour Cells and Characterise Their Gene Expression
Expected completion date	Nov 2015
Estimated size(pages)	200
Requestor Location	Alec Hou 4/99 Mountain Rd Auckland, 1023 New Zealand Attn: Alec Hou
Billing Type	Invoice
Billing Address	Alec Hou 4/99 Mountain Rd Auckland, New Zealand 1023 Attn: Alec Hou
Total	0.00 USD
Total	0.00 USD

Terms and Conditions

Introduction

The publisher for this copyrighted material is Springer Science + Business Media. By clicking "accept" in connection with completing this licensing transaction, you agree that the

following terms and conditions apply to this transaction (along with the Billing and Payment terms and conditions established by Copyright Clearance Center, Inc. ("CCC"), at the time that you opened your Rightslink account and that are available at any time at http://myaccount.copyright.com).

Limited License

With reference to your request to reprint in your thesis material on which Springer Science and Business Media control the copyright, permission is granted, free of charge, for the use indicated in your enquiry.

Licenses are for one-time use only with a maximum distribution equal to the number that you identified in the licensing process.

This License includes use in an electronic form, provided its password protected or on the university's intranet or repository, including UMI (according to the definition at the Sherpa website: http://www.sherpa.ac.uk/romeo/). For any other electronic use, please contact Springer at (permissions.dordrecht@springer.com or permissions.heidelberg@springer.com). The material can only be used for the purpose of defending your thesis limited to university-use only. If the thesis is going to be published, permission needs to be re-obtained (selecting "book/textbook" as the type of use).

Although Springer holds copyright to the material and is entitled to negotiate on rights, this license is only valid, subject to a courtesy information to the author (address is given with the article/chapter) and provided it concerns original material which does not carry references to other sources (if material in question appears with credit to another source, authorization from that source is required as well).

Permission free of charge on this occasion does not prejudice any rights we might have to charge for reproduction of our copyrighted material in the future.

Altering/Modifying Material: Not Permitted

You may not alter or modify the material in any manner. Abbreviations, additions, deletions and/or any other alterations shall be made only with prior written authorization of the author(s) and/or Springer Science + Business Media. (Please contact Springer at (permissions.dordrecht@springer.com or permissions.heidelberg@springer.com)

Reservation of Rights

Springer Science + Business Media reserves all rights not specifically granted in the combination of (i) the license details provided by you and accepted in the course of this licensing transaction, (ii) these terms and conditions and (iii) CCC's Billing and Payment terms and conditions.

Copyright Notice:Disclaimer

You must include the following copyright and permission notice in connection with any reproduction of the licensed material: "Springer and the original publisher /journal title, volume, year of publication, page, chapter/article title, name(s) of author(s), figure number(s), original copyright notice) is given to the publication in which the material was originally published, by adding; with kind permission from Springer Science and Business Media"

Warranties: None

Example 1: Springer Science + Business Media makes no representations or warranties with respect to the licensed material.

Example 2: Springer Science + Business Media makes no representations or warranties with respect to the licensed material and adopts on its own behalf the limitations and disclaimers established by CCC on its behalf in its Billing and Payment terms and conditions for this licensing transaction.

Indemnity

You hereby indemnify and agree to hold harmless Springer Science + Business Media and CCC, and their respective officers, directors, employees and agents, from and against any and all claims arising out of your use of the licensed material other than as specifically authorized pursuant to this license.

No Transfer of License

This license is personal to you and may not be sublicensed, assigned, or transferred by you to any other person without Springer Science + Business Media's written permission.

No Amendment Except in Writing

This license may not be amended except in a writing signed by both parties (or, in the case

of Springer Science + Business Media, by CCC on Springer Science + Business Media's behalf).

Objection to Contrary Terms

Springer Science + Business Media hereby objects to any terms contained in any purchase order, acknowledgment, check endorsement or other writing prepared by you, which terms are inconsistent with these terms and conditions or CCC's Billing and Payment terms and conditions. These terms and conditions, together with CCC's Billing and Payment terms and conditions (which are incorporated herein), comprise the entire agreement between you and Springer Science + Business Media (and CCC) concerning this licensing transaction. In the event of any conflict between your obligations established by these terms and conditions and those established by CCC's Billing and Payment terms and conditions, these terms and conditions shall control.

Jurisdiction

All disputes that may arise in connection with this present License, or the breach thereof, shall be settled exclusively by arbitration, to be held in The Netherlands, in accordance with Dutch law, and to be conducted under the Rules of the 'Netherlands Arbitrage Instituut' (Netherlands Institute of Arbitration).*OR:*

All disputes that may arise in connection with this present License, or the breach thereof, shall be settled exclusively by arbitration, to be held in the Federal Republic of Germany, in accordance with German law.

Other terms and conditions:

v1.3

Questions? customercare@copyright.com or +1-855-239-3415 (toll free in the US) or +1-978-646-2777.

SPRINGER LICENSE
TERMS AND CONDITIONS

Oct 31, 2016

This Agreement between Alec Hou ("You") and Springer ("Springer") consists of your license details and the terms and conditions provided by Springer and Copyright Clearance Center.

License Number	3744720534838
License date	Nov 09, 2015
Licensed Content Publisher	Springer
Licensed Content Publication	Pharmaceutical Research
Licensed Content Title	Click Chemistry, A Powerful Tool for Pharmaceutical Sciences
Licensed Content Author	Christopher D. Hein
Licensed Content Date	Jan 1, 2008
Licensed Content Volume Number	25
Licensed Content Issue Number	10
Type of Use	Thesis/Dissertation
Portion	Figures/tables/illustrations
Number of figures/tables/illustrations	1
Author of this Springer article	No
Order reference number	
Original figure numbers	Fig. 4. Proposed mechanism for the HDC reaction.
Title of your thesis / dissertation	Novel Click Chemistry Probes to Target Hypoxic Tumour Cells and Characterise Their Gene Expression
Expected completion date	Nov 2015
Estimated size(pages)	200
Requestor Location	Alec Hou 4/99 Mountain Rd Auckland, 1023 New Zealand Attn: Alec Hou
Billing Type	Invoice
Billing Address	Alec Hou 4/99 Mountain Rd Auckland, New Zealand 1023 Attn: Alec Hou
Total	0.00 USD
Total	0.00 USD
Terms and Conditions	

Introduction
The publisher for this copyrighted material is Springer Science + Business Media. By clicking "accept" in connection with completing this licensing transaction, you agree that the

following terms and conditions apply to this transaction (along with the Billing and Payment terms and conditions established by Copyright Clearance Center, Inc. ("CCC"), at the time that you opened your Rightslink account and that are available at any time at http://myaccount.copyright.com).

Limited License

With reference to your request to reprint in your thesis material on which Springer Science and Business Media control the copyright, permission is granted, free of charge, for the use indicated in your enquiry.

Licenses are for one-time use only with a maximum distribution equal to the number that you identified in the licensing process.

This License includes use in an electronic form, provided its password protected or on the university's intranet or repository, including UMI (according to the definition at the Sherpa website: http://www.sherpa.ac.uk/romeo/). For any other electronic use, please contact Springer at (permissions.dordrecht@springer.com or permissions.heidelberg@springer.com). The material can only be used for the purpose of defending your thesis limited to university-use only. If the thesis is going to be published, permission needs to be re-obtained (selecting "book/textbook" as the type of use).

Although Springer holds copyright to the material and is entitled to negotiate on rights, this license is only valid, subject to a courtesy information to the author (address is given with the article/chapter) and provided it concerns original material which does not carry references to other sources (if material in question appears with credit to another source, authorization from that source is required as well).

Permission free of charge on this occasion does not prejudice any rights we might have to charge for reproduction of our copyrighted material in the future.

Altering/Modifying Material: Not Permitted

You may not alter or modify the material in any manner. Abbreviations, additions, deletions and/or any other alterations shall be made only with prior written authorization of the author(s) and/or Springer Science + Business Media. (Please contact Springer at (permissions.dordrecht@springer.com or permissions.heidelberg@springer.com)

Reservation of Rights

Springer Science + Business Media reserves all rights not specifically granted in the combination of (i) the license details provided by you and accepted in the course of this licensing transaction, (ii) these terms and conditions and (iii) CCC's Billing and Payment terms and conditions.

Copyright Notice:Disclaimer

You must include the following copyright and permission notice in connection with any reproduction of the licensed material: "Springer and the original publisher /journal title, volume, year of publication, page, chapter/article title, name(s) of author(s), figure number(s), original copyright notice) is given to the publication in which the material was originally published, by adding; with kind permission from Springer Science and Business Media"

Warranties: None

Example 1: Springer Science + Business Media makes no representations or warranties with respect to the licensed material.

Example 2: Springer Science + Business Media makes no representations or warranties with respect to the licensed material and adopts on its own behalf the limitations and disclaimers established by CCC on its behalf in its Billing and Payment terms and conditions for this licensing transaction.

Indemnity

You hereby indemnify and agree to hold harmless Springer Science + Business Media and CCC, and their respective officers, directors, employees and agents, from and against any and all claims arising out of your use of the licensed material other than as specifically authorized pursuant to this license.

No Transfer of License

This license is personal to you and may not be sublicensed, assigned, or transferred by you to any other person without Springer Science + Business Media's written permission.

No Amendment Except in Writing

This license may not be amended except in a writing signed by both parties (or, in the case

of Springer Science + Business Media, by CCC on Springer Science + Business Media's behalf).

Objection to Contrary Terms

Springer Science + Business Media hereby objects to any terms contained in any purchase order, acknowledgment, check endorsement or other writing prepared by you, which terms are inconsistent with these terms and conditions or CCC's Billing and Payment terms and conditions. These terms and conditions, together with CCC's Billing and Payment terms and conditions (which are incorporated herein), comprise the entire agreement between you and Springer Science + Business Media (and CCC) concerning this licensing transaction. In the event of any conflict between your obligations established by these terms and conditions and those established by CCC's Billing and Payment terms and conditions, these terms and conditions shall control.

Jurisdiction

All disputes that may arise in connection with this present License, or the breach thereof, shall be settled exclusively by arbitration, to be held in The Netherlands, in accordance with Dutch law, and to be conducted under the Rules of the 'Netherlands Arbitrage Instituut' (Netherlands Institute of Arbitration).*OR:*

All disputes that may arise in connection with this present License, or the breach thereof, shall be settled exclusively by arbitration, to be held in the Federal Republic of Germany, in accordance with German law.

Other terms and conditions:

v1.3

Questions? customercare@copyright.com or +1-855-239-3415 (toll free in the US) or +1-978-646-2777.

Lin Hou

From: Darla Henderson <D_Henderson@acs.org>
Sent: Monday, 23 November 2015 1:41 p.m.
To: Lin Hou
Subject: FW: Request permission

Dear Alec,

Thank you for the request. I confirm you have permission to reuse Scheme 1 and Table 1 from the article here http://pubs.acs.org/doi/pdf/10.1021/cb6003228 in the thesis you are writing to complete the degree-granting requirements of your university. ACS asks that you:

- Cite the *ACS Chemical Biology* article as the source of Scheme 1 and Table 1;
- Note any modifications you made from the originals; and
- Include in your PhD thesis a direct link to the *ACS Chemical Biology* article – direct link here http://pubs.acs.org/doi/pdf/10.1021/cb6003228

Wishing you the best of luck as you complete your degree,
Darla

Darla Henderson, PhD
Asst Director, Open Access Programs
American Chemical Society

From: Lin Hou [mailto:l.hou@auckland.ac.nz]
Sent: Wednesday, November 18, 2015 6:14 AM
To: Darla Henderson
Subject: RE: Request permission

Dear Dr Henderson,

Thank you so much for your rapid reply. I am planning to use Scheme 1 and Table 1 from the following paper in my PhD thesis. The title of my thesis is "Novel Click Chemistry Probes to Target Hypoxic Tumour Cells and Characterise Their Gene Expression".

Kind regards,

Alec Lin Hou

School of Medical Sciences
University of Auckland

A comparative study of bioorthogonal reactions with azides." (Agard, N. J., Baskin, J. M., Prescher, J. A., Lo, A., & Bertozzi, C. R. (2006). A comparative study of bioorthogonal reactions with azides. ACS Chemical Biology [Electronic Resource], 1(10), 644-648.http://pubs.acs.org/doi/abs/10.1021/cb6003228):

- Scheme 1. Bioorthogonal reactions with the azide: biomolecules containing the azide react via the Staudinger ligation
- Table 1. Selection of reaction depends on application

Kind regards,

Alec Hou

School of Medical Sciences
University of Auckland

From: Darla Henderson [D_Henderson@acs.org]
Sent: Wednesday, 18 November 2015 4:56
To: Lin Hou
Subject: RE: Request permission

Dear Alec Hou,

Please let me know where you wish to reuse the figure and table. Specifically, the name of the journal or book (or thesis) and the publisher, if any.

Thank you,
Darla

Darla Henderson, Ph.D.
Asst. Director, Open Access Programs
American Chemical Society

Lin Hou

From: "Dunncan Suarez" <info@biomedcentral.com> <info@biomedcentral.com>
Sent: Monday, 23 November 2015 11:37 p.m.
To: Lin Hou
Subject: 00600102 re:Request permission

Dear Dr. Hou,

Thank you for contacting BioMed Central.

Yes you may. For your information, reproduction of figures or tables is permitted free of charge and without formal written permission from the publisher or the copyright holder, provided that the figure/table is original, BioMed Central is duly identified as the original publisher, and that proper attribution of authorship and the correct citation details are given as acknowledgement.

If you have any questions please do not hesitate to contact me.

Best wishes

Jerome Juliano
Customer Services
info@biomedcentral.com
www.biomedcentral.com
----------Your Question/Comment ----------

To whom it may concern,

I plan to use one figure from your webpage in my PhD thesis with the title "Novel Click Chemistry Probes to Target Hypoxic Tumour Cells and Characterise Their Gene Expression".

The title of figure is "Target genes transcriptionally activated by HIF-1α". The link of that figure is http://www.genomemedicine.com/content/figures/gm271-1-l.jpg.

I wonder if I need to get specific permission from you? Please let me know.

Thank you so much!

Kind regards,

Alec Hou

School of Medical Sciences

University of Auckland
ref:_00D20CUt._50020spvlBAAQ:ref

Lin Hou

From: Sarah McManaway
Sent: Wednesday, 9 September 2015 9:39 a.m.
To: Lin Hou
Cc: Frederik B. Pruijn; Moana Tercel
Subject: RE: Require the permission to cite your unpublished data in my PhD thesis

Hi Lin,

I'm sorry for my delayed response, I just remembered about this. I am happy for you to use my images in your thesis, no problems at all ☺

Best regards,

Sarah.

From: Lin Hou
Sent: Tuesday, 25 August 2015 4:20 p.m.
To: Sarah McManaway
Cc: Frederik B. Pruijn; Moana Tercel
Subject: Require the permission to cite your unpublished data in my PhD thesis

Hi Sarah,

I plan to use the following 2 images from your previous confocal microscopy work in my thesis.

Those 2 images will be presented in the format attached with this email. I will also mention that they are your unpublished data and acknowledge you.

Could you please let me know if you are happy to offer me a agreement? Thank you so much.

Regards,

Lin

A.

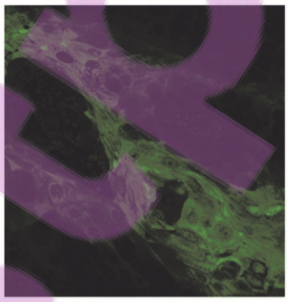

B.